Spring 1974

Synthetically-generated holographic memory system utilizing partially coherent light

William A. Barrett
New Jersey Institute of Technology

Copyright Warning & Restrictions

The copyright law of the United States (Title 17, United States Code) governs the making of photocopies or other reproductions of copyrighted material.

Under certain conditions specified in the law, libraries and archives are authorized to furnish a photocopy or other reproduction. One of these specified conditions is that the photocopy or reproduction is not to be "used for any purpose other than private study, scholarship, or research." If a, user makes a request for, or later uses, a photocopy or reproduction for purposes in excess of "fair use" that user may be liable for copyright infringement,

This institution reserves the right to refuse to accept a copying order if, in its judgment, fulfillment of the order would involve violation of copyright law.

Please Note: The author retains the copyright while the New Jersey Institute of Technology reserves the right to distribute this thesis or dissertation

Printing note: If you do not wish to print this page, then select "Pages from: first page # to: last page #" on the print dialog screen

SYNTHETICALLY-GENERATED HOLOGRAPHIC MEMORY SYSTEM UTILIZING PARTIALLY COHERENT LIGHT

BY

WILLIAM A. BARRETT

A DISSERTATION

PRESENTED IN PARTIAL FULFILLMENT OF

THE REQUIREMENTS FOR THE DEGREE

OF

DOCTOR OF ENGINEERING SCIENCE IN ELECTRICAL ENGINEERING

AT

NEWARK COLLEGE OF ENGINEERING

Newark, New Jersey

1974

ABSTRACT

This dissertation proposes a novel form of optical ROM for the digital computer. This memory makes use of holographic techniques because of the advantages offered by holographic memories over conventional optical ones, especially with regard to dust and scratch sensitivity.

These advantages have long been recognized by workers in the field, indeed several holographic optical memories have already been proposed.

A survey of the state of the art of digital computer memories is offered in the introductory part of the thesis. Particular emphasis is placed on optical memories. A brief review of basic holographic theory is also included for reference.

As shown by the above survey random-access holographic ROM's to this day characteristically offer access times of 1 microsecond or more. This limitation is imposed by the response time of the devices used to deflect the read-out laser beam in order to effect access to the various page addresses.

This dissertation proposes to bypass this difficulty be using the radiation from the phosphor of a CRT tube, rather than laser radiation, for holographic readout. This proposal is based on the hypothesis that a viable random access holographic computer memory can be designed so as not to require for readout the high degree of coherence characterizing laser radiation. The advantage of utili-

zing this specific technique is that current CRT technology, having produced phosphors with nanosecond decay times and deflection circuitry with frequency response in excess of 500 MHz, can be used to reduce the read-out time by a factor of one hundred from that noted above.

To verify this hypothesis, a memory system that employed the CRT as the source of read-out radiation is designed. A mathematical model of this system is formulated from the basic principles of physical optics, taking into account the non-point and non-monochromatic characteristics of the CRT source. The model is meant for digital computer simulation of the system's behavior in order to determine feasibility and optimize system parameters.

A conventional mathematical model, unfortunately, proves to be inadequate in practice because of the excessive computation time required. A second model is formulated based on a less conventional approach, namely on a physical and geometrical interpretation and consequent approximation of various elements of the system.

On the basis of this model a simulation of the system is performed and the parameters of a CRT ROM capable of storing 10^5 bits per square centimeter of film are determined.

The holograms required to implement a memory at such a density cannot be practically produced by optical means. It is shown, however, that production of such holograms can be achieved by means of a computer synthesizing technique.

The design of an appropriate synthesizing system is described. This system uses computer-generated pulse duration modulation on the z-axis input of a CRT to produce the desired hologram.

Practical feasibility of this approach is investigated and proved experimentally by producing test holograms and verifying their information storing ability.

As part of the optimization study of this system the effect of interbit diffraction interference on the bit-to-bit read-out signal non-uniformity is investigated. This non-uniformity, which is not peculiar to the CRT system but constitutes a problem shared by most optical memories, results in output data errors.

A qualitative analysis shows that a tilted rectangular aperture can be selected so as to cause less diffraction interference than is caused by a circular one.

A quantitative theoretical analysis of the phenomenon is presented. For the sake of mathematical convenience this analysis is limited to circular apertures. The relationship between diffraction interference and aperture size is shown to be non-monotonic and to possess local minima of significant depth.

Experimental verification of the above theoretical results is described. These experiments show the presence of other sources of readout non-uniformity and error. In the case of circular apertures the non-uniformity due to interbit diffraction interference is shown

to be dominated by the effect of other sources of disturbance whenever the aperture diameter is larger than 50 mils.

Computer synthesized holograms, as described in this dissertation, are shown to present some advantages in this respect.

APPROVAL OF DISSERTATION

SYNTHETICALLY-GENERATED HOLOGRAPHIC MEMORY SYSTEM

UTILIZING PARTIALLY COHERENT LIGHT

BY

WILLIAM A. BARRETT

FOR

DEPARTMENT OF ELECTRICAL ENGINEERING

NEWARK COLLEGE OF ENGINEERING

BY

FACULTY COMMITTEE

APPROVED: _____

_____

_____

_____

_____

NEWARK, NEW JERSEY

MAY, 1974

DEDICATION

To my wife, Jeanne, for her patience, her understanding, and her encouragement and to our children, Billy, Aileen, Patrick, and Sarah, for their refreshing joy and for their quietness.

ACKNOWLEDGMENTS

The author gratefully acknowledges the guidance and assistance of Dr. Mauro Zambuto, Distinguished Professor of Electrical Engineering. He also expresses his gratitude to the faculty and staff of Newark College of Engineering for the aid that they have rendered, in particular to Dr. Jacob Klapper, Dr. Raj Misra, and Dr. Marshall Natapoff.

The author acknowledges the financial support of Newark College of Engineering and the National Science Foundation.

TABLE OF CONTENTS

Page

APPENDICES

LIST OF FIGURES

LIST OF TABLES

CHAPTER I

SURVEY OF COMPUTER MEMORY TECHNOLOGY

Introduction

The subject of this dissertation is the development of an optical memory system for a digital computer. The goal is to achieve a system with high speed and large capacity while maintaining a favorable cost position with respect to other memory systems. In this chapter, the function of the memory will be briefly discussed as will the manner of its implementation in modern computers. This is done with the intent of giving insight into the properties desired in a memory device. Competitive memory systems, both optical and non-optical, will be examined with the intent of establishing a basis against which a new memory system can be compared. The chapter will conclude with a qualitative description of the proposed optical computer memory system.

Memory Function

In the organizational scheme of a modern digital computer, the memory element serves two purposes. The more obvious is the archival function. In this usage the memory allows vast amounts of data to be quickly available to the user. The second function is, perhaps, less obvious and will therefore be expounded.

The common desk calculator, or 'adding machine', of today is based on the stepped reckoner of Leibniz (1671). It is estimated that a skilled operator can perform only 500 simple arithmetic op-

erations per day using a desk calculator.[1] The limiting factor in this rate is not the speed of the machine, but rather the mental and manual dexterity of the operator. A memory, with its ability to supply a stored program and data to the calculator, eliminates the need for constant operator intervention. Thus, the memory allows the machine to function at 'electronic speed'.

Memory Implementation

Before discussing the properties of the various elements used in memory devices, it seems proper to first sketch out the basic organization of the computer. Figure 1-1 shows the general organization of a modern digital computer. Since the computer's memory is to be the focus of this work, a closer examination of its organization is in order.

From an operational, or characteristic, point of view, the memory may be easily broken into three parts. The operation registers, or control memory, is that portion of the memory in which control instructions are stored immediately prior to being executed and in which currently used data is stored. This area serves as a buffer between the CPU and the main data store. As such, it is characterized by very high speed. Its size is usually between 10 and 10,000 words.[2] The memory on the next highest level is the main storage, or inner memory. This area is frequently referred to as 'core'. It can

---

1 T. C. Bartee, Digital Computer Fundamentals, McGraw Hill, Inc., New York, 1966, p. 4.

2 E. C. Joseph, Computer Design, Vol. 8, No. 11, pp. 165-8, November 1969.

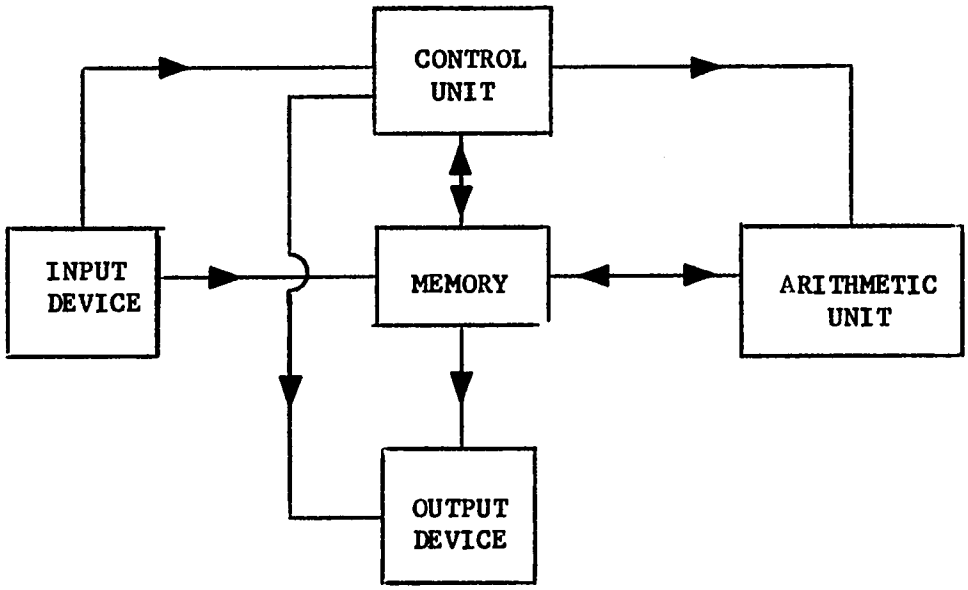

COMPUTER ORGANIZATION

FIGURE 1 - 1

be characterized as a relatively large high speed memory. It is here that the current programs, subroutines, and data are stored. This area also acts as a buffer between the operation registers and the mass store. The inner store has a capacity of 10^3 to 10^6 words.[2] To meet the need for more memory at a lower cost per bit, the mass store, or auxiliary memory, was introduced. The mass store has a capacity in excess of 10^7 words.[2] If still more storage is needed at an even lower cost per bit, punch cards and paper tape are available. In terms of physical components, the control memory is usually composed of semi-conductors, the inner memory is made of ferrite core stacks, and the mass memory consists of magnetic drums, magnetic disks, and magnetic tapes.

In evaluating the different types of memory devices, the permanence, the speed, the capacity, the volatility, the type of access, and the cost need to be indicated. Permanence refers to the erasability of the information stored in the memory. A memory is said to be erasable if the contents of the memory can be changed during the normal operating cycle of the computer; i.e., 'in situ'. An example of a non-erasable memory is the ROM (read only memory). A memory is volatile if its contents would be destroyed by a powering-down of the machine. Two types of access are currently being used; sequential access and random access. In a sequentially accessed memory, the data is available to the sensors in a fixed order. Therefore, it is sometimes necessary to wait for unwanted data to pass the sensors before the desired data becomes available. Sequential

memories are themselves divided into two types; progressive and cyclic. In the progressive, such as punch cards and, to an extent, magnetic tape, the data is available only once. In the cyclic case, such as the magnetic drum, the data is available every period. Sequential memories are also referred to by the terms serial and dynamic.

The random access memory is one in which all the data points are equally available. It is not necessary to wait for unwanted data to pass by first. This type is also referred to by the names parallel and static.

Comparison of Memory Devices (Non-Optical)

As of 1962 computer memory technology had advanced to the state indicated by the devices of Table 1-1.[3] A literal interpretation of the above table may prove misinformative. The difficulty arises in the interpretation of the access times. Some devices; e.g., magnetic cores and electrostatic tubes, have a destructive read cycle. Thus a write cycle must be completed after every read cycle if the data is to preserved. Therefore, it becomes necessary to consider the total memory cycle time (read plus write) if a true understanding of the speed of the device is to be obtained. However, a search of the literature shows what appears to be an interchangeable use (or misuse) of the terms 'access time' and 'cycle time'. A second area of confusion arises when the amount of decoding which the memory will do is taken into consideration; e.g., single-level versus full-decode.

---

[3] Burroughs Corp., Digital Computer Principles, McGraw Hill, Inc., New York, 1962, p. 386.

Storage Device	Typical Capacity (Characters)	Access Time (μsec)	Mode of Access	Volatile	Permanence	Use
Magnetic Cores	$10\text{-}10^5$	1-10	Random	No	Erasable	High Sp. Internal
Magnetic Drums	$20\text{-}2(10^6)$	10-100	Sequential & Cyclic	No	Erasable	Med. Sp. Internal
Magnetic Tape-reels	$2\text{-}2(10^7)$	$(1\text{-}100)10^6$	Sequential & Progressive	No	Erasable	Slow Sp. External
Delay Lines	$5\text{-}10^4$	1-10	Sequential & Cyclic	Yes	Erasable	Med. Sp. Internal
Electrostatic Tubes	$5\text{-}5(10^4)$	1-20	Random	Yes	Erasable	High Sp. Internal
Punched Cards	80-90/card	50-150	Sequential & Progressive	No	Non-Erasable	Low Sp. External

1962 MEMORY TECHNOLOGY

Table 1-1

In late 1968 and early 1969 the state of the memory art had progressed to the point where memories with a capacity of 100 billion bits or with speeds in the order of 10's of nanoseconds were technologically available. This progress is illustrated in Figure 1-2.[4] A chart of the same type, compiled one year later, is shown in Figure 1-3.[5] In early 1973, the position of optical memories was enhanced over that shown in Figure 1-3 when the Precision Instrument Company marketed its 10^{12} bit Unicon 690 at a cost of 10^{-4}¢ per bit.[6] At that time disk memories with 10^{10} bits were priced at approximately 5×10^{-3}¢ per bit. This last chart is significant in two respects. First, it shows that the speed of optical memories had become competitive with that of core memories. Second, the aspect of cost has been introduced. The trade between cost and speed will play a leading role in the following discussion.

Before proceeding to a discussion of semi-conductor memories, it should be stated that some experts are discounting the future of magnetic core memories in the one microsecond market.[7] The main reason for the undesirability of core is the need for extensive interfacing between it and the semi-conductor addressing and arithmetic circuits.

---

4 M. D. Blue and D. Chen, Electronics, Vol. 42, No. 5, p. 109, March, 1969.

5 J. T. LaMacchia, Laser Focus, Vol. 6, No. 2, p. 35, February 1970.

6 O. N. Tufte and D. Chen, IEEE Spectrum, Vol. 10, No. 2, pp. 26-32, February, 1973.

7 D. Roop, Electronic Products, Vol. 12, No. 10, p. 97, February, 1970.

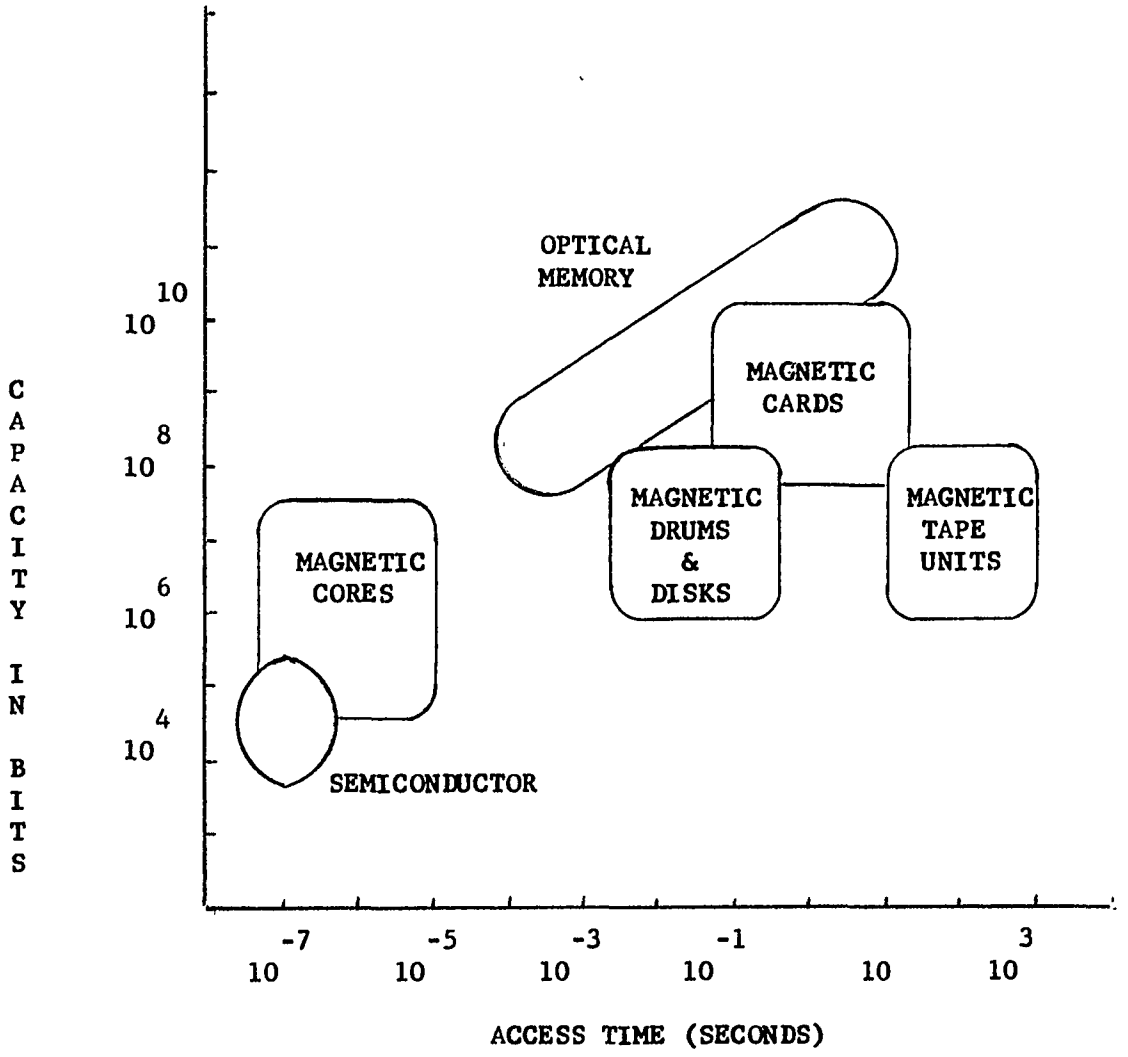

1969 MEMORY TECHNOLOGY

FIGURE 1 - 2

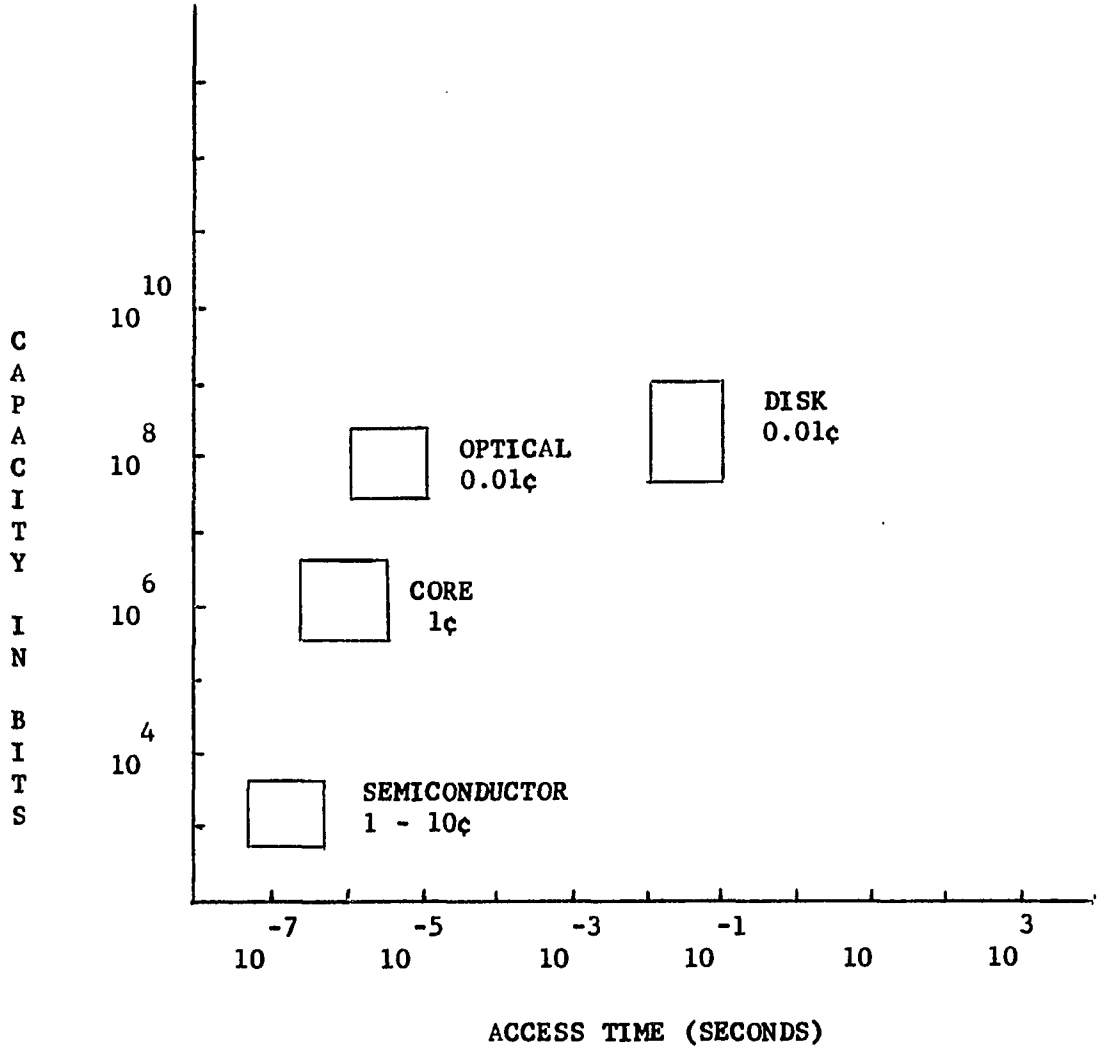

1970 MEMORY TECHNOLOGY

FIGURE 1 - 3

By going to semi-conductor memories, memory, addressing, and arithmetic elements can be formed on the same chip. While optical memories suffer from the same need for buffering, they will be shown to have redeeming values.

At the present time two types of transistors are vying for dominance in the memory market; the MOSFET and the bipolar transistor. Of these the bipolar is the faster. Published data shows 256 bit bipolar RAM's (random access memory) with an access time under 100 nanoseconds and 64 bit bipolar RAM's with times under 5 nanoseconds. The cost is approximately ten cents per bit.[8] The MOS RAM's, with a more economical chip geometry, can be produced with a fully decoding addressing mechanism at a price of 6 to 8¢ per bit for chips with a 1024 by 16 bit system. The time is 1 to 1.5 microseconds. A similar chip with single decode logic costs 8 to 12¢ per bit, but it has an access time of 120 to 250 nanoseconds. The least expensive of the high speed read-write semi-conductor memories are those with large MOS shift registers (1024 bits). These have a bit rate of 5Mhz. They have the advantage of having very few external leads. Furthermore, they can be stopped for up to one microsecond in anticipation of data transfer. The cost is approximately 3¢ per bit.

In the way of non-semi-conductor read-write memories, Sittig and Smits have re-initiated the study of a storage technique of the

---

[8] R. Graham and M. Hoff, Electronic Products, Vol. 12, No. 9, pp. 28-34, January, 1970.

late 1940's; the acoustic delay line.[9] Using Bausch and Lomb's T40 glass and ceramic sodium potassium niobate transducers, they have developed an ultra-sonic delay line with a 100 Mhz bit rate. A 2 inch by 1 inch by 0.1 inch strip of T40 glass will hold 1000 bits. With bit rate higher than that of semi-conductor memories, but the latency of a drum, this device is envisaged as a buffer between a slow external memory and a high speed CPU. Its cost is competitive with a lower speed LSI system.

In the early 1970's the CCD (charge coupled device) and the magnetic bubble memory began to receive serious consideration. While these devices are not sufficiently developed to have firm performance and cost values, some authoritative predictions have been made. It is expected that the cost of a bubble memory will be approximately 10^{-3}¢ per bit[10] and have an access time of 10 microseconds. While the cost of the CCD is predicted to be 0.1¢ per bit, its access time will be compatible with that of semi-conductor memories.

In the operation of a computer, some of the data stored in the memory is of the permanent type. Examples of this are compilers, code converters, trignometric function generators, and display character generators. Since these data need not be written 'in situ', they can be stored in a read-only memory. Many devices and techniques

---

9 E. K. Sittig and F. M. Smits, Bell System Technical Journal, Vol. 48, No. 3, p. 659, March 1969.

10 G. Lapidus, IEEE Spectrum, Vol. 10, No. 7, pp. 50-54, July 1970.

are available for the construction of a ROM which are not suitable for use in constructing a read-write memory. Thus the ROM can be made cheaper, faster, and simpler (no write circuitry) in many cases. A table of some popular ROM's is given in Table 1-2.[11] The fastest ROM currently in production is Signetics' 10139.[12] This 256 bit chip has an access time of 15 nanoseconds.

Optical Memories

As early as 1958 researchers at the Bell Telephone Laboratories were attempting to exploit the high information packing density of photographic film.[13] This particular technique, which had high switching speed as a goal, was called the 'Flying Spot Store'. This system is shown in Figure 1-4.[14] The specifications called for the storing of 2.5×10^6 bits. A phosphor with a decay time of approximately 10^{-7} seconds was called for. P16 type phosphor meets this criterion. In 1958 the beam deflection time had an experimental value of 2×10^{-6} seconds. It should be noted that this system suffered in SNR because each bit was stored as a very small discrete point. A scratch or speck of dust could destroy many bits. This shortcoming can be overcome by holographic techniques.

---

11 J. Marino and J. Sirota, Electronics, Vol. 43, No. 6, pp. 112-6, March 1970.

12 Signetics Corp., IEEE Spectrum, Vol. 11, No. 1, p. 107, January 1974.

13 H. G. Cooper, Bell System Technical Journal, Vol. 40, No. 3, p. 724, May 1961.

14 C. W. Hoover, G. Hangk, and D. R. Herriott, Bell System Technical Journal, Vol. 38, No. 2, p. 367, March 1959.

TABLE OF POPULAR ROM'S

Type	Speed	Comments
Discrete Diode	250nsec to 1 sec	Simple, flexible (change diodes) Expensive: 10 to 25¢/bit handwired Economical capacity 100 to 10000 bits
Monolithic Diode Array	Same	Masks too expensive for small runs
Monolithic Bipolar Transistor Arrays	100nsec	Fabrication complex, expensive masks, highest speed ROM
MOSFET	500nsec to 1 sec	Fabrication complex, expensive masks, ruggedness questioned (charging and discharging of static electricity, as well as excessive voltages, will destroy them), 1¢/bit.
Resistor Arrays	150 to 500 nsec	Excellent reliability and ruggedness, expensive peripheral electronics, high power dissipation and low SNR
Capacitor Arrays	250nsec to 1 sec	Rugged, reliable, tens of thousands of bits
Torodial Transformer		Old, costly because hand-made
Braided Transformer Arrays	150nsec	Reliable, rugged, flexible, machine made, low cost 2 to 9¢/bit

Table 1-2

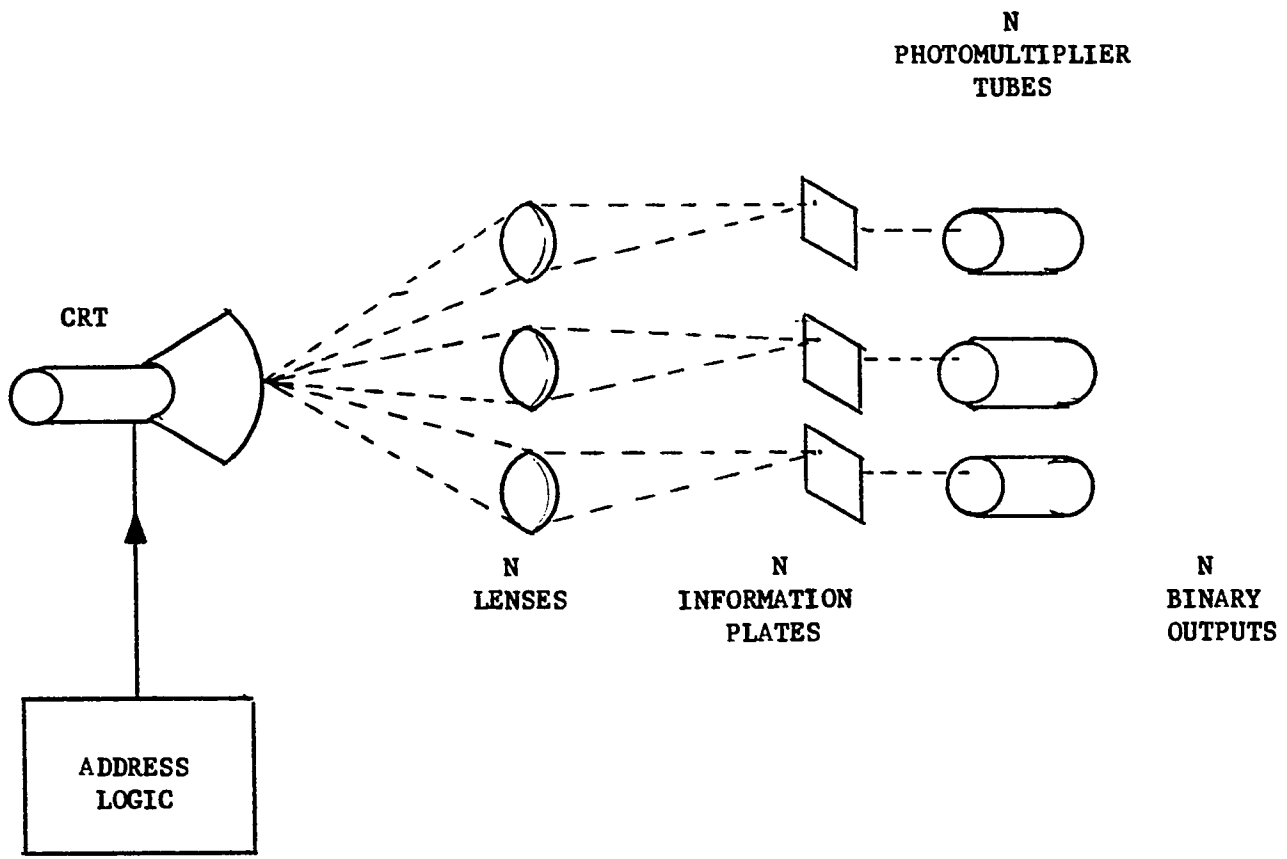

FLYING SPOT STORE

FIGURE 1 - 4

The basic idea of the flying spot store has recently been resurrected by the International Computer and Tabulator Limited of England.[15] Figure 1-5 shows a schematic of ICT's system. In the FSS the parallelism needed to form a word was generated by placing several lenses in a plane. In ICT's version the parallelism is generated by a mirror tunnel. Each position on the CRT produces sixty-nine spots; i.e., a sixty-nine bit word. The access time is rated at five microseconds. As in the FSS, the number of words is set by the 256 x 256 position matrix of the CRT spot. A handicap shared by this store and the FSS is the tediousness of the mask-making process. ICT gives this figure as one hour.

Research in the optical memory field has led to non-photographic devices. The Unicon system of the Precision Instrument Company is representative of one sub-group.[16] Unicon uses a continuous wave argon ion laser to burn or punch one micron holes in a non-magnetic tape. Using a pulse-code modulation scheme, this system can store the contents of four-and-one-half miles of conventional magnetic tape on a three inch by thirty inch strip. The specifications call for a retrieval rate of 2×10^6 bits per second. The company makes a claim for a potential bandwidth of 10^9 bits per second. Similar systems are being studied by the National Cash Register Company and by the Itek Corporation.

---

15 R. J. Botfield, A. N. Hill, and B. J. Steptoe, Journal of Physics E, Vol. 1, Series 2, p. 810, 1968.

16 C. H. Becker, Electronics, Vol. 41, No. 6, p. 50, March 18, 1968.

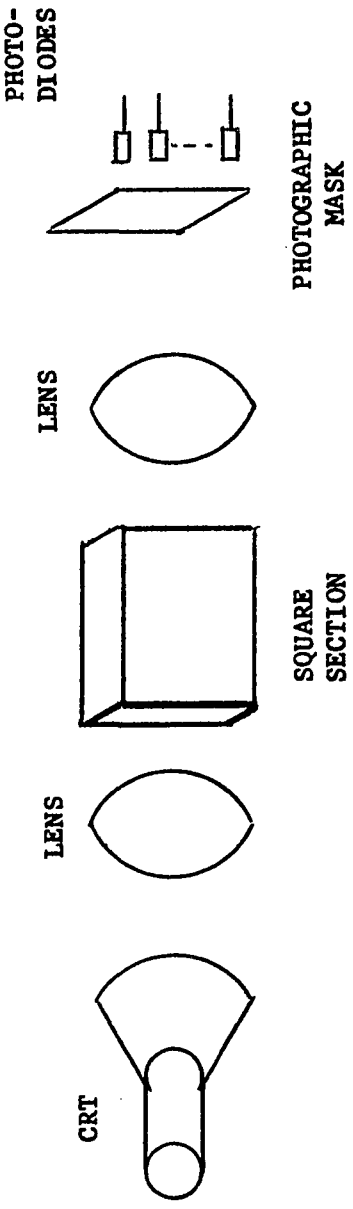

ICT's SYSTEM

FIGURE 1 - 5

A second sub-group makes use of the magneto-optic Faraday Effect. In this type of system a magnetic film of an appropriate material such as manganese-bismuth (Honeywell[17]) is magnetically saturated in one direction. Information is written by raising small areas of the film above the Curie temperature. Subsequent cooling allows the neighboring fields to create a field opposite to the original field of the heated region. The Faraday Effect refers to the ability of a magnetic field to rotate the polarization direction of a light beam. Thus the reading scheme calls for the magnetic film to rotate the light polarization so that a polarization analyzer can distinguish between zeros and ones. Similar Faraday Effect systems are being developed by IBM and by RCA. Other materials especially suited for the technique are EuO and EuS.[18]

A main functional difference between the hole burning techniques and the Faraday Effect systems is that the former are permanent while the latter are erasable. Several companies are working on erasable photographic memory devices. These devices make use of photochromic materials; e.g., organic dyes and alkali halides. "Photochronism" is a reversible change in a compound's absorption spectrum when it is irradiated with a specific wavelength of light. In general, short wavelengths cause the spectrum to be shifted toward the red; longer wavelengths shift it back toward the blue.[19] Thus a material may be darkened by one frequency

---

17 Blue and Chen, op. cit., p. 111.

18 Tufte and Chen, op. cit., p. 30.

19 Blue and Chen, op. cit., p. 110.

and bleached by another. A variation of this scheme has been pursued at the Bell Telephone Laboratories.[20] Using a lithium-niobate crystal 'smaller than a lump of sugar' one thousand phase holograms can be stored. These holograms are angularly separated. To erase the holograms, the crystal temperature is raised to 170°C. It should be noted that this material has a diffraction efficiency maximum of 42% as compared to 6% for photographic film plates. Carson Laboratories Incorporated has developed a similar system, but one with the apparent additional feature of selective erasure.[21] In general, photochromic materials suffer from fatigue, lack of well defined threshold, sensitivity to scattered light, and long-time instability.

At present, holographic optical memories using non-erasable media are being built by IBM and BTL. The most elementary is the cylindrical memory developed at IBM's San Jose Laboratory.[22] Figure 1-6 shows a sketch of this system. It has a theoretical density of 6×10^6 bits per square inch and an experimental density of 2×10^6 bits per square inch. It has a theoretical speed of 160×10^6 bits per second and an experimental speed of 16×10^6 bits per second. However, because of its serial nature, it has a mean access time of 8.5 milliseconds. To overcome this long mean access time, random

---

20 J. T. LaMacchia, F. S. Chen, and D. B. Fraser, Bell Telephone Laboratories Record, January 1969, pp. 30-1.

21 Blue and Chen, op. cit., p. 111.

22 L. F. Shew, Product Engineering, Vol. 40, No. 12, p. 16, June 16, 1969.

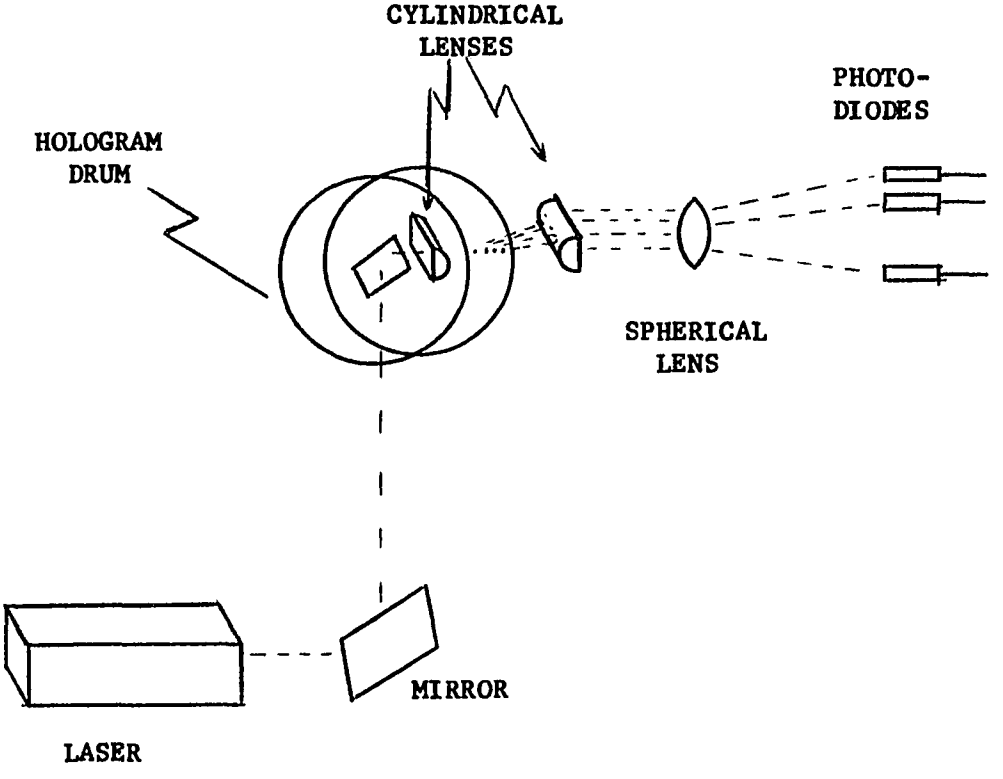

IBM's CYLINDRICAL MEMORY

FIGURE 1 - 6

access memories are being developed by IBM and by BTL. Because of the similarity of the systems, The Bell Telephone Laboratories system alone will be described.

The BTL system is proposed as a semi-permanent random-access mass memory. The contents of the memory are changed by replacing the holographic plate. A schematic of the system is shown in Figure 1-7.[23] The deflector system is a pair of crossed; i.e., x and y, acousto-optic Bragg Diffraction Cells. The acoustic frequency range is 85 to 170 Mhz. Specifications call for the stepping of the frequencies so as to obtain 64 by 64 addresses. Experimentally, a 32 by 32 raster has been obtained. A state of the art cell; e.g., a lithium niobate transducer driving crystalline alpha-iodic acid, can randomly address sixty-four locations with an access time of 1.5 microseconds. Each of the 4096 specified optically addressable subholograms is considered a page of data. Each page will be composed of sixty-four 64-bit words. The subholograms are 1.5 millimeters on edge and have a 2 millimeter center spacing. This gives a packing density of 1024×10^6 bits per square meter. The 4096 bits per page are holographically imaged on an array of photo-transistors; one detector per bit. The words in the page are then accessed as they would be in a standard semi-conductor memory. The specified word access time is 100 nanoseconds.

---

23 L. K. Anderson, Laser Technology, Vol. 9, No. 3, p. 62, March 1970.

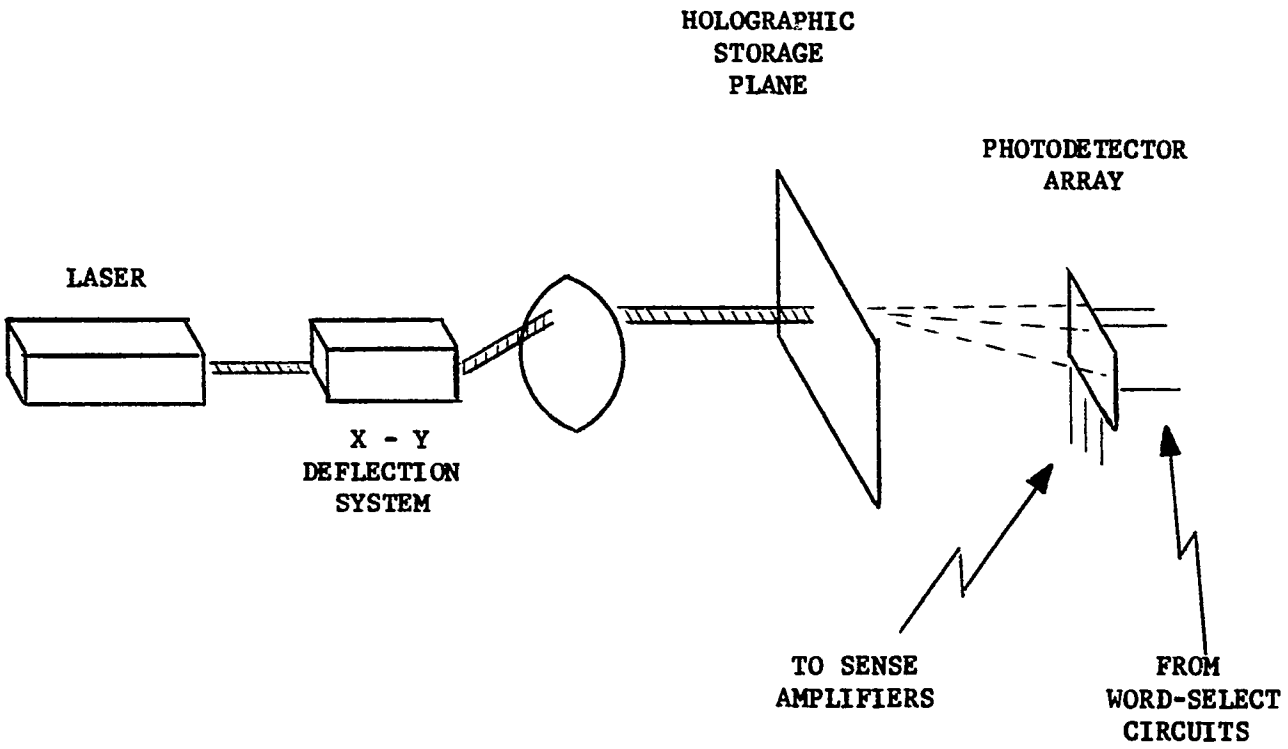

BTL's HOLOGRAPHIC MEMORY

FIGURE 1 - 7

Memory Utilization

The control and arithmetic portions of third generation computers are composed of logic elements; e.g., and-gates, nor-gates, etc. Because of their characteristic high speed, they are usually semiconductor devices. While the cycle time for a single gate is very small, typical operations call for the sequential operation of several gates. Thus, if the intrinsic speed of the semi-conductor device is to be utilized, the designer must limit his logic to single level operation. This constraint leads to very expensive hardware if done with gates. However, this single level logic can be conveniently and economically implemented by employing ROM's. In considering the economics it is noted that ten bits of memory are equivalent to one logic gate on the average.[24] Present technology can place one bipolar logic gate on a ten square mil area of chip or it can place 10 MOSFET ROM bits on the same area. The economy of the ROM occurs because it requires only one custom mask as compared to at least three for the gates. Further economy is present because the memory lends itself to uncomplicated testing procedures. The convenience is in the lack of logic simplification necessary for economic feasibility. It is economical to produce the ROM without minimizing the logic.

As a specific application of this usage of ROM's as logic functions, the technique of microprogramming has been used in the IBM

---

[24] F. Kvamme, Electronics, Vol. 43, No. 5, pp. 88-95, January 5, 1970.

360 series and in the RCA Spectra 70 series. In these machines the control element is not the hard-wired gates of the standard or 'fixed control' computer, but rather is a memory in conjunction with very elementary logic. In the fixed control computers, the logic is designed so as to produce the most efficient operation for a specific type of computer application. This is done at the cost of lower efficiency for other types of applications. In the microprogramable machine the control element has a memory element, either read-write or ROM, which translates the instruction words into elementary commands. To maintain high efficiency, the translator is changed when the application is changed. Control memories are sometimes referred to as 'firm ware'.[25]

The concept of microprogramming has been applied to the minicomputer. The Hewlett Packard 9800 Series Programable Calculator uses a ROM to translate conversational instructions into efficient computer language. The HP 9800 Series also utilizes ROM's to supply its users with specialized programs such as Calculator-Aided Design programs in such areas as network analysis, filter synthesis, and microwave design to name but a few. These ROM's are supplied as interchangable plug-in units.

A new area for the application of ROM's is the 'Communications Terminal'. These devices, such as the Techtran 4100A, presently perform some editing and data compression functions before transmitting

---

[25] W. Roberts, Computer Design, Vol. 8, No. 11, p. 147, November 1969.

their input to the remote computer. ROM's could be used to extend this concept by compiling the conversational language into a language more efficient for transmission.

Another technique used to increase the efficiency of a memory is called 'squaring-up'. The challenge is to use a low-speed less-expensive large memory to feed a high-speed more-expensive control memory. This technique uses long words in the slow memory. The long word, shifted as a unit into the control memory, is broken into several control words. This effectively increases the speed of the interchange by a ratio equal to the number of control words derived from one storage word. A very similar technique is that of page addressing. In this latter technique the computer addresses the large blocks slowly. But once the block, or page, is found, the information in it is accessed at high speed. A third technique is the use of a serially referenced memory. In this variety the blocks are referenced randomly, but the information in each block is accessed serially. The serially referenced memory is sometimes used in conjunction with a random access memory. The data is first read into the RAM. It is then randomly accessible to the CPU.

Proposed System

In examining the literature on optical memories, it was observed that the Flying Spot Scanner and the system designed by ICT used CRT's, photographic film, and projection lenses. It was also noted that BTL's and IBM's random access optical memories used lasers, holograms, and Bragg cells. The system designed herein is

arrived at by combining the best factors of the two above types of optical memories. From the former, the CRT with its high deflection speed is utilized while the photographic bit-by-bit technique with its susceptibility to dust and the lenses with their alignment problems are not. From the latter, the hologram with its image projecting property and its distributed information is utilized while the Bragg cells with their thermal instability are not. The laser was used in the preliminary design to write the hologram.

The initial write configuration is shown in Figure 1-8. It should specifically be noted that the upper or 'reference' beam is focused to a point behind the film plate. The reason for this will be apparent from Chapter III. The circular area on the film plate that is irradiated is referred to as a 'page'. It is assumed that several pages will be arranged on a single film plate. The lens directly ahead of the data mask, sometimes referred to as the Fourier lens, is focused to a point on the film plane in the center of the page to be written. A second page is written by shifting the Fourier lens, data mask, and film module so that the reference beam irradiates another area of the film plate. The mirror and lens system of the data or 'object' beam are readjusted so as to irradiate the newly defined page.

The read configuration is shown in Figure 1-9. The distance from the CRT face to the film is equal to the distance between the film and the focus of the reference beam in the write configuration. The position of the spot of light on the CRT is electronically ad-

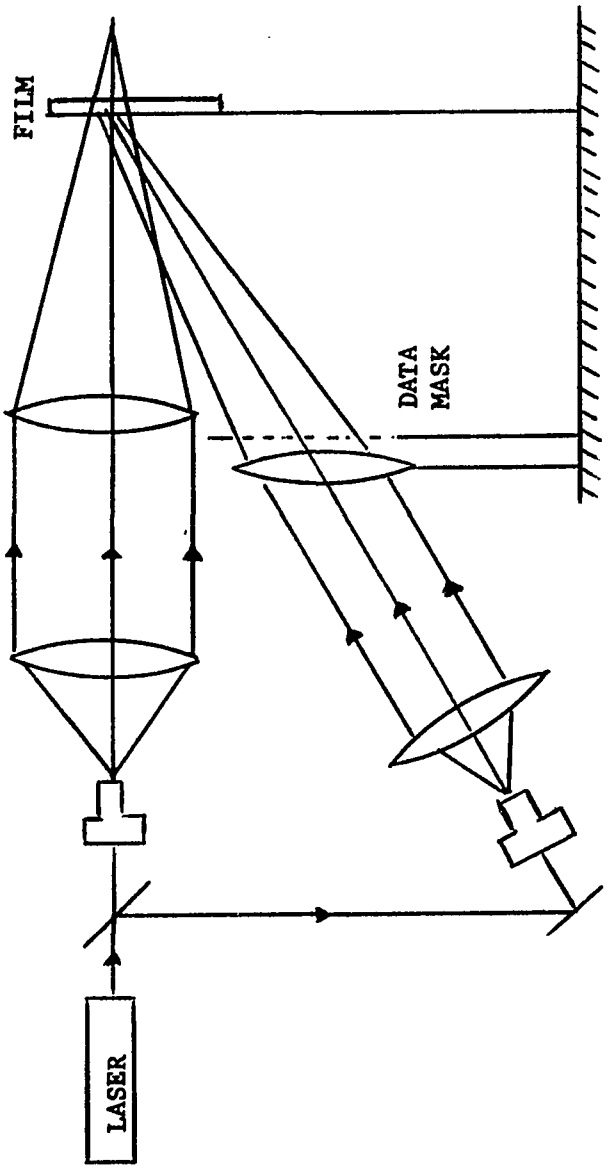

WRITE CONFIGURATION

FIGURE 1 - 8

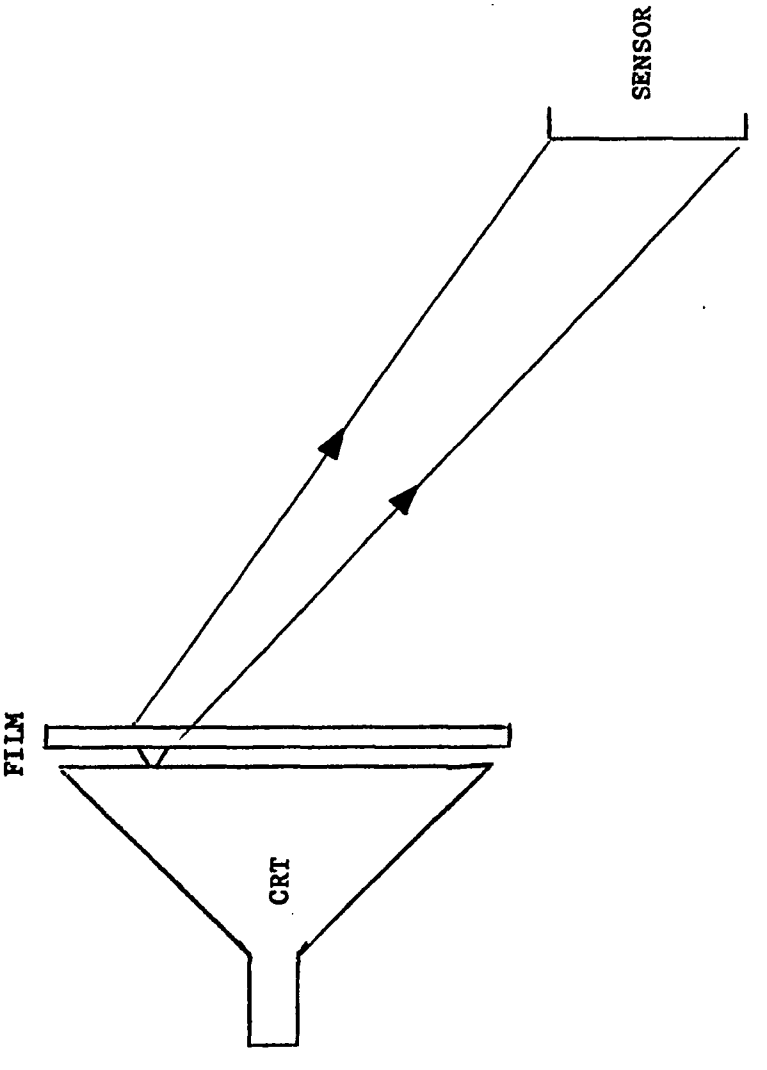

READ CONFIGURATION

FIGURE 1 - 9

justed by means of the deflection plates so that it is centered in front of the page to be read. The hologram's diffraction phenomenon causes a real image to be focused on the sensor plane. The sensor plane is an array of photo-detectors arranged on a one-to-one correspondence with the hole positions of the data mask.

In Chapter III it will be shown that a synthetic write system is more advantageous than the physical system of Figure 1-8. The synthetic system is diagrammed in Figure 1-10. The computer generated hologram is 'painted' on the CRT face and is recorded by an oscilloscope camera. This synthetic hologram is read in exactly the same manner as the previously described physically produced hologram, assuming it has been properly scaled.

SYNTHETIC MODEL

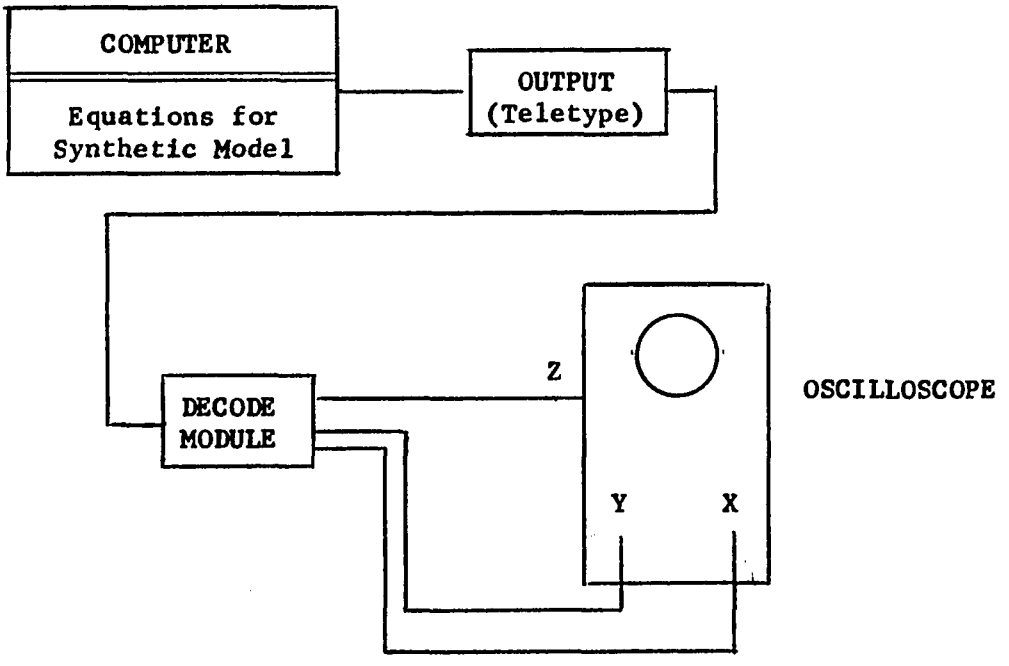

SYNTHETIC WRITE SYSTEM

FIGURE 1 - 10

CHAPTER II

REVIEW OF OPTICAL THEORY

Review of Fundamental Holographic Theory

In 1948 Dennis Gabor envisioned the possibility of improving the performance of electron microscopes by employing the two step lensless process which he called holography. As is well known, the first step of the process entails the recording of the interference pattern between the radiation from the object of interest and that from a background or 'reference' source. In the second step, the recorded interference pattern, or hologram, is illuminated by a 'reconstructing' light. If the reconstructing wave has certain relationships to the reference wave, the diffracted wavefront so generated at the hologram plane contains the information carried by the original object wave and can, therefore, be used to create either a virtual image or a real image of the object.

Synoptically, one can write

$$U(\text{hologram}) = \text{Object} + \text{Background}$$

where U is the complex amplitude of the wave incident on the holographic film, 'Object' is that portion of U that originated at the object, and 'Background' is the remainder of U and serves as a reference signal. Using the symbol * to denote the complex conjugate, the intensity at the hologram plane is

$$I_{holo} = U\,U^* = (O + B)\,(O + B)^*$$
$$= O\,O^* + O\,B^* + O^*B$$

If the holographic film that was exposed to I_{holo} is 'properly' pro-

cessed, the resultant transparency will have a particular amplitude transmittance, T, where

$$T = \sigma(0\ 0^* + B\ B^* + 0\ B^* + 0^* B)$$

in which σ is a function of the film and the development process.

If the reconstruction signal duplicates the original "Background', then the output of the hologram is

$$U(out) = T\ B = \sigma\left[(|0|^2 + |B|^2)\ B + |B|^2\ 0 + |B|^2\ e^{i2b}\ 0^*\right]$$

The first two terms combine in recreating the 'Background' wave. This wave is, however, distorted by the presence of the $|0|^2$ term. The third term recreates the original 'Object' wave, but at $|B|^2$ times its original amplitude. The fourth term creates a conjugate to the recreated 'Object' wave, but it is distorted by the presence of the 'Background' wave's phase, b.

If the reconstruction signal is the conjugate of the original 'Background', then the output of the hologram is

$$U(out) = \sigma\left[(|0|^2 + |B|^2)\ B^* + |B|^2\ e^{i2b}\ 0 + |B|^2\ 0^*\right]$$

Using the same approach as before, the fourth term is now the one of interest. This term creates an undistorted conjugate, or 'real' image of the original 'Object'.

From this qualitative description of holography, it can be seen that the principles of electro-magnetic field theory are integrally involved. A rigorous formulation of holography would require the study of electric and magnetic field vectors coupled through Max-

well's equations. However, it has been shown experimentally[26] that the coupled-vector theory can be reduced to a scalar theory yielding accurate results if 1) the diffracting aperture is large compared to a wavelength of the radiation and 2) the diffracted fields are not observed too close to the aperture.[27,28] This scalar theory is separately applied to the individual polarization components.

For the general polychromatic case,

$$v(p,t) = \int_0^\infty U(P,\nu) \cos 2\pi\nu t \; d\nu$$

where $v(P,t)$ is a function that can represent the physical signal, $U(P,\nu)$ is the amplitude density, and P is the position. Rather than work with the above form of the relationship with its tiresome trignometric identities, it is advantageous to consider the complex analytic signal, $V(P,t)$ where

$$V(P,t) \triangleq V^{(r)}(P,t) + iV^{(i)}(P,t)$$

in which

$$V^{(r)}(P,t) = v(P,t)$$

and $V^{(i)}(P,t)$ is the Hilbert Transform of $V^{(r)}(P,t)$. In integral form

$$V(P,t) = 2 \int_0^\infty U(P,\nu) \, e^{-i2\pi\nu t} \, d\nu$$

---

26 S. Silver, "Microwave Aperture Antennas and Diffraction Theory", JOSA, Vol. 52, p. 131, 1962.

27 J. W. Goodman, Introduction to Fourier Optics, McGraw Hill, Inc., New York, 1968, p. 32.

28 M. Born and E. Wolf, Principles of Optics, Pergamon Press, Long Island City, N. Y., 1965, p. 387.

Now that the relationship between the actual polychromatic signal and its frequency components has been established, if one makes the stipulation that only linear, time-invariant systems be considered, then considerable simplication can be obtained by considering the usual monochromatic case. Thus

$$V(P,t) = U(P,\nu)\, e^{-i2\pi\nu t}$$

Note that in this formulation $U(P,\nu)$ is no longer a density, but rather an amplitude.

Having established the notation, consider now that, if $V(P,t)$ is to be a wave, it must satisfy the scalar wave equation

$$\nabla^2 V - \frac{1}{c^2}\,\frac{d^2V}{dt^2} = 0$$

which for monochromatic radiation reduces to the time-independent Helmholtz equation

$$\nabla^2 U + \frac{4\pi^2\nu^2}{c^2}\, U = 0$$

or more familiarly

$$(\nabla^2 + k^2)\, U = 0$$

From a knowledge of the value of U at a point P_1, its value at a second point, P_0, can be obtained by means of Green's Theorem,[29] i.e.,

$$\iiint (G\nabla^2 U - U\nabla^2 G)\, d\,\text{vol} = \oiint_S (G\,\frac{\partial U}{\partial n} - U\,\frac{\partial G}{\partial n})\, ds$$

---

[29] G. Arfken, Mathematical Methods for Physicists, Academic Press, New York, 1968, pp. 598-611.

where S is the closed surface surrounding the volume, vol, and where G and U are any complex valued functions of P. If G and U satisfy the Helmholtz equation and their first and second derivatives are continuous, then

$$\oiint_S \left(G \frac{\partial U}{\partial n} - U \frac{\partial G}{\partial n}\right) ds = 0$$

The function G(P) is known as a Green's Function. By judiciously choosing the function for G(P), one can use the above equation to find $U(P_0)$ if $U(P_1)$ is available.

In the Kirchhoff formulation, the 'free space' Green's function is used[30]; i.e.,

$$G(P_1) = \frac{e^{ikr_{01}}}{r_{01}}$$

where r_{01} is the distance from P_0 to an arbitrary point, P_1, as shown in Figure 2-1. Because of the constraint on continuity, the volume under consideration must now exclude the point P_0. The surface S is considered as the sum of S' and S". Allowing the sphere S" around P_0 to shrink to the point P_0, integration over S produces

$$U(P_0) = \frac{1}{4\pi} \iint_{S'} \left[U \frac{\partial}{\partial n} \frac{(e^{ikr_{01}})}{r_{01}} - \frac{e^{ikr_{01}}}{r_{01}} \frac{\partial U}{\partial n} \right] da$$

where P_1 is constrained to the surface, S'. This is the Helmholtz-Kirchhoff Integral.

---

30 J. W. Goodman, op. cit., p. 36.

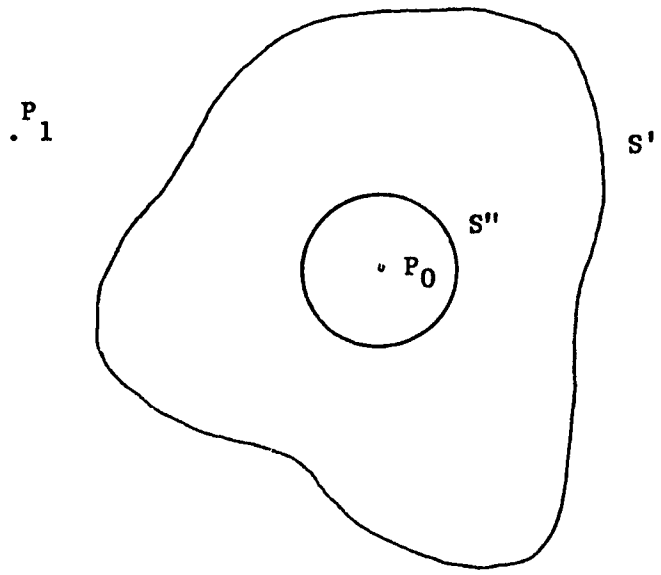

SURFACE OF INTEGRATION

FIGURE 2 - 1

To apply this formula to the transmission of light thru a plane aperture, such as depicted in Figure 2-2, the following boundary conditions can be adopted, as prescribed by the Kirchhoff formulation;

1. over the aperture, A: U and $\partial U/\partial n$ are unaffected by the aperture

2. over the opaque screen, B: $U = 0$, $\partial U/\partial n = 0$

3. over the sphere, C, of infinite radius; U meets the Sommerfeld Radiation Condition; i.e.,

$$\lim_{R\to\infty} R \left[\frac{\partial U}{\partial n} - ikU\right] = 0$$

This leads to the Fresnel-Kirchhoff Diffraction Integral

$$U(P_0) = \frac{1}{4\pi}\iint_A \frac{e^{ikr_{01}}}{r_{01}} \left[\frac{\partial U}{\partial n} - ikU\cos(n,r_{01})\right] ds$$

It should be noted that the assumed boundary values at B are not correct in that if U and $\partial U/\partial n$ vanish together at any point in a plane, they must vanish in the entire plane. The success of this formulation in predicting experimental results was later explained by Kottler when he showed it to be a rigorous solution to a saltus problem of diffraction at a black screen.[31]

Sommerfeld noted the inconsistency of Kirchhoff and proposed a different Green's Function. He chose

---

31 F. Kottler, Ann der Physik, Vol. 70, p. 405, 1923.

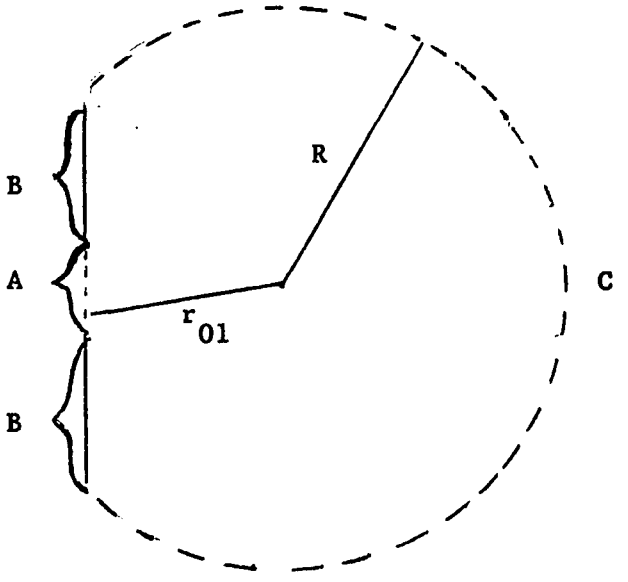

KIRCHHOFF FORMULATION FOR DIFFRACTION
BY A PLANE SCREEN

FIGURE 2 - 2

$$G(P_1) = \frac{e^{ikr_{01}}}{r_{01}} - \frac{e^{ikr'_{01}}}{r'_{01}}$$

where, as shown in Figure 2-3, r'_{01} is the mirror location of r_{01} with respect to the aperture plane. Note the 180° phase shift between the sources. When $r'_{01} \simeq r_{01}$, that is, when P_1 is on the aperture plane, the result is that $G = 0$ and

$$\frac{\partial G}{\partial n} = 2\cos(n,r_{01}) \left[ik - \frac{1}{r_{01}} \right] \frac{e^{ikr_{01}}}{r_{01}}$$

Thus

$$U(P_0) = \frac{1}{4\pi} \iint_{A \neq B} \left[-U \frac{\partial G}{\partial n} \right] ds$$

Now letting $U = 0$ over B, then

$$U(P_0) = \frac{1}{i\lambda} \iint_{A} U(P_1) \cos(n,r_{01}) \frac{e^{ikr_{01}}}{r_{01}} ds$$

This is the Rayleigh-Sommerfeld formulation.

Optical Fourier Transform

Using the symbols defined in Figure 2-4, if one sets $r_{01} = r_0$ for amplitude considerations; i.e., one assumes the paraxial case, then the integral formula becomes

$$U(P_0) = \frac{1}{i\lambda r_0} \iint_{x}\iint_{y} U(P_1)\, e^{ikr_{01}}\, dx\, dy$$

The similarity between the relationship of $U(P_0)$ to $U(P_1)$ and the Fourier Transform should now be apparent. Note that the assumption of $r_{01} \simeq r_0$ for amplitude considerations is far less stringent than the same assumption for the exponent since the exponent is periodic for changes in r_{01} equal to one wavelength of light.

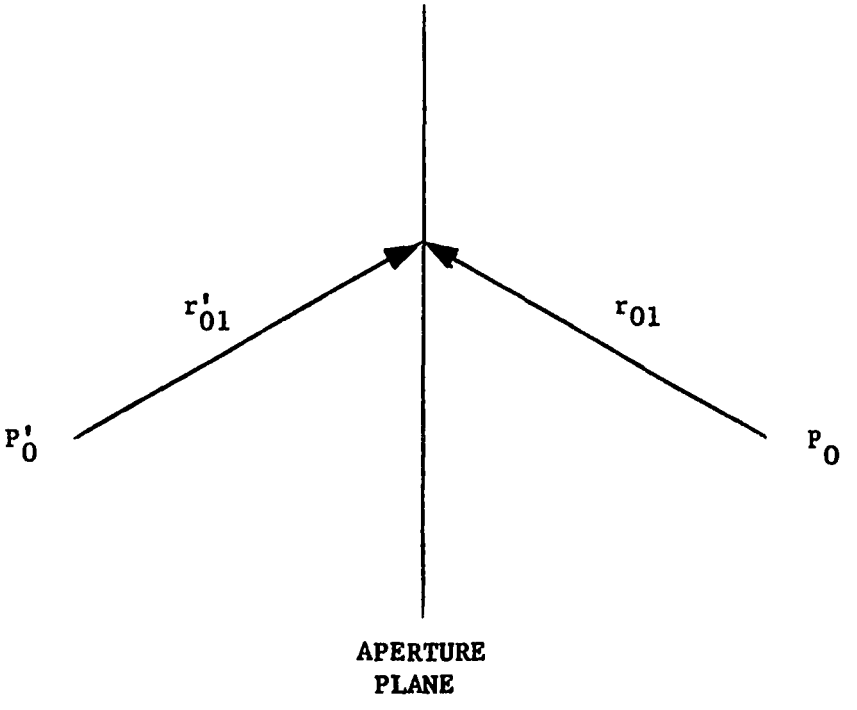

RAYLEIGH-SOMMERFELD FORMULATION

FIGURE 2 - 3

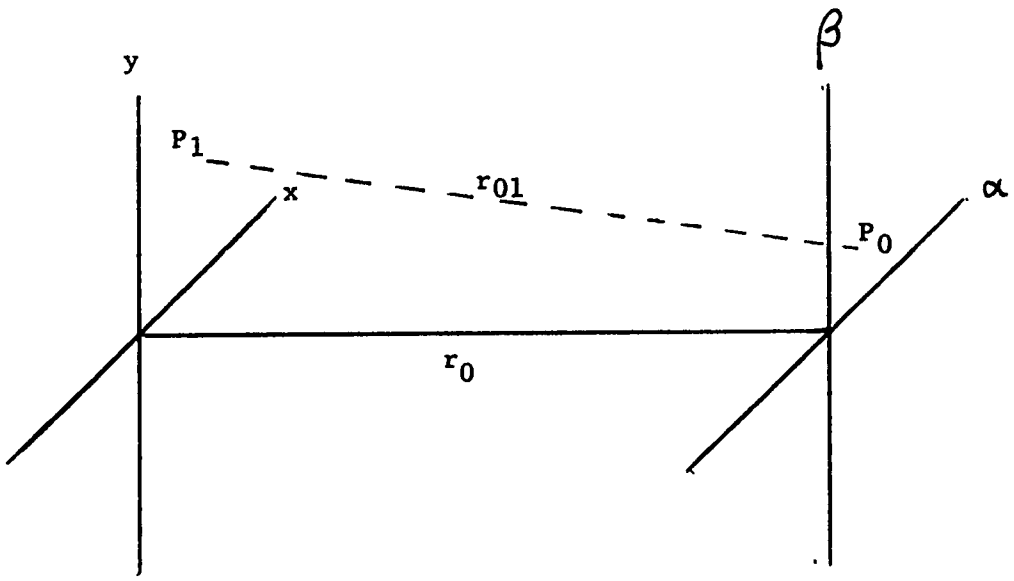

FOURIER TRANSFORM COORDINATES

FIGURE 2 - 4

A further examination of r_{01} is in order. If P_0 is an arbitrary point in the α,β plane, then

$$r_{01} = \left[r_0^2 + (x-\alpha)^2 + (y-\beta)^2\right]^{\frac{1}{2}}$$

If r_0^2 is sufficiently large compared to $(x-\alpha)^2 + (y-\beta)^2$, then the binomial expansion for r_{01} can be approximated by its first two terms; i.e.,

$$r_{01} \approx r_0 + \frac{(x-\alpha)^2 + (y-\beta)^2}{2\,r_0}$$

By sufficiently large is meant that

$$\left| r_{01} - r_0 - \frac{(x-\alpha)^2 + (y-\beta)^2}{2\,r_0} \right| << \lambda$$

Then one can rewrite $U(\alpha, \beta)$ as

$$U(\alpha,\beta) = \frac{e^{ik(r_0 + \frac{\alpha^2+\beta^2}{r_0})}}{i\lambda r_0} \int_x \int_y \left[U(x,y)\, e^{ik\frac{x^2+y^2}{2r_0}}\right] e^{-ik\frac{\alpha x + \beta y}{r_0}}\, dx\, dy$$

Regrouping the terms, this can be written as

$$U(\alpha,\beta) = K(\alpha,\beta)\, \mathcal{F}\left[U'(x,y)\right]$$

where

$$K(\alpha,\beta) = \frac{e^{ik(r_0 + \frac{\alpha^2+\beta^2}{2\,r_0})}}{i\lambda r_0}$$

and

$$U'(x,y) = U(x,y)\, e^{ik\frac{x^2+y^2}{2r_0}}$$

Let

$$U''(\alpha,\beta) = U(\alpha,\beta) \,/\, K(\alpha,\beta)$$

Observe that $U'(\alpha,\beta)$ is the Fourier Transform of $U'(x,y)$ and not of $U(x,y)$. Indeed, for the general case, $U''(\alpha,\beta)$ is the Fresnel Transform of $U(x,y)$, rather than its Fourier Transform. Note, however, that the intensity pattern associated with $U(\alpha,\beta)$ is the intensity pattern of the Fourier Transform of a function whose intensity pattern is that of $U(x,y)$.

For special cases, the Fourier Transform relationship can be obtained. The simplest case is arrived at by choosing x, y, and r_0 such that

$$\frac{x^2 + y^2}{2 r_0 \lambda} \ll 2\pi \qquad \text{i.e., } r_0 \gg \left[x^2 + y^2\right]^{\frac{1}{2}}$$

This produces the result that

$$e^{ik \frac{x^2 + y^2}{2r_0}} \approx 1 \angle 0^\circ \text{ for all x and y}$$

This is the Fraunhofer case.

Another simple case is obtained by premultiplying $U(x,y)$ by a compensating function, $T(x,y)$, such that

$$U(x,y)\, T(x,y) = U(x,y)\, e^{-ik\left(\frac{x^2 + y^2}{2 r_0}\right)}$$

Then

$$U''(\alpha,\beta) = \int_x \int_y U(x,y)\, e^{ik \frac{x^2 + y^2}{2 r_0}}\, e^{ik \frac{x^2 + y^2}{2 r_0}}\, e^{-i\frac{k}{r}(\alpha x + \beta y)}\, dx\, dy$$

Having cancelled the appropriate terms, the Fourier Transform relationship appears. As is well known, a physical device which could

produce the above T(x,y) is a lens of focal length r_0.

Philosophically, one might explain holography as a transform process (recording) and an inverse-transform process (reconstructing). For the special cases that are Fourier Transforms, it is obvious that the image should be recovered since the Fourier Transform possess the quality of duality. For the less familiar case of the Fresnel Transform, one might consider holography as physical confirmation of its possessing duality. This point of view also leads to the interpretation of the focal plane as that plane in which the transform and the inverse-transform relationship possess duality.

Effect of the Processing γ On Holography

The elementary case of a point object and a point reference source is sufficient to afford an insight into the basic recording limitations. Let these sources be the point sources, A_{ref} and A_{obj}, as shown in Figure 2-5. Then,

$$U(\alpha, \beta) = A_{ref} \frac{e^{iku}}{u} + A_{obj} \frac{e^{iks}}{s}$$

Since the silver halides of photographic film, as well as other photosensitive media such as dichromated gelatin and lithium niobate respond, essentially, to the temporally integrated intensity of the radiation rather than to its amplitude, it is necessary to consider the intensity distribution, $I(\alpha, \beta)$ where

$$I(\alpha, \beta) = U(\alpha, \beta)\, U^*(\alpha, \beta)$$

in which the asterisk (*) denotes the complex conjugate. It should be noted, for the sake of rigor, that the assumption is made that

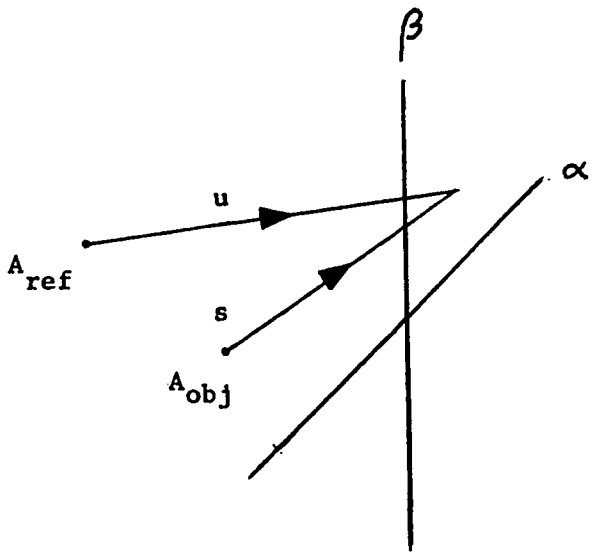

POINT REFERENCE AND OBJECT HOLOGRAM

FIGURE 2 - 5

the exposure time is much longer than the periods of either the reference wave or the object wave, but much shorter than any beat frequency between the reference and object waves.

It is now appropriate to examine a specific recording medium. Since photographic film is the most common, it has been chosen as the material to be examined. In the terminology of photography, the exposure, E, is defined as the intensity, I, integrated over the exposure period, P; i.e., $E = \int IdP$. This exposure, after proper processing, results in a darkening of the film attributable to the precipitation of molecular silver from the exposed silver halide. This darkening is generally expressed in terms of the photographic density, D, where

$$D = \log_{10} (1/\mathcal{T})$$

where $\mathcal{T}$ is the transparency of the film[32] and is defined as the ratio of the transmitted intensity to the incident intensity.[33] The relationship between the exposure and the density is

$$D = \gamma \log_{10} E - D_0$$

in which D_0 is the background density and gamma is a physical constant that depends on the processing and on the type of film used; e.g., Plus-X being a low contrast film has, under standard processing, $\gamma \leq 1$, while High Contrast Copy normally has a $\gamma \geq 2$. These parameters are usually displayed as the slope of the Hurter-Driffield curves for the

---

32 C. E. K. Mees, From Dry Plates to Ektachrom, Ziff-Davis Publishing Company, New York, 1961, p. 21.

33 C. E. K. Mees, The Theory of the Photographic Process, MacMillan Company, New York, 1954, p. 162.

particular film in question. It should be noted that the actual development process; i.e., type of developer solution, time in developer, temperature, etc., determines the developed values of gamma. Combining the above relationships,

$$\log_{10}(I_{in}/I_{out}) = \gamma \log_{10} E - D_0$$

Taking the anti-logarithm, this is rewritten as

$$I_{out}/I_{in} = K I^{-\gamma}$$

where

$$K = 10^{D_0} P^{-\gamma}$$

The function of interest to the holographer is the amplitude of the transmitted wave, not its intensity. Therefore, a new function, the amplitude transmittance, T, is defined such that $T = \sqrt{\tau}$

The amplitude of the transmitted wave is, then, expressed as

$$U_{out} = U_{in} \sqrt{K} \left[U(\alpha, \beta) \; U^*(\alpha, \beta) \right]^{-\gamma/2}$$

$$= U_{in} \sqrt{K} \left[\frac{|A_{ref}|^2}{u^2} + \frac{|A_{obj}|^2}{s^2} + 2 A_{ref} A^*_{obj} \frac{e^{ik(u-s)}}{u\,s} + 2 A^*_{ref} A_{obj} \frac{e^{ik(s-u)}}{u\,s} \right]^{-\gamma/2}$$

For the case of $\gamma = -2$, the solution is straight-forward. U_{in} is judiciously chosen; i.e., from a prior knowledge of the solution, to be

$$U_{in} = A_{recon} \frac{e^{ikv}}{v}$$

This is sketched in Fig. 2-6. Then, the output is

$$U_{out} = \sqrt{K} \left\{ \left[\frac{|A_{ref}|^2}{u^2} + \frac{|A_{obj}|^2}{s^2} \right] A_{recon} \frac{e^{ikv}}{v} \right.$$

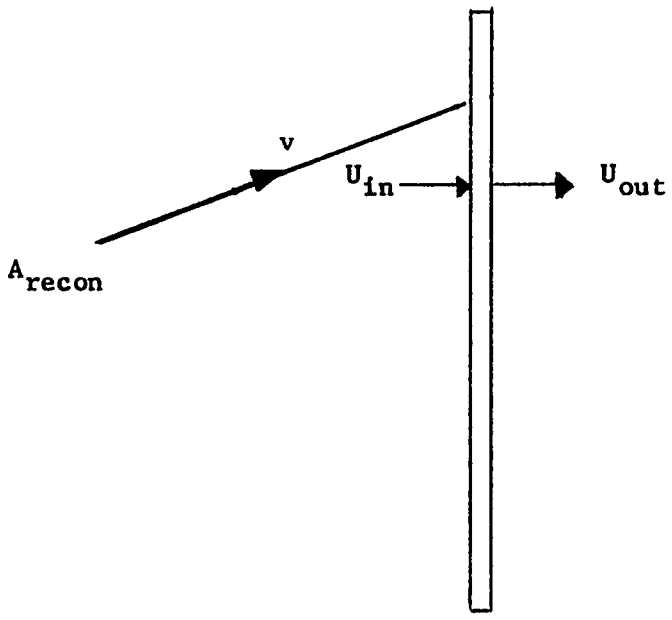

RECONSTRUCTION OF HOLOGRAM

FIGURE 2 - 6

$$\left.\begin{array}{l} + 2\, A_{recon}\, A_{ref}\, A_{obj}^{*}\, \dfrac{e^{ik(v+u-s)}}{v\,u\,s} \\ + 2\, A_{recon}\, A_{ref}^{*}\, A_{obj}\, \dfrac{e^{ik(v-u+s)}}{v\,u\,s} \end{array}\right\}$$

If $v = u$, the last term above becomes

$$U_4(\alpha,\beta) = 2\,\frac{A_{recon}\,A_{ref}\,A_{obj}}{u^2}\,\frac{e^{iks}}{s}$$

$$= C\,A_{obj}\,\frac{e^{iks}}{s}$$

where C is a constant. This result is interpreted to mean that if the developed hologram is irradiated by the original reference source, the original object wave is regenerated. The third term, $U_3(\alpha,\beta)$, generates a second image located at $s' = 2u-s$. This image may be real or virtual, depending upon the algebraic sign of s'. The first two terms, $U_1(\alpha,\beta)$ and $U_2(\alpha,\beta)$, are merely the dimmed reconstruction source.

The question arises as to the effect of $\gamma \neq -2$. The answer is obtained by utilizing the series expansion for an exponential combined with the expansion for the common logarithm; i.e.,

$$a^x = 1 + x \ln a + \frac{(x \ln a)^2}{2} + \cdots$$

$$\ln(1+y) = x - \tfrac{1}{2}x^2 + 1/3\,x^3 - \cdots \quad -1 < x \leq 1$$

If the reference beam is significantly stronger than the object beam, the intensity at the film plane can be described as

$$I(\alpha,\beta) = I_0 + \Delta I(\alpha,\beta)$$

$$= I_0\left(1 + \frac{\Delta I}{I_0}\right)$$

The outcome of the development process is

$$
\begin{aligned}
T &= I_0^{-\gamma/2} \left(1 + \Delta I/I_0\right)^{-\gamma/2} \\
&= I_0^{-\gamma/2} \left[1 - \gamma/2 \ln(1 + \Delta I/I_0 + \gamma^2/8 \ln(1 + \Delta I/I_0) \right. \\
&\quad \left. + \cdots\right] \\
&= I_0^{-\gamma/2} \left\{1 - \gamma/2 \left[\Delta I/I_0 - \tfrac{1}{2} \left(\Delta I/I_0\right)^2 + \cdots\right] \right. \\
&\quad \left. + \gamma^2/8 \left[\Delta I/I_0 - \tfrac{1}{2}(\Delta I/I_0) + \cdots \right.^2 + \cdots\right]\right\}
\end{aligned}
$$

For small values of $\Delta I/I_0$ and moderate values of γ, this can be approximated as

$$
\begin{aligned}
T &= I_0^{-\gamma/2} \left(1 - \gamma/2 \ \Delta I/I_0\right) \\
&= C \left(I_0 - \gamma/2 \ \Delta I(\alpha, \beta)\right)
\end{aligned}
$$

where

$$C = I_0^{1 - \gamma/2}$$

This is interpreted to mean that for the conditions stated, variations in the value of gamma will vary the fringe contrast on the holographic film.

However, gamma is a function of the intensity, I. This means that in general, the relationship of T to ΔI is not linear. To obtain a hologram, I must be constrained to that region of the H-D curves for which gamma is approximately constant.

Another limitation is imposed by the finite resolution capability of the film; i.e., the film's ability to record the separate lines of a grating. From previous expressions, one can observe that T varies as a function of α and β. If T is made to vary at too high a rate, the adjacent dark and clear lines will not be resolved, but,

rather, blended into one gray line. Stated differently, film is a low pass spatial filter. In Chapter III, attention will be given to the effect of this resolution limit on the allowable size of the hologram and on the configuration of the memory.

CHAPTER III

SYSTEM ANALYSIS

System Description

A schematic drawing of the write process is shown in Figure 3-1. The lens located behind the data mask is chosen and positioned so that the light of the illuminating beam is focused at the film plane. The mask, whose function is that of an encoder, may be as simple as a punched card or as sophisticated as an array of nematic liquid crystals. As depicted, the light,diffracted by the 'holes' of the data mask, illuminates only a small portion of the film plate; thereby allowing for an array of pages to be written on a single 4-by-5 inch plate of film. A converging reference beam illuminates the same area of the film plate. To write on a different portion of the film; i.e., to write another page, the angle ϕ , as shown in Figure 3-2, at which the lens is illuminated is varied and the reference beam shifted accordingly.

The reconstruction process is depicted in Figure 3-3. The electron beam of the cathode ray tube (CRT) is adjusted so that it activates the phosphor directly behind the center of the page to be read. The diverging light from the phosphor irradiates an area of the hologram that includes the page to be read. Only the output radiation from the desired page impinges on the sensor bank; the outputs from adjacent pages are made to fall outside the limits of the sensor bank. The technique that causes this discrimination will be detailed later in this Chapter.

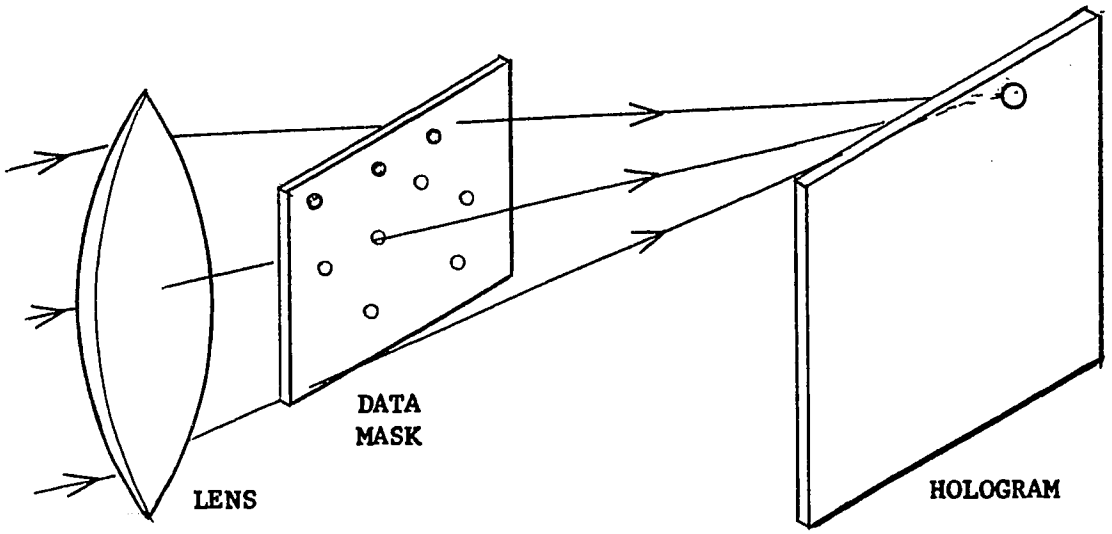

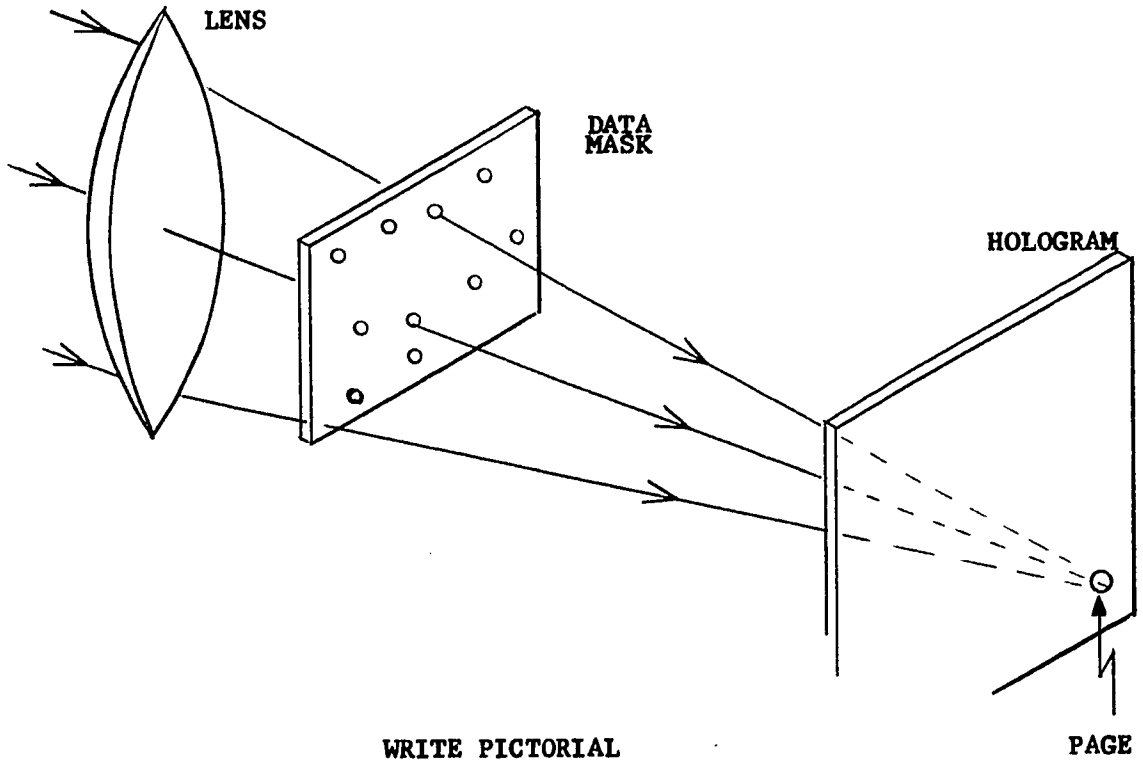

WRITE PICTORIAL

FIGURE 3 - 1

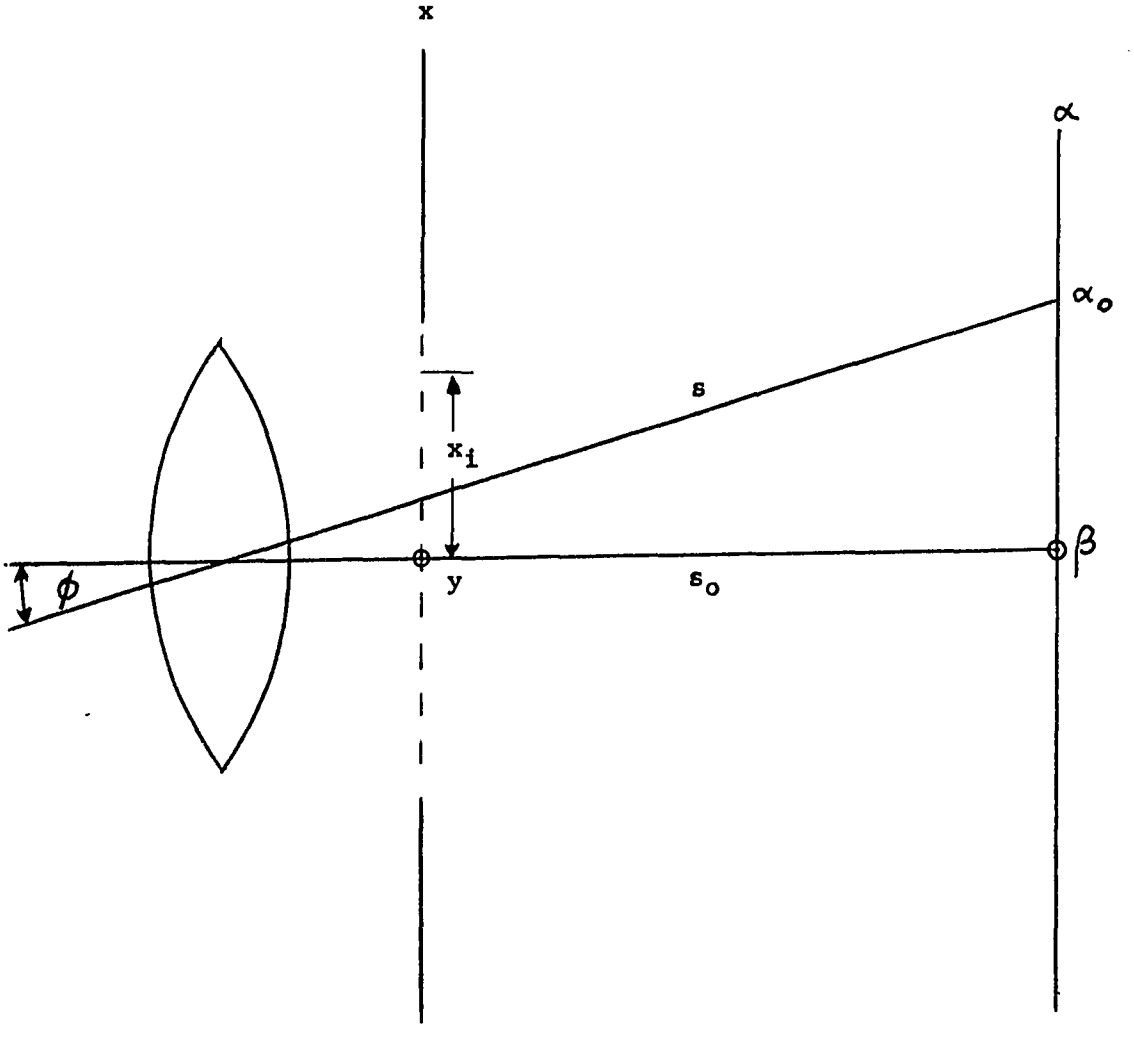

OBJECT BEAM SCHEMATIC

FIGURE 3 - 2

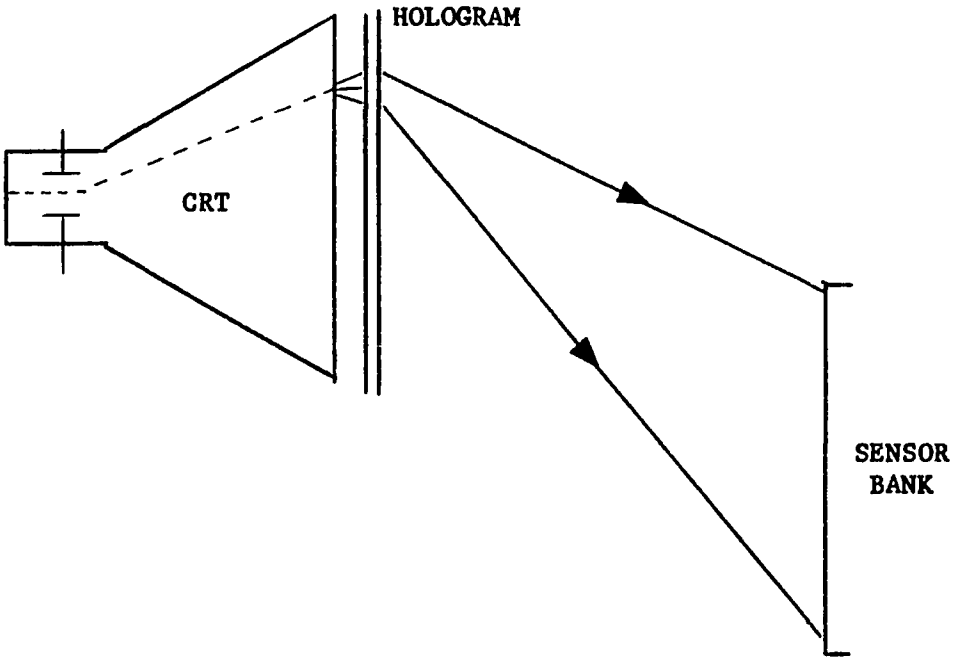

READ PICTORIAL

FIGURE 3 - 3

Derivation of Write Equations

The analytic expression for the radiation incident on the film is found with the aid of Figure 3-4. The complex amplitude of the signal irradiating the data mask is expressed as

$$U(x,y) = A_{obj} \frac{e^{-ikr}}{r}$$

where

$$r = \left[r_0^2 + (x - \alpha_0)^2 + (y - \beta_0)^2 \right]^{\frac{1}{2}}$$

and A_{obj} is a constant and is chosen as the zero phase reference. Physically, the effect of the minus sign in the exponent is, quite evidently, to create a converging wave. Recall that the time factor is $e^{-i\omega t}$. Thus, for a constant phase front, as time increases, the radius, r, must be decreasing; i.e., a sphere collapsing in on itself to the limit of a point.

The complex amplitude of the signal from the data mask arriving at the hologram plane is given by

$$U(\alpha, \beta) = \frac{-i\, A_{obj}}{\lambda} \iint_{x\,y} T(x,y) \frac{e^{ik(-r+s)}}{r\, s}\, dx\, dy$$

where s is defined in Figure 3-5 and T(x,y) is the transmission function of the data mask. This transmission function can be expressed as

$T(x,y) \triangleq 1$ over circles of radius rho zero (ρ_0) centered at the points x_i, y_j that correspond to one bits

$\triangleq 0$ elsewhere

The variable s can be expressed as

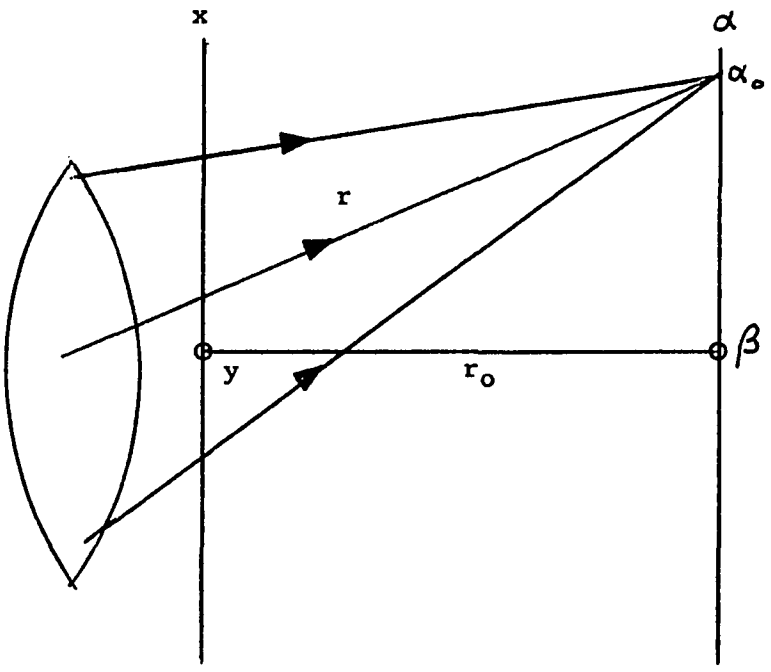

DATA MASK ILLUMINATING BEAM

FIGURE 3 - 4

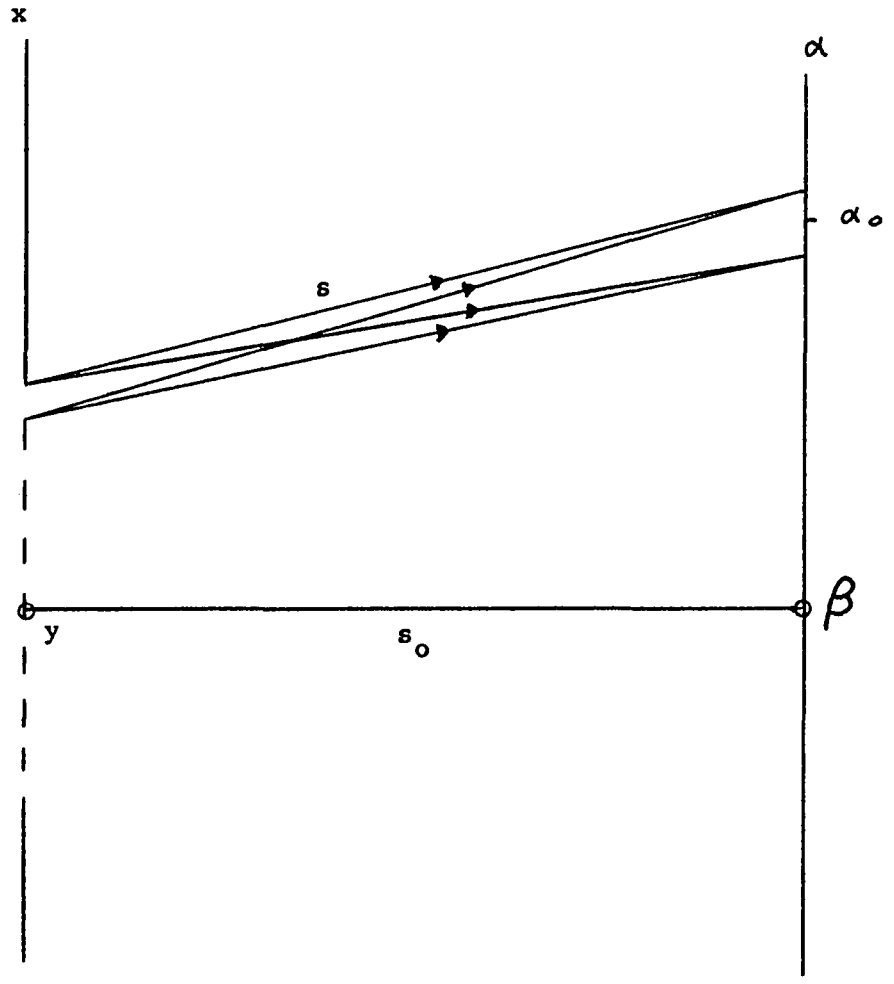

RADIATION FROM ILLUMINATED
DATA MASK

FIGURE 3 - 5

$$s = \left[s_0^2 + (x-\alpha)^2 + (y-\beta)^2 \right]^{\frac{1}{2}}$$

Note that while 'r' depicts the undiffracted illuminating beam, 's' depicts the diffracted radiation from the illuminated data mask. Also note that the r_0 plane is not necessarily coincident with the s_0 plane. Assuming that the sagittal approximation is valid for both r and s, then

$$r = r_0 + \frac{(x-\alpha_0)^2 + (y-\beta_0)^2}{2\, r_0}$$

and

$$s = s_0 + \frac{(x-\alpha)^2 + (y-\beta)^2}{2\, s_0}$$

If r_0 is arbitrarily set equal to s_0, then the amplitude of the radiation from the mask impinging on the film is given as

$$U_{obj}(\alpha,\beta) = \frac{-iA_{obj}}{\lambda} \iint_{x\,y} \frac{T(x,y)}{s_0^2}\, e^{ik\left[-s_0 - \frac{(x-\alpha_0)^2+(y-\beta_0)^2}{2\, s_0}\right]}\, e^{ik\left[s_0 + \frac{(x-\alpha)^2+(y-\beta)^2}{2\, s_0}\right]}\, dx\, dy$$

Extracting the terms not functions of x or y from the integral,

$$U_{obj}(\alpha,\beta) = \frac{-iA_{obj}}{\lambda\, s_0^2}\, e^{ik\frac{\alpha^2-\alpha_0^2+\beta^2-\beta_0^2}{2\, s_0}} \iint_{x\,y} T(x,y)\, e^{-ik/s_0\left[(\alpha-\alpha_0)x + (\beta-\beta_0)y\right]}\, dx\, dy$$

From Chapter II, it should be apparent that this relationship can correctly be expressed as

$$U_{obj}(\alpha,\beta) = K\, \mathcal{F}\left[T(x,y)\right]$$

where $\mathcal{F}$ denotes the Fourier Transform and the phase of K is a function of α and β.

To evaluate this transform, the integral portion of $U_{obj}(\alpha, \beta)$ is rewritten, with the aid of Figure 3-6, as

$$\int_x \int_y T(x,y)\, e^{\frac{-ik}{s_0}\left[(\alpha-\alpha_0)x + (\beta-\beta_0)y\right]} dx\, dy$$

$$= \sum_i \sum_j \int_\rho \int_\theta e^{\frac{-ik}{s_0}\left[(\alpha-\alpha_0)(x_i+\rho\cos\theta) + (\beta-\beta_0)(y_j+\rho\sin\theta)\right]} \rho\, d\rho\, d\theta$$

in which $x = x_i + \rho \cos\theta$

and $y = y_j + \rho \sin\theta$

If the substitution indicated in Figure 3-7 is carried out; i.e.

$$\alpha' = \alpha - \alpha_0 = w \cos\psi$$
$$\beta' = \beta - \beta_0 = w \sin\psi$$

then the transform is rewritten as

$$\sum_i \sum_j e^{\frac{-ik}{s_0}(\alpha' x_i + \beta' y_j)} \int_\rho \int_\theta e^{\frac{-ik\rho w}{s_0}(\cos\psi\cos\theta + \sin\psi\sin\theta)} \rho\, d\rho\, d\theta$$

where the limits of integration are

$$0 \leq \rho \leq \rho_0$$
$$0 \leq \theta < 2\pi$$

Then, making the following mathematical observations,[34]

$$\cos\theta\cos\psi + \sin\theta\sin\psi = \cos(\theta-\psi)$$

and

---

[34] M. Born and E. Wolf, Principle of Optics, Pergamon Press, Long Island City, 1965, p. 395.

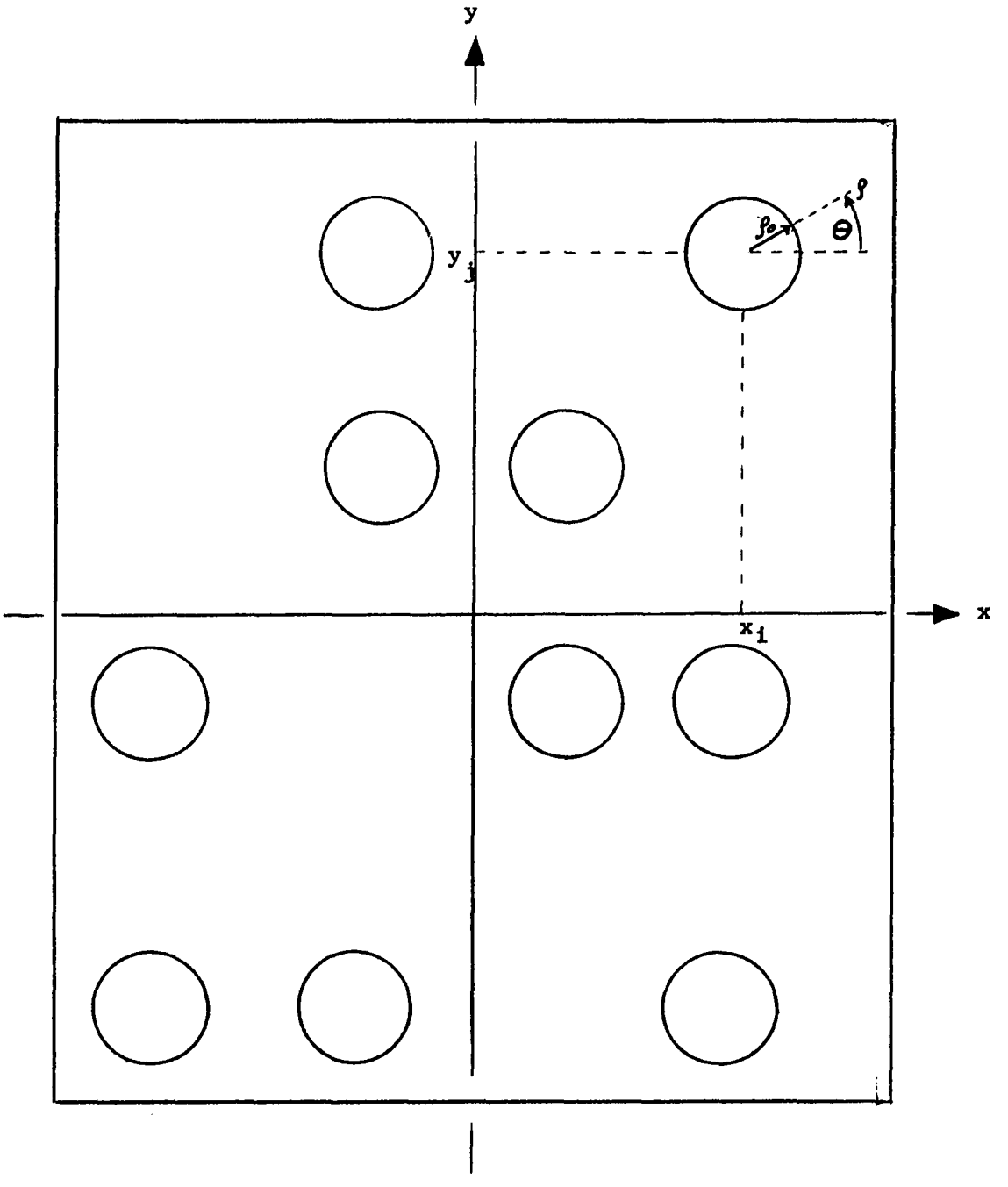

DATA MASK POLAR COORDINATES

FIGURE 3 - 6

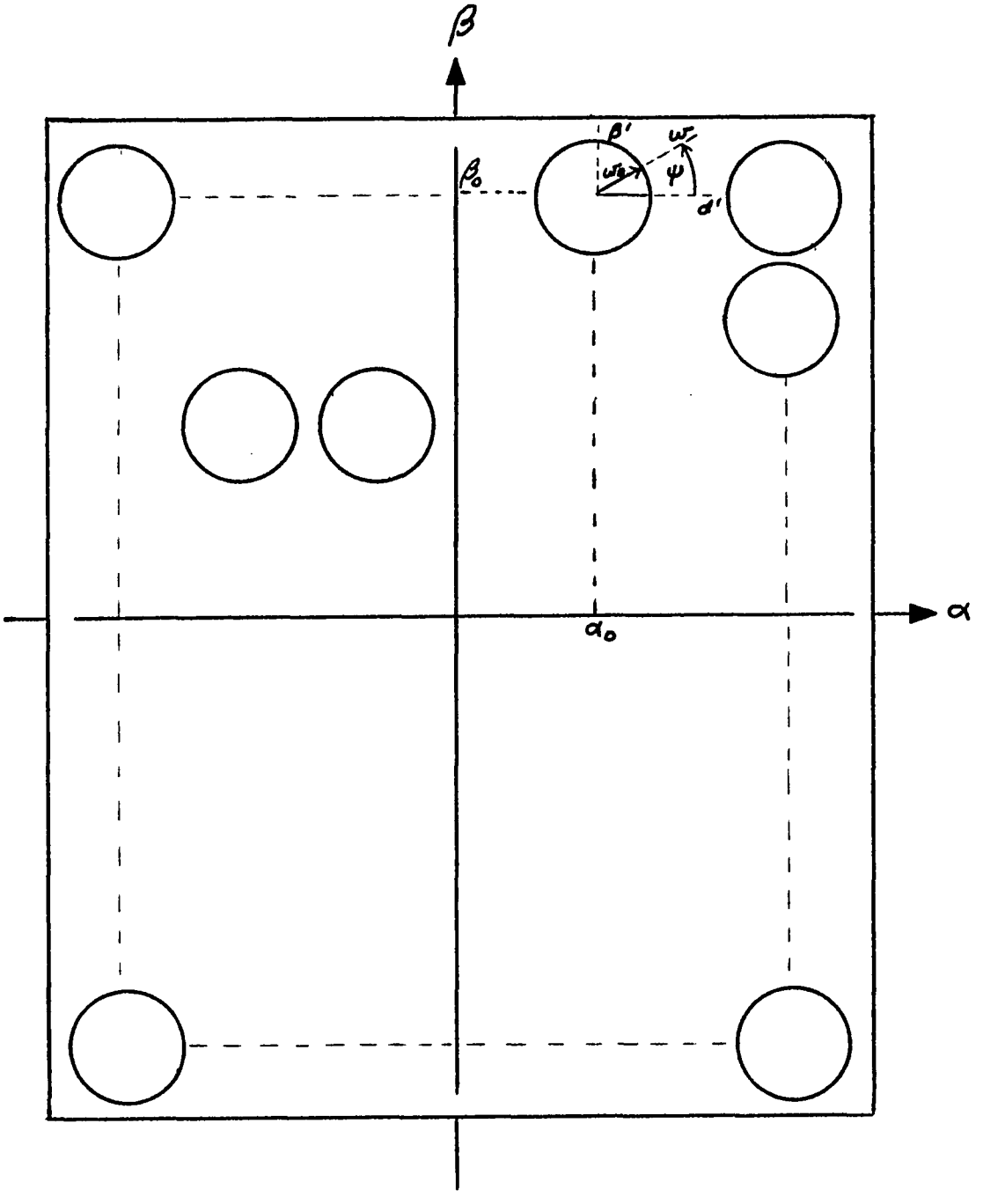

HOLOGRAM POLAR COORDINATES

FIGURE 3 - 7

$$\int_0^{2\pi} e^{\frac{ik\rho w}{s_0}\cos(\theta - \psi)}\, d\theta = 2\pi J_0\left(\frac{k\rho w}{s_0}\right)$$

the expression for the transform can be rewritten as

$$\sum_i \sum_j e^{\frac{-ik}{s_0}\left[(\alpha-\alpha_0)x_i + (\beta-\beta_0)y_j\right]} \int_0^{\rho_0} 2\pi J_0\left(\frac{k\rho w}{s_0}\right) \rho\, d\rho$$

Making use of the identity[35]

$$\int_0^x x' J_0(x')\, dx' = x J_1(x)$$

the term of interest can be expressed as

$$U_{obj}(\alpha,\beta) = \frac{-iA_{obj}\rho_0}{w s_0} e^{\frac{ik}{2s_0}(\alpha^2 - \alpha_0^2 + \beta^2 - \beta_0^2)} J_1\left(\frac{k\rho_0 w}{s_0}\right)$$

$$\sum_i \sum_j e^{\frac{-ik}{s_0}\left[(\alpha-\alpha_0)x_i + (\beta-\beta_0)y_j\right]}$$

To obtain a projected real image of the data mask when a diverging beam emanating from the face of the CRT is used as the reconstruction beam, it is necessary to select a converging reference beam. This beam will be focused thru the film to a point behind the area (page) of the film being used; i.e., on the perpendicular from α_0, β_0. This is shown in Figure 3-8. Let the beam be analytically expressed as

---

35 E. Jahnke and F. Emde, Tables of Functions, Dover Publications, New York, 1945, p. 145.

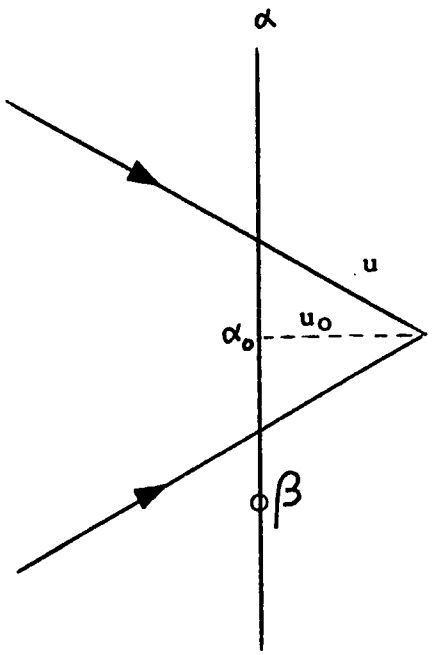

REFERENCE BEAM COORDINATES

FIGURE 3 - 8

$$U_{ref}(\alpha,\beta) = A_{ref}\frac{e^{-iku}}{u}$$

where

$$u = \left[u_0^2 + (\alpha-\alpha_0)^2 + (\beta-\beta_0)^2\right]^{\frac{1}{2}}$$

The irradiance at the film plane during construction is shown as I below

$$I(\alpha,\beta) = |U_{ref}(\alpha,\beta)|^2 + |U_{obj}(\alpha,\beta)|^2$$

$$+ U^*_{ref}(\alpha,\beta)\, U_{obj}(\alpha,\beta) + U_{ref}(\alpha,\beta)\, U^*_{obj}(\alpha,\beta)$$

The real image is constructed from the transmission term that corresponds to the fourth term of the above expression. Making the usual optimistic assumption of an ideal recording medium and ideal processing, the transmittance function of interest is

$$T_4(\alpha,\beta) = \sigma\frac{A_{ref}}{u_0}e^{-iku}\; i\frac{A_{obj}}{w\, s_0}\; J_1\left(\frac{k\rho_0 w}{s_0}\right)\; \rho_o$$

$$e^{\frac{-ik}{2s_0}(\alpha^2-\alpha_0^2+\beta^2-\beta_0^2)}\sum_i\sum_j e^{\frac{ik}{s_0}\left[(\alpha-\alpha_0)x_i+(\beta-\beta_0)y_j\right]}$$

Derivation of Reed Equations

The analytic expression for the reconstruction radiation is found with the aid of Figure 3-9. The coordinates mu (μ) and nu (ν) are used to denote the non-point, or extended, nature of the reconstruction beam source, i.e. the excited phosphor spot on the CRT.

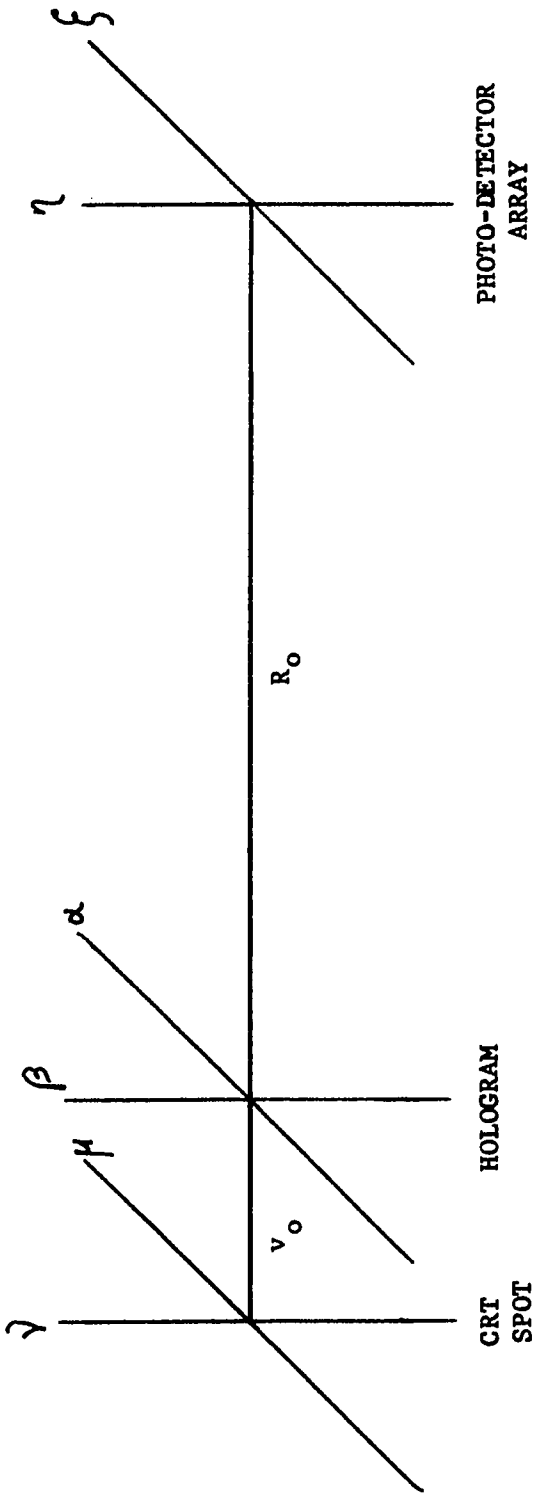

READ-OUT GEOMETRY

FIGURE 3 - 9

Also, before expressing this radiation in analytic form, it is necessary to closely examine the frequency (temporal) of the radiation from the CRT. Normally, it is several hundred Angstroms in bandwidth for common fast decay phosphors. As such, it would not be correct to use the equations developed in Chapter II since they were derived under the assumption of monochromatic radiation. To overcome this, the phosphor will be modeled as a collection of spatially distributed monochromatic sources. The model of the phosphor will set the frequency of a segment of the spot at one value for a time interval Δt, and then change to another frequency for the next interval.[36] In general, it is not permissible to assume that all the segments are simultaneously radiating at the same frequency or even that a deterministic relationship exists amongst the segments. Furthermore, only a probablistic relationship exists between the frequency of a particular segment at time t, and its frequency at time $t \neq \Delta t$; i.e., it is not valid to assume that the phosphor's radiation is coherent.

Since holography is normally thought of as employing coherent light, it is appropriate to outline the role that coherence plays in holography and to explore the ramifications arising from the use of the phosphor's radiation for reading the hologram. Recall that the interference pattern of two waves is given by

---

[36] G. R. Fowles, Introduction to Modern Optics, Holt, Rinehart, and Winston, Inc., New York, 1968, p. 72.

$$I = I_1 + I_2 + 2\sqrt{I_1 I_2}\ \mathrm{Re}\left[\gamma_{12}\right]$$

where γ_{12} is the complex coefficient of coherence.[37] The effect of $\gamma_{12} = 1$ and $\gamma_{12} = 0$ are displayed in Figure 3-10, showing the distributions of I from the previous formula for sinusoidal incident waves. From this figure, it can be seen that a high value of coherence is necessary if the interference is to create the diffraction lines on the holographic film. More rigorous proofs of this are available in the literature.[38]

The coherence requirements of the readout process are quite different. In terms of the problem at hand, let $f(\mu, \nu, \xi, \eta, t)$ represent the complex amplitude of the radiation at the image point ξ, η emanating from the source point μ, ν during the time interval Δt beginning at time t. The total value of the amplitude at this ξ, η point can be expressed as

$$A(\xi, \eta, t) = \int_{\mu}\int_{\nu} f(\mu, \nu, \xi, \eta, t)\ d\mu\ d\nu$$

Since the phosphor spot will be modeled as a finite collection of segments, this total value can be expressed as

$$A(\xi, \eta, t) = \sum_{m}\sum_{n} f(m, n, \xi, \eta, t)$$

If the m x n source segments are completely coherent, then the intensity in the image plane is given by

---

37 J. DeVelis and G. Reynolds, Theory and Application of Holography, Addison-Wesley Publishing Co., Reading, Mass., 1967, p. 21.

38 Ibid, pp. 111-128.

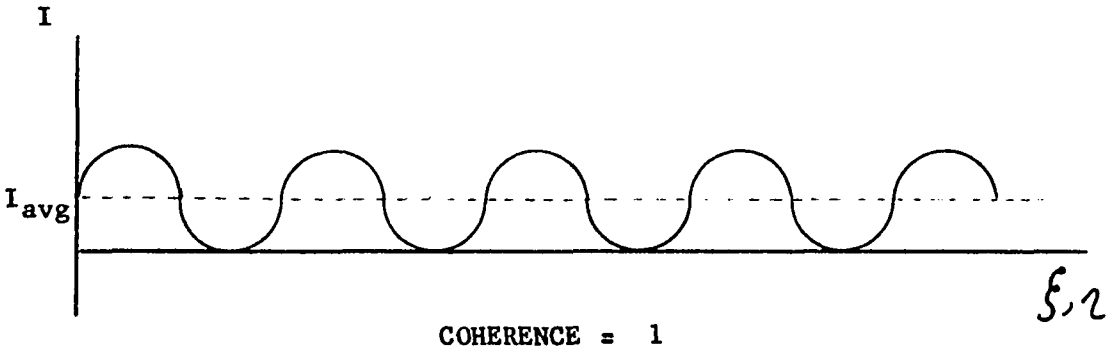

COHERENCE = 1

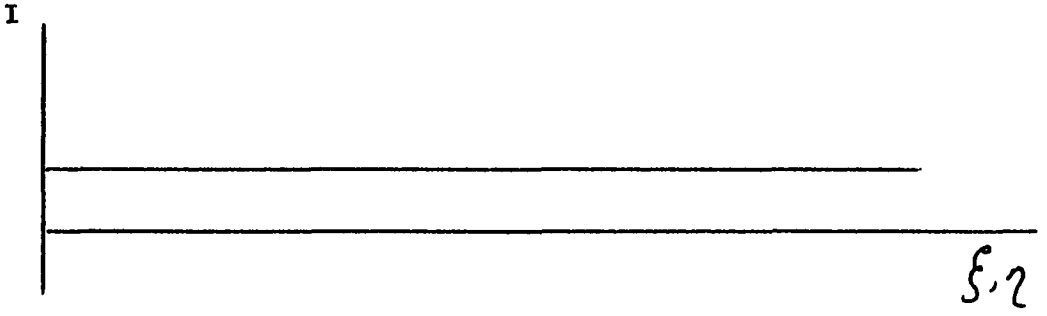

COHERENCE = 0

EFFECT OF COHERENCE

FIGURE 3 - 10

$$I_{COH}(\xi, \eta, t) = A(\xi, \eta, t)\, A^*(\xi, \eta, t)$$

If the m x n segments are independent, i.e. $\gamma_{12} = 0$, then the intensity in the image plane is given by[39]

$$I_{INCOH}(\xi, \eta, t) = \sum_m \sum_n f(m,n,\xi,\eta,t)\, f^*(m,n,\xi,\eta,t)$$

From the Law of Conservation of Energy, it is apparent that

$$\int_{\xi}\int_{\eta} I_{COH}(\xi, \eta, t)\, d\xi\, d\eta = \int_{\xi}\int_{\eta} I_{INCOH}(\xi, \eta, t)\, d\xi\, d\eta$$

if the source of the radiation is a hemispherical radiator and the limits on the integrations are plus and minus infinity. If the equality, on a bit-by-bit basis, is valid for the finite limits of the corresponding photodetectors, then the lack of coherence will not affect the data output. The specific constraints on the system required to achieve this condition will be found later in this chapter.

The radiation at the point α, β on the hologram from a segment μ, ν of the phosphor spot can be expressed, using Figure 3-9, as

$$\Delta U_{recon}(\alpha, \beta, \mu, \nu, t) = A_{recon} \frac{e^{ik_2 v}}{v}$$

where

$$v = \left\{ v_0^2 + \left[\mu - (\alpha - \alpha_{RC})\right]^2 + \left[\nu - (\beta - \beta_{RC})\right]^2 \right\}^{\frac{1}{2}}$$

---

39 Goodman, op. cit., p. 106.

It is understood that k_2 is $k_2(\mu, \nu, t)$ and that A_{recon} is $A_{recon}(\mu, \nu, t)$. The total instantaneous amplitude of the reconstruction beam at the point α, β on the hologram can be represented as

$$U_{recon}(\alpha, \beta, t) = \iint_{\mu}\iint_{\nu} \frac{A_{recon}\, e^{ik_2 v}}{v} \, d\mu \, d\nu$$

The expression for the complex amplitude of the signal radiation at the image plane is then

$$U(\xi, \eta, t) = -i \iint_{\alpha}\iint_{\beta} T_4(\alpha, \beta)\, U_{recon}(\alpha, \beta, t)\, \frac{e^{ik_2 R}}{\lambda_2 R} \, d\alpha \, d\beta$$

in which

$$R = \left[R_0^2 + (\alpha - \xi)^2 + (\beta - \eta)^2 \right]^{\frac{1}{2}}$$

Consolidating the work to this point; i.e., expanding the expression for $U(\xi, \eta, t)$

$$U(\xi, \eta, t) = \sigma A_{obj} A_{ref} \rho_0 \iint_{\alpha}\iint_{\beta} \frac{e^{-iku}}{u_0} \, \frac{e^{\frac{-ik}{2s_0}(\alpha^2 - \alpha_0^2 + \beta^2 - \beta_0^2)}}{s_0}$$

$$\frac{J_1\left(\frac{k \rho_0 w}{s_0}\right)}{w} \sum_i \sum_j e^{\frac{ik}{s_0}\left[(\alpha - \alpha_0)x_i + (\beta - \beta_0)y_j\right]}$$

$$\iint_{\mu}\iint_{\nu} \frac{A_{recon}\, e^{ik_2 \left\{ v_0 + \frac{\left[\mu - (\alpha - \alpha_{RC})\right]^2 + \left[\nu - (\beta - \beta_{RC})\right]^2}{2v_0} \right\}}}{\lambda_2 \, v_0}$$

$$\frac{e}{R_0} \qquad ik_2 \left[R_0 + \frac{(\alpha-\xi)^2 + (\beta-\eta)^2}{2 R_0} \right] \qquad d\mu \; d\nu \; d\alpha \; d\beta$$

Note the sagittal approximation for v and R in the above equation.

$U(\xi, \eta, t)$ as computed above represents the signal on the sensors for the arbitrary period t to $t + \Delta t$. During that period, the segments of the phosphor spot were assigned particular amplitudes, phases, and wavelengths. Therefore, to obtain a valid representation of the physical signal, $U(\xi, \eta, t)$ must be obtained by properly weighting the many possible $U(\xi, \eta, t)$ solutions. Toward this end, one would separately compute each $U(\xi, \eta, m, n, \lambda)$ and store their individual outputs. Then using the distribution statistics of the phosphor's radiation, one would sum these individual outputs.

Digitalization of Read Source Model

The solution of the above equation for $U(\xi, \eta, t)$ be means of a digital computer program requires that, as already stated, the continuous variables of integration; e.g., μ, ν, t, be transformed into discrete variables. In the attempt to keep the computer time within reasonable limits such digitalization must imply relatively rough approximations. Models are formulated for the spatial and temporal (frequency) variables of the CRT spot.

CRT Spatial Model. The intensity of the reconstruction source (CRT) spot is assumed to vary as a Gaussian function of μ and ν, i.e.,

$$I(\mu, \nu) = I_0 \, e^{\frac{-\mu^2+\nu^2}{2\sigma^2}}$$

For the straight-forward case, one would now construct Gaussian random number generators to obtain the sample points of μ, ν . It should be recalled that a large number of sample points are necessary to preclude the possibility of a skewed sample distribution. For the previously indicated reason and for those that will become apparent from the succeeding work, it is not possible to utilize a large number of sample points. The skewness problem will be avoided by means of a structured sampling technique; i.e.,constraints will be placed on the randomness of the sample points.

The spatial distribution of the source intensity is Rayleigh if expressed in polar coordinates. The cumulative distribution function $P(r,\theta)$ is written as

$$P(r,\theta) = \int_0^r \int_0^\theta I_0 \, e^{\frac{-r'^2}{2\sigma^2}} \, r'dr'd\theta$$

where I_0 is a constant with respect to r and θ. This can be simplified to

$$P(r) = 2\pi I_0 \int_0^r e^{\frac{-r'}{2\sigma^2}} \, r'dr'$$

The normalized cumulative distribution function can be shown to be

$$P(r) = \int_0^r \frac{1}{\sigma^2} \, r' \, e^{\frac{-r'^2}{2\sigma^2}} \, dr'$$

Using this function, p(r), the spot is broken into N annular regions, or rings, of equal power. The boundaries of these regions are obtained from the following equations;

$$1/N = 1/\sigma^2 \int_{r_{L-1}}^{r_L} r' \, e^{\frac{-r'^2}{2\sigma^2}} \, dr'$$

$$= - e^{\frac{-r^2}{2\sigma^2}} \Bigg|_{r_{L-1}}^{r_L}$$

or

$$r_L = - \sqrt{2}\,\sigma \ln(1-L/N)$$

where $1 \leq L \leq N$.

Within each band, the position of the average r is found from the following equation;

$$\bar{r}_L = \frac{\int_{r_{L-1}}^{r_L} r' \, 1/\sigma^2 \, r' \, e^{\frac{-r'^2}{2\sigma^2}} \, dr'}{1/N}$$

If in the interest of notational simplicity, one sets

$$\rho = \frac{r}{\sqrt{2}\,\sigma}$$

then

$$\bar{\rho}_L = N \int_{\rho_{L-1}}^{\rho_L} 2\rho'^2 \, e^{-\rho'^2} \, d\rho'$$

Integrating by parts

$$\bar{\rho}_L = N\left[-\rho' e^{-\rho'^2} \Big|_{\rho_{L-1}}^{\rho_L} + \int_{\rho_{L-1}}^{\rho_L} e^{-\rho'^2} d\rho' \right]$$

and recognizing the second part as the integral representation of the Error Function "erf"; then

$$\bar{\rho}_L = N\left\{ \rho_{L-1} e^{-\rho_{L-1}^2} - \rho_L e^{-\rho_L^2} + \sqrt{\pi/2}\,\left[\mathrm{erf}(\rho_L) - \mathrm{erf}(\rho_{L-1}) \right] \right\}$$

This function is evaluated using the approximation[40]

$$\mathrm{erf}(\rho) = 1 - (a_1 t + a_2 t^2 + a_3 t^3)\, e^{-\rho^2} + \epsilon(\rho)$$

where

$$|\epsilon(\rho)| \leq 2.5 \times 10^{-5} \text{ for } 0 \leq \rho < \infty$$

$$t = 1/(1+p)$$

$$p = 0.47047$$

$$a_1 = 0.3480242$$

$$a_2 = -0.0958798$$

$$a_3 = 0.7478556$$

Randomization is achieved, within the above constraints, by allowing the points within each ring to vary randomly from $\bar{\rho}_L - (\bar{\rho}_L - \rho_{L-1})/2$ to $\bar{\rho}_L + (\bar{\rho}_L - \rho_{L-1})/2$. This is subject to the ad-

---

40 M. Abromowitz and I. Stegun, Handbook of Mathematical Functions, Dover Publications, Inc., New York, 1965, p. 299.

ditional conditions that the points alternate about $\bar{\rho}_L$ and that they be separated by equal angles. A further degree of randomization is obtained by rotating each ring by a random fraction of 2π radians. The randomizations were accomplished using an in-line generator that produced a uniform distribution.[41]

The Fortran Program used to compute the model's values is included as Appendix 3-1. A graphic display of the digitalized CRT spot is shown in Figure 3-11 for the case of four rings with twelve points per ring.

CRT Frequency Model. The dependence of intensity on wavelength for this proposed model was chosen with a particular input format in view. The bandwidths of standard fast-decay CRT phosphors are fairly broad; too broad to be of much use in the envisaged application. By simply placing a narrow band-pass filter between the phosphor and the output sensors of the image plane, an acceptable bandwidth can be produced, although of course, at the expense of power. The complexity of the intensity variations with temporal frequency usually necessitates a graphical presentation.

---

41 G. Marsaglia and T. Bray, "One Line Random Number Generators and Their Use in Combinations", Communications of the Assoc. for Computing Machinery, Vol. 11, No. 11, Nov. 1968, pp. 757-9.

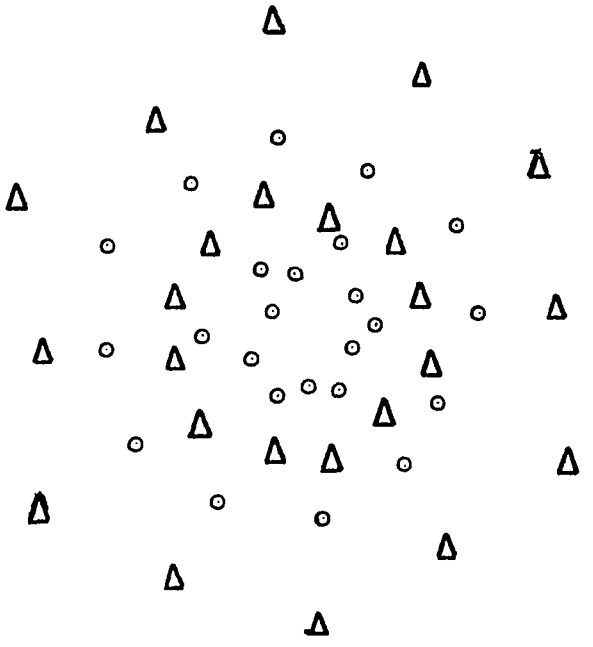

CRT SPATIAL MODEL

FIGURE 3 - 11

It should be noted that some of the europium activated phosphors, such as Gd_2O_3:Eu and Y_2O_2S:Eu[42] and YVO_4:Eu and Y_2O_3:Eu[43] have single or double lines with bandwidths of less than 20A°. While the decay times of these phosphors, which are in excess of 800 microseconds, are not compatible with the demands of a high speed memory, they could be utilized in a lower speed device.

To diitalize this graphical data, convenient, arbitrary scales are chosen for the abscissa and the ordinate. An appropriate number of data-points' coordinates are recorded. The abscissa values are changed to wavelength by applying the relationship

$$w = \frac{\Delta w}{\Delta x} x \neq w_0$$

A similar relationship converts ordinate values to intensity. This technique is desirable since the quadruled divisions on the graph paper used for the filter characteristic curves are not necessarily aligned with convenient intensity and frequency values; rather scale markers are superimposed on the paper. These markers are conveniently used to establish the values of $\frac{\Delta w}{\Delta x}$ and $\frac{\Delta A}{\Delta y}$.

It is now necessary to convert these 'appropriate data-points' into a set of properly weighted points. In the scheme adopted, the

---

42 W. T. Maloney, "Real-Time Holographic Filtering of Oscilloscope Traces", Applied Optics, Vol. 10, No. 11, Nov. 1971, pp. 2554-5.

43 A. Levine and F. Pallila, "YVO_4:Eu, A New Highly Efficient Phosfor Color Television", Electro-Chemical Technology, Vol. 4, No. 1-2, p. 16.

points are selected so as to be equally weighted. Let the arbitrary data points be W(ML) and AMP(ML) where $1 \leq ML \leq NL$ and NL is the total number of data-points selected. If these points are considered to outline a curve, then the area under the curve is the total power of the source. The distribution function, DAMP(ML), is the power up to the wavelength W(ML) where

$$DAMP(ML) = DAMP(ML-1) + (AMP(ML) - AMP(ML-1))/2 * (W(ML) - W(ML-1))$$

The total power of the source is DAMP(NL). If NF weighted points are desired, each point has DAMP(NL)/NF power. The power below the MF^{th} weighted point is

$$RAMP(MF) = DAMP(NL)/(2*NF) * (2*MF - 1)$$

e.g., if a total of 10 points is chosen, then the wavelength at the 4th point is chosen so that 7/20ths of the power is emitted within the spectral range below that wavelength. One must now find the wavelength RW(MF) that corresponds to a distribution function of magnitude RAMP(MF). Once it is determined that

$$DAMP(ML) \geq RAMP(MF) > DAMP(ML-1)$$

it is necessary to find Δw where

$$\Delta w = RW(MF) - W(ML-1)$$

to obtain RW(MF).

Referring to Figure 3-12, the cross-hatched area is approximately

$$DAREA = AMP(ML-1)* \Delta W + \tfrac{1}{2}(AMP(ML)-AMP(ML-1))* (\Delta W*\Delta W)/(W(ML)-W(ML-1))$$

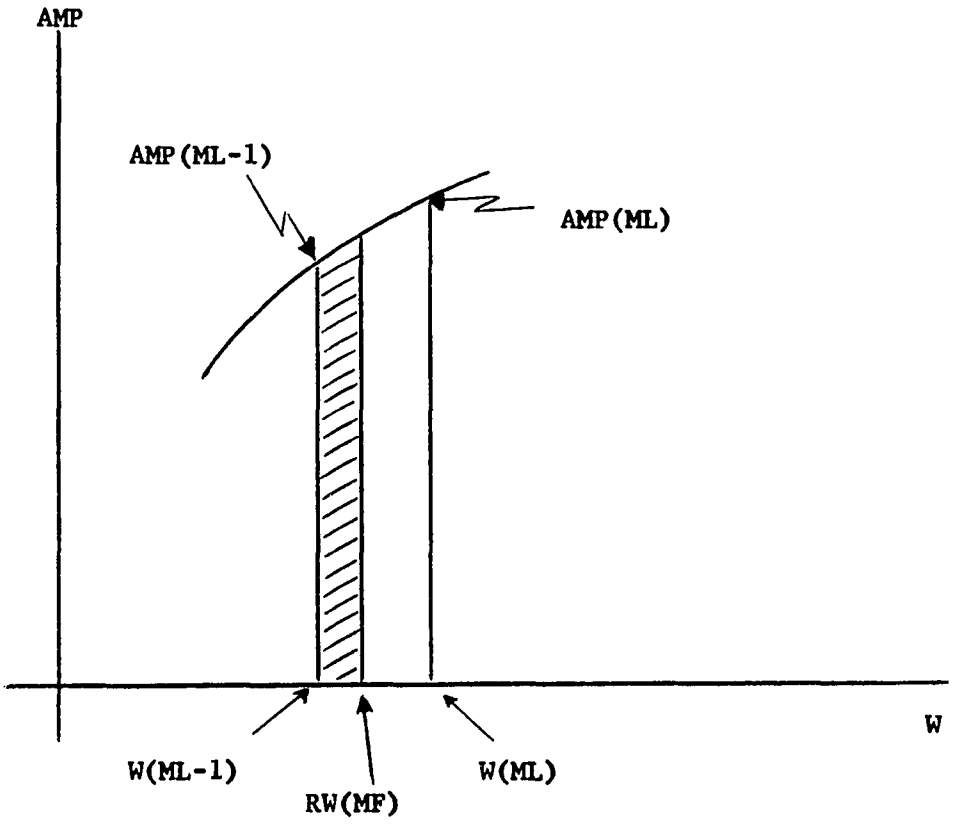

METHOD OF SELECTING FREQUENCY POINTS

FIGURE 3 - 12

This expression can be solved for ΔW by the quadratic formula. Having obtained ΔW, then

$$RW(MF) = W(ML-1) + \Delta W$$

The Fortran program implementing the above approach is shown in Appendix 3-2. This program was used to obtain the weighted points for two specific cases. The transmission curves for these cases are shown as Figures 3-13 and 3-14. The curves are those of 100A° and 30A° commercial laser line filters. The computed points are indicated on these graphs as well as appearing in the computer printouts associated with the program.

Analytically Derived Computer Simulation

As a preparatory step for evaluating $U(\xi, \eta, t)$ on the digital computer, the integration with respect to α and β was simplified. By making extensive use of the previously defined relationships that $\alpha - \alpha_0 = w \cos\psi$ and $\beta - \beta_0 = w \sin\psi$; e.g. $\alpha^2 - \alpha_0^2 = w^2 \cos^2\psi + 2\alpha_0 w \cos\psi$, the exponent can be reduced to

$$i(Cw^2 + Dw \cos\psi + Ew \sin\psi + G)$$

where

$$C = -\frac{k}{2}(1/u_0 + 1/s_0) + \frac{k_2}{2}(1/v_0 + 1/R_0)$$

$$D = k\left[\frac{x_i - \alpha_0}{s_0}\right] + k_2\left[\frac{\alpha'_0 - \alpha_{Rc} - \mu}{v_0} + \frac{\alpha_0 - \xi}{R_0}\right]$$

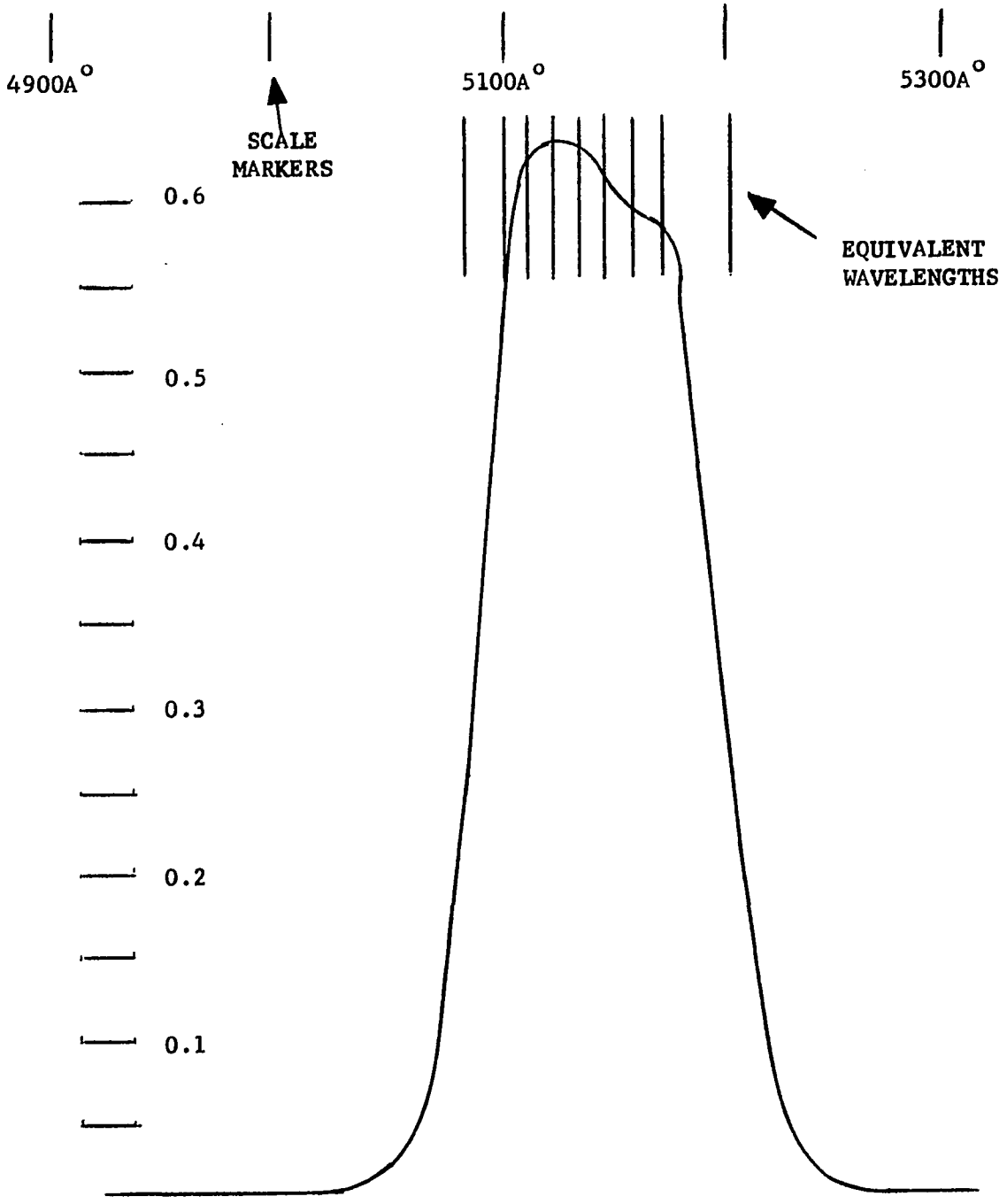

5145A° / 100A° FILTER

FIGURE 3 - 13

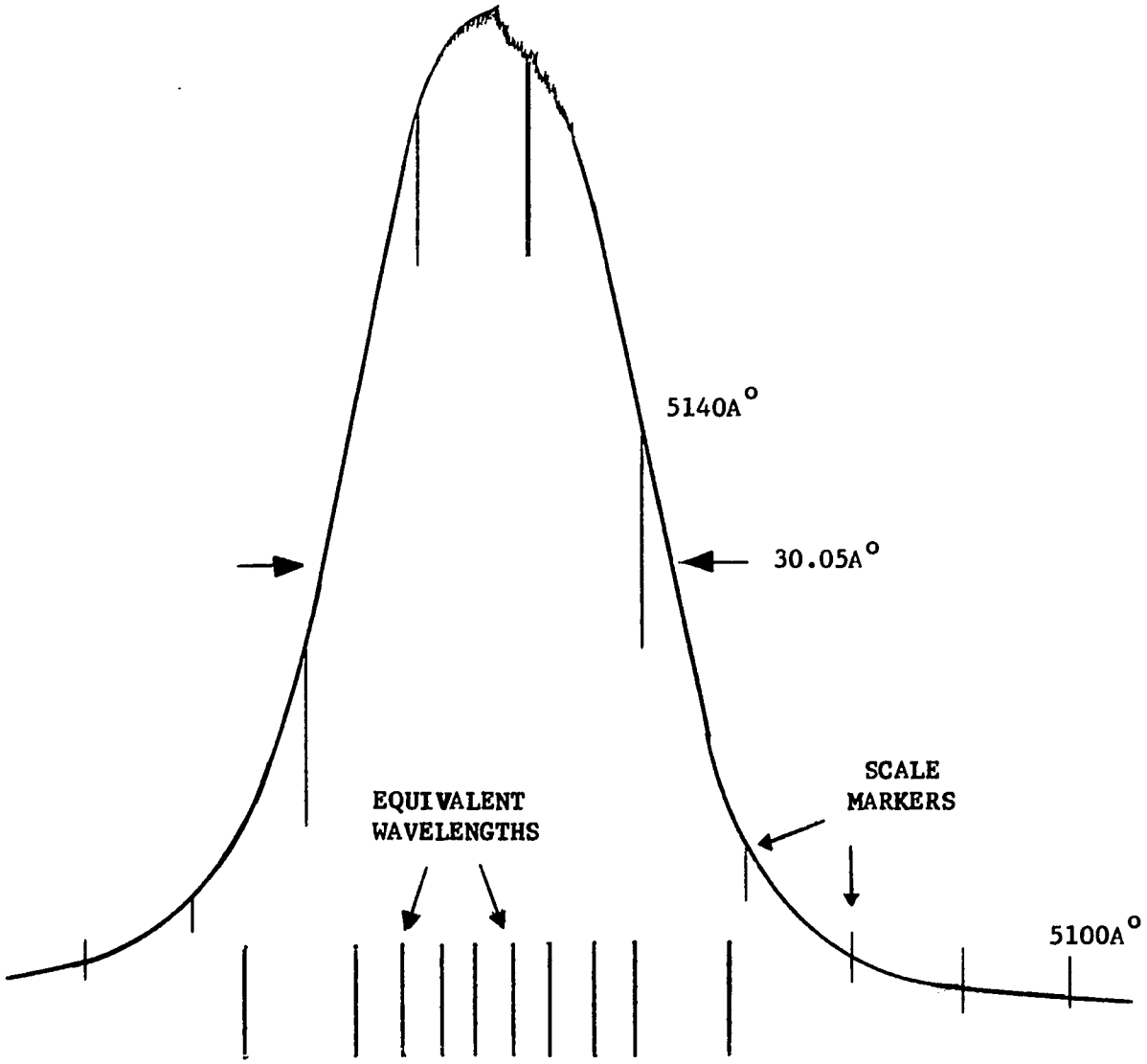

5145A° / 30A° FILTER

FIGURE 3 - 14

$$E = k\left[\frac{y_j - \beta_0}{s_0}\right] + k_2\left[\frac{\beta_0 - \beta_{Rc} - \nu}{v_0} + \frac{\beta_0 - \eta}{R_0}\right]$$

$$G = -ku_0 + k_2\left[v_0 + \frac{(\alpha_0 - \alpha_{Rc})^2 + (\beta_0 - \beta_{Rc})^2}{2\,v_0}\right.$$

$$+ \frac{\mu^2 + \nu^2}{2\,v_0} - \frac{\mu(\alpha_0 - \alpha_{Rc}) + \nu(\beta_0 - \beta_{Rc})}{v_0}$$

$$\left. + \frac{(\xi - \alpha_0)^2 + (\eta - \beta_0)^2}{2\,R_0}\right]$$

Then one can rewrite $U(m, n, \xi, \eta, t)$ as

$$U(m,n,\xi,\eta,t) = \frac{A_{obj} A_{ref} A_{recon} \rho_0}{\lambda^2 u_0 s_0 v_0 R_0} e^{iG}$$

$$\int_w J_1(k\rho_0 w/s_0)\, e^{iCw^2}$$

$$\int_\psi \sum_{x_i} \sum_{y_j} e^{iw(D\cos\psi + E\sin\psi)}\, d\psi\, dw$$

The integration over ψ can be performed using the relationships

$$D\cos\psi + E\sin\psi = (D^2+E^2)^{\frac{1}{2}} \cos(\psi - \tan^{-1}E/D)$$

and

$$\int_0^{2\pi} e^{iZ\cos(\theta - \phi)}\, d\theta = 2\pi J_0(Z)$$

Letting

$$F = (D^2 + E^2)^{\frac{1}{2}}$$

then

$$U(m,n,\xi,\eta,t) = \frac{A_{obj} A_{ref} A_{recon} \rho_0}{\lambda_2 u_0 s_0 v_0 R_0} e^{iG}$$

$$\int_w J_1(k\rho_0 w/s_0)\, e^{iCw^2} \sum_i \sum_j 2\pi J_0(Fw)\, dw$$

This integration can not be accomplished without approximation. The expansion of the integrand as to permit integration is achieved by setting

$$e^{iCw^2} = 1 + iCw^2 - \frac{C^2 w^4}{2} - \frac{iC^3 w^6}{3} + \cdots$$

and

$$J_1(k\rho_0 w/s_0) = J_1(Aw) = \frac{Aw}{2} - \frac{A^3 w^3}{2^3\ 1\ 2} + \frac{A^5 w^5}{2^5\ 2\ 3} + \cdots$$

The integration is accomplished by using the relationship

$$\int_0^{w_0} w^n J_0(Fw)\, dw = \frac{w^n}{F} J_1(Fw_0) - (n-1) \frac{w_0^{n-1}}{F^2} J_2(Fw_0)$$

$$- (n-1)(n-3) \frac{w_0^{n-2}}{F^3} J_3(Fw_0) - \cdots$$

The resultant expression for the radiation in the image plane is

$$U(m,n,\xi,\eta,t) = \frac{A_{obj} A_{ref} A_{recon} \rho_0}{\lambda_2 u_0 s_0 v_0 R_0} e^{iG}$$

$$\sum_{\ell=1}^{L} g_\ell \sum_x \sum_y \frac{J_\ell(Fw_0)}{F^\ell}$$

where g_ℓ is a coefficient. Recall that F is F(m,n, ξ , η , x,y,t).

Coincident with this development of the equations for $U_3(m,n,\xi,\eta,t)$, a second set of equations were developed for a special case of the above system. The special case, which was originally construed to be of only academic interest, set the bit-hole of the data-mask to a point; i.e., $\rho_0 = 0$. As is shown later in this chapter, this special case became the center of interest. The detailed mathematics of its development is included as Appendix III-3. The Fortran program is given in Appendix III-4.

As a preliminary step to executing the Fortran program CMPOUT, an estimate of the central processing unit (CPU) run time was made. The number of wavelengths chosen was 10, the number of spatial CRT spot positions was 48, and the number of non-zero mask bits was 3. With the bit positions selected as in Figure 3-15, it was decided to select the ξ, η sample points as shown in that figure. If twelve points are considered sufficient to map the amplitude contour for each spot's radius, two hundred sample points are required. The Bessel Function was found by experiment to have a CPU time of 11 milliseconds. A simple calculation shows that the Bessel Function execution time would consume 3168 seconds (52.8 minutes). A fair estimate of the entire CPU time would double this value. Since it was intended to repeatedly use this program for various combinations of the system parameters in an attempt to find an optimum set of these parameters, this time factor must be considered as excessive. Therefore, it was necessary to find another approach.

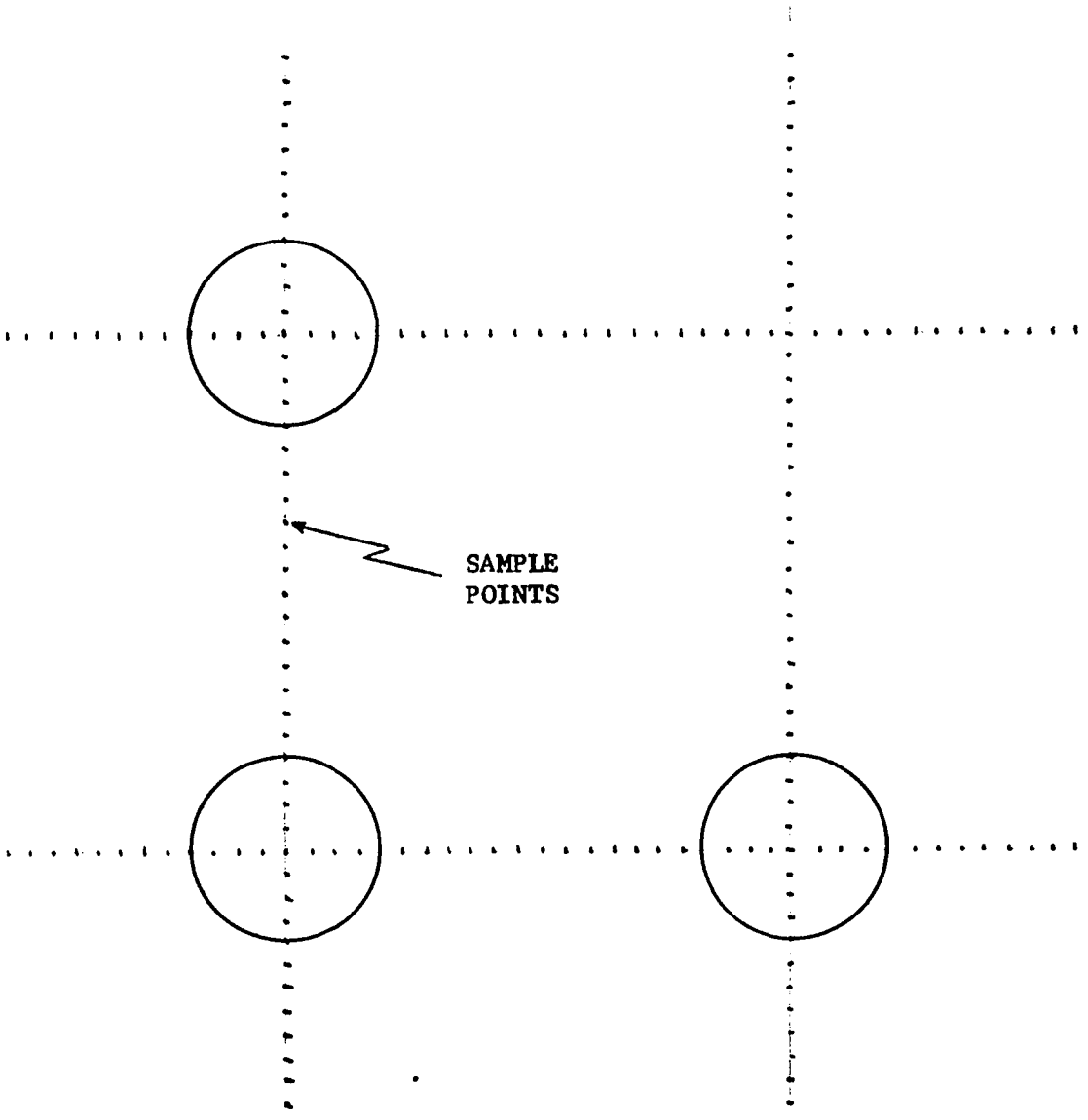

SAMPLE POINTS

FIGURE 3 - 15

Interpretively Derived Computer Simulation

In the preceding section, the radiation on the output, or sensor, plane was to be computed as a result of the strict mathematical manipulation of the equations. In this section, the output radiation is computed with the aid of insights into the physical processes involved.

The essence of this approach lies in the interpretive exploitation of the exponent in the integral expression for $U(\xi, \eta)$. First note that G is constant with respect to α and β. Therefore it can be extracted from that integral. Thus, in the ξ, η image intensity term, it is cancelled with its conjugate term. Next, consider the effect of the coefficient of the quadratic term. Recall that in an imaging system, the focus plane is that in which the coefficient of the quadratic term of the exponent equals zero.[44,45] For the problem at hand, then, the focus plane is that in which C equals zero, i.e.

$$-k/2\ (1/u_0 \neq 1/s_0) \neq k_2/2\ (1/v_0 \neq 1/R_0) = 0$$

Defining

$$\Delta k = k_2 - k$$

and approximating

$$k/k_2 = 1 - \Delta k/k$$

---

[44] Goodman, op. cit., pp. 92-4.

[45] DeVelis and Reynolds, op. cit., p. 71.

then from the expression for C equals zero, one can obtain

$$\frac{1}{R_0} = -\frac{1}{v_0} + \frac{1}{u_0} + \frac{1}{s_0} - \frac{\Delta k}{k}\left[\frac{1}{u_0} + \frac{1}{s_0}\right]$$

Observe that if Δk equals zero, then

$$1/R_0 = -1/v_0 + 1/u_0 + 1/s_0 \triangleq 1/R_{oc}$$

where R_{oc} is R_o for the center wavelength. Using this, one can establish the relationship

$$1/R_0 = 1/R_{oc} - \Delta k/k\ (1/u_0 + 1/s_0)$$

and

$$\frac{R_0}{R_{oc}} = \frac{1}{1 - R_{oc}\frac{\Delta k}{k}\left[\frac{1}{u_0} + \frac{1}{s_0}\right]}$$

If the sensors are located in the R_{oc} plane, then the effect of $R_o \neq R_{oc}$ is inferred with the aid of Figure 3-16. Light at the frequency corresponding to k_2 focuses a point object into the R_o plane at the position ξ_0. Geometrically, this strikes the sensor plane, R_{oc}, at the position ξ_c. From the application of the theorem on similar triangles, it becomes obvious that

$$\xi_c = \xi_0\ \left[R_{oc}/R_o\right]$$

and

$$\frac{w_0}{(R_0^2 + \xi_0^2)^{\frac{1}{2}}} = \frac{\xi_s}{\left[(R_{oc}-R_o)^2 + (\xi_c - \xi_o)^2\right]^{\frac{1}{2}}}$$

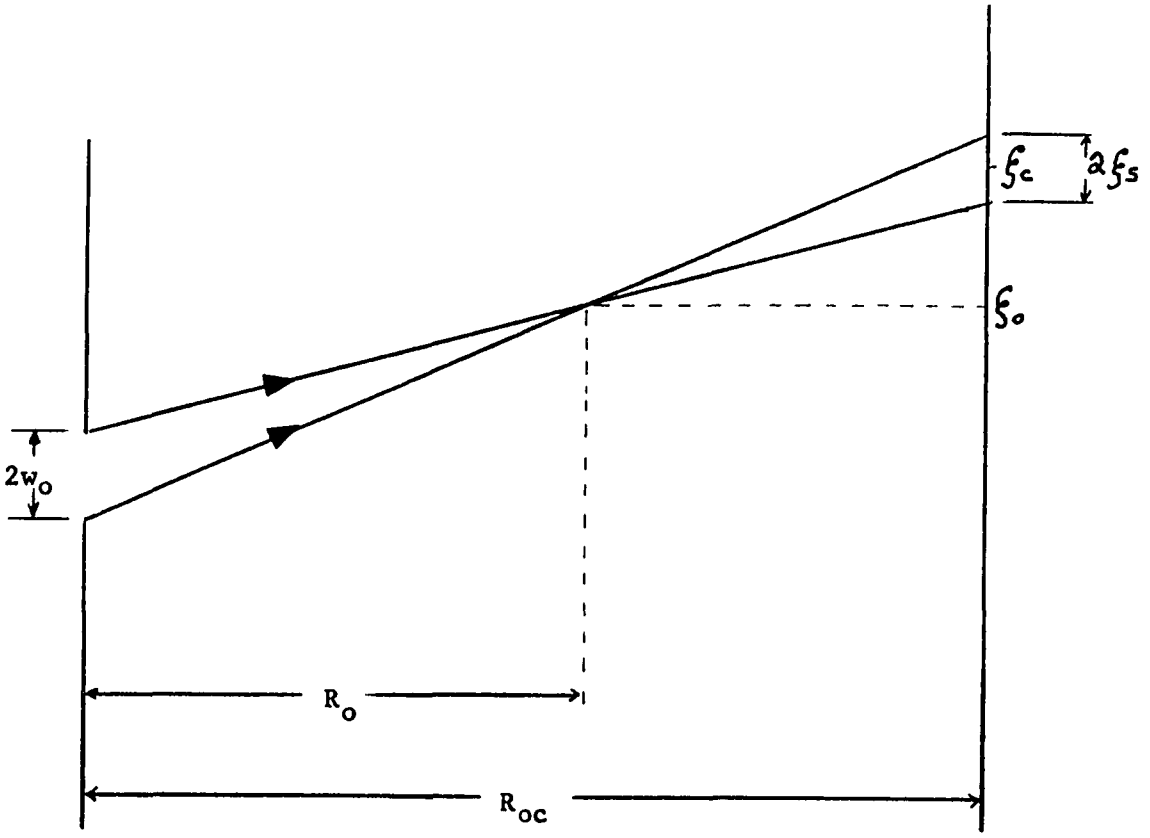

EFFECT OF MISFOCUS

FIGURE 3 - 16

This second expression reduces to

$$\xi_s = \pm w_0 R_{oc} \frac{\Delta k}{k} \quad (1/u_0 \pm 1/s_0)$$

The term ξ_s is interpreted as the spread, or smear, in the ξ direction on the sensor plane due to the mis-focusing of the image. This is comparable to chromatic aberration in a lens.[46] To emphasize the continuous nature of this effect, it is helpful to replace w_0 by Δw_0. The minus sign is suppressed and the expression becomes one of absolute value, i.e.

$$\xi_s = \Delta w_0 R_{oc} \frac{\Delta k}{k} \quad (1/u_0 \pm 1/s_0)$$

Having found the size of the spread for a given wave-number, $k \pm \Delta k$, it is now appropriate to find its centroid. If the hologram page aperture were infinite, the image would form at a point where the coefficients of α and β were zero.[47] For the ξ coordinate, this requires that

$$k \left[\frac{-\alpha_0}{u_0} - \frac{-x_i}{s_0} \right] = k_2 \left[\frac{-\alpha_{RC} \pm \mu}{v_0} - \frac{\xi_0}{R_0} \right]$$

This reduces to

---

46 F. Jenkins and H. White, Fundamental of Optics, McGraw-Hill Book Co., New York, 1957, p. 157.

47 DeVelis and Reynolds, op. cit., p. 71.

$$\xi_c = R_{oc}\left[\frac{\alpha_0}{u_0} + \frac{x_i}{s_0} - \frac{\alpha_{RC} + \mu}{v_0} - \frac{\Delta k}{k}\left(\frac{\alpha_0}{u_0} + \frac{x_i}{s_0}\right)\right]$$

with the aid of

$$\frac{\xi_0}{R_0} = \frac{\xi_{oc}}{R_{oc}}$$

This second spread term resulting from the frequency bandwidth merits explanation. If one recalls that a hologram is a composite of familiar diffraction gratings, then based on experience, one expects different wavelengths to be bent different amounts.[48] This bending, or angular dispersion, determines the position of the image just as a line grating separates the spectrum into different lines when it is irradiated with white light.

Since the aperture is finite, it is necessary to account for the diffraction pattern that this aperture generates. This pattern will be accounted for as a spread equal to the central disk of the Airy pattern; i.e., the first zero of the diffraction pattern will be used as the bound for the problem at hand. Thus

$$\xi_{CD} = \frac{R_0}{k\, w_0}\ 3.832$$

in the k_2 image plane, or

$$\xi_{CD} = \frac{R_{OC}}{k\, w_0}\ 3.832$$

in the sensor plane.

---

[48] Born and Wolf, op. cit., p. 408.

Combining all the spread contributions, one obtains

$$\xi_C = R_{OC}\left[\frac{\alpha_0}{u_0} + \frac{x_i}{s_0} - \frac{\alpha_{RC} + \Delta\mu}{v_0} - \frac{\Delta k}{k}\left(\frac{\alpha_0}{u_0} + \frac{x_i}{s_0}\right)\right]$$

$$+ R_{oc}\,\Delta w_o\,\frac{\Delta k}{k}\left[\frac{1}{u_0} + \frac{1}{s_0}\right] + R_{oc}\,\frac{\Delta p}{k w_o}$$

where

Δ_μ represents the finite extent of the reconstruction source

Δ_p represents the continuous nature of the diffraction pattern and $0 \leq p \leq 3.832$.

As an aid in understanding the various mechanisms involved in this last equation, it will be separated into meaningful groupings. Thus

$$\xi_C = R_{oc}\,\frac{x_i}{s_0}$$ location of point center if aligned

$$+ R_{oc}\left[\frac{\alpha_0}{u_0} - \frac{\alpha_{RC}}{v_0}\right]$$ offset due to non-alignment of reconstruction source

$$+ R_{oc}\,\frac{\Delta k}{k}\left[\frac{\alpha_0}{u_0} + \frac{x_i}{s_0} + \Delta w_0\left(\frac{1}{u_0} + \frac{1}{s_0}\right)\right]$$ smear due to frequency bandwidth

$$+ R_{oc}\,\frac{\Delta p}{k w_0}$$ smear due to diffraction of finite aperture

$$+ R_{oc}\,\frac{\Delta\mu}{v_0}$$ smear due to non-point nature of reconstruction source

It is also helpful to rewrite the equation in another configuration;

$$\xi_c = \xi_{position} + \xi_{offset} + \xi_{spread}$$

where

$$\xi_{position} = R_{oc} \left[\frac{x_i}{s_0} \right]$$

$$\xi_{offset} = R_{oc} \left[\frac{\alpha_0}{u_0} - \frac{\alpha_{RC}}{v_0} \right]$$

$$\xi_{spread} = R_{oc} \left\{ \frac{\Delta k}{k} \left[\frac{\alpha_0}{u_0} + \frac{x_i}{s_0} + \Delta w_0 \left(\frac{1}{u_0} + \frac{1}{s_0} \right) \right] + \frac{\Delta p}{k w_0} + \frac{\Delta \mu}{v_0} \right\}$$

This derivation was duplicated for the η direction.

By means of these equations for ξ_c and η_c, one can compute the effects of system parameter changes on the output of the system. In the design of the system, it should be apparent that the spacing between bit positions on the data mask must be such that adjacent bit images do not overlap if there is to be no inter-bit crosstalk; i.e., $|x_i - x_{i-1}| \geq 2 \xi_s / \mathcal{M}$ where $\mathcal{M}$ is the system magnification. Thus the minimum data mask dimension is $2N \xi_s / \mathcal{M}$ where N is the number of bits per page in the x-direction.

Interpage Crosstalk - Optical Suppression. In the previous section, the term ξ_{offset} seemed to represent only a potential problem. It could reasonably be assumed that it would cause inter-bit

crosstalk if the reconstruction source was misaligned from the exact position of the reference source. However, a second look showed that it could be used to suppress inter-page crosstalk. As was noted previously, the size of the output image in the ξ direction is $2N\xi_s$. If, as shown in Figure 3-17, any stray radiation from the reconstruction source at position α_n irradiates an adjacent page; i.e., $\alpha_{n\neq 1}$, then it is necessary that the misalignment between the sources be such that

$$\xi_{offset} \triangleq 2N\,\xi_{spread}$$

The variable of interest is the distance that must exist between adjacent α_{RC}'s to insure a large enough ξ_{offset}. This distance will be called h , where

$$h = \alpha_0 - \alpha_{RC}$$

Then

$$\xi_{offset} = R_{oc}\left[\frac{\alpha_0}{u_0} - \frac{\alpha_{RC}}{v_0}\right] = R_{oc}\left[\frac{\alpha_0}{u_0} - \frac{\alpha_0 - h}{v_0}\right]$$

Before proceeding to find the minimum page separation, it is necessary to obtain the maximum value of α_0. This is required since the maximum value of ξ_s occurs at $\alpha_{0\,max}$. In the background material of Chapter II, it was noted that the $|B|^2$ and $|O|^2$ terms of the hologram transmission resulted in a dimmed, but otherwise unaltered, reconstruction source wavefront. If this energy were allowed to impinge on the sensors, it would be considered a noise signal. To overcome this problem, one need only place the data mask to the side of the film since

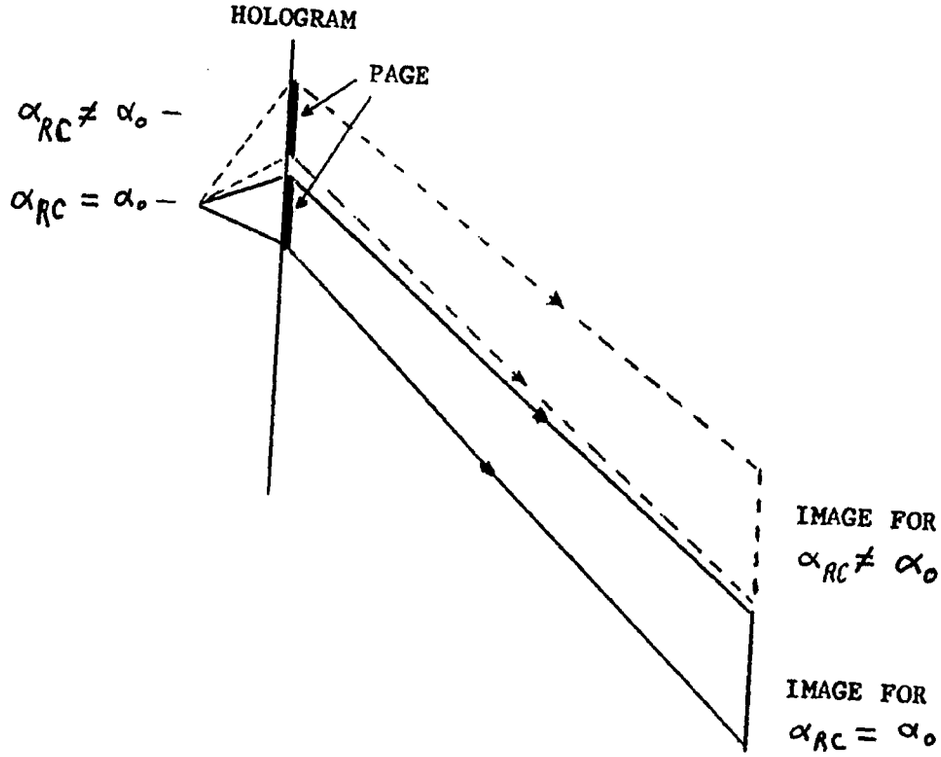

OPTICAL SUPPRESSION
OF
INTERPAGE CROSSTALK

FIGURE 3 - 17

the undiffracted noise signal will not be bent to the sensor position. This technique is commonly referred to as side-band holography. If the film size is 'c', then, as shown in Figure 3-18,

$$\alpha_{0\ max} = c - w_0 + N f_s$$

If, for the sake of simplicity, one allows $u_0 = v_0$, then $R_{oc} = s_0$ and

$$f_{offset} = \frac{R_{oc} h}{u_0}$$

Noting that for the limiting case,

$$x_i = (N-1) f_s$$

$$\Delta p = p$$

$$\Delta w = w_0$$

then

$$h = \frac{2N \frac{\Delta k_{max}}{k} \left[c + \frac{w_0 u_0}{s_0} \right] + \frac{u_0 p}{k w_0} + \Delta_{\mu max}}{1 + \frac{\Delta k_{max}}{k} - N \frac{\Delta k_{max}}{k} \left[\frac{R_{oc}}{u_0} + 1 \right]}$$

This value of h is the minimum page separation. Rewriting this equation, one obtains

$$N = \frac{\frac{1}{2} h \left(1 + \frac{\Delta k_{max}}{k}\right)}{\frac{\Delta k_{max}}{k} \left(c + \frac{w_0 u_0}{r_0}\right) + \frac{u_0 p}{k w_0} + \Delta_\mu + h \frac{\Delta k_{max}}{2k} \left(\frac{R_{oc}}{u_0} + 1\right)}$$

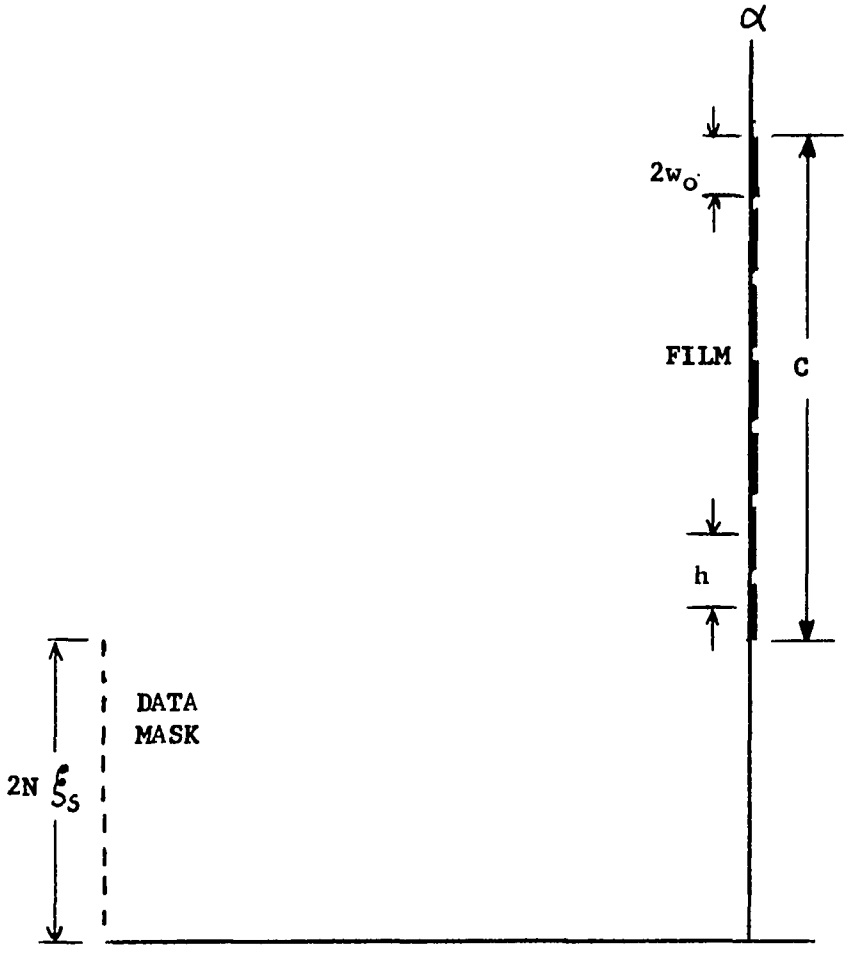

SIDEBAND HOLOGRAPHY

FIGURE 3 - 18

where N is the maximum number of rows that a page can have without inter-bit or inter-page crosstalk.

As a preliminary step to evaluating N for various values of the system parameters, it is logical to first search for maxima by more sophisticated mathematics. However, in terms of the system bit packing density, it is not the number of bits per page that is of prime importance, but rather the number of bits recorded per square centimeter of film. If the length of the film edge is L, then the number of rows of pages is Q where

$$Q = \frac{L}{h}$$

and the total number of rows of points is T where

$$T = Q \times N = \frac{\frac{1}{2}\left(1 + \frac{\Delta k_m}{k}\right) L}{\frac{\Delta k_m}{k}\left(c + w_0 \frac{u_0}{s_0}\right) + \frac{u_0 p}{k w_0} + \Delta\mu_{max} + h \frac{\Delta k_m}{k}\left(\frac{R_{oc}}{u_0} + 1\right)}$$

An attempt was made to optimize this with respect to h, r_0, w_0, and u_0 simultaneously. The result was non-physical. The best that could be achieved was simultaneous optimization with respect to w_0 and u_0. The expressions are

$$w_0 = (r_0 \, p/\Delta k)^{\frac{1}{2}}$$

and

$$u_0 = \tfrac{1}{2}\left(h \, r_0 \, (r_0 \, \Delta k/p)^{\frac{1}{2}}\right)^{\frac{1}{2}}$$

These relationships were used in the computerized evaluation of N.

A similar development was done for the η direction to calculate the maximum number of columns, M. The program used to evaluate M and N for various values of c, Δk, $\Delta\mu$, h, w_0, u_0, and r_0 is included as Appendix III-5.

The selection of the value of all but one of these system parameters; i.e., c, h, w_o, u_o, r_o, and Δk, was, within reason, at the discretion of the designer. Δk is included in this group since the system designer, subject to power considerations, can choose the filter bandwidth. On the other hand, the minimum size of the CRT spot, $\Delta\mu$, is not under his control. Therefore, it was necessary to obtain information on available $\Delta\mu$ values from CRT manufacturers. A sampling of this information is supplied as Table 3-1. On the basis of this data, three nominal spot sizes were selected; 5×10^{-3}cm as representative of the large diameter magnetic deflection tubes, 20×10^{-3}cm as representative of the large diameter, high resolution electrostatic deflection tubes, and 50×10^{-3}cm as representative of the group that includes the available Fairchild 765H series Oscilloscopes. As an additional result of the correspondence required to generate Table 3-1, information on current phosphor decay times was obtained. Philco data shows P16 phosphor with a decay time to the 10% point of 0.1 microsecond and P24 with a value of 1 microsecond. For extremely high speed use, Westinghouse lists its PX42 phosphor as having a decay time of 1 nanosecond.

The computed values of N and M are given in Table 3-2 for a selected sample of system parameters. These examples are for the

Manufacturer	Designation	Resolution $x10^{-3}$cm	Diameter inches	Phosphor	Focus & Deflection
Philco	4XP16	0.976	2.8	P16	Mag - Mag
	4WP16	0.725	2.8	P16	Mag - Mag
	5ECP16	1.27	5	P16	Mag - Mag
	5ECP24	1.27	5	P24	Mag - Mag
Note:	P16 0.1 microseconds decay to 10% pt.				
	P24 1.0 " " " " "				
General Electric	Z4836	5.0	2	Specify	ES - Mag
	Z4880	2.5	3	"	ES - Mag
	Z4790	5.0	5	"	ES - Mag
	Z4915	1.25	5	"	Mag - Mag
	Z4665	16.0	5	"	ES - ES
Fairchild	5CWP	25.0	5	Specify	ES - ES
	K2202	3.7	2	"	ES - ES
	K2252	3.5	2½	"	ES - ES
	K1871	1.8	5	"	Mag - Mag
	* K21321P-2/B	45.0	4	"	ES - ES
	* 765H Series Oscilloscope				
Westinghouse	WX4903P	1.6	4½	Specify	ES - Mag
	WX30890	1.3	4½	"	ES - Mag
Note:	PX42 Phosphor 1.0 nanosecond decay to 10% pt.				

CATHODE RAY TUBE CHARACTERISTICS

Table 3-1

$h = 0.1cm$
$c = 2.0cm$
$s_o = 15cm$

$\Delta\lambda$ A°	Δ_μ cm	w_o cm	v_0 cm	N	M
30	0.005	0.03	3.0	2.3	6.9
		*0.2841	*4.45	2.6	8.1
100		0.03	3.0	0.96	3.4
		*0.156	*6.01	1.0	3.5
30	0.02	0.03	3.0	1.4	3.4
		*0.284	*4.45	1.5	3.7
100		0.03	3.0	0.75	2.3
		*0.156	*6.01	0.79	2.3
30	0.05	0.03	3.0	0.76	1.7
		*0.284	*4.45	0.79	1.8
100		0.03	3.0	0.52	1.4
		*0.156	*6.01	0.54	1.4

* Optimum values of w_o and v_0

VALUES OF N AND M

Table 3-2

desirable case of reasonably large film size and small page size which combine to form a large capacity memory. Note that optimization of u_o and w_o leads to only modest increases in capacity while resulting in page overlap, i.e., $w_o \geq h$. This overlapping necessitates multiple film exposure.

A more extensive set of values of N and M is listed in Table 3-3. In examining this list, recall that the maximum number of rows of pages in a direction on the film sheet of dimension c is c/h. Thus if the film dimension is 0.5 cm and the page separation, h, is 0.1 cm, then five rows of pages can be formed. Using this table to compare the values of N to those of M, one can clearly see the high price in bit-packing density that is paid for sideband holography.

In-Line or Gabor Type Hologram. As was previously stated, the motivation for side-band holography was that it removed the noise signal caused by the $|B|^2$ and $|O|^2$ terms. Another well-known advantage, which was not mentioned in the above, is that it also angularly separates the real image from the virtual image as shown in Figure 3.19.[49] Because of the high price in bit-storage density being paid for this noise suppression, a closer examination of the need for it was made.

As in the preceding work, the focus plane is that plane in which the coefficients of α^2 and β^2 in the exponent are zero. Thus for the

---

[49] Goodman, op. cit., p. 218.

					h = 0.1 cm		0.15		0.3		0.5	
					w_o = 0.05 cm		0.05		0.15		0.05	
c	$\Delta\lambda$	s_o	$\Delta\mu$	v_o								
cm	A°	cm	cm	cm	N	M	N	M	N	M	N	M
0.5	30	10	.005	0.5	3.5	13.6					6.5	51.8
				3.0	4.5	11.1					15.5	44.3
		15		0.5	2.9	13.7					4.7	51.8
				3.0	4.3	11.2					13.5	44.5
			.02	0.5	1.6	4.5					3.7	20.4
				3.0	1.9	4.2					7.5	19.1
		30	.005	0.5	1.9	13.7					2.6	51.9
				3.0	3.9	11.2					9.7	44.6
			.02	0.5	1.2	4.5					2.2	20.4
				3.0	1.8	4.2					6.1	19.1
1.0		15	.005	0.5	2.5	11.4	3.0	16.6	4.0	30.8	4.3	45.1
				3.0	3.5	9.6	4.9	14.0	8.9	26.2	11.7	39.4
			.02	0.5	1.4	4.2	1.9	6.3	2.8	12.2	3.5	19.2
				3.0	1.7	4.0	2.4	5.8	4.7	11.8	6.9	18.1
		30	.005	0.5	1.7	11.4	2.0	16.6	2.3	30.8	2.5	45.1
				3.0	3.1	9.7	4.3	14.1	7.1	29.1	8.7	39.5
			.02	0.5	1.1	4.2	1.4	6.3	1.9	12.2	2.2	19.2
				3.0	1.6	4.0	2.3	5.9	4.2	12.0	5.7	18.1
			.05	0.5					1.3	5.5	1.7	9.0
				3.0					2.3	5.5	3.4	8.7
2.0		15	.005	0.5	1.9	8.6	2.5	12.5	3.4	23.7	4.1	35.7
				3.0	2.5	7.5	3.6	11.1	6.6	22.6	9.2	32.0
			.02	0.5	1.2	3.8	1.7	5.6	2.6	10.9	3.3	17.3
				3.0	1.4	3.6	2.1	5.3	4.0	10.6	5.9	16.4
		30	.005	0.5	1.4	8.6	1.7	12.6	2.2	23.8	2.4	35.8
				3.0	2.3	7.5	3.2	11.1	5.6	22.7	7.3	32.1
			.02	0.5	1.0	3.8	1.3	5.6	1.8	10.9	2.1	17.3
				3.0	1.4	3.6	2.0	5.3	3.6	10.7	5.1	16.4
			.05	0.5					1.3	5.5	1.7	8.5
				3.0					2.1	5.2	3.2	8.3

SAMPLED VALUES OF N AND M

Table 3-3

c cm	$\Delta\lambda$ Å	s_o cm	$\Delta\mu$ cm	v_o cm	h = 0.1 cm, w_o = 0.05 cm N	M	h = 0.15, w_o = 0.05 N	M	h = 0.3, w_o = 0.15 N	M	h = 0.5, w_o = 0.05 N	M
0.5	100	15	.005	0.5	1.1	8.4					1.5	25.6
				3.0	2.3	7.3	2.2	7.8			5.5	23.5
1.0				0.5							1.5	20.6
				3.0					3.5	13.5	4.6	19.2
			.02	0.5							1.3	12.8
				3.0							3.6	12.3
			.05	0.5							1.2	7.3
				3.0							2.5	7.1
2.0			.005	0.5							1.3	14.8
				3.0							3.4	14.1
			.02	0.5							1.2	10.3
				3.0							2.8	9.9
			.05	0.5							1.1	6.4
				3.0							2.1	6.3

SAMPLED VALUES OF N AND M

Table 3-3 (con'd)

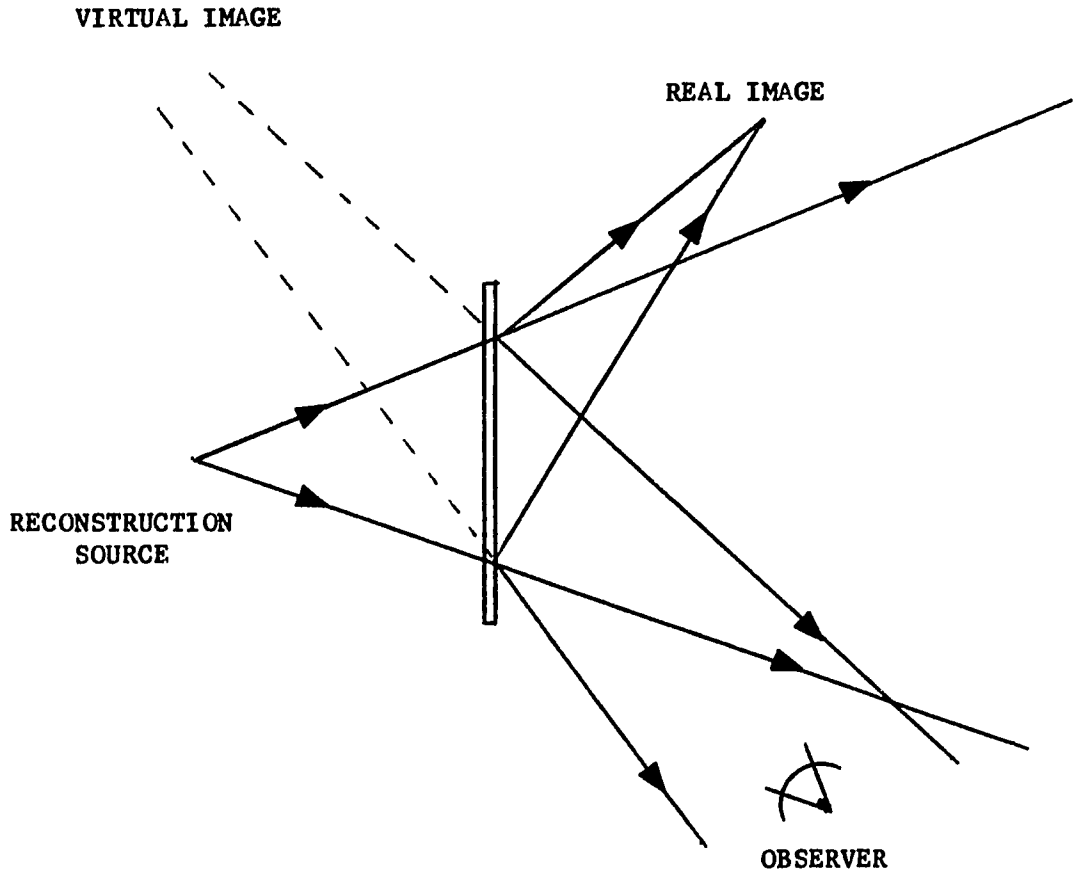

ANGULAR IMAGE SEPARATION
OF
SIDE-BAND HOLOGRAPHY

FIGURE 3 - 19

desired term,

$$0 = 1/R + 1/v_0 - 1/u_0 - 1/s_0$$

If $u_0 = v_0$, then

$$R = s_0 = R_0 \quad \therefore \text{ real image}$$

For its conjugate image term,

$$0 = 1/R + 1/v_0 + 1/u_0 + 1/s_0$$

$$1/R = -(1/v_0 + 1/u_0 + 1/s_0) \quad \therefore \text{ virtual image}$$

For the source - source conjugate term,

$$0 = 1/v_0 + 1/R$$

$$R = -v_0 \quad \therefore \text{ virtual image}$$

For the object - object conjugate term,

$$0 = 1/v_0 + 1/R$$

$$R = -v_0 \quad \therefore \text{ virtual image}$$

Since all the noise wavefronts are seemingly generated on the far side of the hologram, one would expect the power density at the sensor plane due to the noise wavefronts to be small compared to the power density of the focused signal wavefront. Therefore, it appears that the Gabor type hologram can be used effectively. A schematic of the proposed system is shown in Figure 3-20.

While this may increase the value of N, it can not make it equal to that of M. The reason for this is evident from Figure 3-21. As can be seen, the data mask must be set to the side so that the radiation from it is not intercepted by the reference beam converging lens. To those unfamiliar with holography, the apparent solution might be to place the reference beam behind the film, as shown in

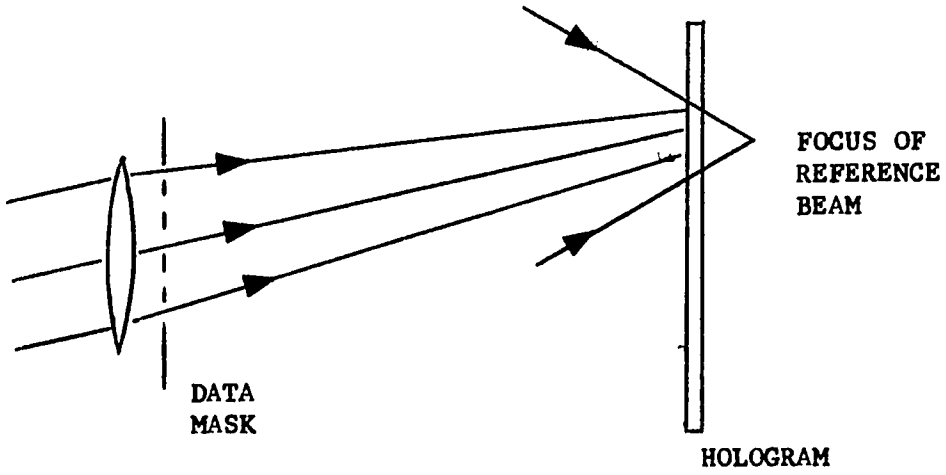

SCHEMATIC OF DESIRED
GABOR SYSTEM

FIGURE 3 - 20

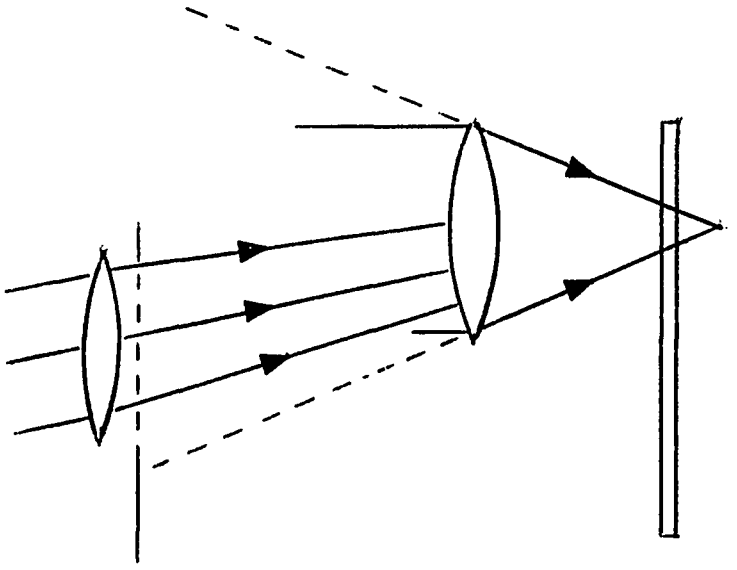

DASHED RAYS INDICATE CONE OF BLOCKAGE

EFFECT OF REFERENCE BEAM LENS

FIGURE 3 - 21

Figure 3-22. This, however, produces a reflection hologram in which the image is viewed with reflected light.[50]

Since the obstacle to the higher bit-storage density is the presence of the physical converging lens in the reference beam, a solution is to remove the physical lens. This can be accomplished by abandoning the physical 'write' process in favor of a synthetic write process; i.e.,generate the hologram on a computer. As will be shown later, this technique makes it possible to eliminate the $|B|^2$ and $|O|^2$ noise. This synthetic system is the subject of Chapter IV. Having thus removed the obstacle of the lens, the hologram can be made so that N = M.

Interpage Crosstalk - Mechanical Suppression. In examining Table 3-3, one observes that as the page separation is increased, the allowable number of bits per page increases also. However, one notes that the number of pages per fixed size hologram decreases as page separation increases. The advantage of the optical suppression of interpage crosstalk is that the user need only position the hologram in a set plane in front of the CRT with no concern as to the detailed alignment in that plane. The alignment would be done by electronically positioning the CRT spots' coordinate axes to coincide with those of the hologram. However, if the price in bit storage density that must be paid for this system convenience is too high, the interpage crosstalk can, of course, be suppressed mechanically. A scheme for this

---

50 Ibid, p. 251.

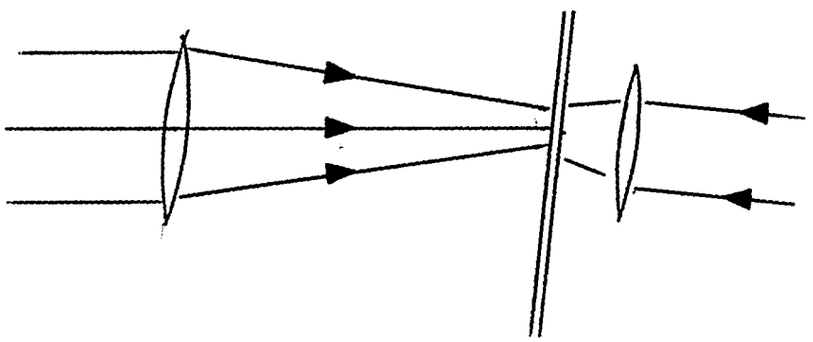

REFLECTION HOLOGRAM

FIGURE 3 - 22

is shown in Figure 3-23.

An estimate of the price in storage density being paid for the optical suppression can be obtained from Table 3-3. Consider the h = 0.5 cm columns as indicative of the increase in density that would be afforded by a mechanical system; i.e., the values in the h = .5 column are attainable for separations of $h = 2w_o = 0.1$ cm. On a two dimensional basis, the price is a decrease in density of between twenty and twenty-five-to-one. As an example, consider the case of c = 2cm, $w_0 = 0.05$cm, $\Delta\lambda = 30A^o$, $s_0 = 15$cm, $\Delta\mu = 0.02$cm, and $v_0 = 0.5$cm. If h = 0.1cm, $M^2 = 3.8^2 \approx 4^2 = 16$; but if h = 0.5cm, then $M^2 = 17.3^2 \approx 17^2 = 289$. For c = 2, the total number of bits for the h = 0.5cm case is 115,600 if mechanical separation used. The higher resolution CRT would increase this to over one-half million bits.

The h = 0.5cm case is only indicative of the density possible if mechanical suppression is used. Employing the mathematics developed in the previous section entitled 'Interpretively Derived Computer Simulation', one can write

$$\eta_{spread} = R_{oc}\left\{\Delta k/k\left[\beta_o/u_o + y_j/s_o + \Delta w_o(1/u_o + 1/s_o)\right] + \Delta p/(kw_o) + \Delta\nu/v_o\right\}$$

Using $\beta_{0max} = c/2 - w_o$ and $y_{j_{max}} = (M-1)\eta_s$

one obtains

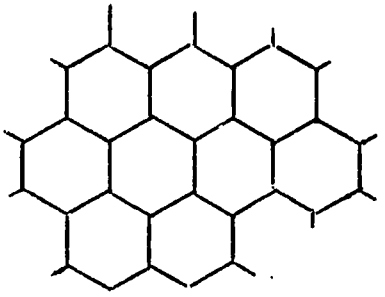

END VIEW

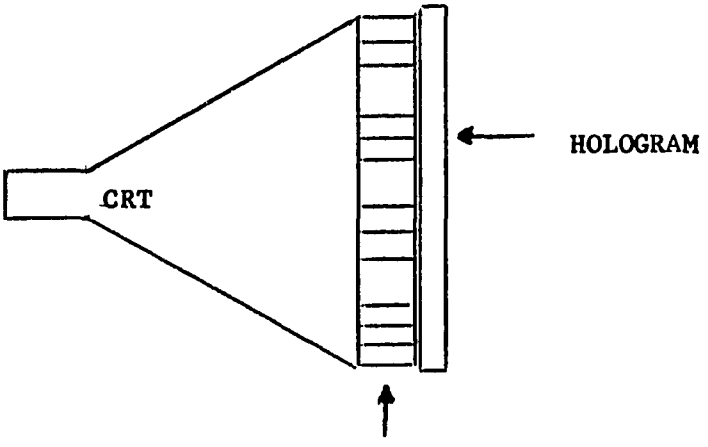

SIDE VIEW

MECHANICAL SUPPRESSION
OF
INTERPAGE CROSSTALK

FIGURE 3 - 23

$$\eta_s = \frac{R_{oc}\left\{\frac{\Delta k}{k}\left[\frac{c}{2u_o}+\frac{w_o}{s_o}\right]+\frac{\Delta p}{kw_o}+\frac{\Delta\mu}{v_o}\right\}}{1-R_{oc}\,\frac{\Delta k}{k}\,\frac{M-1}{s_o}}$$

A Fortran program was written to evaluate η_s for the following values:

$\Delta\lambda$ = 30, 100 A°

c = 0.5, 1.0, 2.0cm

s_o = 3, 10, 15, 30cm

$\Delta\mu$ = 0.005, 0.02, 0.05cm

v_o = 0.05, 1.0, 3.0cm

w_o = 0.03, 0.1, 0.15, 0.5cm

The program was executed by setting values of M up to 20 and examining the effect of the variation on η_s. From the equation, observe that as M increases, η_s increases to infinity. Further increases in M results in negative values of η_s.

In all the cases computed, η_s remained positive; i.e., realizable. As specific examples of this consider

$\Delta\lambda$ = 100 A°

c = 2cm

s_o = 15cm

$\Delta\mu$ = 0.02cm

w_o = 0.03cm

v_o = 0.5cm 3.0cm

M = 20

Then

$$\eta_s = 1.9\text{cm} \qquad 0.34\text{cm}$$

Interpreting this, at least 400 bits can be stored on a 0.03cm page and 33^2 pages or 435K bits on a 2cm square piece of film.

Expanded System. If the capacity of the system, as described to this point, is not great enough, several methods exist to increase it. One of the more obvious methods is to increase the number of bits per page by increasing the size of the data mask. However, in examining the expression for η_{spread}, one notes that as $y_{j_{max}}$ is increased; i.e., as more data points are added, η_{spread} is increased. The larger η_{spread}, of course, requires more spacing between data points and this results in an even larger value for $y_{j_{max}}$. The outcome is a cumbersome data mask. More important, however, is the fact that there is a limit to the field of view that the holographic film can faithfully record; i.e., the film, as noted in Chapter IV, has a finite resolution limit. Using this technique for increasing the system capacity would eventually expand the data mask to the point that it would exceed that field of view. A second obvious method, that of increasing the number of pages per hologram, will lead to the same problem. This, likewise, can be seen by examining the expression for η_{spread}.

Two other methods will be described here. Both call for increasing the addressing nomenclature by on level. Standard systems have the bit, the word, the page, and the memory. A new subdivision, the chapter, is proposed. As its name implies, it would be composed of

pages; i.e.,it would be a new level between the page and the memory.

The first method is predicated on the assumption that a suitable photo-detector read-out array is available at a low cost. If so, several detector arrays could be positioned, as indicated in Figure 3-24, so that each array sensed the signal from a specified portion of the hologram; that portion being a chapter. The outputs of each array would be connected in parallel to the corresponding outputs of all the other arrays. It is important to note that while the addressing nomenclature has been increased, the actual addressing code has not.

The second method utilizes a system of mirrors placed so as to apparently duplicate the multiple array technique of the first system. This system is shown in Figure 3-25. It should be mentioned that the hologram-to-image distance could easily be varied between chapters to conform to the geometry of the mirror system. The same could be done for the apparent angle of the image.

Using a four inch CRT, the capacity of the system could be increased twenty-five fold by means of the 'chapter' technique. Using the values of a previous example, this would allow for the storage of over 10 Megabits.

Conclusions

The feasibility of using a CRT as the source of radiation for a computer ROM has been proven. While it has been shown possible to

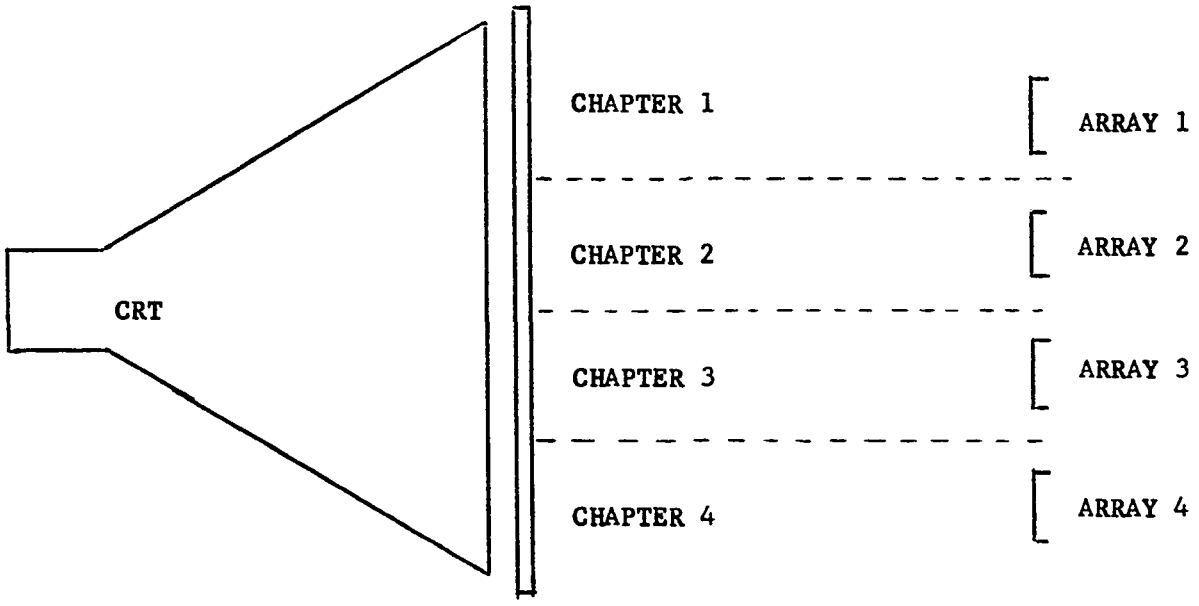

EXPANDED SYSTEM UTILIZING MULTIPLE ARRAYS

FIGURE 3 - 24

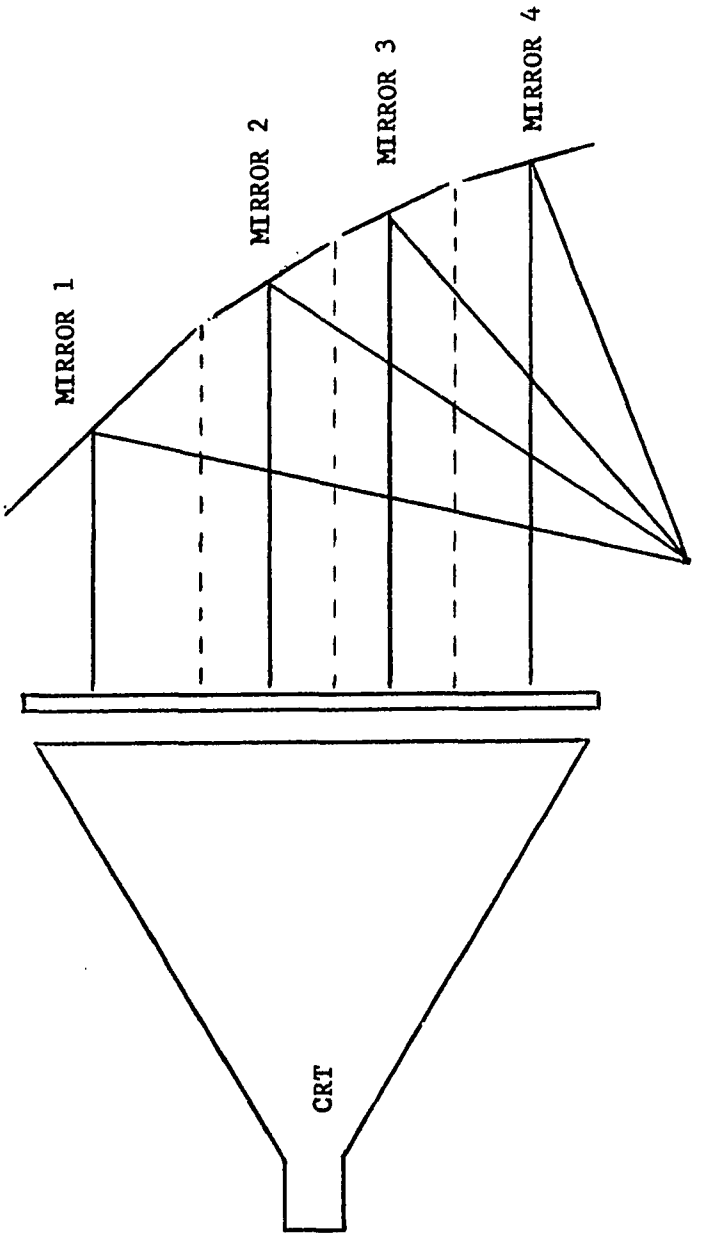

EXPANDED SYSTEM UTILIZING MIRRORS

FIGURE 3 - 25

suppress inter-page cross-talk by a purely optical technique, the mechanical page separation technique was proven desirable from a bit density point of view. Using this latter approach and a synthetically generated hologram, a RAM system was designed that has a bit storage density capability in excess of 100K bits per cm^2 and an access time of approximately 10 nanoseconds.

CHAPTER IV

SYNTHETIC HOLOGRAM

Introduction

On the basis of the bit-storage density considerations developed in Chapter III, it was determined that a synthetically generated hologram should be produced. In the present Chapter, the ability of the synthetic approach to suppress unwanted terms that are present in the optically produced hologram is shown. Also noted is the diffusion advantage of the synthetic data mask point sources. As is shown in Chapter V, there are other benefits to be derived from utilizing a synthetic hologram. For example, the synthetic hologram can be made free from the detrimental effects of lens imperfections and mechanical vibrations.

In this Chapter, the necessary equations are developed to calculate the transmittance pattern of the synthetic hologram. To implement this theory a modem was designed and fabricated for the production of synthetic holograms; and that modem was connected to a remote computer terminal so that a sample synthetic hologram could be made to show the feasibility of this approach. This Chapter contains a description of the actual system and the results of system testing as well as an example of synthetic holograms produced by the system.

Derivation of Transmission Pattern Equation

First, the appropriate expression for the transmission pattern of the hologram must be determined. As previously stated, the syn-

thetic nature of this process allowed the utilization of an otherwise impractical data mask, i.e. a mask configured of ideal point sources. Using the coordinates of Figure 4-1, the radiation from the data mask incident on the film plane was expressed as

$$U_{obj}(\alpha, \beta) = \sum_{ij} A_{ij} \frac{e^{iks_{ij}}}{s_{ij}}$$

where

$$s_{ij} = \left[s_o^2 + (\alpha - x_i)^2 + (\beta - y_j)^2 \right]^{\frac{1}{2}}$$

and ij is considered as a single subscript. As previously described, the reference beam was expressed as

$$U_{ref}(\alpha, \beta) = A_{ref} \frac{e^{-iku}}{u}$$

where

$$u = \left[u_o^2 + (\alpha - \alpha_o)^2 + (\beta - \beta_o)^2 \right]^{\frac{1}{2}}$$

Thus the complex signal amplitude at the hologram plane is

$$U_{holo}(\alpha, \beta) = U_{obj}(\alpha, \beta) + U_{ref}(\alpha, \beta)$$

and the corresponding intensity is

$$I_{holo}(\alpha, \beta) = \left[U_{obj}(\alpha, \beta) + U_{ref}(\alpha, \beta) \right] \left[U_{obj}(\alpha, \beta) + U_{ref}(\alpha, \beta) \right]^*$$

$$= |U_{obj}|^2 + |U_{ref}|^2 + U_{ref}^* U_{obj} + U_{ref} U_{obj}^*$$

For the case of $\gamma = -2$, the last expression is, except for a multi-

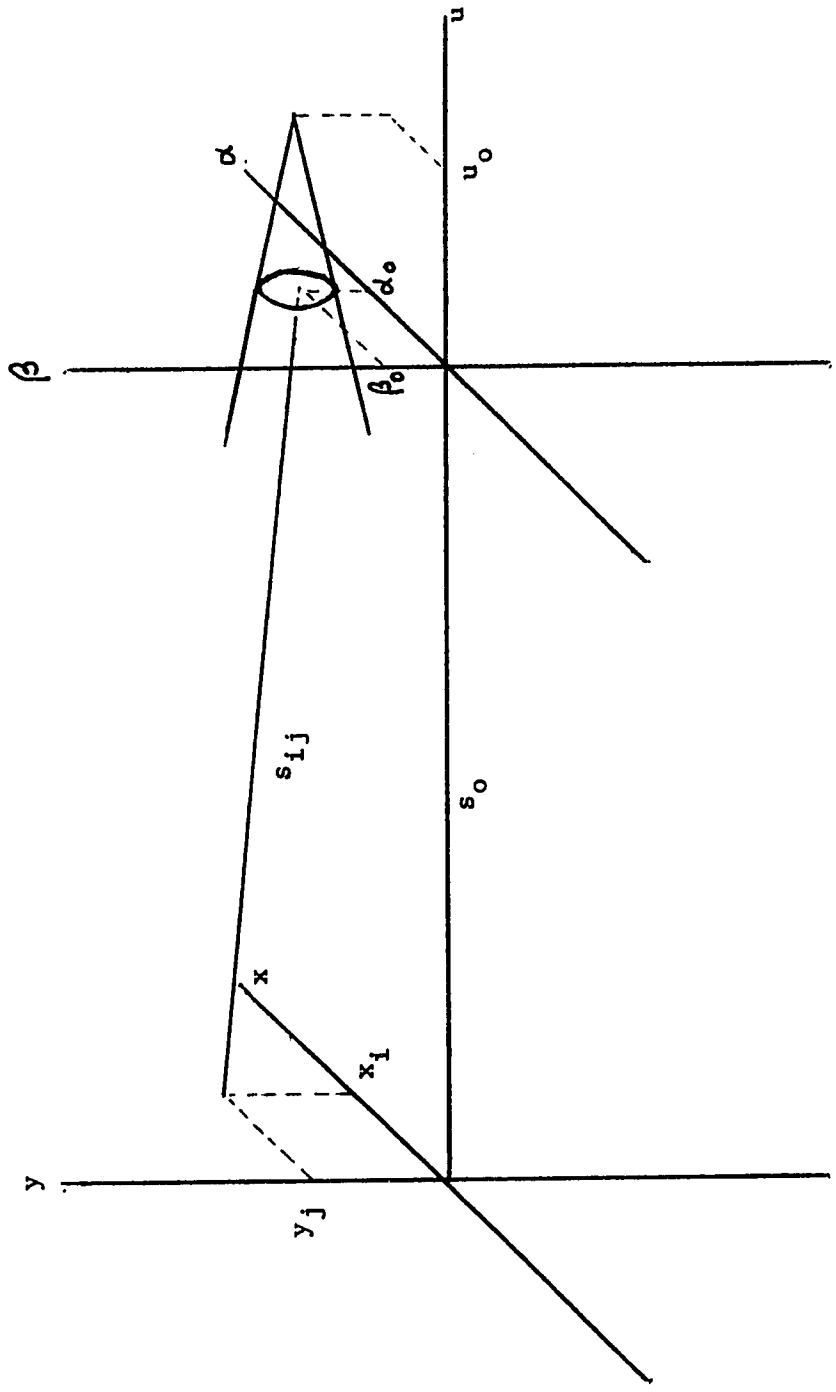

COORDINATES FOR SYNTHESIS

FIGURE 4 - 1

plicative constant, also the expression for the hologram's amplitude transmittance, $T_{holo}(\alpha, \beta)$. Using the notation of Chapter II,

$$T_{holo}(\alpha, \beta) = \sigma I_{holo}(\alpha, \beta)$$

As previously noted, the first two terms of $T_{holo}(\alpha, \beta)$ are noise terms that can mathematically be discarded from the hologram process. Since the synthetic computer generated hologram is not encumbered by the same constraints as the physical holographic process, these terms can be suppressed. Recalling that the complex amplitude, U, was defined as the time-independent portion of the complex analytic signal, it is apparent that the virtual image term, T_3, cannot be discarded. Rather, it must be combined with T_4 to form the real, or physical signal. Note that T_3 and T_4 are the transmittance terms corresponding to the third and fourth terms of the above expression for I_{holo}. Thus, the transmittance function to be synthesized becomes

$$T_{3\&4}(\alpha, \beta) = 2 \text{ RE} \left[U^*_{ref}(\alpha, \beta) \, U_{obj}(\alpha, \beta) \right]$$

$$= 2 \frac{A_{ref}}{u} \sum_{ij} \frac{A_{ij}}{s_{ij}} \cos \left[k(s_{ij} + u) + \phi_{ij} \right]$$

where ϕ_{ij} is the phase of $A_{ij} A^*_{ref}$.

Closer examination of $T_{3\&4}$ reveals that it is capable of assuming negative values. This is not consistent with the properties of the recording medium. In the optically produced case, the U_1 and U_2 terms, serving as a bias, prevent this from occurring. In the synthetic case, a bias term is also required. Let this term be

$$T_{bias} = 2 \frac{A_{ref}}{u_{min}} \sum_{ij} \frac{A_{ij}}{s_{ij\,min}}$$

Noting that $u \geq u_o$ and $s_{ij} \geq s_o$, this bias can safely be adopted as

$$T_{bias} = 2 \frac{A_{ref}}{u_o s_o} \sum_{ij} A_{ij}$$

The expression for the transmission of the synthetic hologram then becomes

$$T_{syn}(\alpha, \beta) = 2 \frac{A_{ref}}{u_o s_o} \sum_{ij} A_{ij}$$

$$+ 2 \frac{A_{ref}}{u} \sum_{ij} \frac{A_{ij}}{s_{ij}} \cos \left[k(s_{ij} + u) + \phi_{ij} \right]$$

Employing the paraxial approximation as before, i.e.

for amplitude considerations

$u = u_o$

$s = s_o$

for phase considerations

$$u = u_o + \frac{(\alpha - \alpha_o)^2 + (\beta - \beta_o)^2}{2u_o}$$

$$s_{ij} = s_o + \frac{(\alpha - x_i)^2 + (\beta - y_j)^2}{2s_o}$$

the transmission function is

$$T_{syn}(\alpha, \beta) = 2 \frac{A_{ref}}{u_o s_o} \sum_{ij} A_{ij} \left\{ 1 + \cos \left[u_o + s_o \right. \right.$$

$$+ \frac{(\alpha - \alpha_o)^2 + (\beta - \beta_o)^2}{2\, u_o} + \frac{(\alpha - x_i)^2 + (\beta - y_j)^2}{2\, s_o} \Big] \Big\}$$

It should be noted that in the actual production of the synthetic hologram, a T_{offset} was added to raise T_{syn} above the fog level of the film.

An interesting side effect of utilizing point sources for the data mask should also be noted. In normal photography, any portion of the scene being recorded is recorded only on one area of the film. If that area of the photograph is destroyed, all information about that portion of the scene is lost. Likewise, if a hologram of a data mask with large bit holes is made using non-diffuse light, a similar result occurs. To overcome the possibility of a small scratch or a speck of dust destroying information completely, holographers can diffusely illuminate objects. This results in light from every portion of the object scattering to every area segment of the film. Consider the effect of decreasing the size of the data bit holes. As the holes are decreased in size, their diffraction patterns at the hologram plane increase. For the limiting case of point 'holes', the diffraction pattern becomes infinite. As a result, the information from any one bit is stored everywhere on the hologram. Thus, the synthetic hologram developed in this Chapter possesses the properties of a diffuse hologram.

Digitalization

Inherent in this synthesis was the need to convert the transmission function, $T_{syn}(\alpha, \beta)$, from a continuous function of α and β in-

to a discrete function of those coordinates. In accomplishing this, it is, of course, necessary to sample the α, β plane. To this end, the sampling rate had to be determined.

Since frequency is defined as[53]

$$f \triangleq \frac{1}{2\pi} \frac{\text{d phase}}{\text{d variable}}$$

the spatial frequency component of $T_{syn}(\alpha, \beta)$ in the α direction is

$$f_\alpha = \frac{1}{2\pi} \frac{d\ (k(s_{ij} \mp u) \mp \phi_{ij})}{d\ \alpha}$$

$$f_\alpha = \frac{1}{\lambda} \left[\frac{\alpha' - \alpha_o}{u_o} \mp \frac{\alpha - x_i}{s_o} \right]$$

Thus the Nyquist Rate is

$$N.R_\alpha = \frac{2}{\lambda} \left[\frac{\alpha - \alpha_o}{u_o} \mp \frac{\alpha - x_i}{s_o} \right]$$

For the example of page 113 of Chapter III,

$$N.R._\alpha = \frac{2}{5145(10^{-8})} \left[\frac{0.03}{3} \mp \frac{7.8}{15} \right]$$

$$= 19{,}400 \text{ lines per cm.}$$

$$= 1{,}940 \text{ lines per mm.}$$

Since the resolution limit of Agfa 10E70, a high resolution film used for holography is 2800 lines per mm, it is possible to generate such

---

53 A. Carlson, Communications Systems: An Introduction to Signals and Noise in Electrical Communication, McGraw Hill, New York, 1968, p. 223.

a hologram. It should be noted that the validity of using the Nyquist rate as the minimum rate to prevent aliasing of the Fresnel transform has been shown in the literature.[54,55,56]

A more stringent requirement was placed on the film's resolution limit when the effect of sample pulse width was considered. As is well known in communications theory,[57,58] the effect of permitting the Nyquist rate sampling pulse width to approach a duty cycle of fifty percent is to de-emphasize the high frequency portion of the signal's spectrum. In terms of the memory system, this means that, as the synthetic hologram's sample pulse width increases, the outer data bits of the imaged data mask are subject to a relative decrement in intensity. Provided that this decrement is not too severe, it can be compensated for by varying the sensor amplification with position. Interpreting this requirement, the resolution limit of the film must be greater than the Nyquist rate; exactly how much greater depends on the sensors' sensitivity and dynamic range.

---

54 T. Haung, "Digital Holography", IEEE Spectrum, Vol. 59, No. 9, Sept. 1971, p. 1344.

55 W. Cathey Jr., "The Effect of Finite Sampling in Holography", Optik, Vol. 27, 1968, pp. 317-26.

56 W. Carter, "Aliasing in Sampled Holograms", Proceedings of IEEE, Vol. 56, Jan. 1968, pp. 96-8.

57 A. Carlson, Op. Cit., pp. 283-6.

58 E. Craig, Laplace and Fourier Transforms for Electrical Engineers, Holt, Rinehart, and Winston, New York, 1966, pp. 394-8.

This discussion would not be complete without acknowledging the presence of quantization noise. A theoretical analysis of the effect of this quantization noise on the output image would be extremely complicated since the quantization is taking place in the Fresnel domain of that image. Therefore, if it is desired to know the specific effects of the quantization on that output image, the experimental avenue appears to be the best approach. For the memory system, the quantization noise's effects were minimized by utilizing sixteen levels of exposure. It should be noted that the effects of binary, or two level, quantization have been analyzed in the literature.[59,60]

Implementation

As a first step toward implementing production of a synthetic hologram, a Fortran program was written to evaluate $T_{syn}(\alpha,\beta)$. This program is supplied in Appendix IV

The second step was the design of a system capable of converting the numerical output of the computer into a hologram. A block schematic of the system selected is shown as Figure 4-2. This particular system was chosen because, in utilizing the available acoustic coupler, teletype, oscilloscope, and camera, its incremental cost of approximately $300.00 was within the project's budgetary con-

---

59 A. Kozma and D. Kelly, "Spatial Filtering for the Detection of Signals Submerged in Noise", Applied Optics, Vol. 4, Apr. 1965, pp. 387-92.

60 J. Goodman, Op. Cit., pp. 235-40.

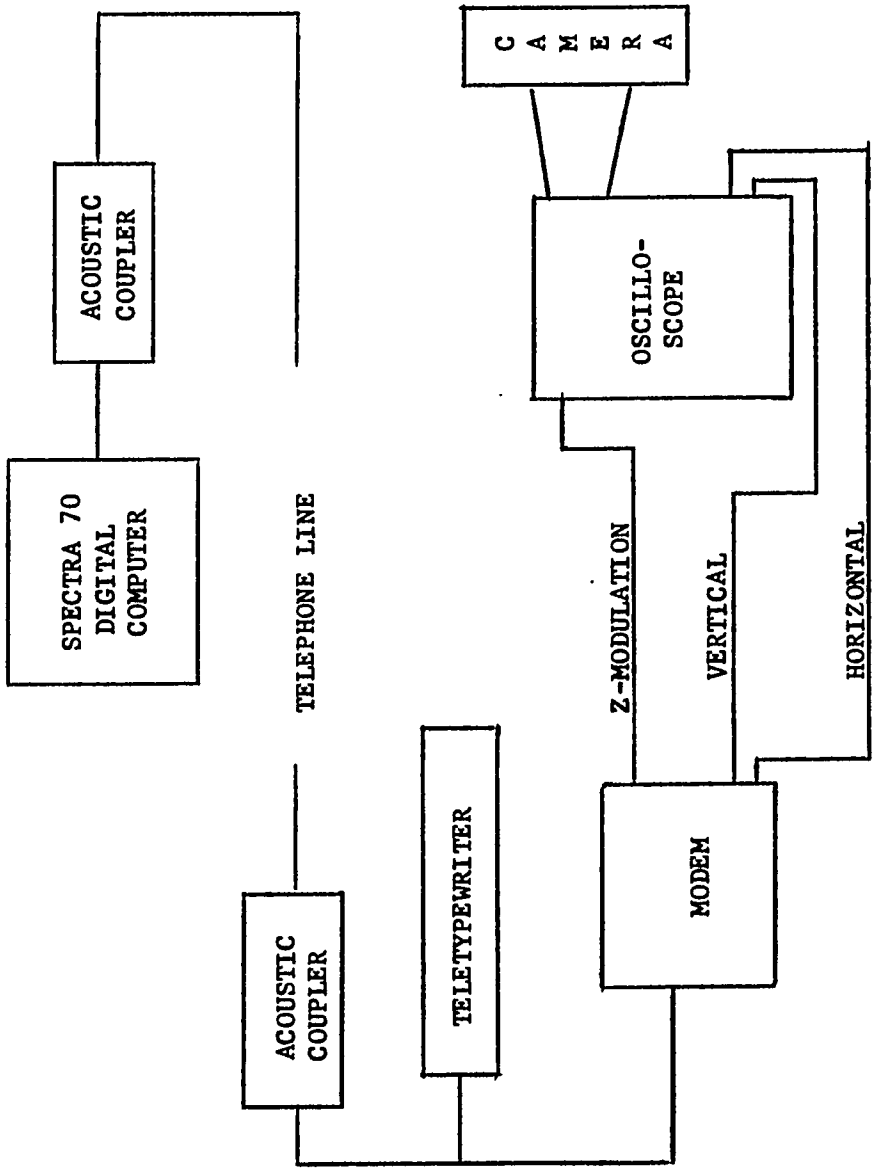

SYSTEM SCHEMATIC

FIGURE 4 - 2

straints. Furthermore, in not requiring special concessions from the Computer Center, it allowed for flexibility of scheduling.

An examination of the available teletype system indicated that the output of the acoustic coupler was the point in the teletype system most suitable to serve as the input to the hologram generator. Its suitability arises from the fact that the audio frequency-shift keying has been transformed into the standard voltage-level ASCII pulse-code modulation signal and from the fact that the output of the acoustic coupler, being a jack connector, lent itself to a temporary intercept that did not require a modification of the existing teletype system hardware.

From a system design point of view, the modem of Figure 4-2 transforms the serial PCM output of the acoustic coupler into a PDM signal. This PDM signal is then applied to the z-axis input of the oscilloscope. This input switches the CRT spot 'on' for the duration of the PDM pulse.

It was originally intended to convert the serial PCM output of the acoustic coupler into a PAM signal. An examination of the available Fairchild 766 oscilloscope showed that its intensity circuitry interacted with its focusing circuitry. As a result, an attempt to amplitude modulate the CRT spot would produce de-focused spots. This could not be tolerated since high resolution was needed to meet the sampling rate requirements. Examination of the oscilloscope also revealed that the Z-modulation input was capacitor-coupled to the -1400

volt cathode of the CRT. Since the asynchronous nature of the input data would produce undesirable transients if a-c coupled to the cathode, it was necessary to devise a d-c coupling scheme. The scheme, utilizing photo-electric devices, is shown in a subsequent figure.

At the end of the PDM pulse, the α position is stepped to the right by one increment, and then the process is repeated. The increment is chosen to be equivalent to 1/256 of a line width. After 256 points have been recorded in the α direction, one increment is made in the β direction and the α position is re-initialized. This procedure continues until the 256 by 256 position matrix of the synthetic hologram has been completed. To prevent computer command signals, e.g. carriage control and line feed, from producing erroneous points on the hologram, a digital filter was designed to discriminate against all but the desired sixteen character codes.

The third step in the investigation, the component specification and the hardware fabrication was assigned to R. Mozzone as part of his Master's Thesis work. For the details of this step, the reader is, therefore, referred to his thesis.[61] However, for the sake of completeness, the system diagrams are included as Figures 4-3A,B,C.

Next, a rough check of the step scale of gray generated by the complete system was performed to ensure reasonable linearity within

---

[61] R. Mozzone, "A System for Generating Digital Holograms", Master's Thesis, Newark College of Engineering, E.E. Dept., 1974.

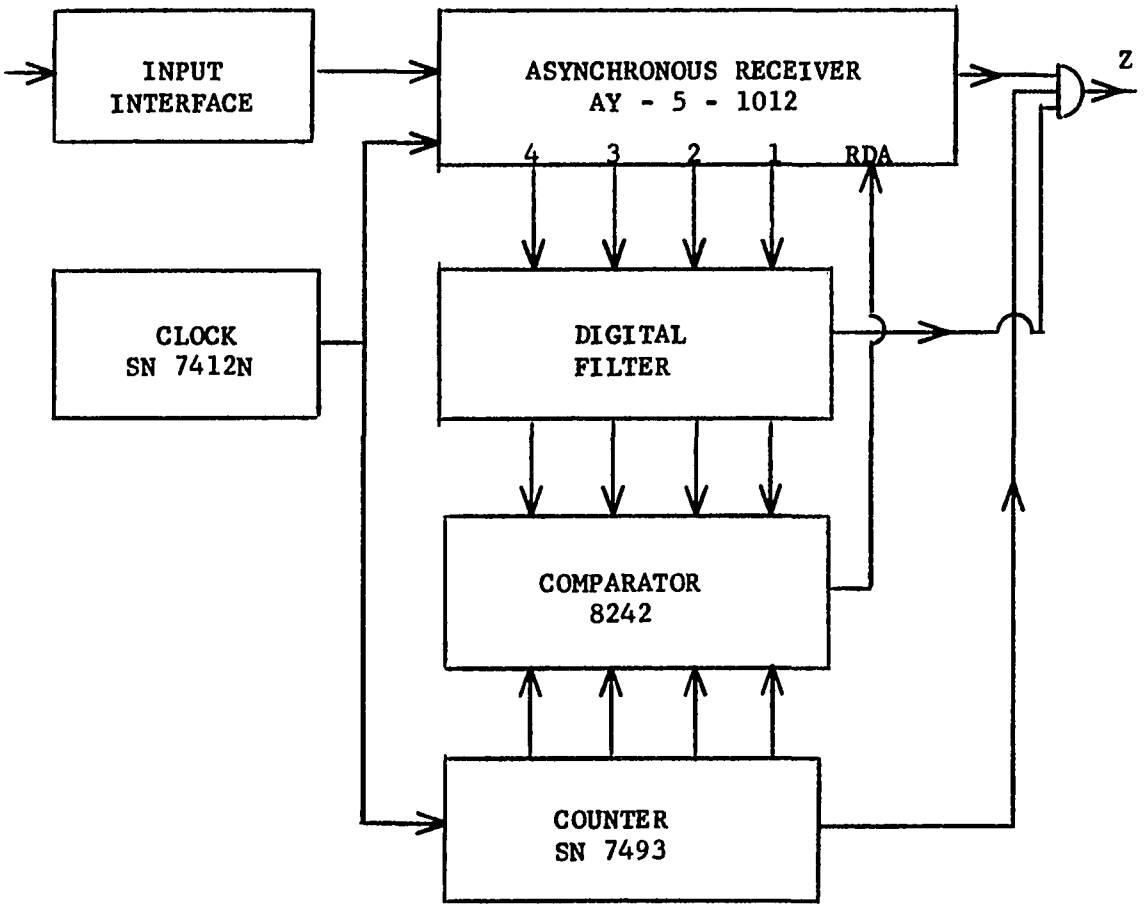

MODEM RECEIVER

FIGURE 4 - 3A

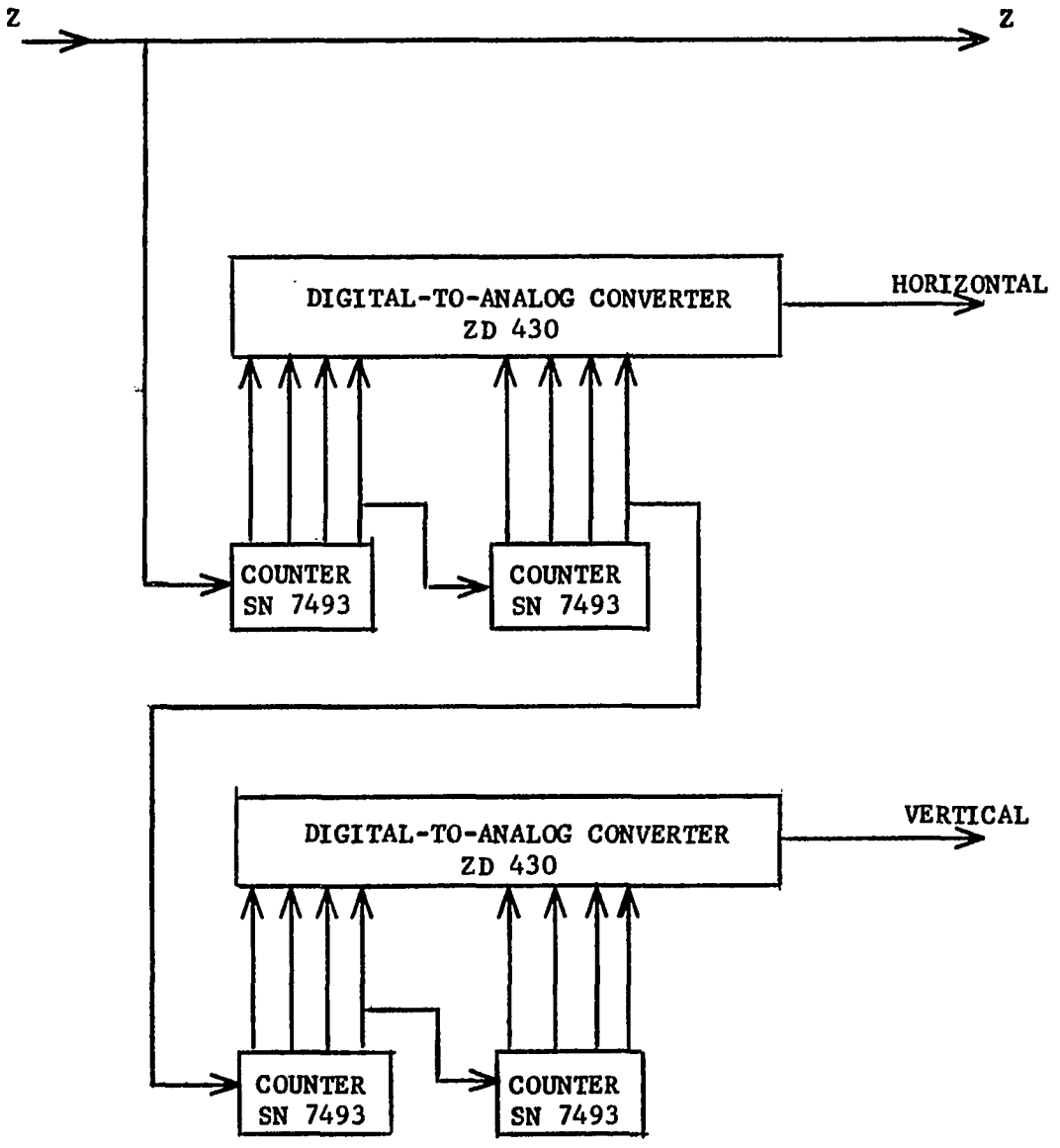

HORIZONTAL & VERTICAL
STEP GENERATORS

FIGURE 4 - 3B

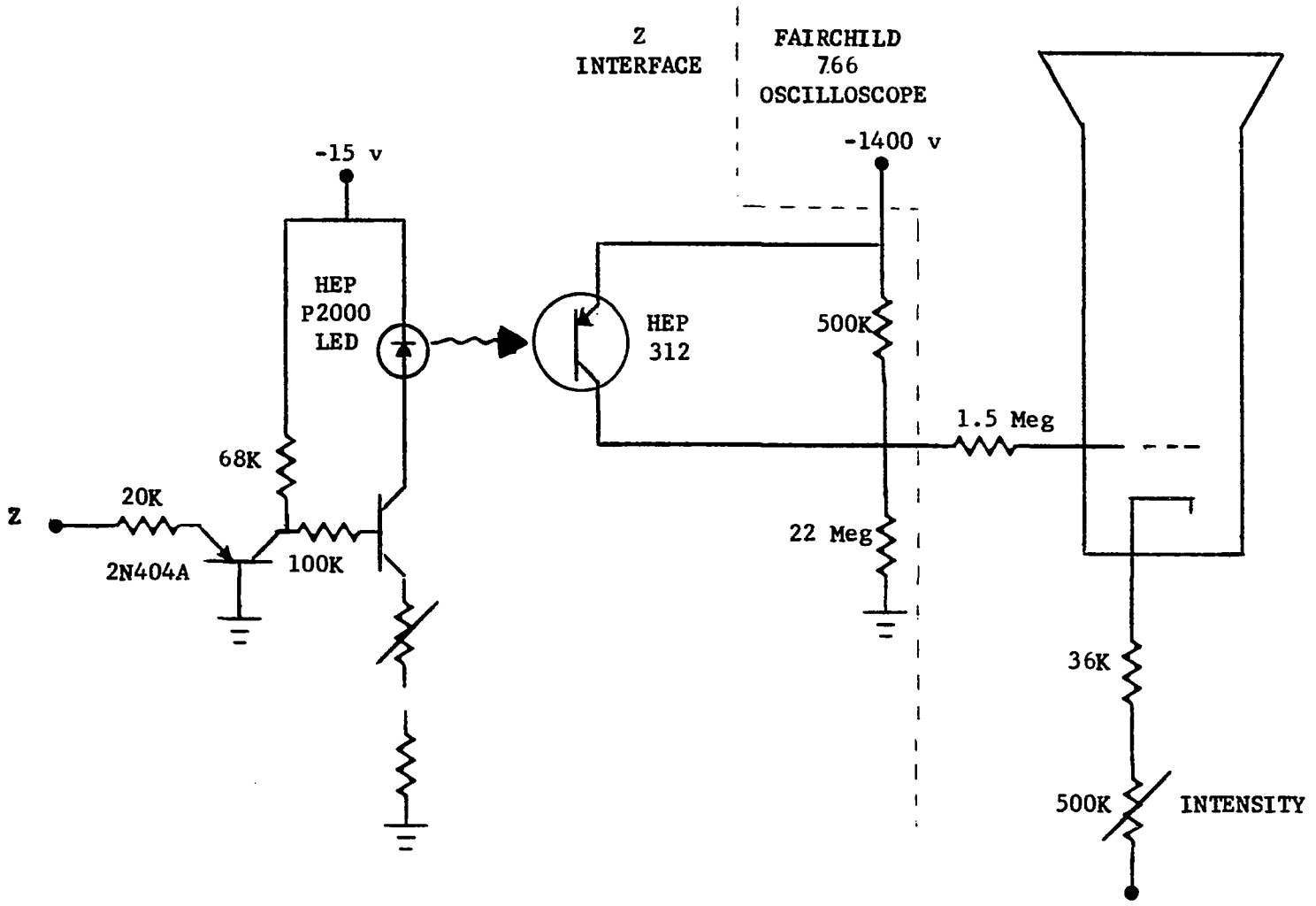

Z - INTERFACE

FIGURE 4 - 3C

the film exposure latitude. Using a high-speed PCM generator, the preliminary test supplied forty-five seconds of continuous 'ones' to the input of the modem; this was followed by fifteen seconds of 'zeros'. This sequence was repeated for ascending input values, i.e. forty-five seconds of 'twos' followed by fifteen seconds of 'zeros', then forty-five seconds of 'threes' followed by fifteen seconds of 'zeros', etc. It should be noted that a line of 'fifteens' was first produced to identify the starting point on the film.

The result was a gray scale as shown in Figure 4-4A,B. An exact analysis of this gray scale would require a 'Microdensitometer', an optical instrument used to measure the densities of transparencies. A qualitative visual analysis was made since this instrument was not readily available. This analysis indicated that the exposure due to a 'one' exceeded that necessary to rise above the toe, or gross fog, level of the film as defined in Figure 4-4C. The analysis also indicated that the exposure due to a 'fifteen' was below that corresponding to the "shoulder" of the curve, or saturation, level of the film. From this it was concluded that the exposures were in the region where the γ of the developed picture was essentially constant. Interpreting this, it appears that the film was acting as an 'ideal' medium.

As a final system test, the input parameters of the program HOLOGR were chosen so as to produce a known output pattern. The input geometry synthesized by these parameters is shown in Figure 4-5. The program, with these particular parameter values, was labeled FRING3.

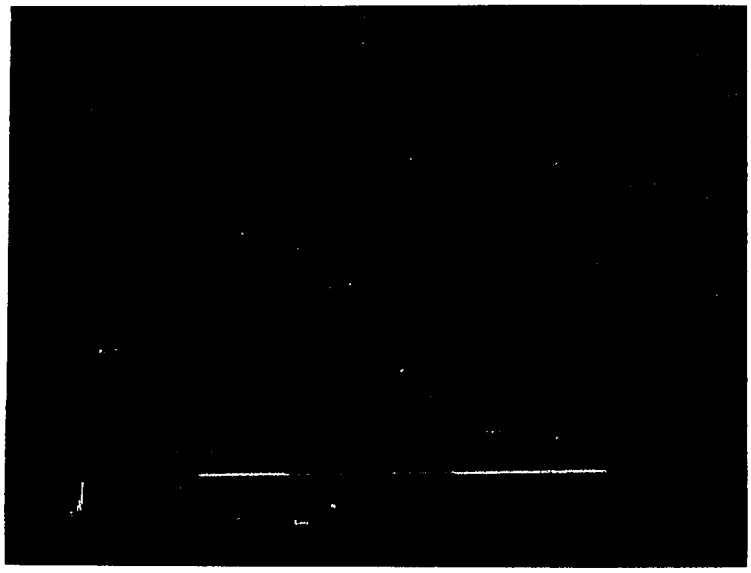

EXAMPLE OF GRAY SCALE

FIGURE 4 - 4A

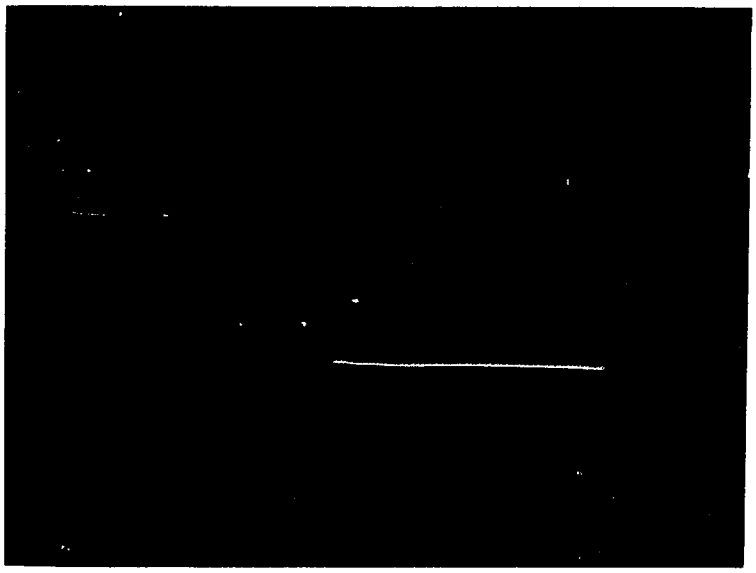

EXAMPLE OF GRAY SCALE

FIGURE 4 - 4B

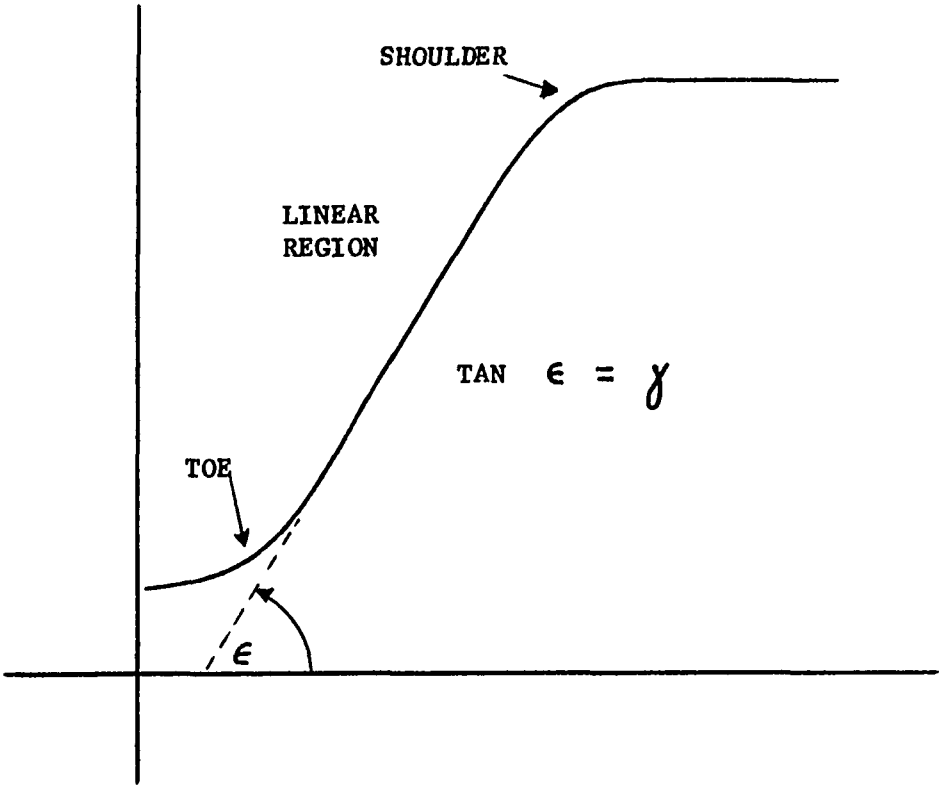

HURTER-DRIFFIELD CURVE

FIGURE 4 - 4C

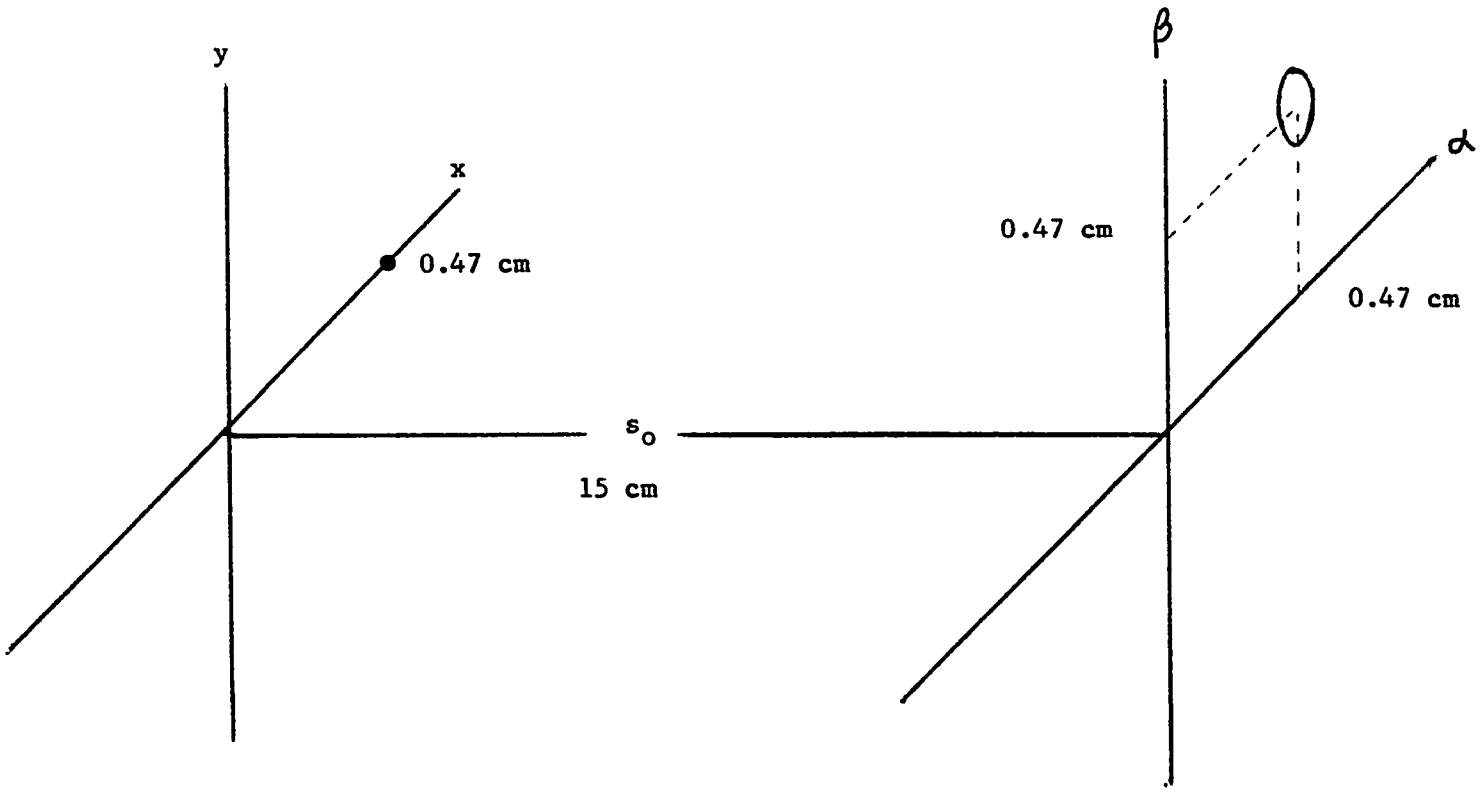

SYNTHESIZED GEOMETRY

FIGURE 4 - 5

The hologram pattern for this configuration should be the familiar one of Fresnel Rings. An example of these rings is shown in Figure 4-6. These rings occur at distances d_n from the center, where

$$d_n = \sqrt{2 s_o n \lambda}$$

For the test page, $d_{min} = 0.44$ cm, $d_{max} = 0.50$ cm, $s_o = 15$ cm, and $\lambda = 5145$ A°. A simple calculation indicated that $n_{min} = 125$ and $n_{max} = 162$. Thus, the text pattern should show approximately 37 lines. From the figure, it can be shown that the individual lines subtend less than 3.6° of arc. Thus they are approximately straight lines and are oriented parallel to the α axis.

The initial execution of FRING3 produced the output shown in Figure 4-7. It should be noted that since the minimum transmission time was 1.65 hours, the test runs were, as in this case, frequently terminated before completion. The 1.65 hour time figure is the result of using the low-frequency telephone line to transmit data from the computer to the teletypewriter. The teletype's 110 baud rate allows only eleven 10-bit characters to be transmitted per second. Thus, provided no time-sharing delays are encountered, 5,958 seconds are required to transmit the 256-by-256 characters of the hologram. However, it should be noted that during a typical three hour transmission period, only ten minutes of computer time was used. If one's intent were to design a system suitable for the 'full-scale' production of these synthetic holograms, it is assumed that he would take advantage of this order of magnitude time reduction. This might be accomplished by connecting the modem directly to a mini-computer.

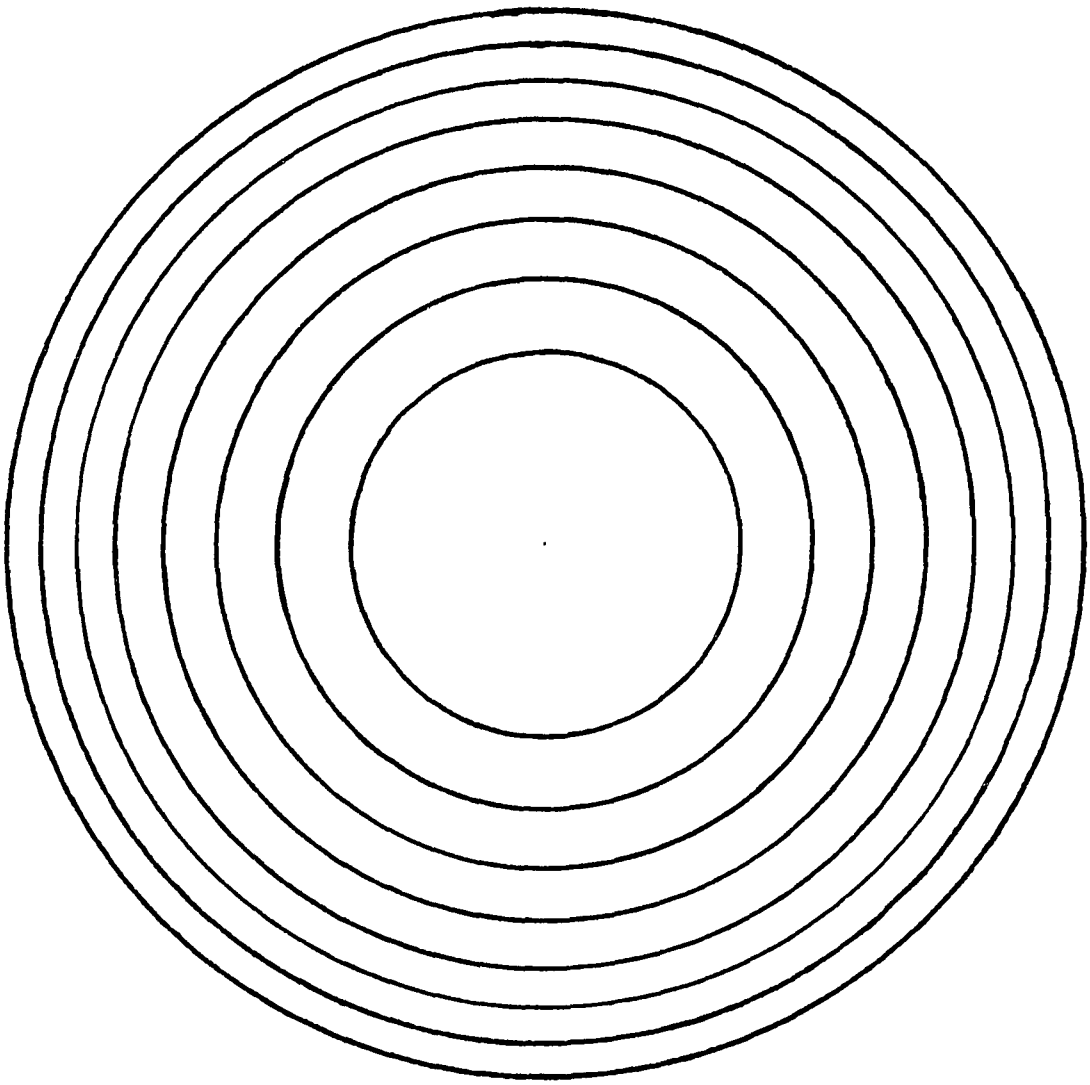

FRESNEL RINGS

FIGURE 4 - 6

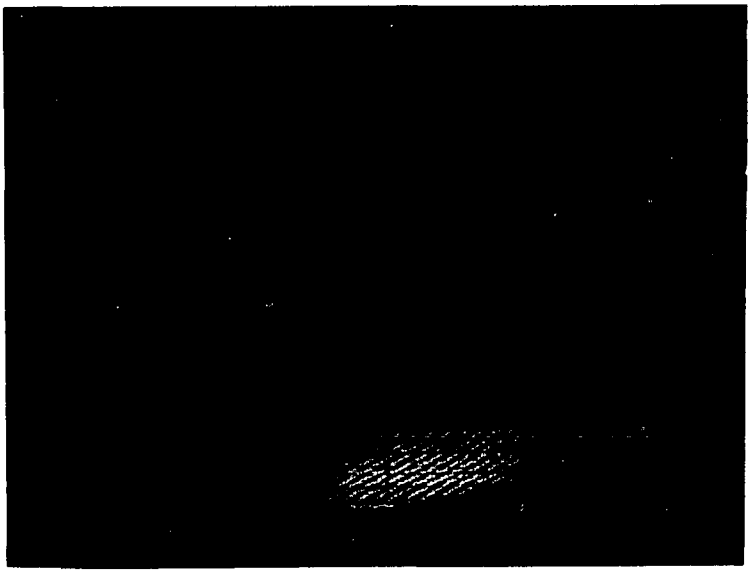

EFFECT OF NOISE BITS

FIGURE 4 - 7

However, since the intent of this study was to show the feasibility of producing synthetic holograms through the utilization of a particular technique, it was not necessary to acquire such a mini-computer.

An analysis of the pattern in Figure 4-7 indicated that extra bits were being produced; i.e.,

line 1: 254 legitimate bits, 2 illegitimate bits

line 2: 247 legitimate bits, 9 illegitimate bits

line 3: 248 legitimate bits, 8 illegitimate bits

etc.

It was these extra, or non-legitimate, bits that accounted for the non-circular shape of the page. The source of these extra bits was traced to a mal-adjusted modem interface. The mal-adjustment resulted in the interface acting as a linear amplifier for the noise on the input line rather than a binary switch with a threshold that eliminated the noise.

The interface was re-adjusted to correct this and FRING3 was executed again. The result is shown in Figure 4-8. The page appeared to have the proper circular shape. However, it was noted that the lines were not vertical, but were canted to the right. To check the assumption that the cause of the canting was thermal drift in the oscilloscope's vacuum tube horizontal amplifier, a uniform signal was supplied to the modem. The result is Figure 4-9, proving the assumption to be correct. The drift was reduced by replacing the oscilloscope's horizontal amplifier.

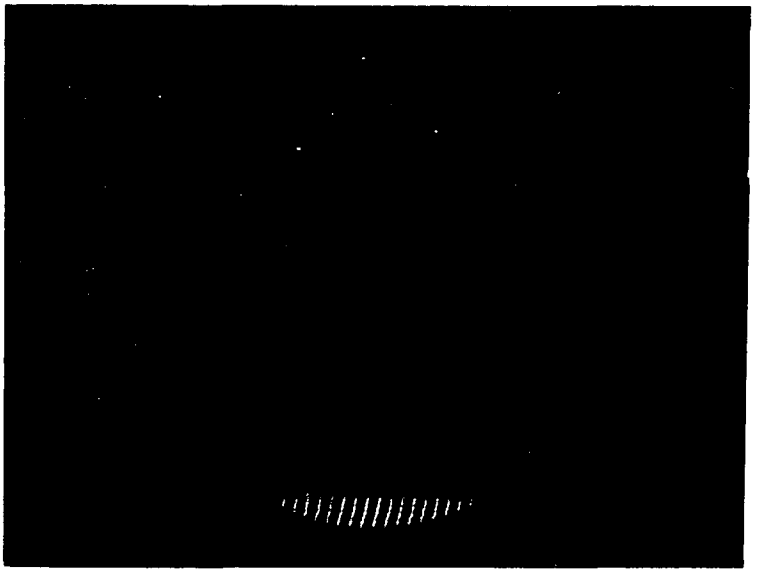

HORIZONTAL DRIFT

FIGURE 4 - 8

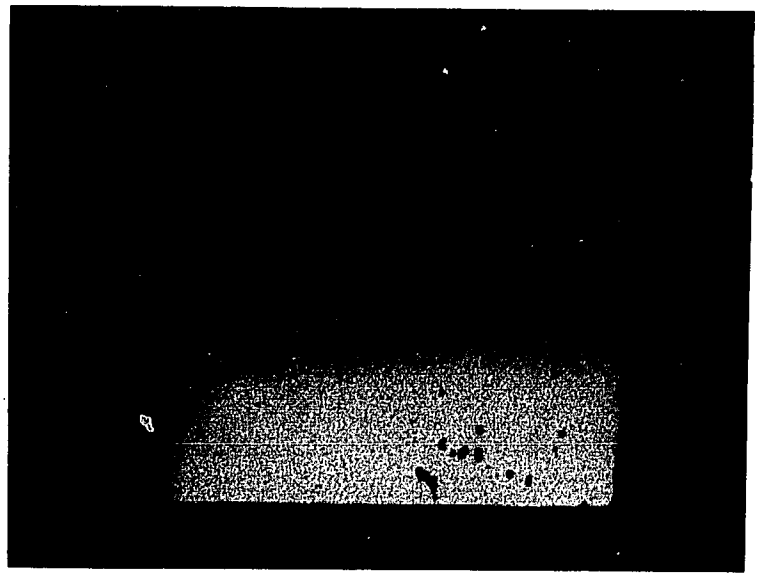

CONFIRMATION OF HORIZONTAL DRIFT

FIGURE 4 - 9

A subsequent execution of FRING3 resulted in Figure 4-10. This picture, which required approximately three hours to construct, revealed another problem; i.e., an intensity drift. It should be noted that the intensity was set before each program execution through a trial and error technique; i.e., the intensity control on the oscilloscope was adjusted until a suitable gray scale was photographed. A suitable scale was defined as one that included both knees of the Hurter-Driffield curve. To substantially reduce the severity of the intensity drift, it was necessary to allow a warm-up period of approximately ninety minutes for the oscilloscope. During the period, it was required that the CRT beam intensity be adjusted to approximately the value used in making the hologram. To protect the phosphor, the beam was directed off-screen.

An examination of Figure 4-10 showed that it possessed thirty-seven lines and that those lines were approximately straight and parallel to the axis. Since this agreed with the predicted output, it was concluded that FRING3 proved the correctness of the program HOLOGR. It should be noted that this output, being six centimeters in diameter, is a 100X magnification of the desired hologram.

Because the modem was connected in parallel with the teletypewriter, a hard copy of the output of FRING3 was produced simultaneously with the production of Figure 4-10. Several of the middle rows of the output are shown as Figure 4-11 where the symbols 0,1,2,3,4,5,6, 7,8,9,J,K,L,M,N,Ø are the hexadecimal code in ascending order. While Figure 4-11 confirms the presence of 37 lines, it also indicates the gray scale that should be displayed in Figure 4-10.

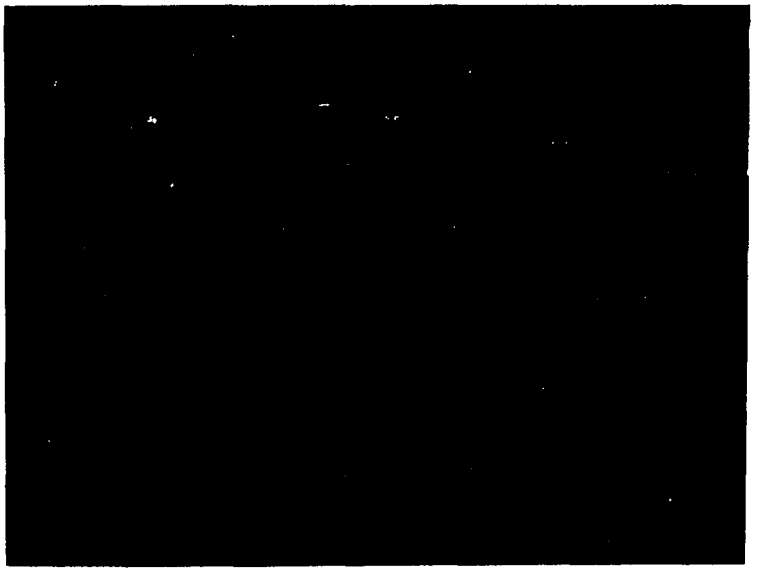

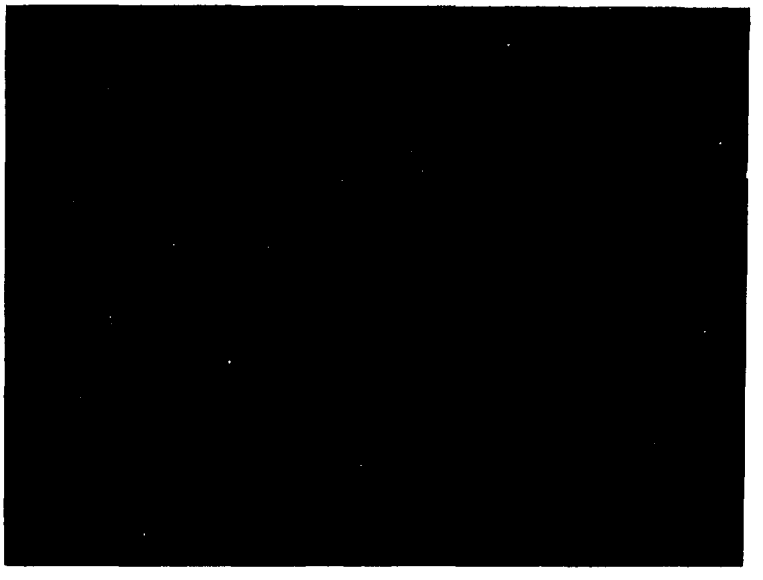

PARTIAL AND COMPLETED FRING3 OUTPUT

FIGURE 4 - 10

```
028NØK5115KØM82039NØJ4016LØM7104JØN93028NØK5016LØM7104KØN82039NNJ4028M
ØK5016LØL6105KØM7204JØN8203JNN93039NNJ3029NØJ4028NØJ4028NØJ4028NØJ4028
NØJ4028NNJ3039NN9303JNN8204JØM8205KØM7116LØL5017MØK4028NN9303JØN8205KØ
L6117MØK4029NN9204KØM6116MØK4029NN8204KØL6117M
028NØK5115KØM82059NØK4016LØM7104JØN93028NØK5016LØM7104KØN82039NNJ4028M
ØK5016LØL6105KØM7204JØN8203JNN93039NNJ3029NØJ4028NØJ4028NØJ4928NØJ4028
NØJ4028NØJ3039NN9303JNN8204JØN8205KØM7116LØL5017MØK4028NN9303JØN8205KØ
L6117MØK4029NN9204KØM6116MØK4029NN8204KØL6117M
028NØK5115KØM82039NØK4016LØM7104JØN93028NØK5016LØM7104KØN82039NNJ4028M
ØK5016LØL6105KØM7204JØN8203JNN93039NNJ3029NØJ4028NØJ4028NØJ4028NØJ4088
NØJ4028NØJ3039NN9303JNN8204JØN8205KØM7116LØL5017MØK4028NN9303JØN8205KØ
L6117MØK4029NN9204KØM7116MØK4029NN9204KØL6117M
028NØK5115KØM82039NØK4016LØM7104JØN93028NØK5016LØM7104KØN82039NØJ4027M
ØK5016LØL6105KØM7204JØN8203JNN93039NNJ3028NØJ4028NØJ4028NØJ4028NØJ4028
NØJ4028NØJ3039NN9303JNN9204JØN8205KØM7116LØL5017MØK4028NN9303JØN8205KØ
L6117MØK4029NN9204KØM7116MØK4029NN9204KØL6117M
028MØK5115KØM82039NØK4016LØM7104JØN93028NØK5016LØM7104KØN82039NØJ4027M
ØK5016LØL6105KØM7204JØN8203JNN93039NNJ3028NØJ4028NØJ4028NØJ4028NØJ4028
NØJ4028NØJ3039NN93039NN9204JØN8204KØM7116LØL5117MØK4028NN9303JØN8205KØ
L6117MØK4029NN9204KØM7116MØK4029NN9204KØL6117M
```

FRING3 HARD COPY SAMPLE WITH LINE STRUCTURE EMPHASIZE

Figure 4-11

Furthermore, Figure 4-11 shows that each intensity cycle, i.e. line, of Figure 4-10 is composed of seven spots.

The effects of two additional signal problems that were experienced are displayed in Figures 4-12 and 4-13. It was determined that the first problem was the result of noise triggering the reset line of the counter. This problem was solved by shielding that line. The second problem was identified as being the result of messages from the computer console operator. This unwanted intervention was decreased to a minimum by employing the computer command statements that suppress computer system broadcasts and messages; i.e., /BCNTRL MES=NO,BCST=NO. Figure 4-14 is an example of the combined effect of these two problems.

Having tested the system and validated its correctness, and having identified the operational problem areas and remedied them as well as possible, the next step was to synthesize a hologram representative of the type suitable for application as a computer memory. Therefore, the system depicted in Figure 4-15 was synthesized. The data mask bit separation corresponds to that required by η_{spread} for the case of $\Delta\lambda$ = 100A^{o}, chapter size = 1cm, s_o = 15cm, CRT spot size = 0.05cm, u_o = 3cm, m = n = 20, and mechanical interpage cross-talk suppression. For the sake of simplicity, only three of the data mask bits were 'ones'. Note that these three bits are adjacent bits and that they straddle the center of the data mask. The resultant synthetic hologram is shown in Figure 4-16. The calibration gray scale that was made after a warm-up period of one-and-a-

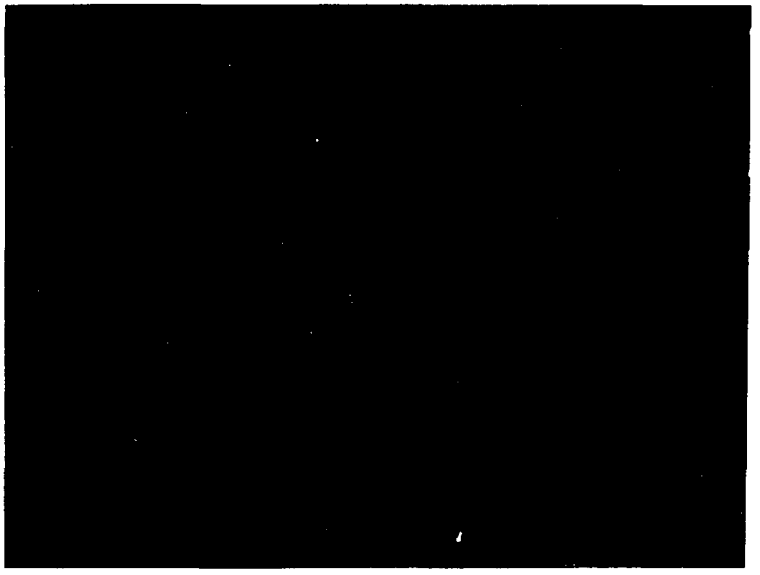

EFFECT OF UNWANTED RESET

FIGURE 4 - 12

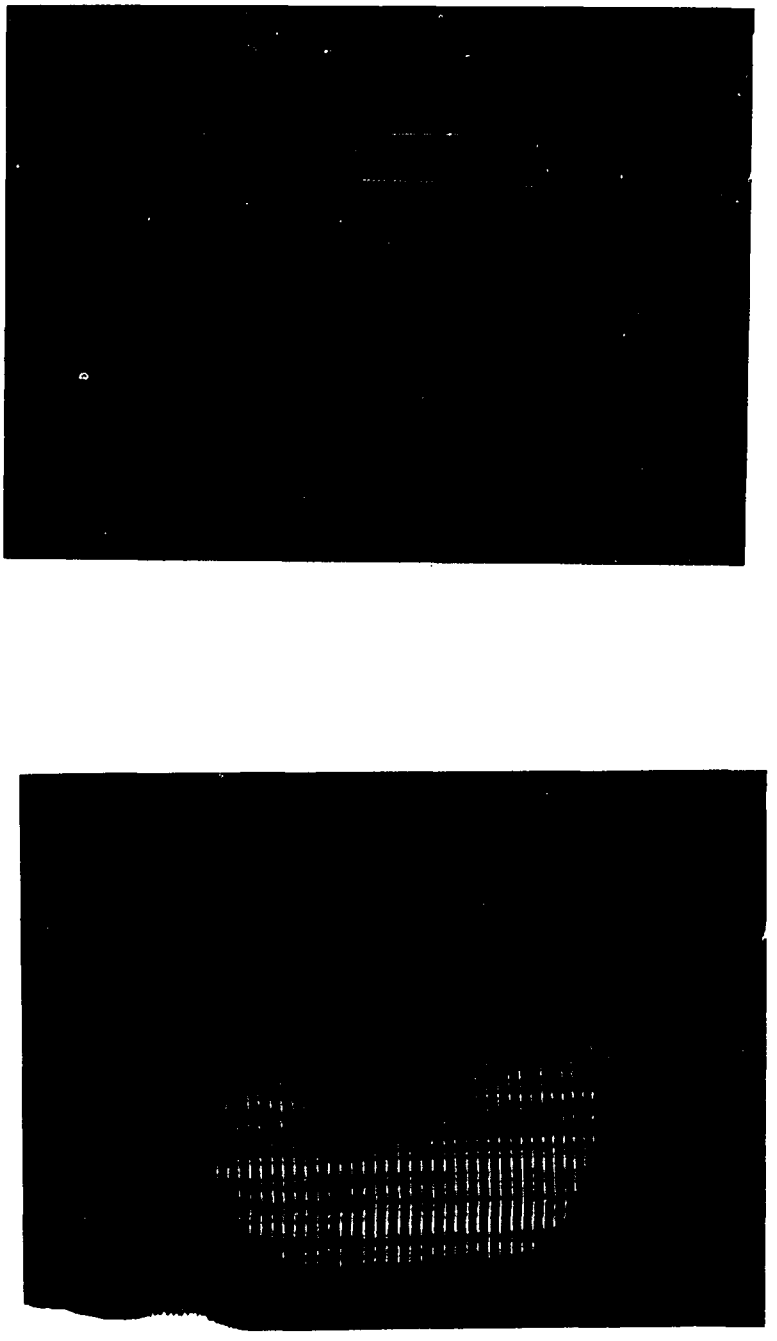

EFFECT OF UNWANTED MESSAGES

FIGURE 4 - 13

COMBINED EFFECT OF UNWANTED MESSAGES AND RESETS

FIGURE 4 - 14

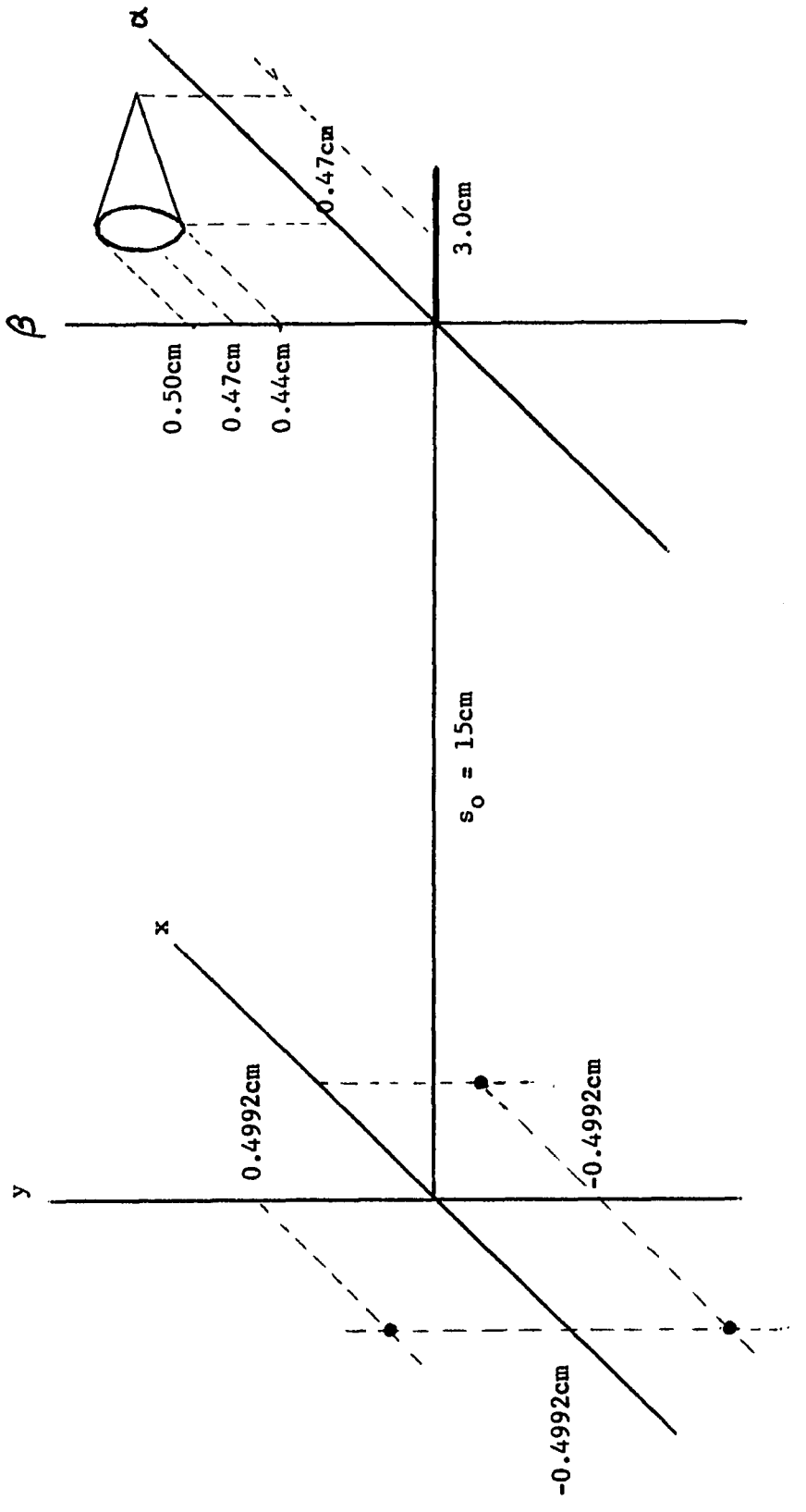

SYNTHESIZED GEOMETRY

FIGURE 4 - 15

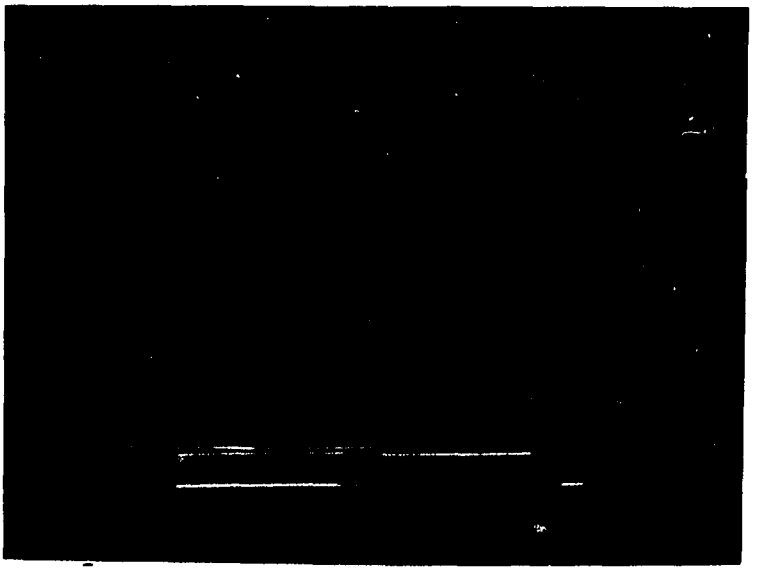

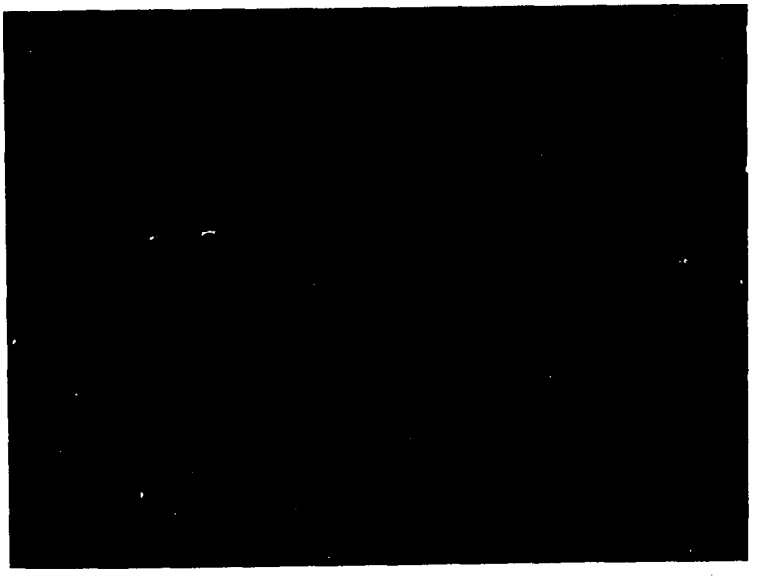

MEMORY HOLOGRAM

FIGURE 4 - 16

half hours and immediately before the hologram is included in that figure. As can be seen, the intensity drift problem is still evident. So that a clearer visualization of the fine structure of the hologram can be obtained, Figure 4-17 is included. This latter figure has, quite evidently, suffered an unwanted 'reset'.

With the attainment of the synthetic hologram of Figure 4-16, the feasibility of producing a synthetic hologram, using this technique, was shown. It was, therefore, decided to halt this phase of the experimental work. This decision was also prompted by the fact that the digital computer was suffering from a malfunction in its communications controller. This malfunction was such that it had become very improbable that the communications link would continuously operate for the required three hours.

Furthermore, it appeared that the recurring problem of intensity drift over the three hour period could only be solved by obtaining an oscilloscope, or other CRT device, which was especially constructed for thermal stability in its intensity circuitry or to which special feedback circuitry was fitted. This equipment was not reasonably available. An alternative solution to the drift problem was to decrease the time necessary to 'paint' the hologram. This time reduction could be accomplished by attaching the modem to a high bit-rate output line of the computer. Note that this would also overcome the problem with the communications controller up-time. This time reduction could also have been accomplished with the aid of a variable speed digital recorder, e.g. record at teletypewriter speed and

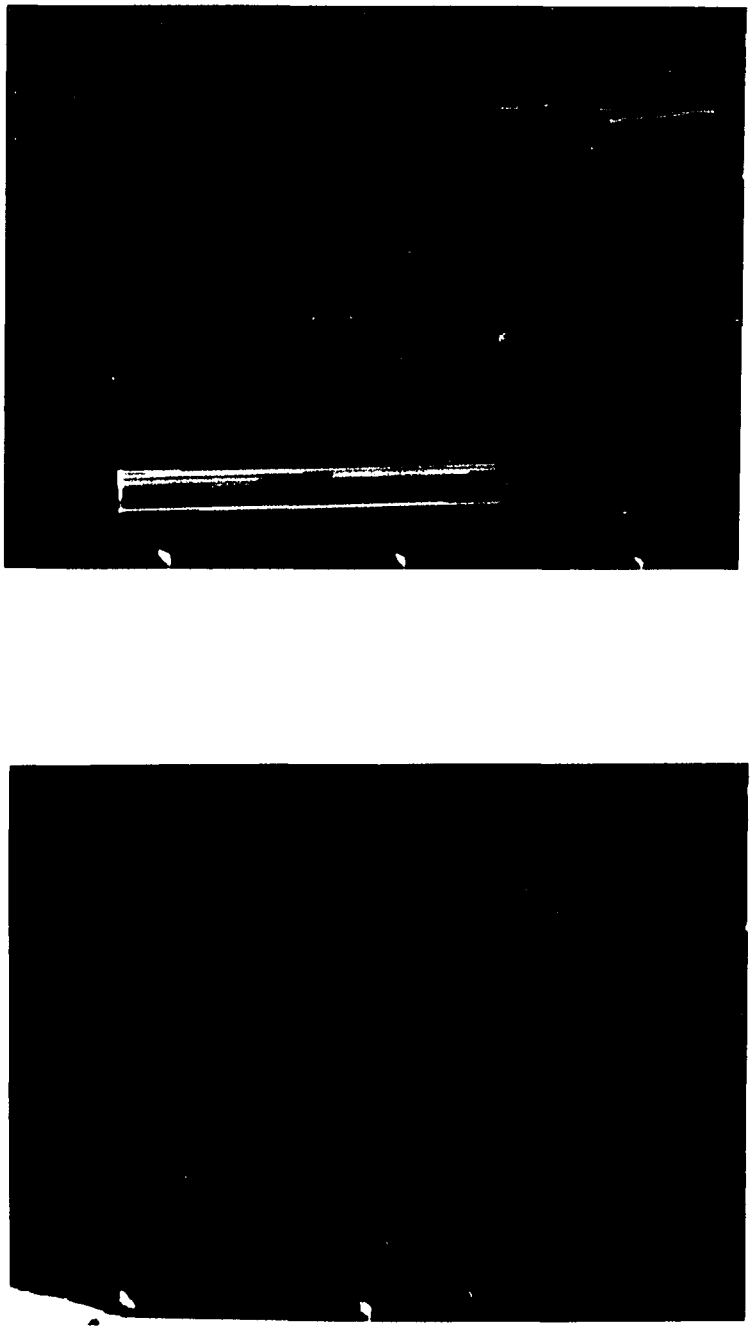

MEMORY HOLOGRAM WITH MESSAGE BITS

FIGURE 4 - 17

play back to the modem at a higher speed. Unfortunately, these options were not available for this project.

Conclusions

While the devices necessary to overcome the production problems were not available to this project, their existence,[62] together with the obtained output shown in Figure 4-16, indicate the feasibility of this approach to the development of a synthetic hologram.

---

[62] Techtran Industries, 580 Jefferson Rd., Rochester, N.Y., produces variable speed recording communications terminal (4100A) which can record at 110 baud rate and play back at 2400 baud rate (factory option).

CHAPTER V

BIT INTENSITY NONUNIFORMITY

Introduction

The preceding chapters were devoted to the system design aspects of a specific optical holographic computer memory system. In this chapter, some consideration will be given to a major problem that has been found when holographic memories, in general, are tested. The problem is that of uniform detectability of the data points. By this is meant that the detected values, in terms of the light energy impinging on the photodetectors, of 'ones' and of 'zeros' fluctuate greatly for the various bits distributed throughout the memory. The values vary to the point that a particular 'zero' may produce a higher output than a particular 'one'. This makes it impossible to design an error free threshold detection scheme.

There are several sources of this nonuniformity. Five are listed in Table 5-1, along with their relative contributions to the nonuniformity problem.[63,64] Of these five causes, interbit diffraction interference was examined in some detail by this research-

---

63 J. T. LaMacchia, W. A. Barrett, & R. L. Townsend, "Non-Uniformity of the Reconstructed Image from Holograms Used in Data Storage", presented at Fall Meeting, Optical Society of America, Oct. 1970, Hollywood, Florida.

64 Dr. LaMacchia was a technical supervisor at BTL assigned the task of reducing non-uniformity in the holographic memory output. Mr. Barrett was assigned the particular task of evaluating the affect of diffraction interference by Dr. LaMacchia. The experimentation was performed in the laboratory of Dr. Townsend and frequent use was made of his expertise with experimentation.

LASER POWER FLUCTUATIONS	(20%)
DEFLECTION EFFICIENCY	(2:1)
HOLOGRAM DIFFRACTION EFFICIENCY	(2:1)
PHOTODETECTOR SENSITIVITY	(2:1)
INTER-BIT DIFFRACTION INTERFERENCE	(2:1)

CAUSES OF NON-UNIFORMITY
AND
THE RANGES OF THEIR INDIVIDUAL VARIATIONS

Table 5-1

er since it showed promise of partial correction through the application of diffraction theory.[65]

The extent of this problem is shown in Figure 5-1. This figure was obtained by horizontally scanning a row of eight bits with a photomultiplier head that was mounted on a motor driven carriage. A servo-system attached to this carriage produced an output voltage that corresponded to the horizontal position of the head. This signal was used to drive the "X" channel of an XY recorder. The output of the PM amplifier was, of course, used to drive the "Y" channel of that recorder. Since the data masks used through-out the experiment reported in this Chapter consisted of bit holes having a nominal radius of 50.8 microns and spaced at 254 micron intervals, a 5 micron pinhole was placed over the face of the PM tube to obtain sufficient resolution to observe the shape of the individual bit images. It should be noted that the images were always produced with a magnification of unity.

Notice that for the hologram produced with the 65 mil diameter aperture at the film plane, the maximum to minimum intensity ratio is approximately 1.4:1; while for the 35 mil hologram, the variation approaches 2:1. This effect of aperture size suggests that one source of the bit-to-bit variation is the diffraction interference

---

65 W. A. Barrett and R. L. Townsend, "Bit Intensity Nonuniformity in an Optical Memory", Technical Memorandum MM71-2212-2, Bell Telephone Laboratories.

35 MIL APERTURE

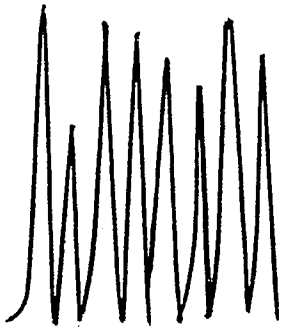

65 MIL APERTURE

INTENSITY OF BIT PATTERN
FOR TWO APERTURE SIZES

FIGURE 5 - 1

between the neighboring bits of the data mask.

Of course, the diffraction interference is not the only source of bit-to-bit non-uniformity in the data of Figure 5-1. The other factors listed in Table 5-1 plus mechanical factors such as data mask hole non-uniformity, dust, and movement are also involved. Furthermore, the non-linear nature of the recording media tends to amplify the other causes of non-uniformity.[66]

Qualitative Discussion

The diffraction interference effects may be qualitatively described as follows. Upon reconstruction, the bits of the data mask are imaged by the hologram onto the reconstruction plane. Centered at each bit position in this plane there will appear the diffraction pattern associated with the hologram's aperture, rather than a perfect dot of light. Since a finite aperture produces a spatially infinite diffraction pattern, the tails of the diffraction patterns from each bit will overlap all of the other bit position. At each bit location, the field amplitude, then, is the coherent summation of the amplitude of that particular main lobe and the amplitudes of the neighboring diffraction tails. Therefore, that field amplitude depends on the distance from the position of the bit under consideration to that of each of the other bit positions in the array.

---

66 L. H. Lin and H. L. Beauchamp, "Hologram Formation in a Near Fourier Transform Plane for High Density Optical Memory", Technical Memorandum MM68-222404, Bell Telephone Laboratories.

Thus, it can be seen that the variability in the intensity of the bits is determined, diffraction-wise, by the variability of the side-lob contributions; i.e., in a periodic array the amplitude of a bit is influenced by whether its neighbors are 'ones' or 'zeros'.

As a preliminary design criterion, two geometrical shapes were considered for the aperture; circular and rectangular. The diffraction pattern for the circular aperture has, of course, circular symmetry; whereas the primary pattern for the rectangle is a four-pointed star. The form of the intensity distributions for the circular and for the rectangular cases are, respectively[67]

$$I(r) \propto \left[\frac{J_1(r)}{r} \right]^2$$

and

$$I(x,y) \propto \left[\frac{\sin x}{x}\right]^2 \left[\frac{\sin y}{y}\right]^2$$

in the Fraunhofer region. In considering design criteria, both the amplitude and the geometric characteristics of the diffraction pattern were studied.

From the above equations, which are only approximate in the region of interest, it is seen that the amplitudes of the side lobes are smaller for the circular case than for the rectangular case.

---

67 J. Stone, Radiation and Optics, McGraw Hill, New York, 1963, pp. 172-6.

Thus the circular aperture would appear to be the better choice for low inter-bit diffraction interference. Closer examination, however, reveals that the rectangular aperture possesses two interesting properties that should receive consideration. Firstly, its diffraction pattern is directional, having primary maxima only along directions perpendicular to the aperture sides. Secondly, the diffraction pattern has nulls at periodic positions.

Advantage can be taken of this first property of the rectangular aperture by tilting the aperture at an angle with respect to the array of bits of the data mask. This results in the individual diffraction pattern of every bit being tilted with respect to the rows and columns of the reconstructed bits in the image plane. By properly choosing the tilt angle, the star pattern can be made to overlap a bit position at the 3rd or 4th nearest neighbor rather than the first nearest neighbor. This lessens the effects of the interference because of the lower value of the higher order lobes.

The nulls of the diffraction pattern of a uniformly illuminated square aperture occur at integral multiples of $\lambda R/w_o$ where λ is the wavelength of the radiation, R is the aperture to image plane distance, and w_o is the aperture size. This second property of the rectangular aperture, namely the periodicity of its diffraction pattern, can be taken advantage of by placing bits at the nulls of the diffraction patterns of the other bits. This is accomplished by adjusting the aperture size and/or the bit spacing.

The natural extension of this train of thought is the combination of the use of these two properties. Thus, when the tilted star pattern does overlap a bit position at the 3rd or 4th nearest neighbor, it can be made to do so at a null.

While the symmetry of the circular aperture rules out the directional advantages of the rectangular aperture's pattern, the second effect, that of positioning the nulls of the diffraction pattern, could still be utilized. However, the benefit of this second effect is lessened by the aperiodic nature of the Airy pattern.

Consider, in the case of the rectangular aperture, placing neighbors at distances corresponding to the n^{th} null. Because of periodicity, all the bits in the same row or column will fall at the nulls of the diffraction pattern.

For the circular aperture case, the significant near neighbor distances in a square array are d, $\sqrt{2}d$, 2d, $\sqrt{5}d$, etc. The roots of $J_1(r)$ are 3.83, 7.02, 10.13, 13.32, etc. Since they do not fall at multiple bit distances, a multiple null scheme cannot be fabricated for this aperture shape. If the first nearest neighbor is placed at a null of $J_1(r)$, the succeeding neighbors are not, in general, at nulls.

Thus, the effects of diffraction leading to bit non-uniformity can be minimized for the circular aperture, but not the extent that these effects can be minimized for the rectangular case.

Theoretical Analysis

The system to be analyzed is shown pictorially in Figure 5-2 and schematically in Figure 5-3.

It should be noted that the system includes the random $0^0/180^o$ phase plate of C. B. Burckhardt.[68] With Burckhardt's system, a phase plate consisting of a random distribution of squares of 0^o and 180^o relative phase shift is placed on the input side of the data mask. The squares of the phase plate are aligned with the holes of the data mask so that all the light passing through any one of the data holes receives a constant relative phase shift of 0^o or 180^o. Burckhardt has shown that this procedure reduces the peak values of the light intensity at the hologram plane and, thus, helps to prevent saturation of the film.

The theoretical predictions were obtained using the Fresnel-Kirchhoff diffraction integral[69]

$$U(\alpha,\beta) = \frac{-i}{\lambda} \iint_{x\ y} \frac{e^{ik(r+s)}}{r\ s}\ dx\ dy$$

where r is the distance from the source to the data mask point (x,y), s is the distance from that data mask point to the hologram point (α,β), and λ and k are the wavelength and the wavenumber, respectively, of the light. The obliquity factor has been approximated

---

68 C. K. Burckhardt, Technical Memorandum, Bell Telephone Laboratories

69 J. Stone, op. cit., p. 162.

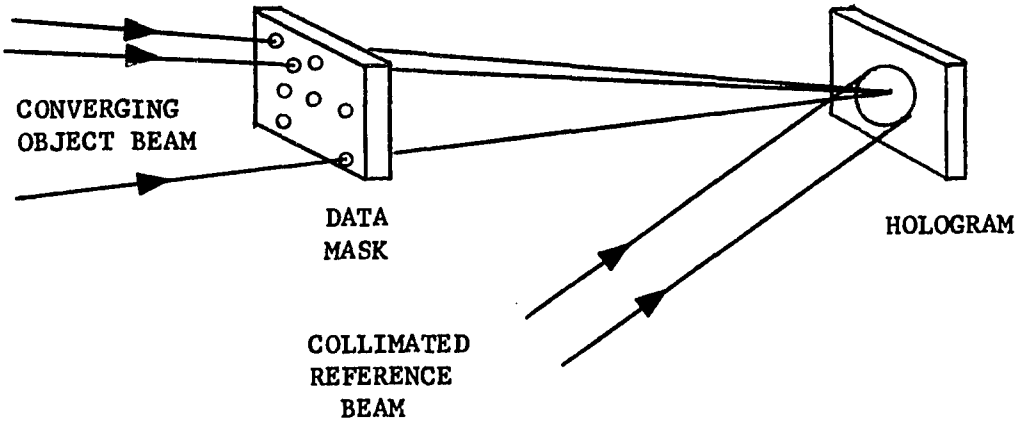

(a) WRITE

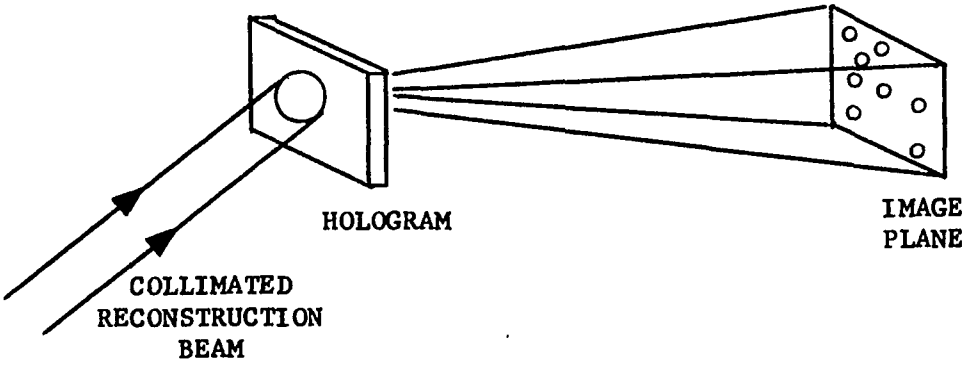

(b) READ

WRITE AND READ PICTORIAL

FIGURE 5 - 2

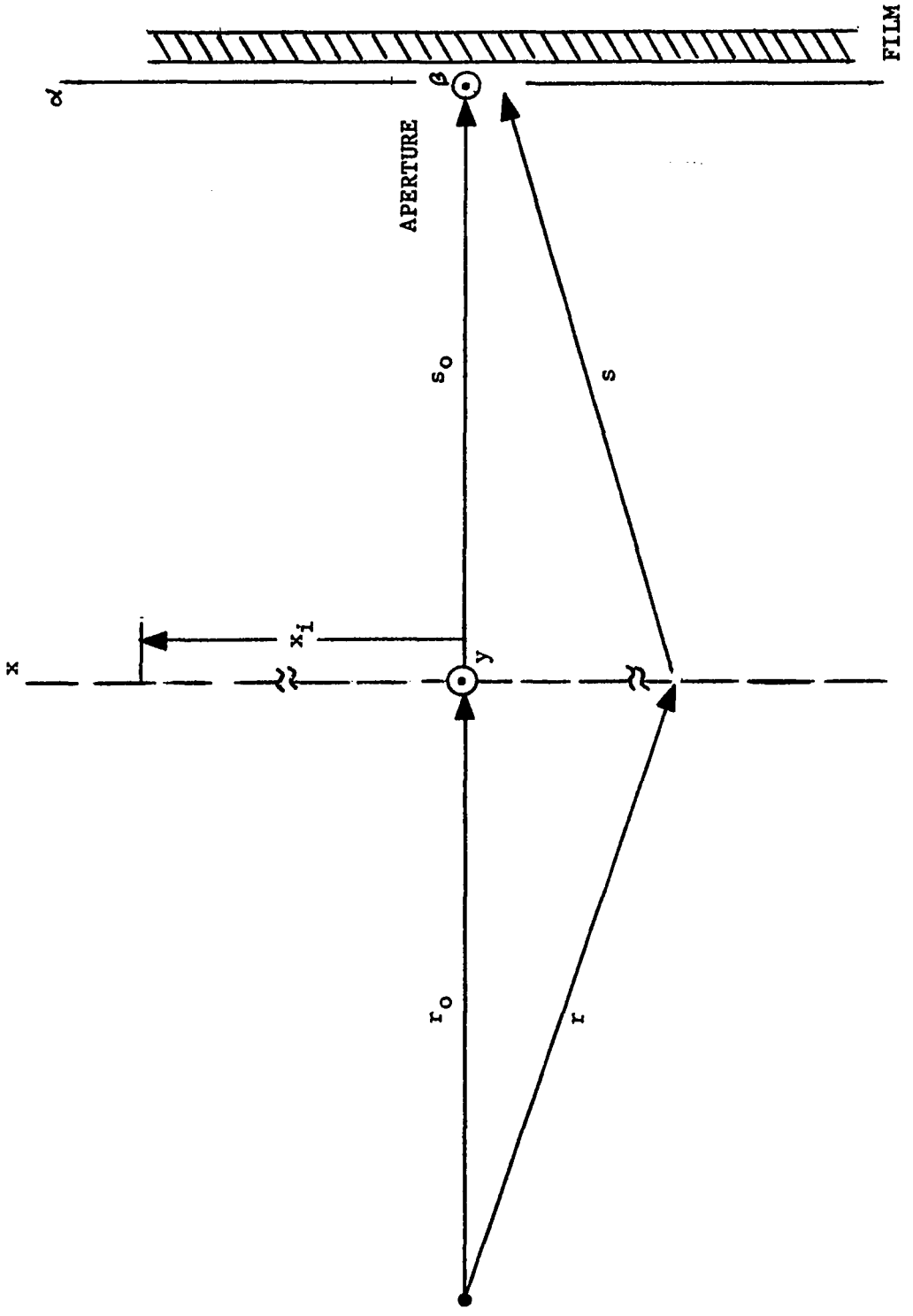

RECORDING GEOMETRY - OBJECT BEAM

FIGURE 5 - 3A

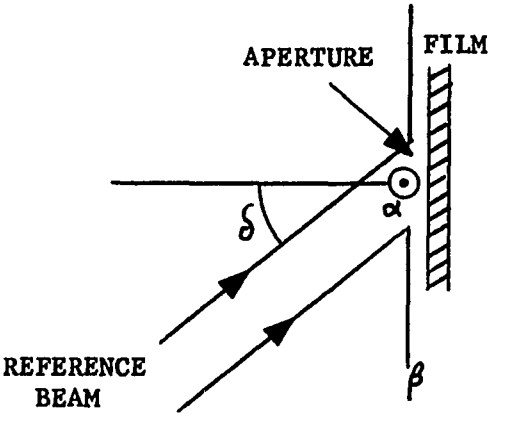

RECORDING GEOMETRY - REFERENCE BEAM

FIGURE 5 - 3B

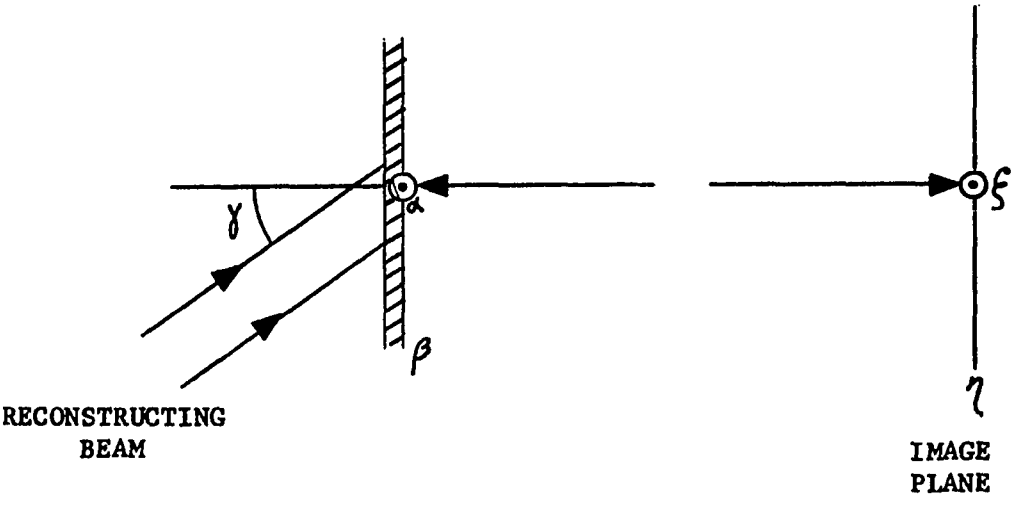

RECONSTRUCTION GEOMETRY

FIGURE 5 - 3C

as unity. The detail of this mathematical approach is presented in Appendix V-1. It was assumed that the recording medium and its processing are ideal, i.e. $\gamma = -2$, non-saturable, uniform, etc. While this theoretical analysis was limited to circularly apertured holograms for mathematical convenience, before actually constructing a memory, other geometric shapes for the aperture that provide a higher page packing density should receive consideration. This is expecially true in light of the previous discussion on the benefit of a tilted rectangular aperture.

Using the computer program of Appendix V-1, the amplitude due to the radiation from all sixty-four bits of an 8-by-8 data mask array was computed at each of the sixty-four corresponding points in the image plane. Thus the intensity computed at each of the image points was the result of contributions from each of the sixty-four data mask points. The theoretical output intensity distribution for the 8-by-8 array is shown as the histogram of Figure 5-4. The system parameters were, with the notation of Figure 5-3C,

R_o = 30cm

ρ_o = data bit hole radius = 0.00508cm

w_o = aperture radius = 0.074cm

$\Delta x = \Delta y$ = bit spacing = 0.0254cm

It should be noted that the array was limited to an 8-by-8 instead of BTL's standard 64-by-64 bit array to limit computation costs. The 64-by-64 array computation would have cost approximately 4096 times the $11.00 of the 8-by-8.

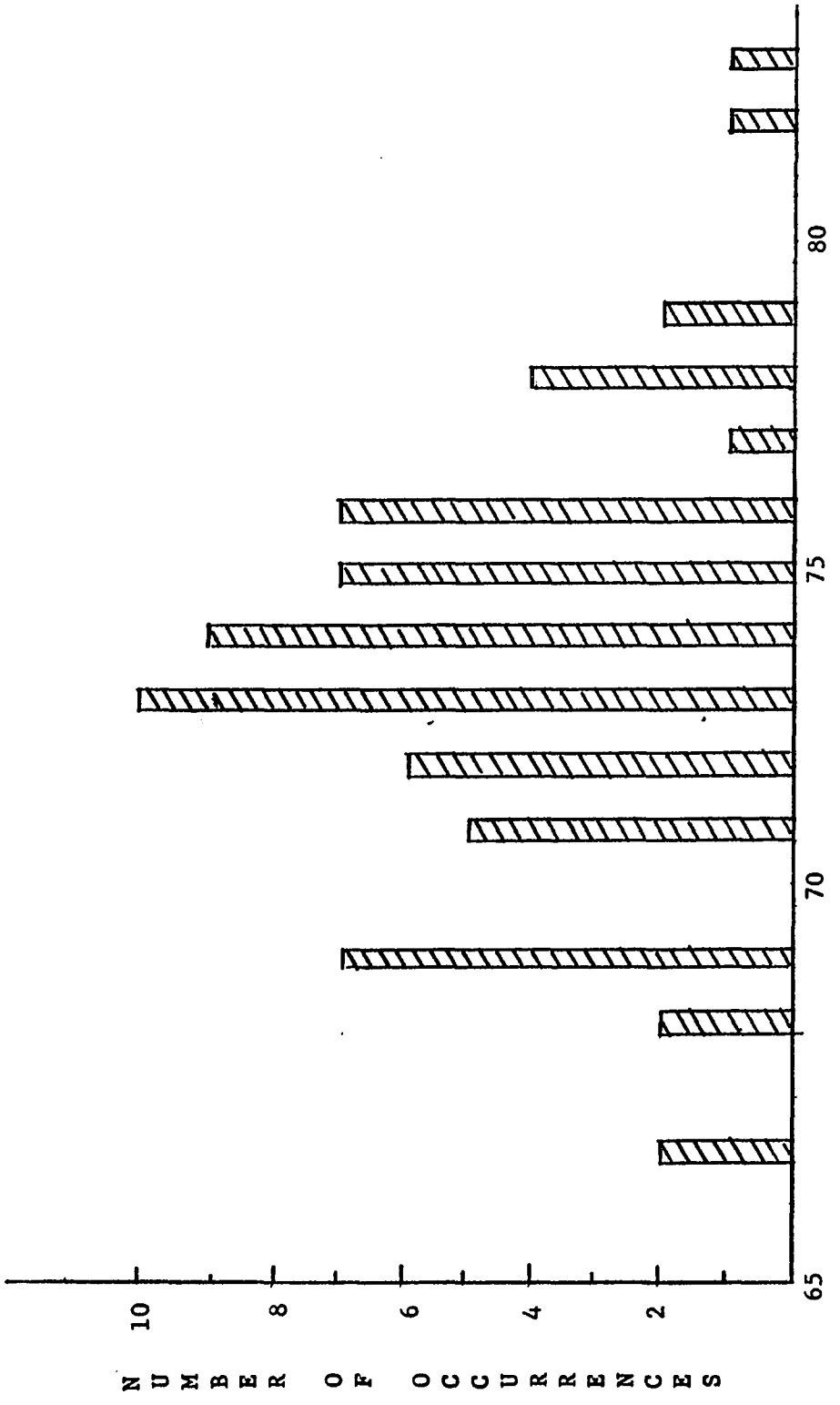

INTENSITY DISTRIBUTION OF BITS FOR 58 MIL APERTURE

FIGURE 5 - 4

To compare the non-uniformity of the bit values for different system parameters a figure of merit was chosen as a measure of the non-uniformity. This is the normalized standard deviation (NSD) of the bits of the 8-by-8 array. The computer program was executed so as to carry out the imaging procedure and to compute the NSD for the circularly apertured holograms with diameters from 0.020" to 0.070" at 0.002" increments. The results are plotted in Figure 5-5 for two different phase plates and for no phase plate.

The curves for the two phase plate conditions give nearly identical results, differing only in detail. There are definite ranges of aperture sizes for which the NDS has local minima, i.e. aperture sizes for minimum inter-bit diffraction interference.

It is easy to visualize why the NDS curve decreases non-monotonically. First, consider imaging through an aperture an infinite array of bits with no phase plate. It is clear from translational symmetry that the NSD curve versus aperture size would be uniformly zero. As the array is decreased to a finite size, a boundary would be formed such that bits near this border would have fewer near neighbors than interior points would have. This would produce a non-zero NSD.

The large initial magnitude of the NSD is due to the overlap of the first side lobe of the Airy pattern with the nearest neighbor bit. As the aperture size increases, a null moves to the nearest neighbor position and a local minimum of the NSD occurs.

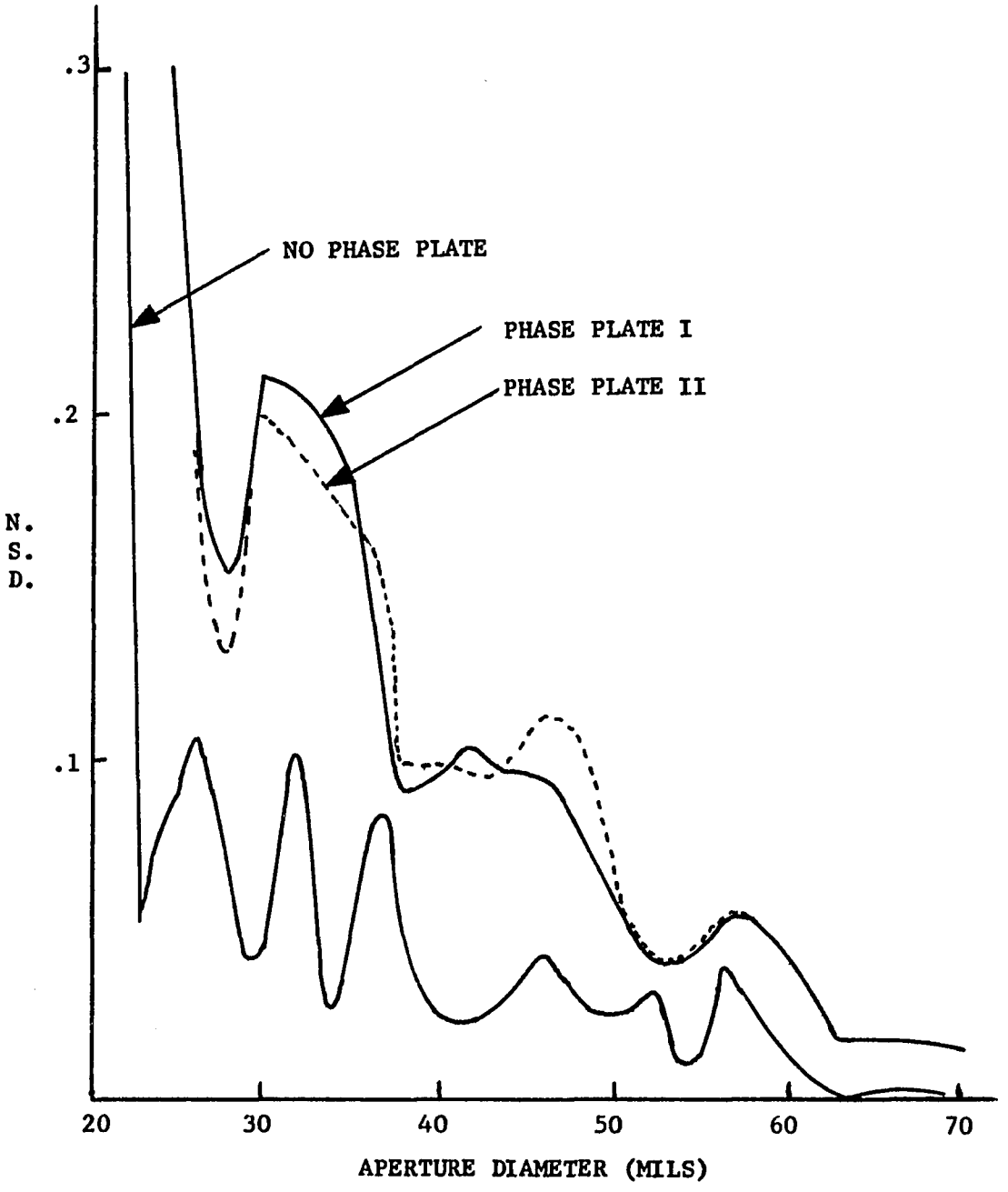

NORMALIZED STANDARD DEVIATION VS. APERTURE DIAMETER

FIGURE 5 - 5

For the case of the circular aperture, the minimum value of the NSD is not zero because of the non-periodicity of the Airy pattern and of the radial distances of the near neighbors. As the aperture size increases further, the amplitudes of the side lobes at the near neighbor bit positions increase and the NSD increases. For still larger aperture sizes, the NSD decreases and increases in an oscillatory fashion as the nulls and maxima of the Airy pattern move through the near neighbor positions.

For the case of the phase plate in front of the data mask, the randomness of the phase squares adds more variability to the overlapping diffraction patterns and, therefore, increases the standard deviation.

Experimental Results

The theoretical analysis was based on the use of an 'ideal' medium. This ideal medium can be modeled by a system with a lens which has an aperture equal to the diameter of the hologram and a focal length equal to one-half the data mask to hologram spacing. For such a system, as shown in Figure 5-6, the data mask and the image plane are 1:1 conjugates. The proof of this assertion is offered in Appendix V-2. Using this technique, it is possible to see the effects of a non-ideal medium by comparing the lens model's results to an actual hologram's results.

Using the experimental layout shown in Figure 5-7, bit-by-bit intensity scans were obtained for an 8-by-8 array of imaged data points. A brief, simplified functional analysis of that layout may

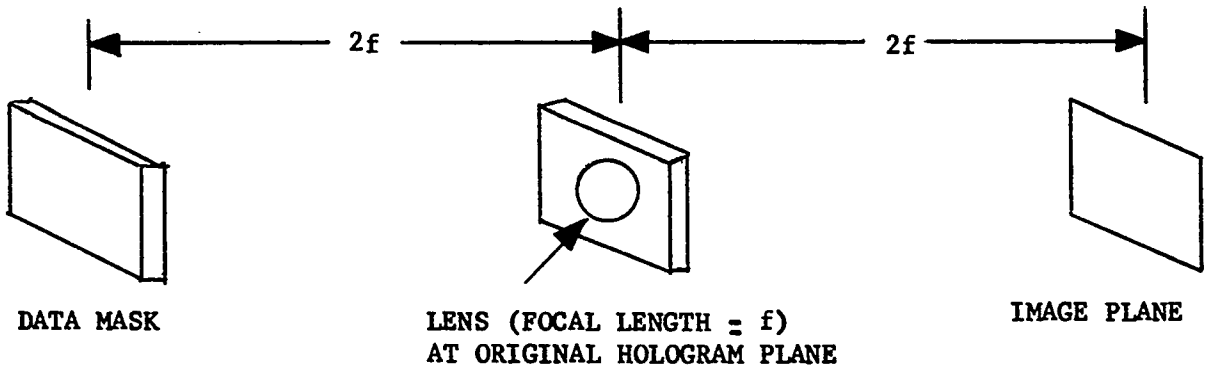

MODEL OF IMAGING SYSTEM

FIGURE 5 - 6

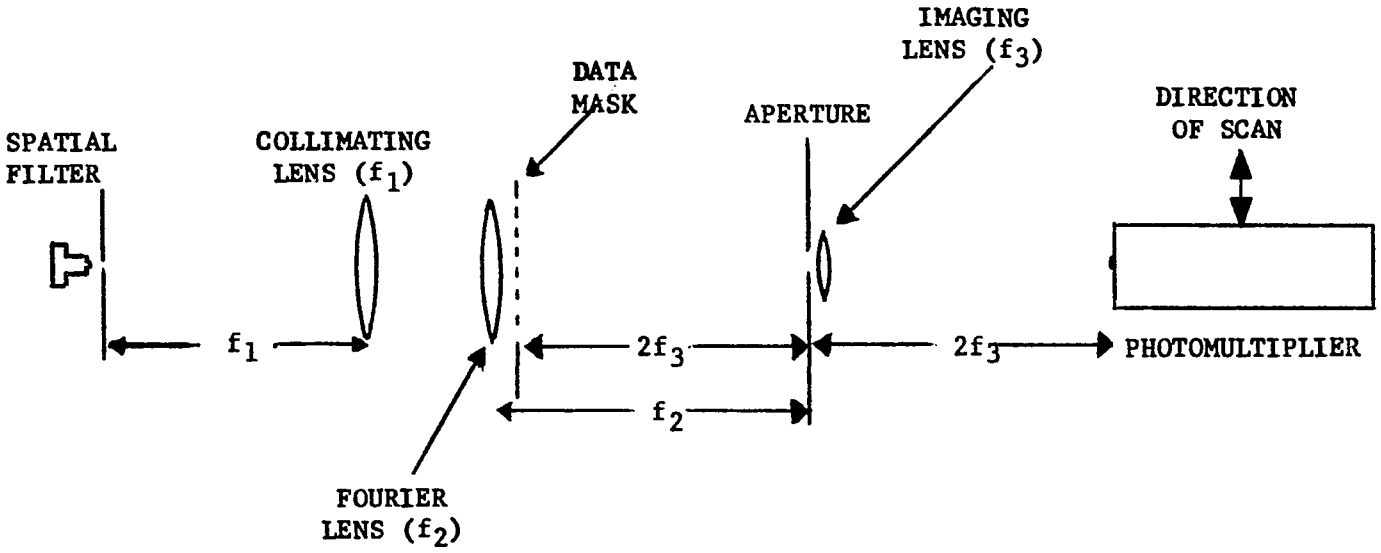

EXPERIMENTAL SETUP FOR IMAGING DATA MASK THROUGH APERTURE

FIGURE 5 - 7

be helpful. The spatial filter, being a low-pass filter, was used to remove spatial variations from the beam; thereby creating a more uniform beam intensity. The 'collimating lens', as its name implies, was used to collimate the output of the spatial filter. From the point of view of geometric optics, the 'Fourier lens' concentrates, or focuses, the output of the collimating lens into the area of the aperture. The effect of this lens, as seen from the point of view of physical optics, is found in Appendix V-1. Up to this point, the layout is the same as used to form the object beam for the making of the holograms. Continuing with the geometric viewpoint, the data mask, which has been illuminated so as to appear brightest when observed from the aperture, is imaged by the 'imaging lens' onto the plane scanned by the photomultiplier.

The experimental procedure adopted called for scanning the image of the data mask without an aperture in the imaging lens plane, then scanning with an aperture in that plane, and, after a pause, again scanning without the aperture. The first part of this proceddure was adopted because the unapertured scan would indicate the level of bit-to-bit non-uniformity not attributable to aperture diffraction. This assumes that, because of the focusing effect of the Fourier lens, the edge effects of the imaging lens are negligible. The last portion of this procedure, when linked to the first part, would provide data that would indicate the presence and degree of temporal fluctuations in the system. This entire procedure was repeated for a series of circular apertures and for one square, untilted aperture.

The sizes used were chosen only because they were available and spanned the region of interest.

Holograms were made using the same apertures. The images from these holograms were scanned using the layout of Figure 5-8.

Figure 5-9 shows examples of the data for two aperture sizes. A comparison of Figure 5-9A with Figure 5-9B indicates the presence of temporal noise.

In analyzing the data, two approaches have been followed. In the first approach, an attempt was made to remove the effects of spatial non-uniformities; e.g.,non-standard data hole sizes, non-uniform beam irradiance, imperfections in the glass lenses, etc.

This was accomplished by comparing the image of a given data hole only with other images of itself under the various conditions; i.e.,apertured versus non-apertured, apertured versus hologram, etc. For example, if the individual bits of the data mask array are identified by a double subscript notation; i.e., bits 1,1 to 8,8, the bit 2,6 of the apertured scan, or bit set, is only compared to the 2,6 bit of the unapertured scan. The actual comparison consisted of individually subtracting the intensity of each of the 64 bits as measured under a particular condition or scan; e.g.,no-aperture, from each of the corresponding 64 bits measured under a different condition; e.g.,no-aperture later. The result of this procedure was a 64 bit array of the differences in output of the two different scans being compared. The effect of long term laser power fluctuations

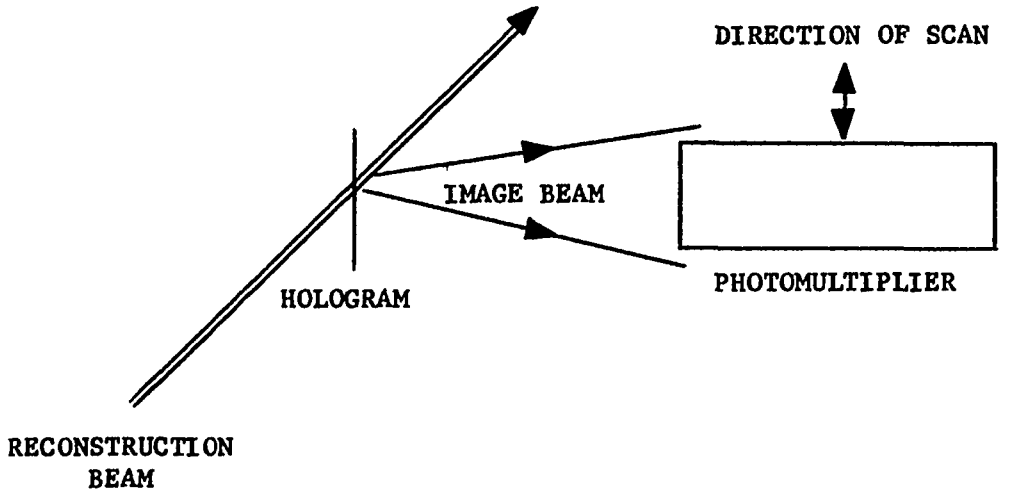

EXPERIMENTAL SETUP FOR MEASURING
OUTPUT FROM HOLOGRAMS

FIGURE 5 - 8

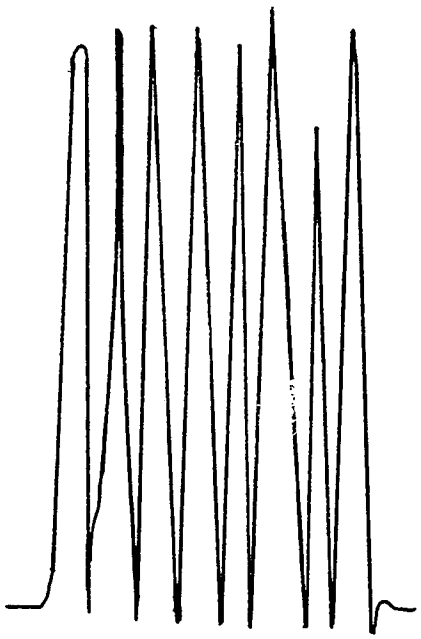

(a) NO APERTURE

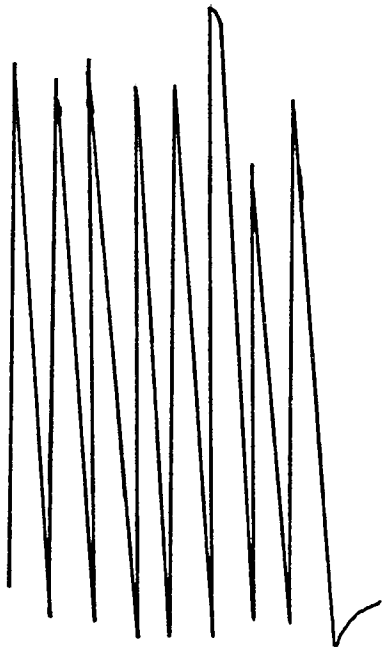

(b) NO APERTURE LATER

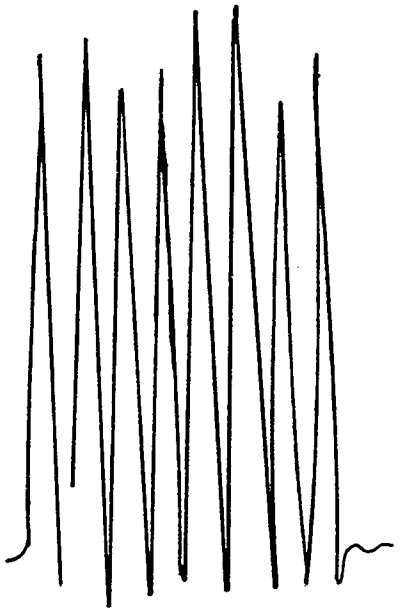

(c) 65 MIL APERTURE

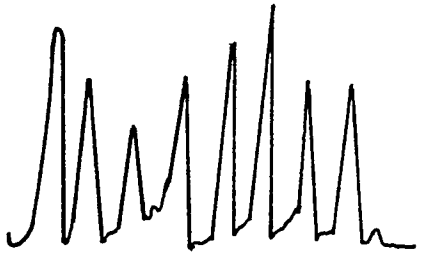

(d) 65 MIL HOLOGRAM

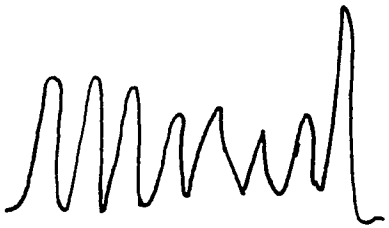

(e) 25 MIL APERTURE

(f) 25 MIL HOLOGRAM

EXAMPLES OF OUTPUT SCANS

FIGURE 5 - 9

and other power variations were accounted for by normalizing the bit sets to unity intensity before making any of the above cross comparisons; n.b., the term 'cross comparison' refers to the comparison of corresponding bits of different scans. The normalized intensities of the corresponding bits were subtracted and the standard deviation of these 64 remainders computed. Figure 5-10 depicts this NSD data for several aperture diameters. It is observed that the aperture - no-aperture standard deviation does follow the expected trend of a general decrease with increasing aperture. Note that the square aperture shows a significantly greater NSD than the corresponding circular aperture.

Attention is particularly called to the data represented by the solid black bars. This is the cross comparison for the no-aperture case with the no-aperture later case. This value thus represents the standard deviation of the temporal noise. Since these black bars are not all of the same amplitude, it can be concluded that the temporal noise is non-stationary. It should be noted that this noise level dominates the effect of the diffraction at the larger aperture sizes. The 65NP refers to a case in which the glass phase plate was removed, thus depriving the thin data mask of some of its mechanical rigidity. This would account for the rise in temporal fluctuation over the normal fluctuation level.

The second approach to analyzing the data was based on the actual problem encountered in the optical memory system; i.e., non-uniformity of the intensity within a given array scan. This internal

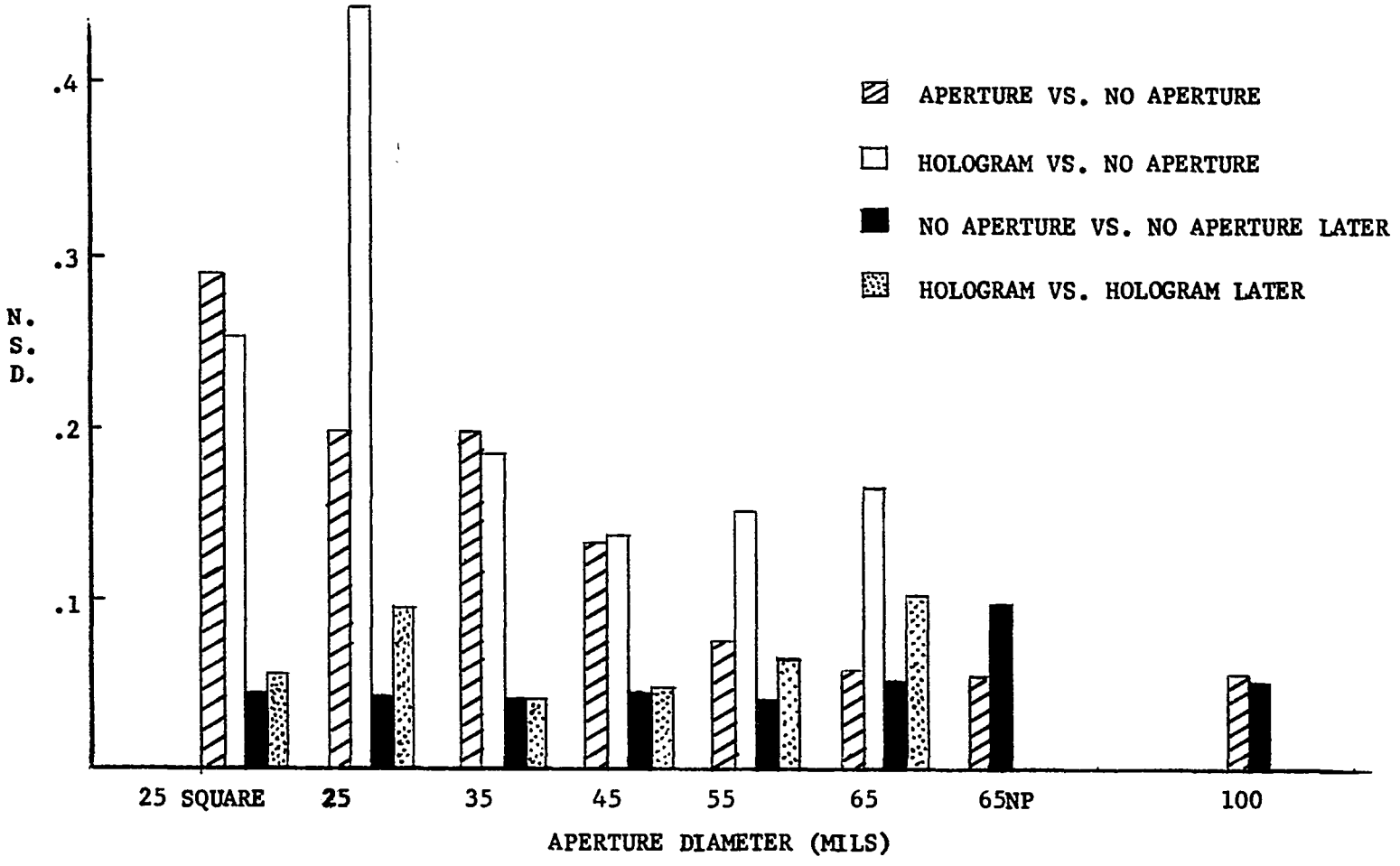

CROSS COMPARISONS

FIGURE 5 - 10

comparison was accomplished by separately computing the NSD of the bit variations within each array of non-apertured, apertured, and holographic output images. This data is graphically displayed in Figure 5-11. With the exception of the 25mil aperture, the experimental values follow the theoretical predictions quite well. The NSD generated in the no-aperture case is what may be termed spatial noise. This noise dominates the diffraction effects for the larger apertures. A disconcerting observation is that the NSD for the hologram is, in several of the displayed cases, less than that for the apertured lens case. In other words, the hologram generated a more uniform image than did the lens for the 65- 35mil cases. One would expect the gelatin imperfections to make the non-uniformity worse.

Because of this unexpected result, the experiment was partially repeated. To reduce air-transmitted vibrations, the elements of the system were more firmly attached to the rigid 'floating' table, to reduce lens contamination, each lens was carefully cleaned with acetone; and finally, to reduce the amount of airborne dust affecting the uniformity, a plexiglass housing was constructed and the entire system placed inside it. As a further precaution, filtered air was pumped into the plexiglass housing so as to maintain a slight positive pressure with respect to the laboratory.

For this second set of data, the spatial noise level decreased from an NSD of 0.10 to one of 0.075; but the temporal noise level rose. For this second set of data, the hologram's image is more uni-

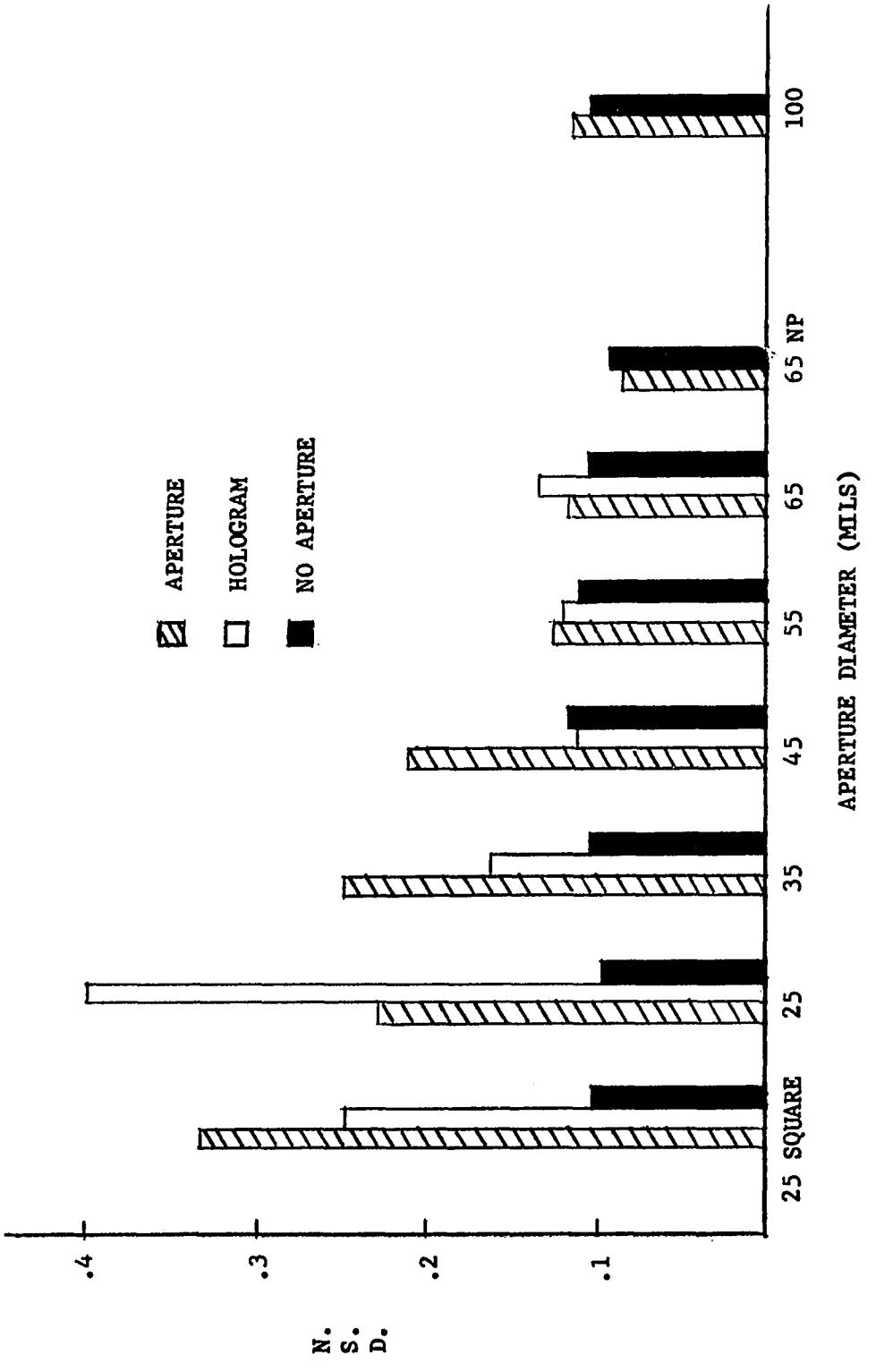

INTERNAL COMPARISONS

FIGURE 5 - 11

form than the image formed using the lens technique. Later work showed that some of the inconsistencies of the data from the holograms could be eliminated by variably aperturing one hologram instead of using several holograms of various sizes.

In attempting to uncover the characteristics of the non-uniformity caused by other than diffraction effects, the photomultiplier tube was positioned so as to scan a line of output data points. The data mask was then removed and the image plane scanned where the row of data points would have been. Figure 5-12 shows the data that was obtained. This represents a spatially dependent variation of approximately $\pm$ 30%. Cleaning the lenses and placing them in the filtered, positive pressure atmosphere reduced this variation to approximately $\pm$ 15%.

Conclusions

As to the agreement between theoretical and experimental results, consider the following. If the noise is assumed to be independent, random Gaussian noise, then

$$\sigma_M^2 = \sigma_T^2 + \sigma_N^2$$

where σ_M^2, σ_T^2, and σ_N^2 are the variances of the measured data, the theoretical data, and the noise. Using this relationship, Figure 5-13 shows very good agreement between the theoretical and the experimental effects of diffraction.

From the theoretical predictions of Figure 5-5, it is concluded that certain combinations of aperture size and bit spacing are sig-

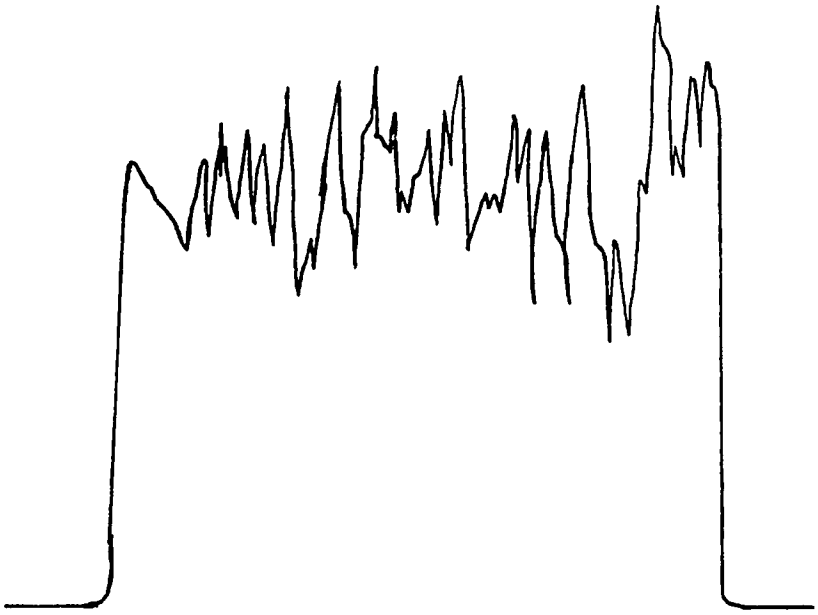

SCAN OF IMAGE PLANE WITH DATA MASK REMOVED

FIGURE 5 - 12

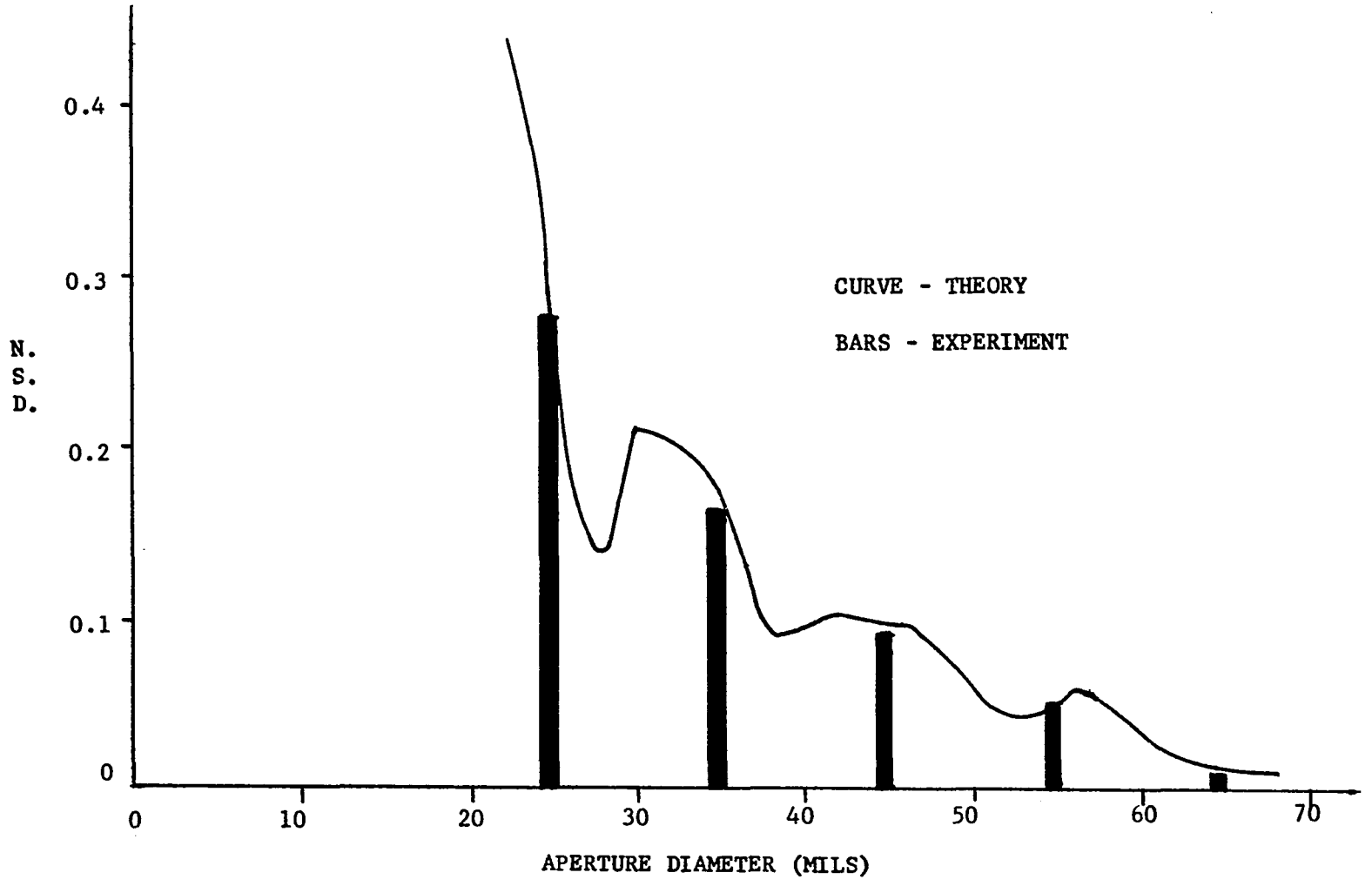

NORMALIZED STANDARD DEVIATION VS. APERTURE DIAMETER

FIGURE 5 - 13

nificantly more desirable than others. This is especially true at the smaller relative aperture sizes. From Figure 5-10 and Figure 5-11, it is apparent that aperture diffraction interference is not the only phenomenon causing the bit non-uniformity. Furthermore, at the larger aperture sizes, these phenomena, which have been labeled as noise, are the dominant causes of non-uniformity.

Since this noise is not an inherent, or theoretically mandated, result of the holographic process, and therefore must be the result of non-ideal physical components, one would expect that it could be reduced if the role of physical components were reduced. One method of achieving this is to employ the synthetic hologram technique developed in Chapter IV.

CHAPTER VI

CONCLUSIONS

The feasibility of an optical holographic ROM system utilizing partially coherent light from a CRT luminescent dot for the hologram reproduction has been proved.

Substitution of the CRT for the usual acousto-optic Bragg-cell-deflected laser beam as the source of read out radiation results in a one hundred fold decrement in random access time.

The techniques described permit one to design a system that achieves a storage density in excess of 10^5 bits per square centimeter of holographic film.

The problem of analysis and design of the system was approached by the use of a computer simulation of the process. Such analysis, having to take into account the effects on holographic reconstruction of the extended spectrum of the CRT luminescence and the finite size of the luminous dot used as a reconstruction source, resulted in the development of a novel approach to the simulation. In this case conventional computer simulation, as shown in this dissertation, requires excessive run times. The approach described is derived from a physical interpretation and approximation of the components of the system. Optimization of the system to obtain the highest packing density minimizing error sources was based on this simulation.

The extended spectrum of the CRT spot, with its consequent limited time coherence, and the limited spatial resolution of the CRT display have been shown to generate inter-page crosstalk. One of the methods here described for the suppression of this source of error is based on purely optical techniques, but it proves too costly in terms of bit packing density for presently available CRT's. The system proposed by this dissertation utilizes a 100Å optical filter and a mechanical technique of interpage crosstalk applied to a currently available medium resolution (0.02 cm spot size) CRT.

The optical method of interpage crosstalk suppression previously referred to could be utilized in practice, if phosphor technology were to produce fast decay phosphors with a spectral bandwidth of the order of magnitude of some of the present-day europium-activated compounds in a high resolution device. Development of such a device, on the basis of the requirements and limitations indicated in this dissertation, could represent a valuable subject for future research in its appropriate field.

While the CRT phosphor has been used as the source of the read-out radiation, it is only a vehicle for permitting detailed analysis. The technique is, in itself, quite general and applicable to use with other sources of partially coherent light. In particular, future work in this area should follow the development of light emitting semi-conductor arrays as a possible replacement for the CRT as the source of read-out radiation.

The system described and analyzed uses circularly apertured holograms. The analysis of inter-bit crosstalk developed in this disserta-

tion, however, shows that use of a rectangularly apertured page permits further reduction of this diffraction-related cause of bit-to-bit non-uniformity. The theoretical analysis indicates that the density circuit can be increased by a factor of two by judicious choice of page size. The technique described to obtain this result appears a promising point of departure for future investigation and refinement of the system; promising, as it does, a more efficient utilization of film surface. Such future investigation could make use of the computer simulation methods here described, extending them to the special case of square-apertured holograms.

Some experimentation has been conducted to verify the predictions of the theoretical analysis of interbit diffraction interference. This experimentation shows that other effects, also described in the dissertation, and best labeled as "noise", dominate the diffraction-caused non-uniformities for apertures greater than 50 mils. This noise is the result of non-ideal physical conditions introduced by the technological implementation of both the hologram recording and reproduction system. Future investigations could consider such causes of bit non-uniformity and propose further solutions to this problem.

The system here described effectively eliminates the above causes of non-uniformity during the recording process by obtaining the holograms through a process of computer generated synthesis, rather than by physical holography of a data mask.

Many other advantages are shown to result from this approach, including higher information storage density, the elimination of optical

noise due to unwanted components of the hologram reconstruction, the use of theoretical point sources for the bits, and others as analyzed in the dissertation.

Computer generated synthesis of the holograms, using 16 levels of gray scale rather than the more usual binary holography technique, was obtained by PDM modulation of a CRT presentation. The design of a device providing the necessary interface between the computer and the CRT to perform this modulation is described in the dissertation, together with the computer program for the generation of the required hologram transmittance.

The feasibility of this design has been proved by fabricating the system and using it for the production of a sample hologram. The particular form of the implementation described refers to a feasibility study using available computer facilities. Its extension to a faster and more convenient system for the production of such holograms under more restrictive conditions of practical use appears quite straight forward. Further work in this context could utilize high speed data links or specialized programming on a minicomputer.

For this use the interface could utilize other forms of CRT modulation. For instance PAM, rather than PDM, could be used to display the entire transmittance pattern for a single exposure photography, rather than use the slower time exposure photographic system imposed by availability of facilities during this investigation.

The holograms produced by this method are digitalized on 16 gray-scale steps. This decreases the number of spurious images that would be generated by a binary hologram and improves the resolution. In this investigation the problem was only roughly analyzed. Further work might consider optimization of the number of quantization levels.

Further experimental investigation in the characteristics of the image reconstructed by the use of a CRT spot as a reference source would also constitute a valuable contribution and a promising avenue of research.

In conclusion, by the techniques described and by using available components, it would be possible to assemble a system of this type to store 10 megabits over a 4-inch square CRT with a random access time of the order of 10 nanoseconds.

REFERENCES

1. Abramowitz, M. and Stegun, I., Handbook of Mathematical Functions, Dover Publications, Inc., New York, 1965, p. 299.

2. Anderson, L. K., Laser Technology, Vol. 9, No. 3, p. 62, March 1970.

3. Arfken, G., Mathematical Methods for Physicists, Academic Press, New York, 1968, pp. 598-611.

4. Barrett, W. A. and Townsend, R. L., "Bit Intensity Nonuniformity in an Optical Memory", Technical Memorandum MM71-2212-2, Bell Telephone Laboratories.

5. Bartee, T. C., Digital Computer Fundamentals, McGraw Hill, Inc., New York, 1966, p.4.

6. Becker, C. H., Electronics, Vol. 41, No. 6, p. 50, March 18, 1968.

7. Beran, M. J. and Parrent, G. B. Jr., Theory of Partial Coherence, Prentice Hall, Inc., Englewood Cliffs, New Jersey, 1964.

8. Blue, M. D. and Chen, D., Electronics, Vol. 42, No. 5, p. 109, March 1969.

9. Born, M. and Wolf, E., Principle of Optics, Pergamon Press, Long Island City, 1965, p. 395.

10. Botfield, R. J., Hill, A. N., and Steptoe, B. J., Journal of Physics E, Vol. 1, Series 2, p. 810, 1968.

11. Burckhardt, C. K., Technical Memorandum, Bell Telephone Laboratories.

12. Burroughs Corp., Digital Computer Principles, McGraw Hill, Inc., New York, 1962, p.386.

13. Carlson, A., Communications Systems: An Introduction to Signals and Noise in Electrical Communication, McGraw Hill, New York, 1968, p. 223.

14. Carter, W., "Aliasing in Sampled Holograms", Proceeding of IEEE, Vol. 56, Jan. 1968, pp. 96-8.

15. Cathey, W. Jr., "The Effect of Finite Sampling in Holography", Optik, Vol. 27, 1968, pp. 317-26.

16. Cochran, G., "New Method of Making Fresnel Transforms with Incoherent Light", JOSA, Vol. 56, No. 11, Nov. 1966, pp. 1513-7.

17. Cooper, H. G., Bell System Technical Journal, Vol. 40, No. 3, p. 724, May 1961.

18. Craig, E., Laplace and Fourier Transforms for Electrical Engineers, Holt, Rinehart and Winston, New York, 1966, pp. 394-8.

19. DeVelis, J. and Reynolds, G., Theory and Application of Holography, Addison-Wesley Publishing Co., Reading, Mass., 1967, p. 21.

20. Frecska, S. A., "Characteristics of the Agfa-Gevaert Type 10E70 Holographic Film", Applied Optics, Vol. 7, No. 11, Nov. 1968, pp. 2312-4.

21. Friesem, A. A. and Zelenka, J. S., "Effects of Film Nonlinearities in Holography", Applied Optics, Vol. 6, No. 10, October 1967, pp. 1755-9.

22. Fowles, G. R., Introduction to Modern Optics, Holt, Rinehart, and Winston, Inc., New York, 1968, p. 72.

23. Goodman, J. W., Introduction to Fourier Optics, McGraw Hill, Inc., New York, 1968, p. 32.

24. Goodman, J. W. and Knight, G. R., "Effects of Film Nonlinearities on Wavefront-Reconstruction Images of Duffuse Objects," JOSA, Vol. 58, No. 9, Sept. 1968, pp. 1276-83.

25. Graham, R. and Hoff, M., Electronic Products, Vol. 12, No. 9, pp. 28-34, January 1970.

26. Haung, T., "Digital Holography", IEEE Spectrum, Vol. 59, No. 9, Sept. 1971, p. 1344.

27. Hoover, C. W., Hangk, G., and Herriott, D. R., Bell System Technical Journal, Vol. 38, No. 2, p. 367, March 1959.

28. Jahnke, E. and Emde, F., Tables of Functions, Dover Publications, New York, 1945, p. 145.

29. Jenkins, F. and White, H., Fundamental of Optics, McGraw Hill, Inc., New York, 1957, p. 157.

30. Joseph, E. C., Computer Design, Vol. 8, No. 11, pp. 165-8, November 1969.

31. Keeton, S. C., "A Sampled Computer-Generated Binary Hologram", IEEE Proc., March 1968, pp. 325-7.

32. Kottler, F., Ann der Physik, Vol. 70, p. 405, 1923.

33. Kozma, A., "Photographic Recording of Spatially Modulated Coherent Light", JOSA, Vol. 56, No. 4, April 1964, pp. 428-32.

34. Kozma, A. and Kelly, D., "Spatial Filtering for the Detection of Signals Submerged in Noise", Applied Optics, Vol. 4, April 1965, pp. 387-92.

35. Kvamme, F., Electronics, Vol. 43, No. 5, pp. 88-95, Jan. 5, 1970.

36. LaMacchia, J. T., Laser Focus, Vol. 6, No. 2, p. 35, February 1970.

37. LaMacchia, J. T., Barrett, W. A., and Townsend, R. L., "Non-Uniformity of the Reconstructed Image from Holograms Used in Data Storage", presented at Fall Meeting, Optical Society of America, Oct. 1970, Hollywood, Florida.

38. LaMacchia, J. T., Chen, F. S., and Fraser, D. B., Bell Telephone Laboratories Record, January 1969, pp. 30-1.

39. Lapidus, G., IEEE Spectrum, Vol. 10, No. 7, pp. 50-4, July 1970.

40. Leith, E. N. and Upatnieks, J., "Reconstructed Wavefronts and Communication Theory", JOSA, Vol. 52, 1962, p. 1123.

41. Leith, E. N. and Upatnieks, J., "Wavefront Reconstruction with Diffused Illumination and Three-Dimensional Objects", JOSA, Vol. 54, 1964, p. 1295.

42. Levine, A. and Pallila, F., "YVO_4:Eu, A New Highly Efficient Phosphor for Color Television", Electro-Chemical Technology, Vol. 4, No. 1-2, p. 16.

43. Lin, L. H. and Beauchamp, H. L., "Hologram Formation in a Near Fourier Transform Plane for High Density Optical Memory", Technical Memorandum MM68-2224-4, Bell Telephone Laboratories.

44. Lohmann, A. W., "Wavefront Reconstruction for Incoherent Objects", JOSA, Vol. 55, 1965, p. 1555.

45. Lohmann, A. W. and Paris, D. P., "Binary Fraunhofer Holograms, Generated by Computer", Applied Optics, Vol. 6, No. 10, Oct. 1967, pp. 1739-48.

46. Maloney, W. T., "Real-Time Holographic Filtering of Oscilloscope Traces", Applied Optics, Vol. 10, No. 11, Nov. 1971, pp. 2554-5.

47. Mandall, L and Wolf, E., "Coherence Properties of Optical Fields", Rev. Mod. Phys., Vol. 37, 1965, p. 231.

48. Marino, J. and Sirota, J., Electronics, Vol. 43, No. 6, pp. 112-6, March 1970.

49. Marsaglia, G. and Bray, T., "One Line Random Number Generators and Their Use in Combinations", Communications of the Assoc. for Computing Machinery, Vol. 11, No. 11, Nov. 1968, pp. 757-9.

50. Mees, C. E. K., From Dry Plates to Ektachrom, Ziff-Davis Publishing Company, New York, 1961, p. 21.

51. Mees, C. E. K., The Theory of the Photographic Process, MacMillan Company, New York, 1954, p. 162.

52. Meir, R. W.,"Magnification and Third-Order Oberrations in Holography", JOSA, Vol. 55, 1965, p. 987.

53. Mozzone, R., A System for Generating Digital Holograms, Master's Thesis, Newark College of Engineering, E.E. Dept., 1974.

54. Pfahnl, A., "Properties of Fast-Decay Cathode-Ray Tube Phosphors", Bell System Technical Journal, January 1963, pp. 181-93.

55. Roberts, W., Computer Design, Vol. 8, No. 11, p. 147, Nov. 1969.

56. Roop, D., Electronic Products, Vol. 12, No. 10, p. 97, Feb. 1970.

57. Shew, L. F., Product Engineering, Vol. 40, No. 12, p. 16, June 16, 1969.

58. Signetics Corp., IEEE Spectrum, Vol. 11, No. 1, p. 107, Jan. 1974.

59. Silver, S., "Microwave Aperture Antennas and Diffraction Theory", Vol. 52, p. 131, 1962.

60. Sittig, E. K. and Smits, F. M., Bell System Technical Journal, Vol. 48, No. 3, p. 659, March 1969.

61. Stroke, G. W., An Introduction to Coherent Optics and Holography, Academic Press, New York, 1966.

62. Thomas, G., Calculus and Analytic Geometry, Addison-Wesley Pub., Co., Reading, Mass., 1961, pp. 797-8.

63. Tufte, O. N. and Chen, D., IEEE Spectrum, Vol. 10, No. 2, pp. 26-32, February 1973.

64. Vander Lugt, A., "Signal Detection by Complex Spatial Filtering", IEEE Trans. on Information Theory, April 1964, pp. 139-45.

65. Waters, J. P., "Three Dimensional Fourier-Transform Method for Synthesizing Binary Holograms", JOSA, Vol. 58, No. 9, Sept. 1968, pp. 1284-8.

APPENDIX III-1

CRT SPATIAL MODEL FORTRAN PROGRAM

```
C       PROGRAM TO DETERMINE SPATIAL MODEL VALUES FOR RECONSTRUCTION SOURCE
        DIMENSION RHO(14),E(14),B(14),RHOAVG(14),RNGPHA(14),RHOIN(14,14)
        DIMENSION RHOOUT(14,14),RHORAN(14,29),PTPHA(14,29),NR(10),NPPR(10)
C       NT MUST EQUAL NP
        READ12,NT,NR(1),NR(2),NR(3),NR(4),NR(5),NR(6)NR(7)
   12 FORMAT(815)
        READ 47, NP, NPPR(1),NPPR(2),NPPR(3),NPPR(4),NPPR(5),NPPR(6)
   47 FORMAT(815)
C       COMPUTE RHO
        D0100 MT=1/NT
        MP = MT
        NNR=NR(MT)
        ANR=NRR
        NRP1= NNR + 1
        DO 21 M=2,NNR
        AM = M - 1
        RHO(M) = SQRT( -ALOG(1.0 - AM/ANR)  )
   21 CONTINUE
C       APPROXIMATION FOR ERROR FUNCTION
        A1 = 0.3480242
        A2 = - 0.0958798
        A3 = 0.7578558
        P = 0.4707
        RHO(1) = 0.0
C       APPROXIMATE INFINITY BY 20
        RHO(NRP1) = 20.0
        NNRP1= NNR + 1
        DO 40 M = 1, NNRP1
        T = 1.0 / ( 1.0 + P* RHO(M))
        EXPT = EXP( - RHO(M)*RHO(M))
        E(M) = 1.0 - (A1*T + A2*T*T +A3*T*T*T) *EXPT
        B(M) = RHO(M) * EXPT
   40 CONTINUE
        DO 41 M = 1, NNR
        MP1 = M + 1
        RHOAVG(M) = -ANR*(B(MP1) - B(M) -0.8862269*(E(MP1) - E(M)))
   41 CONTINUE
C       SET RANDOM GENERATORS
        INR = 4048151
        INI = 81525722
        INO = 53931333
        NA = NPPR(MP)
        ANA = NA
        ANA02 = ANA/2.0
        NA02 = ANA02
        BNA02 = NA02
```

```
      DIF = ANA02 - BNA02
      DO 51 M = 1,NNR
C     SUFFIX "R" FOR RING PHASE
      INR = INR * 27
      RSULTR = 0.5 / FLOAT (INR)*0.2328306E-9
C     RSULTR VARIES FROM 0 TO 1.0
      RNGPHA(M) = 2.0*3.14159265*RSULTR
C     TEST FOR EVEN OF ODD
      IF(DIF -0.3) 53,53,54
C     IF EVEN 53   IF ODD 54
   53 NK = NA/2
      GO TO 55
   54 NK = ( NA -1)/2
      RHORAN(M,NA) = RHOAVG(M)
   55 CONTINUE
      DO 57MK=1,NK
C     SUFFIX "I" FOR POINTS INSIDE RHOAVG:  "0" POINTS OUTSIDE RHOAVG
      INI = INI * 15003
C     RSULTI and RESULTO VARY BETWEEN / AND 0.5
      RSULTI = 0.5 / FLOAT(INI)*0.2328306E-9
      RSULTI = 0.5*RSULTI
C     BOTH RHOIN AND RHOOUT ARE CONSTRAINED TO VARY RANDOMLY IN A RANGE
C     FROM 0 TO 1/2 THE DISTANCE BETWEEN RHOAVG AND THE INSIDE BOUNDRY
C     OF THE ANNULAR REGION IN CONSIDERATION ; I.E., RHO(M)
      RHOIN(M,MK) = - (RHOAVG(M) - RHO(M  ))*RSULTI / RHOAVG(M)
      INO = INO * 2121
      RSULTO = 0.5 / FLOAT(INO)*0.2328306E-9
      RSULTO = 0.5*RSULTO
      RHOOUT(M,MK) =-(RHO(M) - RHOAVG(M)) * RSULTO / RHOAVG(M)
   57 CONTINUE
C     ALTERNATE INSIDE POINTS WITH OUTSIDE PPOINTS
      DO 58 MA =1,NA
      MB = 2*MA -1
      RHORAN(M,MB) = RHOIN(M,MA)
      MBP1 = MB / 1
      RHORAN(M,MBP1) = RHOOUT(M,MA)
   58 CONTINUE
      DO 59 MA = 1, NA
      AMA = MA
      PTPHA(M,MA) = RNGPHA(M) / 2.0*3.14159265 *( AMA - 1.0)/ ANA
   59 CONTINUE
   51 CONTINUE
      DO 72 M = 1, NNR
      PRINT 64
   64 FORMAT(1HO)
      PRINT 65,M,RHOAVG(M),M,RNGPHA(M)
   65 FORMAT(1H ,'RHOAVG',13,' = 1,F14.8,4X,'RNGPHA',13,1 = 1,F14.8)
      PRINT 70
   70 FORMAT ( 1H ,'   RADIUS        PHASE ')
      DO 72 MA = 1, NA
      PRINT 71,RHORAN(M,MA),PTPHA(M,MA)
```

```
   71 FORMAT ( 2F14.7)
   72 CONTINUE
      DO 80 M = 1, NNR
      PRINT 64
      PRINT 65,M,RHOAVG(M),M,RNGPHA(M)
      PRINT 75
   75 FORMAT (1H , '     MU              NU')
      DO 80 MA = 1, NA
      AMU = RHORAN(M,MA)*COS(PTPHA(M,MA))
      ANU = RHORAN(M,MA)*SIN(PTPHA(M,MA))
      PRINT 81 ,AMU,ANU
   81 FORMAT(2F14.8)
   80 CONTINUE
  100CONTINUE
      STOP
      END
*RUN
```

APPENDIX III-2

CRT FREQUENCY MODEL FORTRAN PROGRAM

```
C       DECK 1
C       B SERVES TO CREAT A SECOND MATRIX FOR AMP & POSIT, BMP & BOSIT
        DIMENSION POSIT(120),AMP(120),W(120),DAMP(120),RAMP(25),RW(25)
        DIMENSION CW(12),CP(12)  ,BMP(120),BOSIT(120)
C       INPUT NUMBER OF POINTS AND NO. OF CALIBRATION POINTS
        DO200 MT=1,2
        READ5,NP,NC,NF
      5 FORMAT(3110)
C       INPUT 12 DATA CARDS  - AMP VS POSITION
        DO 3 I=1,12
        READ 1,AMP(1),POSIT(1),AMP(2),POSIT(2),AMP(3),POSIT(3),
       1AMP(4),POSIT(4),AMP(5),POSIT(5),AMP)6),POIT(6),AMP(7),POSIT(7),
       2AMP(8).POSIT(8)
      1 FORMAT(16F5.1)
        DO3J=1,8
        K=8*(I-1)+J
        BOSIT(K)=POSIT(J)
        BMP(K)=AMP(J)
      3 CONTINUE
C       INPUT 3 FREQ CARDS - WAVELENGTH VS POSITION
        READ4,CW(1),CP(1),CW(2),CP(2),CW(3),CP(3),CW(4),CP(4)
        READ4,CW(5),CP(5),CW(6),CP(6),CW(7),CP(7),CW(8),CP(8)
        READ4,CW(9),CP(9),CW(10),CP(10),CW(11),CP(11),CW(12),CP(12)
      4 FORMAT(8F10.4)
        WSLOPE = (CW(1)-CW(NC))/(CP(1)-CP(NC))
        DO42 MP=1,NP
        W(MP)= WSLOPE*(BPSIT(MP)-CP(1)) + CW(1)
     42 CONTINUE
        DO500 MP=1,NP
        PRINT 700,BMP(MP),BOSIT(MP)  ,W(MP)
    700 FORMAT(1H ,3F14.6)
    500 CONTINUE
        CALL XYPLOT(NP,W,RMP)
        PRINT 100
    100 FORMAT(1H1)
C       COMPUTE DISTRIBUTION FUNCTION
        DAMP(1)=0.0
        DO8MP=2,NP
        MPM1=MP-1
        DAMP(MP)=DAMP(MPM1)+(MBP(MP)+BMP(MPM1))/2.0*ABS(W(MP)-W(MPM1))
      8 CONTINUE
C       COMPUTE EQUIVALENT VALUES
        ANE = NE
        DO9ME=1,NE
        AME=ME
```

```
      RAMP(ME)=DAMP(NP)*(2.0*AME-1.0)/(2.0*ANE)
    9 CONTINUE
C     COMPUTE EQUIVALENT WAVELENGTHS
      MP=1
      DO13 ME=1,NE
   12 CONTINUE
      IF(RAMP(ME)-DAMP(MP))11,11,10
   10 MP=MP/1
      GO TO 12
   11 MPM1=MP-1
      A=BMP(MPM1)
      A2=A*A
      SLOPE = (BMP(MP)-BMP(MPM1))/ABS(W(MP)-W(MPM1))
      DAREA = RAMP(ME)-DAMP(MPM1)
      DW = (-A/SQRT(A2/2.0*SLOPE*DAREA))/SLOPE
      IF(W(MP) -W(MPM1))16,16,17
   16 DW = - DW
   17 CONTINUE
      RW(ME)=W(MPM1)/DW
      PRINT 14,ME,RW(ME)
   14 FORMAT(1H ,'EQUIVALENT WAVELENGTH',I3,' = 1, E14.7)
   13 CONTINUE
  200 CONTINUE
      STOP
      END
 *RUN


EQUIVALENT WAVELENGTH 1 =   .5131507E/04
EQUIVALENT WAVELENGTH 2 =   .5139757E/04
EQUIVALENT WAVELENGTH 3 =   .5144265E/04
EQUIVALENT WAVELENGTH 4 =   .5147996E/04
EQUIVALENT WAVELENGTH 5 =   .5151453E/04
EQUIVALENT WAVELENGTH 6 =   .5154773E/04
EQUIVALENT WAVELENGTH 7 =   .5158907E/04
EQUIVALENT WAVELENGTH 8 =   .5161667E/04
EQUIVALENT WAVELENGTH 9 =   .5166226E/04
EQUIVALENT WAVELENGTH 10 =  .5175886E/04


EQUIVALENT WAVELENGTH 1 =   .5199496E/04
EQUIVALENT WAVELENGTH 2 =   .5181980E/04
EQUIVALENT WAVELENGTH 3 =   .5169691E/04
EQUIVALENT WAVELENGTH 4 =   .5157886E/04
EQUIVALENT WAVELENGTH 5 =   .5146375E/04
EQUIVALENT WAVELENGTH 6 =   .5135242E/04
EQUIVALENT WAVELENGTH 7 =   .5124281E/04
EQUIVALENT WAVELENGTH 8 =   .5113277E/04
EQUIVALENT WAVELENGTH 9 =   .5101433E/04
EQUIVALENT WAVELENGTH 10 =  .5083031E/04
```

APPENDIX III-3

DETAILED MATHEMATICS FOR POINT SOURCE ARRAY

The analytic expression for the radiation from the point-sources data array is found with the aid of Figure AIII-1. The complex amplitude of the object, or data, beam is

$$U_{obj}(\alpha,\beta) = \sum_i \sum_j A_{ij} e^{iks_{ij}} / s_{ij}$$

where

$$s_{ij} = \left[s_o^2 + (\alpha - x_i)^2 + (\beta - y_j)^2 \right]^{\frac{1}{2}}$$

The converging reference beam is expressed as

$$U_{ref}(\alpha,\beta) = A_{ref} e^{-iku} / u$$

where

$$u = \left[u_o^2 + (\alpha - \alpha_o)^2 + (\beta - \beta_o)^2 \right]^{\frac{1}{2}}$$

Note that the reference beam converges through the hologram plane to a point u_o distance behind the α_o, β_o point of the hologram plane. The complex amplitude of the radiation impinging on the film is

$$U(\alpha,\beta) = U_{ref} + U_{obj}$$

The intensity is

$$I(\alpha,\beta) = |U_{ref}|^2 + |U_{obj}|^2 + U_{ref} U_{obj}^* + U_{ref}^* U_{obj}$$

If a gamma of minus two is assumed, the transmission function of the hologram will be directly proportional to these terms. The first two terms are noise as far as the image reconstruction is concerned.

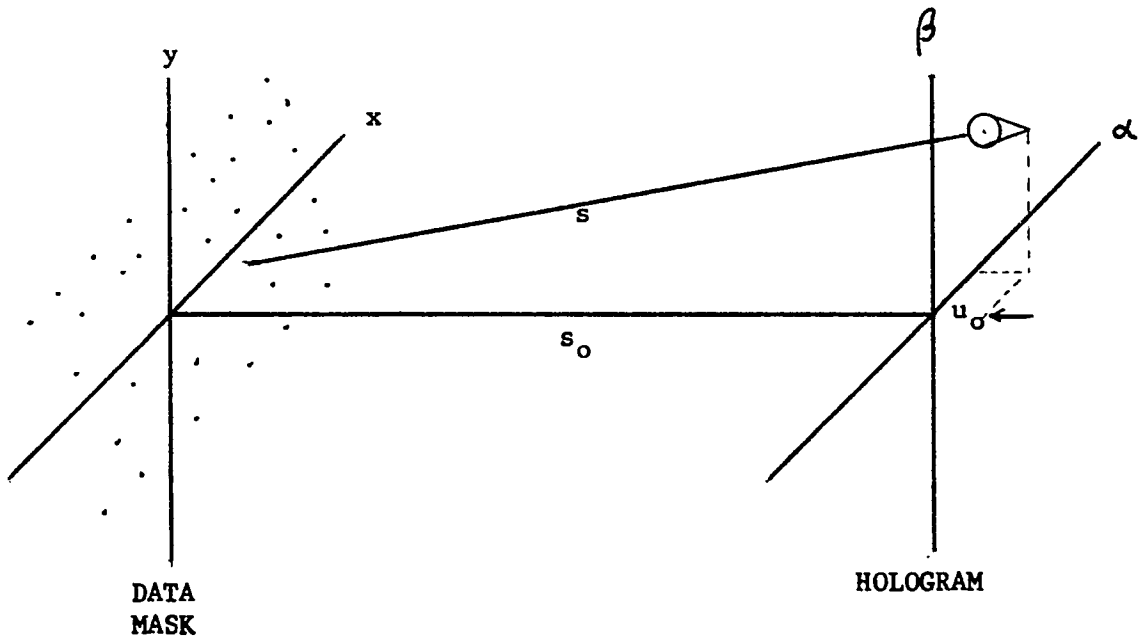

POINT SOURCE DATA MASK GEOMETRY

FIGURE AIII - 1

Since the computer will be generating the hologram, these first two terms will be deleted from the picture. Notice that this is not possible in physically produced holograms and constitutes one advantage of the computer generated hologram of Chapter IV. The third and fourth terms are the terms of interest. In particular, it is the third term that forms the desired real image. The fourth term generates a virtual image. For the purposes of this system, this virtual image is also noise and, therefore, it would be desirable to suppress the fourth term. However, the sum of $U_{ref}U^{*}_{obj}$ and $U^{*}_{ref}U_{obj}$ is the real function and, since it is impractial to generate complex functions, it is the sum that is used in making the hologram.

The term of interest is

$$T_3(\alpha,\beta) = \sigma A_{ref}\, e^{-ik\left[u_o + (\alpha-\alpha_o)^2/(2u_o) + (\beta-\beta_o)^2/(2u_o)\right]}$$

$$\sum_i \sum_j A^{*}_{ij}\, e^{-ik\left[s_o + (\alpha-x_i)^2/(2s_o) + (\beta-y_j)^2/(2s_o)\right]}$$

The reconstruction source is modeled exactly as it was in the previous section of Chapter III. Thus, using the coordinates of Figure AIII-2.

$$U_{recon}(\alpha,\beta,\mu,\nu,t) = A_{recon}(\mu,\nu,t)\,\frac{e}{v}^{ik_2(\mu,\nu),t)v}$$

where

$$v = \left[v_o^2 + (\alpha-\alpha_{RC}-\mu)^2 + (\beta-\beta_{RC}-\nu)^2\right]^{\frac{1}{2}}$$

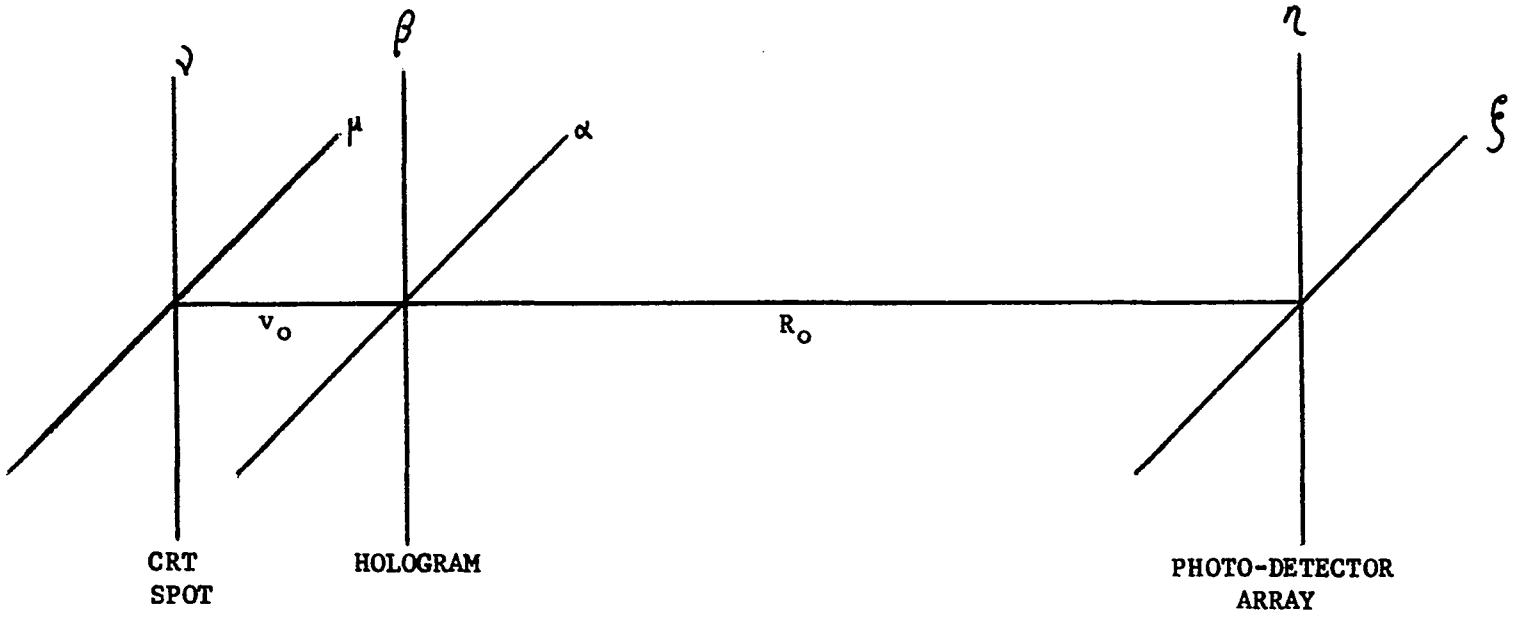

READ-OUT GEOMETRY

FIGURE AIII - 2

Using the Rayleigh-Sommerfeld formulation and labelling U_3 as U_{image}

$$U_{image}(\xi,\eta,\mu,\nu,t) = \frac{1}{i\lambda_2}\iint T_3(\alpha,\beta)\,\frac{e^{ikR}}{R}\,U_{recon}(\alpha,\beta,\mu,\nu,t)\,d\alpha\,d\beta$$

where

$$R = \left[R_o^2 + (\xi-\alpha)^2 + (\eta-\beta)^2\right]^{\frac{1}{2}}$$

Initial concentration is centered on the exponent of the integrand. Using the paraxial, or sagittal, approximation, this expands to

$$(\alpha^2+\beta^2)\left[\frac{-k}{2u_0} - \frac{k}{2s_0} + \frac{k_2}{2v_0} + \frac{k_2}{2R_0}\right]$$

$$+ \alpha\left[-k\left(\frac{-\alpha_o}{u_o}\ \frac{-x_i}{s_o}\right) + k_2\left(\frac{-\alpha_{RC}}{v_o}\ \frac{-\mu}{v_o}\ \frac{-\xi}{R_o}\right)\right]$$

$$+ \beta\left[-k\left(\frac{-\beta_o}{u_o}\ \frac{-y_j}{s_o}\right) + k_2\left(\frac{-\beta_{RC}}{v_o}\ \frac{-\nu}{v_o}\ \frac{-\eta}{R_o}\right)\right]$$

$$-k\left[u_o + \frac{\alpha_o^2}{2u_o} + \frac{\beta_o^2}{2u_o} + s_o + \frac{x_i^2}{2s_o} + \frac{y_j^2}{2s_o}\right]$$

$$+ k_2\left[v_o + \frac{\alpha_{RC}^2}{2v_o} + \frac{\mu^2}{2v_o} + \frac{\alpha_{RC}\mu}{v_o} + \frac{\beta_{RC}^2}{2v_o} + \frac{\nu^2}{2v_o} + \frac{\beta_{RC}\nu}{v_o} + \frac{\xi^2}{2R_o} + \frac{\eta^2}{2R_o}\right]$$

$$= (\alpha^2+\beta^2)\,C' + \alpha D' + \beta E' + G'$$

After separating the variable, one would then need to integrate

$$\int e^{i\alpha^2 C + i\alpha D}\,d\alpha$$

in the α direction. A similar integration must be performed over β. As it involves Fresnel Integrals, this integration is not convenient, to say the least.[51] The substitutions of

$$\alpha = z \cos \psi$$

$$\beta = z \sin \psi$$

lead to

$$\int_z \int_\psi e^{iC'z^2} \quad e^{iF'z} \quad d\psi \, z dz$$

$$= \int_z e^{iCz^2} \; 2\pi J_o(F'z) \; z dz$$

For the cases of interest, further integration is impeded because a series approximation of the exponential is not convenient since C' is too large. As an example, let

$$k_2 = k + \Delta k$$

$$u_o = v_o$$

$$s_o = R_o$$

then

$$C = \tfrac{1}{2} \Delta k \left[\frac{1}{v_o} + \frac{1}{R_o} \right]$$

If $\alpha_{max} = 1.0\text{cm}$, $\Delta k_{max} = 2\pi \frac{50}{(5000)^2} \; 10^8 \; \text{cm}^{-1}$, $v_o = 3\text{cm}$, and $R_o = 15\text{cm}$, then

$$(\alpha^2 + \beta^2) \; \frac{\Delta k}{2} \quad \left[1/v_o + 1/R_o \right] = 2\pi(80)$$

---

51 G. Thomas, Calculus and Analytic Geometry, Addison-Wesley Publishing Co., Reading, Mass., 1961, pp. 697-8.

However, consider the fact that a reasonable page size is in the order of 1.5mm. To use this information, set

$$\alpha = \alpha' + \alpha_o$$

$$\beta = \beta' + \beta_o$$

$$\alpha = w \cos \phi$$

$$\beta = w \sin \phi$$

then

$$u = u_o + \frac{w^2}{2u_o}$$

$$s = s_o + \frac{w^2}{2s_o} + \frac{(\alpha_o - x_i)}{s_o} w \cos \phi + \frac{(\beta_o - y_j)}{s_o} w \sin \phi$$

$$+ \frac{(\alpha_o - x_i)^2}{2s_o} + \frac{(\beta_o - y_j)^2}{2s_o}$$

$$v = v_o + \frac{w^2}{2v_o} + \frac{(\alpha_o - \alpha_{RC} - \mu)}{v_o} w \cos \phi + \frac{(\beta_o - \beta_{RC} - \nu)}{v_o} w \sin \phi$$

$$+ \frac{(\alpha_o - \alpha_{RC} - \mu)^2}{2v_o} + \frac{(\beta_o - \beta_{RC} - \nu)^2}{2v_o}$$

and

$$R = R_o + \frac{w^2}{2R_o} + \frac{(\alpha_o - \xi)}{R_o} w \cos \phi + \frac{(\beta_o - \eta)}{R_o} w \sin \phi$$

$$+ \frac{(\alpha_o - \xi)^2}{2R_o} + \frac{(\beta_o - \eta)^2}{2R_o}$$

Using these relationships, the exponent can be rewritten as

$$w^2 \left[-\frac{k}{2u_o} - \frac{k}{2s_o} + \frac{k_2}{2v_o} + \frac{k_2}{2R_o} \right]$$

$$+ w \cos \phi \left[-k \frac{(\alpha_o - x_i)}{s_o} + k_2 \frac{(\alpha_o - \alpha_{RC} - \mu)}{v_o} + k_2 \frac{(\alpha_o - \xi)}{R_o} \right]$$

$$+ w \sin \phi \left[-k \frac{(\beta_o - y_j)}{s_o} + k_2 \frac{(\beta_o - \beta_{RC} - \nu)}{v_o} + k_2 \frac{(\beta_o - \eta)}{R_o} \right]$$

$$- k \left[u_o + s_o + \frac{(\alpha_o - x_i)^2 + (\beta_o - y_j)^2}{2s_o} \right]$$

$$+ k_2 \left[v_o + R_o + \frac{(\alpha_o - \alpha_{RC} - \mu)^2}{2v_o} + \frac{(\beta_o - \beta_{RC} - \nu)^2}{2v_o} + \frac{(\alpha_o - \xi)^2}{2R_o} + \frac{(\beta_o - \eta)^2}{2R_o} \right]$$

$$= Cw^2 + Dw \cos \phi + Ew \sin \phi + G$$

Using this simplified notation, the reconstruction term is written as

$$U_3(\mu, \nu, \xi, \eta, t) = \frac{1}{i\lambda_2} \int_w \int_\phi \frac{A_{ref}}{u_o} \sum_i \sum_j \frac{A_{ij}^*}{s_o} \frac{A_{recon}}{v_o} \frac{1}{R_o}$$

$$e^{i (Cw^2 + Dw\cos \phi + Ew\sin \phi + G)} \, d\phi \, w dw$$

Letting

$$F = (D^2 + E^2)^{\frac{1}{2}}$$

$$U_3(\mu, \nu, \xi, \eta, t) = \frac{1}{i\lambda_2} \sum_i \sum_j e^{iG} \, A_{ref} A_{ij}^* A_{recon}$$

$$\int_w e^{iCw^2} \int_0^{2\pi} e^{iFw\cos(\phi - \tan^{-1}E/D)} \, d\phi \, w\,dw$$

$$= \frac{1}{i\lambda_2} \frac{A_{ref} A_{recon}}{u_o s_o v_o R_o} \sum_i \sum_j A_{ij} e^{iG} \int_w e^{iCw^2} 2\pi J_o(Fw) \, w\,dw$$

Using the values of the previous example and the hologram size of 1.5mm; i.e. $C_{max} \approx 80$ and $w^2_{max} = (0.075)^2$, one finds

$$C_{max} w^2_{max} = 1.4$$

Recalling that

$$e^{iX} = \cos X + i \sin X$$

and

$$\cos X = 1 - X^2/2 + X^4/4 - X^6/6 + X^8/8 \ldots\ldots$$

$$\sin X = X - X^3/3 + X^5/5 - X^7/7 + X^9/9 \ldots\ldots$$

then the evaluated trignometric series can be written as

$$\cos(1.4) = 1 - 0.980 + 0.1600667 - 0.0104577 + 0.0003660 - 7.971082(10^{-6}) + 1.183585(10^{-7}) - 1.274630(10^{-9})\ldots$$

$$\sin(1.4) = 1.4 - 0.4573333 + 0.0448187 - 0.0020915 + 0.0000569 - 1.014501(10^{-6}) + 1.274630(10^{-8}) - 1.189654(10^{-10})\ldots$$

Since $U(\xi,\eta)$ is composed of (t)·(m)·(n)·(i)·(j) components, a specific case is required to compute the required accuracy of each component; i.e., $U(\xi,\eta,\mu,\nu,t)$ and, thence, the required number of terms for the trignometric series. For this development, let mn = 50, t = 10, and ij = 10. If 1% overall accuracy is desired, each term must be accurate

to one part in 500,000, or two parts per one million. As is well known,[51] the sine and cosine series are in error by less than the first term dropped. Therefore, to determine the required number of terms in each one need only to perform the following computations;

$$\text{cosine: } @6 \text{ terms } \frac{1.1836(10^{-7})}{1.7(10^{-1})} = \frac{.695}{10^6}$$

$$@5 \text{ terms } \frac{7.971(10^{-6})}{1.7(10^{-1})} = \frac{46.7}{10^6}$$

$$\text{sine: } @5 \text{ terms } \frac{1.0145(10^{-6})}{0.98} = \frac{1.04}{10^6}$$

$$@4 \text{ terms } \frac{5.69(10^{05})}{0.98} = \frac{58.1}{10^5}$$

Therefore, for the cosine, six terms are required and for the sine, five terms are needed. Thus, the integrand is

$$\left[1 - \frac{C^2 w^4}{2!} + \frac{C^4 w^8}{4!} - \frac{C^6 w^{12}}{6!} + \frac{C^8 w^{16}}{8!} - \frac{C^{10} w^{20}}{10!} \right.$$

$$\left. + i \left(Cw - \frac{C^3 w^6}{3!} + \frac{C^5 w^{10}}{5!} - \frac{C^7 w^{14}}{7!} + \frac{C^9 w^{18}}{9!} \right) \right] w J_o(Fw)$$

Using the relationship,[52]

---

[52] Born and Wolf, op. cit., p. 395.

$$\int X^{p\neq1} J_p(X)\, dX = X^{p\neq1} J_{p\neq1}(X)$$

and its expanded version

$$\int X^{m\neq p\neq1} J_p(X)\, dX = \int X^m X^{p\neq1} J_p(X)\, dX$$

$$= X^{m\neq p\neq1} J_{p\neq1}(X) - \int m X^{m\neq p} J_p(X)\, dX$$

obtained from integration-by-parts, the series integrand can be integrated as shown below;

$$\int_0^{w_o} w J_o(Fw)\, dw = w_o J_1(Fw_o)$$

$$\int_0^{w_o} -\frac{c^2 w^4}{2} w J_o(Fw)\, dw = -\frac{c^2}{F^6 2!}\left[F^5 w_o^5 J_1(Fw_o) \right.$$

$$\left. -4\int_0^{w_o} F^3 w^3 Fw J_1(Fw)\, dFw \right.$$

$$= -\frac{c^2}{2!F^6}\left[F^5 w_o^5 J_1(Fw_o) - 4 F^4 w_o^4 J_2(Fw_o)\right.$$

$$\left. \neq 8 F^3 w_o^3 J_3(Fw_o)\right]$$

or in general

$$\int_0^{w_o} w^n J_o(Fw)\, dw = \frac{1}{F^{n\neq1}}\left[(Fw_o)^n J_1(Fw_o) - (n-1)(Fw_o)^{n-1} J_2(Fw_o)\right.$$

$$+ (n-1)(n-3)(Fw_o)^{n-2} J_3(Fw_o)$$

$$- (n-1)(n-3)(n-5)(Fw_o)^{n-3} J_4(Fw_o)$$

$$+ (n-1)(n-3)(n-5)(n-7)(Fw_o)^{n-4} J_5(Fw_o)$$

$$- (n-1)(n-3)(n-5)(n-7)(n-9)$$

$$(Fw)^{n-10} (Fw)^5 J_5(Fw)\, dFw \Big]$$

Note that this series is finite if "n" is odd.

The integral can be expressed as

$$\frac{w_o}{F} J_1(Fw_o) + iC\left[\frac{w_o^3}{F} J_1(Fw_o) - \frac{2w_o^2}{F^2} J_2(Fw_o)\right]$$

$$- \frac{C^2}{2}\left[\frac{w_o^5}{F} J_1(Fw_o) - \frac{4w_o^4}{F^2} J_2(Fw_o) + \frac{8w_o^3}{F^3} J_3(Fw_o)\right]$$

$$- \frac{iC^3}{6}\left[\frac{w_o^7}{F} J_1(Fw_o) - \frac{6w_o^6}{F^2} J_2(Fw_o) + \frac{24w_o^5}{F^3} J_3(Fw_o)\right.$$

$$\left. - \frac{48w_o^4}{F^4} J_4(Fw_o)\right] + \text{etc.}$$

This expression can be regrouped as

$$\sum_{b=1}^{11} f_b J_b(Fw_o)$$

where

$$f_1 = \frac{1}{F}\left[w_o - \frac{C^2 w_o^5}{2} + \frac{C^4 w_o^9}{24} - \frac{C^6 w_o^{13}}{720} + \frac{C^8 w_o^{17}}{40320} - \frac{C^{10} w_o^{21}}{3628800} + i\left(C w_o^3 - \frac{C^3 w_o^7}{6} + \frac{C^5 w_o^{11}}{120} - \frac{C^7 w_o^{15}}{5040} + \frac{C^9 w_o^{19}}{362880} \right) \right]$$

$$f_2 = \frac{1}{F^2}\left[2C^2 w_o^4 - \frac{C^4 w_o^8}{3} + \frac{C^6 w_o^{12}}{60} - \frac{C^8 w_o^{16}}{2540} + \frac{C^{10} w_o^{20}}{181440} + i\left(-2C w_o^2 + C^3 w_o^6 - \frac{C^5 w_o^{10}}{12} + \frac{C^7 w_o^{14}}{360} - \frac{C^9 w_o^{18}}{20160} \right) \right]$$

f_3 etc.

The real image reconstruction signal is written as

$$U_{image}(\xi,\eta,\mu,\nu,t) = \frac{A_{ref} A_{recon}}{i \lambda_2 u_o s_o v_o R_o} \; 2\pi \sum_i \sum_j \left[A_{ij}^* \, e^{iG} \sum_{b-1}^{11} f_b J_b(F w_o) \right]$$

For computational efficiency, one would allow

$$f_b = \frac{g_b}{F^b}$$

At this point, as a prelude to programming the expression for U_3, it is worthwhile to explicitly note the dependencies. Therefore,

$$k_2 = k_2(\mu,\nu,t)$$

$$A_{recon} = A_{recon}(\mu,\nu,t)$$

$$G = G(\mu,\nu,t,x,y,\xi,\eta)$$

$$F = F(\mu, \nu, t, x, y, \xi, \eta)$$

$$g = g(\mu, \nu, t)$$

$U_{image}(\xi, \eta, t)$ is obtained by summing $U_{image}(\xi, \eta, \mu, \nu, t)$ over all the points of the μ, ν source model.

APPENDIX III-4

CMPOUT FORTRAN PROGRAM

```
      PROGRAM CMPOUT
      DIMENSION WL2(15),AMU(50),X(4),Y(4),  PDM(50),PEN(50)
      DIMENSION PGN(50),PDZ(100),PEE(100),PGE(100),PDX( 4),PEY( 4)
      DIMENSION REPGXY( 4),QEPGXY( 4),AK2
      DIMENSION ZETA(100),ETA(100),PGM(50),GPZ(100)
      DIMENSION REPGN(50),QEPGN(50),REPGZ(100),QEPGZ(100)
      DIMENSION REPGE(100),QEPGE(100)
      DIMENSION DSQ(4,50,100),ESQ(4,50,100)
      READ 454, WO
  454 FORMAT(F10.4)
C     READ UO IN CENTIMETERS - RECONSTRUCTION SOURCE DISTANCE
      READ 400, UO
  400 FORMAT(F10.4)
C     READ OBJECT DISTANCE, RO, IN CENTIMETERS
      READ400, RO
C     READ ALPHA ZERO, REFERENCE SOURCE CENTER POSITION, IN CM AND
C     ALPHA RC, RECONSTRUCTION SOURCE CENTER POSITION; FROM ONE CARD
      READ 401, AO,ARC
  401 FORMAT(2F10.4)
      ALPO = AO
C     SAME FOR BETAS
      READ 401, BO,BRC
      BETO=BO
      AOMARC = AO - ARC
      BOMBRC = BO - BRC
C     READ THE NUMBER OFFREQUENCY POINTS TO BE USED
      READ 402, NK
  402 FORMAT(I5)
      READ 404,WL2(1),WL2(2),WL2(3),WL2(4),WL2(5),WL2(6)
      READ404,WL2(7),WL2(8),WL2(9),WL2(10),WL2(11),WL2(12)
  404 FORMAT(6F10.4)
      READ 405,WL
  405 FORMAT(F10.4)
  403 FORMAT(6F10.4)
C     READ THE FREQUENCIES  IN ANGSTROMS
C     READ RECONSTRUCTION SOURCE POSITION STRUCTURE, MU, IN CM
C     READ NUMBER OF MU POINTS
      READ403,AMU( 1),ANU(1),AMU(2),ANU(2),AMU(3),ANU( 3)
      READ403,AMU( 4),ANU( 4),AMU( 5),ANU( 5),AMU( 6),ANU( 6)
      READ 403,AMU( 7),ANU( 7),AMU( 8),ANU( 8),AMU( 9),ANU( 9)
      READ403,AMU(10),ANU(10),AMU(11),ANU(11),AMU(12),ANU(12)
      READ403,AMU(13),ANU(13),AMU(41),ANU(14),AMU(15),ANU(15)
      READ403,AMU(16),ANU(16),AMU(17),ANU(17),AMU(18,ANU(18)
      READ403,AMU(19),ANU(19),AMU(20),ANU(20),AMU(21),ANU(21)
      READ403,AMU(22),ANU(22),AMU(23),ANU(23),AMU(24),ANU(24)
```

```
      READ403,AMU(25),ANU(25),AMU(26),ANU(26),AMU(27),ANU(27)
      READ403,AMU(28),ANU(28),ANU(29),ANU(29),AMU(30),ANU(30)
      READ403,AMU(31),ANU(31),AMU(32),ANU(32),AMU(33),ANU(33)
      READ403,AMU(34),ANU(34),AMU(35),ANU(35),AMU(36),ANU(36)
      READ403,AMU(37),ANU(37),AMU(38),ANU(38),AMU(39),ANU(39)
      READ403,AMU(40),ANU(40),AMU(41),ANU(41),AMU(42),ANU(42)
      READ403,AMU(43),ANU(43),AMU(44),ANU(44),AMU(45),ANU(45)
      READ403,AMU(46),ANU(46),AMU(47),ANU(47),AMU(48),ANU(48)
      READ403,AMU(49),ANU(49),AMU(5),ANU(50)
      READ 402, NMU
      READ 402, NNU
      MNUNU = NMU * NNU
      NMU = NMUNU
      NNU = NMU
C     READ EQUIVALENT WAVELENGTHS IN
C     READ NUMBER OF X POINTS
      READ 402, NXY
C     I WANT X&Y PAIRS, NOT ROWS AND COLUMNS
      READ404,X(1),Y(1),X(2),Y(2),X(3),Y(3),X(3),Y(3),X(4),Y(4)
C     SET MY = MX AND DROP MY LOOPS
      READ 450, ZETAA,ZETAB
  450 FORMAT(2F10.4)
      DO 451 MZETA =1,NZETA
      AMZETA = MZETA
      ANZETA = NZETA
      ZETA(MZETA)=ZETAA+(ZETAB -ZETAA)*(AMZETA -1.0)/(ANZETA -1.0)
  451 CONTINUE
      READ452,ETAA,ETAB
  452 FORMAT(2F10.4)
      READ NETA
      DO 453 META = 1,NETA
      AMETA = META
      ANETA = NETA
      ETA(META)=ETAA +(ETAB -ETAA)*(AMETA -1.0)/(ANETA -1.0)
  453 CONTINUE
      PI = 3.1415
      AK = 2.0*PI/WL *1.0E8
      RUO =1.0/UO
      RRO=1.0/RRO
      ARECON=1.0
      AREF=1.0
      RGCON1= COS(-AK*(UO+RO)) * AREF * ARECON * (RRO*RRO*RUO*RUO)
      QGCON1 = SIN(-AK*(UO+RO))* AREF * ARECON * (RRO*RRO*RUO*RUO)
      GC1 = 1.0/24.0
      GC2 =  1.0/720.0
      GC  3 = 1.0 /40320.0
      GC 4 = 1.0/3628800.0
      GC 4 = 1.0/3628800.0
      GC5=1.0/6.0
      GC6=1.0/120.0
      GC7=1.0/5040.0
```

```
GC8=1.0/362880.0
GC9=1.0/9.0
GC10=1.0/60.0
GC11=1.0/2540.0
GC12=1.0/181440.0
GC13=1.0/12.0
GC14=1.0/360.0
GC15=1.0/20160.0
GC16=1.0/6.0
GC17=1.0/180.0
GC18=1.0/10080.0
GC19=2.0/3.0
GC20=1.0/30.0
GC21=1.0/1260.0
GC22=4.0/3.0
GC23=1.0/15.0
GC24=1.0/630.0
GC25=1.0/3.0
GC26=1.0/90.0
GC27=2.0/3.0
GC28=1.0/45.0
GC29=8.0/3.0
GC30=2.0/15.0
GC31=16.0/3.0
GC32=4.0/15.0
GC33=4.0/3.0
GC34=8.0/3.0
GC35=32.0/3.0
GC36=64.0/3.0
W02 = W0*W0
W03 =W02 *W0
W04 = W03 * W0
W05 =W03 *W02
W06 = W05 * W01
W07 = W06 * W0
W08 = W07 * W0
W09 = W08 * W0
W010 = W09 * W0
W011 = W010 * W0
W012 = W011 * W0
W013 = W012 * W0
W014 = W013 * W0
W015 = W014 * W0
W016 = W015 * W0
W017 = W016 * W0
W019 = W018 * W0
W020 = W019 * W0
W021 = W020 * W0
W022 = W021 * W0
W023 = W022 * W0
W024 = W023 * W0
```

```
      WO25 = WO24 * WO
      WO26 = WO25 * WO
      WO27 = WO26 * WO
      WO28 = WO27 * WO
      WO29 = WO28 * WO
      DO300MMU=1,NMU
C     AAOMARC - AO MINUS ARC
C      AMU - A PREFIXED TO MU FOR REAL TYPE
C      PPD  - PART OF PART OF     D
      PPD=AOMARC - AMU(MMU)
C      PDM - PART OF D DUE TO MU
      PDM(MMU)=PPD*RUO
C      PGM - PART OF G DUE TO MU
      PGM(MMU)=PDM(MMU)*PPD*0.5
      MNU = MMU
      PPE= BOMBRC a ANU(MNU)
      PEN(MNU)= PPE*RUO
      PGN(MNU)= PEN(MNU)*PPE*0.5
  300 CONTINUE
      DO 304 MZETA=1,NZETA
      AMZ= ALPO -ZETA(MZETA)
      PDZ(MZETA)=AMZ*RRO
      PGZ(MZETA)= PDZ(MZETA)*AMZ*0.5
  304 CONTINUE
      DO 305 META=1,NETA
      BME=BETO - ETA(META)
      PEE(META)=BME*RRO
      PGE(META)=PEE(METZ)*BME*0.5
  305 CONTINUE
      DO308 MX=1,NX
      AOMX=ALPO -X(MX)
      PDX(MX)= -AOMX*RRO*AK
      PGX=PDX(MX)*AOMX*0.5
C      REPGX - REAL PART OF THE EXPONENTIAL OF G DUE TO X
      REPGX    = COS(PGX)
      QEPGX    = SIN(PGX)
      MY = MX
      BOMY= BETO - Y(MY)
      PEY(MY)= -AOMX*RRO*AK
      PGY=PEY(MY)*BOMY)0.5
      REPGY    = COS(PGY)
      QEPGY     = SIN(PGY)
      QEPGXY(MX   )=REPGX     *QEPGY    / QEPGX     *REPGY
      REPGXY(MX   )= REPGX     *REPGY    -QEPGX     *QEPGY
  308 CONTINUE
      DO600 MK=1,NK
      AK2(MK) = 2.0*PI/WL2(MK)    *1.0E8
      C1 = (-AK / AK2(MK)) *(RUO / RRO)
      C = CL
      C2 = C1 *C1
      C3 = C2 * C1
      C4 = C2 * C1
```

```
      C5 = C4 * C1
      C6 = C5 * C1
      C7 = C6 * C1
      C8 = C7 * C1
      C9 = C8 * C1
      C10 = C9 * C1
      CWO2=C*WO*WO
      RSMALL = (0.5/C)*SIN(CWO2)
      QSMALL = (0.5/C)*(1.0-COS(CWO2))
      RGAM1 = WO -0.5*C2*WO5 + GC1*C4*WO9 - GC2*C6*WO13 + GC3*C8*WO17
     1 -GC4*C10*WO21
      QGAM1 = C1*WO3 - GC5*C3*WO7 + GC6*C5*WO11 - GC7*C7*WO15 + GC8*C9IW
     1 019
      RGAM2 = 2.0*C2*WO4 - GC9*C4*WO8 + GC10*C6*WO12 -GC11*C8*WO16 +
     1 GC12*C10*WO20
      QGAM2 = -2.0*C1*WO2 + C3*WO6 - GC13*C5*WO10 + GC14*C7*WO14
     1 -GC15*C9*WO18
      RGAM3 = -4.0*C2*WO3 +2.0*C4*WO7 -GC16*C6*WO11 + GC17*C8*WO15
     1 - GC18*C10*WO19
      QGAM3 = -4.0*C3*WO5 + GC19*C5*WO9 -GC20*C7*WO13 +GC21*C9*WO17
      RGAM4 = -8.0*C4*WO6 +GC22*C6*WO10 - GC23*C8*WO14 + GC24*C10*WO18
      QGAM4 = 8.0*C3*WO4 - 4.0*C5*WO8 + GC5*C7*WO12 -GC26*C9*WO16
      RGAM5 = 16.0*C4*WO5 - 8.0*C6*WO9+GC27*C8*WO13 -GC28*C10*WO17
      QGAM5 = 16.0*C5*WO7 -GC29*C7*WO11 + GC30*C9*WO15
      RGAM6 = 32.0*C6*WO8 -GC31*C8*WO12 + GC32*C10*WO16
      QGAM6 = -32.0*C5*WO6 +16.0*C7*WO10 -GC33*C9*WO14
      RGAM7 = -64.0*C6*WO7 + 32.0*C8*WO11 - GC34*C10*WO15
      QGAM7 = -64.0*C7*WO9 + GC35*C9*WO13
      RGAM8 = -128.0*C8*WO10 + GC36*C10*WO14
      QGAM8 = 128.0*C7*WO8 - 64.0*C9*WO12
      RGAM9 = 256.0*C8*WO9 -128.0*C10*WO13
      QGAM9 = 256.0*C9*WO11
      RGAM10 = 512.0*C10*WO12
      QGAM10 = -512.0*C9*WO10
      RGAM11 = -1024.0*C10*WO11
      QGAM11 = 0.0
      QGTV= AK2
      REGTV= COS(QGTV)
      QEGTV = SIN(QGTV)
      RGCON2= RGCON1*REGTV - QGCON1*QEGTV
      QGCON2= RGCON1*QEGTV + QGCON1*REGTV
C     GCON3 IS A DUMMY CREATED TO ALLOW FOR THE DIVISION BY I
      RGCON3 = QGCON2
      QGCON3 = -RGCON2
      RGCON2 = RGCON3  *AK2(MK)
      QGCON2 = QGCON3  *AK2(MK)
      DO 320 MMU=1,NMU
      QUAD=AK2(MK)*PGM(MMU)
      REPGM(MMU)= COS(QUAD)
      QEPGM(MMU) = SIN(QUAD)
  320 CONTINUE
```

```
      DO322 MNU=1,NNU
      QUAD=AK2(MK)*PGN(MNU)
      REPGN(MNU)= COS (QUAD)
      QEPGN(MNU) = SIN(QUAD)
  322 CONTINUE
      DO324 MZETA = 1,NZETA
      QUAD = AK2(MK) *PGZ(MZETA)
      REPGZ(MZETA) = COS (QUAD)
      QEPGZ(MZETA) = SIN (QUAD)
      DO324 MMU=1,NMU
      PART = AK2(MK)*(PDM(MMU)/PDZ(MZETA)
      DO324 MX=1,NX
      D = PDX(MX) / PART
      DSQ(MX,MMU,MZETA) = D * D
  324 CONTINUE
      DO326 META=1,NETA
      QUAD=AK2(MK)*PGE(META)
      REPGE(META)= COS(QUAD)
      QEPGE(META) = SIN(QUAD)
      DO 326 MNU=1,NNU
      PART = AK2(MK)*(PEN(MNU) / PEE(META))
      DO 326 MY = 1, NY
      E = PEY(MY) / PART
      ESQ(MY,MNU,META) = E * E
  326 CONTINUE
      DO 390 MMU=1,NMU
      REXPG= RGCON2*REPGM(MMU) - QGCON2*QEPGM(MMU)
      QEXPG = RGCON2*QEPGM(MMU) / QGCON2*REPGM(MMU)
      MNU = MMU
      REXPG=REXPG *REPGN(MNU) - QEXPG*QEPGN(MNU)
      QEXPG= QEXPG*REPGN(MNU) / REXPG*QEPGN(MNU)
      MZTET = 0
      DO390 MZETA=1,NZETA
      REXPG1=REXPG *REPGZ(MZETA)- QEXPG*QEPGZ(MZETA)
      QEXPG1= QEXPG*REPGZ(MZETA)/ REXPG*QEPGZ(MZETA)
      IF(MZETA - 25) 110,111,110
  110 IF(MZETA - 76) 112,111,112
  112 META1=25
      META2=100
      META3=51
      GO TO 113
  111 META1=1
      META2=100
      META3=1
  113 CONTINUE
      DO 380 META = META1, META2,META3
      MZTET = MZTET / 1
C     MZTET IS A COUNTER SET UP TO AVOID THE 100 BY 100 MATRIX NECESSARY
C     TO HOLD THE 4  100 POINTS STRAIGTH LINES
      REXPG2=REXPG/*REPGE(META) - QEXPG1*QEPGE(META)
      QEXPG2= QEXPG1*REPGE(METZ) / REXPG1*QEPGE(META)
```

```
      RBSTOT=0.0
      QBSTOT=0.0
      DO 370 MX=1,NX
      MY = MX
      REXPG =REXPG * REPGXY(MX    ) - QEXPG * QEPGXY(MX    )
      QEXPG = QEXPG* REPGXY(MX    ) + REXPG * QEPGXY(MX    )
      FSQ = DSQ(MX,MMU,MZETA) * ESQ(MY,MNU,META)
      F=SQRT(FSQ)
      FWO=F*WO
      FWO2=FWO*FWO
      FWO3=FWO*FWO2
      FWO4=FWO*FWO3
      FWO5=FWO*FWO4
      IF( 90.0-FWO)10,10,11
   10  PO=1.0 -(9.0/(128.0*FWO2)) + (11025.0/(98304.0*FWO4) )
       QO=(-.125/FWO) + (225.0/(3072.0*FWO3)) +((-893025.0)/(3932160.0*
     1 FWO5))
       P1= 1.0 + (15.0/(128.0*FWO2)) + (14175.0/(98304.0*FWO4))
       Q1=0.375/FWO - (315.0/(3072.0*FWO3)) + (1091475.0/(31457280.0*
     1 FWO5))
       AJO=(SQRT(2.0/(PI*FWO)))*(PO*COS(FWO-PI/4.0) -QO*SIN(FWO-PI/4.0)
     1 )
       AJ1 =(SQRT(2.0/(PI*FWO)))*(PI*COS(FWO-(3.0*PI)/4.0)
     1 -QL*SIN(FWO-(3.0*PI)/4.0))
      RFWO=1.0/FWO
      AJ2=2.0*RFWO*AJ1-AJO
      AJ3=4.0*RFWO*AJ2-AJ1
      AJ4=6.0*RFWO*AJ3-AJ2
      AJ5=8.0*RFWO*AJ4-AJ3
      AJ6=10.0*RFWO*AJ5-AJ4
      AJ7=12.0*RFWO*AJ6-AJ5
      AJ8=14.0*RFWO*AJ7-AJ6
      AJ9=16.0*RFWO*AJ8-AJ7
      AJ10=18.0*RFWO*AJ9-AJ8
      AJ11=20.0*RFWO*AJ10-AJ9
       GO TO 12
   11  IF(FWO -0.001)13,13,14
   13 AJO=1.0
      RBESUM= RSMALL
      QBESUM=QSMALL
       GO TO 16
   14  CONVER = 0.000001
      XB = FWO
C     I HAVE MODIFIED THE STANDARD BESSEL FUNCTION ROUTINE SO AS TO
C     PRODUCE J N+1 AS WELL AS J N. J N+1 IS JNP1.
C     I HAVE DELETED THE TESTS FOR NEGATIVE ORDER (N) AS WELL AS FOR
C     ZERO ORDER ALSO I HAVE ELIMINATED THE TEST FOR N TOO LARGE
C     TO SET UP FOR SUM TO 11, MUST SET N = 10
      N=10
      BJ=0.0
C     DECIDE ON MMAX AND TEST FOR ALLOWABLE ORDER
   31 IF(F-15.0) 32,32,34
```

```
   32 NTEST = 20.0 / 10.0*XB - XB**2 /3.0
      GO TO 36
   34 NTEST = 90.0 / XB/2.0
   36 IF(N-NTEST) 40,38,38
   38 IER = 4
C     NEED ERROR MESSAGE
   40 IER = 0
      N1 = N/1
      BPREV = 0.0
C     DECIDE ON MSTART;I.E., MZERO
      IF(XB - 5.0) 50.60,50
   50 MA = XB/ 6.0
      GO TO 70
   60 MA = 1.4*XB/ 60.0/XB
   70 MB = N / IFIX(XB)/4 / 2
      IF(MA - MB) 71,71,72
   71 MZERO = MB
      GO TO 73
   72 MZERO = MA
   73 CONTINUE
      MMAX=NTEST
C     START LOOP TRYING M FROM MO TO MMAX IN STEOS OF 3
  100 DO 190 M=MZERO,MMAX,3
      FM1=1.OE-28
      FM=0.0
      ALPHA=0.0
C     TEST FOR M EVEN OR ODD
      IF(M-(M/2)*2)  120,115,120
  115 JT = -1
      GO TO 130
  120 JT=1
  130 M2=M-2
      DO160 K=1,M2
C     RUNS INDEX BACKWARDS
      MK=M-K
C     IF K=M-2, THEN MK=2
C     WHEM MK =2, BMK IS B1
      BMK =2.0*FLOAT(MK)*FM1/XB - FM
      FM=FM1
      FM1=BMK
      IF(MK-N-1) 150,140,150
C     IF MK=2, THEN BMK IS B1
  140 BJ=BMK
      BJMP1= FM
  150 JT= -JT
C     IF N ODD,S=0; IF N EVEN,S=2
      S=1/JT
C     RECALL ALPHA = FO / SUM OVER EVEN M OF 2*FM
  160 ALPHA = ALPHA / BMK*S
C     THIS IS FO
```

```
      BMK=2.0*FM1/XB - FM
  180 ALPHA = ALPHA + BMK
C     JN = FN / ALPHA
      BJ=BJ/ALPHA
      BJNP1=BJNP1/ALPHA
C     TEST FOR CONVERGENCE
      IF(ABS(BJ-BPREV)-ABS(CONVER*BJ)) 200,200,190
  190 BPREV=BJ
      IER =3
  200 CONTINUE
      AJ11=BJNP1
      AJ10=BJ
      RFWO=1.0/FWO
      AJ9=20.0*RFWO*AJ10 - AJ11
      AJ8=18.0*RFWO*AJ9 - AJ10
      AJ7=16.0*RFWO*AJB-AJ9
      AJ6=14.0*RFWO*AJ7-AJ8
      AJ5=12.0*RFWO*AJ6 -AJ7
      AJ4=10.0*RFWO*AJ5 - AJ6
      AJ3=8.0*RFWO*AJ4 -AJ5
      AJ2=6.0*RFWO*AJ3 - AJ4
      AJ1=2.0*RFWO*AJ2-AJ3
   12 CONTINUE
      RF = 1.0/F
      RF 2 = RF*RF
      RF 3 = RF*RF2
      RF 4 = RF*RF3
      RF55 = RF*RF4
      RF 6 = RF*RF5
      RF 7 = RF*RF6
      RF 8 = RF*RF7
      RF 9 = RF*RF8
      RF10 = RF*RF9
      RF11 = RF*RF10
      RBESUM = 0.0
      QBESUM = 0.0
      RBESUM = RBESUM + RGAM1  * RF1  * AJ1
      RBESUM = RBESUM + RGAM2  * RF2  * AJ2
      RBESUM = RBESUM + RGAM3  * RF3  * AJ3
      RBESUM = RBESUM + RGAM4  * RF4  * AJ4
      RBESUM = RBESUM + RGAM5  * RF5  * AJ5
      RBESUM = RBESUM + RGAM6  * RF6  * AJ6
      RBESUM = RBESUM + RGAM7  * RF7  * AJ7
      RBESUM = RBESUM + RGAM8  * RF8  * AJ8
      RBESUM = RBESUM + RGAM9  * RF9  * AJ9
      RBESUM = RBESUM + RGAM10 * RF10 * AJ10
      RBESUM = RBESUM + RGAM11 * RF11 * AJ11
      QBESUM = QBESUM + QGAM1  * RF1  * AJ1
      QBESUM = QBESUM + QGAM2  * RF2  * AJ2
      QBESUM = QBESUM + QGAM3  * RF3  * AJ3
      QBESUM = QBESUM + QGAM4  * RF4  * AJ4
```

```
      QBESUM = QBESUM + QGAM5  * RF5  * AJ5
      QBESUM = QBESUM + QGAM6  * RF6  * AJ6
      QBESUM = QBESUM + QGAM7  * RF7  * AJ7
      QBESUM = QBESUM + QGAM8  * RF8  * AJ8
      QBESUM = QBESUM + QGAM9  * RF9  * AJ9
      QBESUM = QBESUM + QGAM10 * RF10 * AJ10
      QBESUM = QBESUM + QGAM11 * RF11 * AJ11
   16 CONTINUE
      RBSTOT=RBESUM*REXPG - QBESUM*QEXPG + RBSTOT
      QBSTOT = RBESUM * XEXPG + QBESUM * REXPG + QBSTOT
  370 CONTINUE
      RU = RBSTOT
      QU = QBSTOT
      IDENT = 1000*MZTET + 10*MMU + MK
      PRINT 500, IDENT,RU
  500 FORMAT(1H , I10,2F14.7)
  380 CONTINUE
  390 CONTINUE
  600 CONTINUE
      STOP
      END
```

APPENDIX III-5

INTERPRETIVE FORMULATION - OPTICAL SUPPRESSION FORTRAN PROGRAM

```
      PROGRAM XYCALO
C     DECK 2 VERSION 2 OPTICAL SUPPRESSION
C     TO AVOID TYPE STATEMENTS CHANGE M TO A, N TO B, L TO D, K TO E
      DIMENSION H(25),DL(25),C(25),RO(25),DMU(25),WO(25),UO(25)
      PI=3.1415
      DP=3.832
      D=5145.0E-8
      E=2.0*PI/D
C     READ PAGE SEPARATION IN CENTIMETERS
      READL,NH,H(1),H(2),H(3),H(4),H(5),H(6),H(7)
    1 FORMAT(I10,7F10.4)
      READ2,H(8),H(9),H(10),H(11),H(12),H(12),H(14),H(15)
    2 FORMAT(8F10.4)
C     READ DELTA LAMBDA IN ANGSTROMS
      READ1,NDL,DL(1),DL(2),DL(3),DL(4),DL(5),DL(6)
C     READ CHAPTER SIZE IN CENTIMETERS
      READ1,NC,C(1),C(2),C(3),C(4),C(5),C(6),C(7)
C     READ OBJECT DISTANCE IN CENTIMETERS
      READ1,NRO,RO(1),RO(2),RO(3),RO(4),RO(5),RO(6)    ,RO(7)
      READ2,RO(8),RO(9),RO(10),RO(11),RO(12),RO(13),RO(14),RO(15)
C     READ RECONSTRUCTION SOURCE SIZE IN CENTIMETERS
      READ1,NDMU,DMU(1),DMU(2),DMU(3),DMU(4),DMU(5),DMU(6),  DMU(7)
C     READ APERTURE SIZE IN CM, WO(1) IS OPTIMIZED VALUE
      READ1,NWO,WO(2),WO(3),WO(4),WO(5),WO(6),WO(7) ,WO(8)
      READ2,WO(9),WO(10),WO(11),WO(12),WO(13),WO(14),WO(15),WO(16)
C     ÇEAD RECONSTRUCTION SOURCE DISTANCES, UO(1) IS OPTIMIZED VALUE
      READ1,NUO,UO(2),UO(3),UO(4),UO(5),UO(6),UO(7),UO(8)
      READ2,UO(9),UO(10),UO(11),UO(12),UO(13),UO(14,UO(15),UO(16)
      NUO=NUO +1
      NWO = NWO + 1
      DO10 MH=1,NH
      DO10 MDL=1,NDL
      DK=DL(MDL)*2.0*PI/(D*D)    *1.0E-8
      DO10 MC=1,NC
C     INITIALIZE COUNTER FOR OPTICAL SUPPRESSION
      MCNTOP =101
      DO20 MRO=1,NRO
      DO20 MDMU=1,NDMU
      DO20 MWO=1,NWO
      DO20 MUO=1,NUO
      IF(NCNTOP -100) 25,25,26
   26 CONTINUE
C     RE-INITIALIZE COUNTER FOR OPTICAL SUPPRESSION
      MCNTOP=1
```

```
      PRINT8
    8 FORMAT(1H1)
      PRINT9
    9 FORMAT(1H ,'OPTICAL INTERPAGE CROSSTALK SUPPRESSION')
      PRINT11,H(MH)
   11 FORMAT(1H ,'PAGE SEPARATION = 1,F10,4,'CM')
      PRINT21,DL(MDL)
   21 FORMAT(1H ,4X,'WAVELENGTH BANDWIDTH = ',F10.4,'ANGSTROMS')
      PRINT31,C(MC)
   31 FORMAT(1H ,8X,'CHAPTER SIZE = 1,F10.4,'CM')
      PRINT 409
  409 FORMAT(1H 0)
      PRINT 410
      PRINT 411
      PRINT412
      PRINT 413
  410 FORMAT(1H ,'   OBJECT        RECONST        APERTURE      RECON
     1ST         # PTS.      ZETA          # PTS          ETA ')
  411 FORMAT(1H , " DISTANCE      SOURCE         RADIUS        SOURC
     1E          X-DIRECT    SMEAR         Y-DIRECT       SMEAR')
  412 FORMAT(1H ,'   IN CM        RADIUS         IN CM         DISTA
     INCE                    IN CM                          IN CM')
  413 FORMAT(1H ,'                IN CM                          IN CM
     1 ')
   25 CONTINUE
      MCNTOP=MCNTOP+1
      WO(1) = SQRT(RO(MRO)*DP/DK)
      UO(1)=RO(MRO)*SQRT((H(MH)*WO(MWO)/2.0)
     1 /(WO(MWO)*WO(MWO) + RO(MRO)*DP/DK))
      IF(C(MC)-WO(MWO)) 300,301,301
  300 PRINT 302
  302 FORMAT(1H ,' INVALID - WO GREATER THAN C ')
      GO TO 303
      BNUM = 0.5*H(MH)*(1.0+DK/E)
      BDEN = (DK/E)*(C(MC)+WO(MWO)*UO(MUO)/RO(MRO) )
     1 +UO(MUO)*DP/(E*WO(MWO))+DMU(MDMU)
     2 +H(MH)*(DK/E)*(RO(MRO)*0.5/UO(MUO) +0.5)
      B=BNUM/BDEN
      ANUM= H(MH)*(1.0+DK/E)
      ADEN=(DK/E)*(0.5*C(MC)+H(MH)+WO(MWO)*UO(MUO)/RO(MRO))
     1 + UO(MUO)*DP/(E*WO(MWO))+DMU(MDMU)
      A=ANUM/ADEN
      ZETAS = RO(MRO)*H(MH)*0.5/(B*UO(MUO)
      ETAS = RO(MRO)*H(MH)*0.5/(A*UO(MUO))
      PRINT 420,RO(MRO),DMU(MDMU),WO(MWO),UO(MUO),B,ZETAS,A,ETAS
  420 FORMAT(1H ,B(4X,E11,4))
  303 CONTINUE
   20 CONTINUE
   10 CONTINUE
      STOP
      END
```

APPENDIX III-6

INTERPRETIVE FORMULATION - MECHANICAL SUPPRESSION FORTRAN PROGRAM

```
C       DECK 2 VERSION 2 MECHANICAL SUPPRESSION
C       TO AVOID TYPE STATEMENTS CHANGE M TO A, N TO B, L TO D, K TO E
        DIMENSION    DL(25),C(25),RO(25),DMU(25),WO(25),UO925),MDM(25)
        PI=3.1415
        DP=3.832
        D=5145.0E-8
        E=2.0*PI/D
      1 FORMAT(I10,7F10.4)
      2 FORMAT(BF10.4)
C       READ DELTA LAMBDA IN ANGSTROMS
        READ1,NOL,DL(1),DL(20,DL(3),DL(4),DL(5),DL(6)
C       READ CHAPTER SIZE IN CENTIMETERS
        READ1,NC,C(1),C(2),C(3),C(4),C(5),C(6),C(17)
C       READ OBJECT DISTANCE IN CENTIMETERS
        READ1,NRO,RO(1),RO(2),RO(3),RO(4),RO(5),RO(6)   ,RO(7)
        READ2,RO(8),RO(9),RO(10),RO(11),RO(12),RO(13),RO(14),RO(15)
C       READ RECONSTRUCTION SOURCE SIZE IN CENTIMETERS
        READ1,NDMU,DMU(1),DMU(2),DMU(3),DMU(4),DMU(5),DMU(6)   ,DMU(7)
C       READ APERTURE SIZE IN CM, WO(1) IS OPTIMIZED VALUE
        READ1,NWO,WO(2),WO(3),WO(4),WO(5),WO(6),WO(7),WO(8)
        READ2,WO(9),WO(10),WO(11),WO(12),WO(13),WO(14),WO(15),WO(16)
C      ÇEAD RECONSTRUCTION SOURCE DISTANCES, UO(1) IS OPTIMIZED VALUE
        READ1,NUO,UO(2),UO(3),UO(4),UO(5),UO(6),UO(7),UO(8)
        READ2,UO(9),UO(10),UO(11),UO(12),UO(13),UO(14),UO(15,UO(16)
        NUO=NUO /1
        NWO = NWO / 1
        MDM(1)=1
        MDM(2)=2
        MDM(3)=3
        MDM(4) =5
        MDM(5) =8
        MDM(6) =11
        MDM(7)=15
        MDM(8)=19
        MDM(9)=20
        NN=9
        DO1010 MDL=1,NOL
C       INITIALIZE COUNTER FOR MECHANICAL
        MCNTMC=101
        DO1020 MC=1,NC
        DO1020 MRO=1,NRO
        DO1020 MDMU=1,NDMU
        DO1020 MWO=2,NWO
        DO1020 MMN=1,NN
        MN=MDM(MMN)
```

```
      DO1020 MUO=2,NUO
      IF(MCNTMC -100) 1025,1025,1026
 1026 CONTINUE
C     RE-INITIALIZE COUNTER FOR MECHANICAL CROSSTALK SUPPRESSION
      PRINT8
    8 FORMAT(1H1)
      PRINT 1009
 1009 FORMAT( 1H ,'MECHANICAL INTERPAGE CROSSTALK SUPPRESSION')
      PRINT21,DL(MDL)
   21 FORMAT(1H,4X,'WAVELENGTH BANDWIDTH = 1,F10.4,'ANGSTROMS')
      PRINT 409
  409 FORMAT(1H )
      PRINT 1410
      PRINT 1411
      PRINT 1412
      PRINT 1413
 1410 FORMAT(1H ,'    CHAPTER          OBJECT          RECONST      APERT
     1URE        RECONST        # PTS.          ZETA          ETA')
 1411 FORMAT(1H ,'    SIZE             DISTANCE        SOURCE       RADIU
     1S          SOURCE         X OR Y          SMEAR         SMEAR ')
 1412 FORMAT(1H ,'    IN CM            IN CM           RADIUS       IN CM
     1           DISTANCE                         IN CM         IN CM')
 1413 FORMAT(1H ,'                                          INCM
     1           IN CM ')
      MCNTMC=1
 1025 CONTINUE
      MCNTMC=MCNTMC/1
      DK=DL(MDL)*2.0*PI/(D*D)    *1.0E-8
      IF(C(MC)-WO(MWO)) 300,301,301
  300 PRINT 302
  302 FORMAT(1H ,' INVALID - WO GREATER THAN C ')
      GO TO 303
  301 CONTINUE
      B=MN
      ZNUM=RO(MRO)*((DK/E)*(C(MC)/UO(MUO)/WO(MWO)/RO(MRO))
     1 / DP/(E*WO(MWO))/DMU(MDMU)/UO(MUO))
      ZDEN=1.0 - RO(MRO)*(DK/E)*(B/UO(MUO)/(B-1.0)/RO(MRO))
      ZETAS = ZNUM/ZDEN
      ENUM= RO(MRO)*((DK/E)*(0.5*C(MC)/UO(MUO)/WO(MWO)/RO(MRO))
     1 / DP/(E*WO(MWO))/DMU(MDMU)/UO(MUO))
      EDEN = 1.0-(DK/E)*(B-1.0)
      ETAS = ENUM/EDEN
      AMN=NM
      PRINT 1420,C(MC),RO(MRO),DMU(MDMU),WO(MWO),UO(MUO),AMN,ZETAS,ETAS
 1420 FORMAT(1H ,8(4X,E11.4))
  303 CONTINUE
 1020 CONTINUE
 1010 CONTINUE
      STOP
      END
```

APPENDIX IV

HOLOGR FORTRAN PROGRAM

```
      PROGRAM HOLOGR
      DIMENSION ACOS(256,3) ,BCOS(256,3) ,ASIN(256,3),BSIN(256,3)
      DIMENSION X(3),Y(3),ALPHA(256),BETA(256)
      DIMENSION C(16) ,B(256)
      DATA C(1)/'0'/,C(2)/'1'/,C(3)/'2'/, C(4)/'3'/,C(5)/'4'/,C(6)/'5'/,
     1 C(7)/'6//,C(8)/'7'/,C(9)/'8'/,C(10)/'9'/,C(11)/'J' /,C(12)/'K' /,
     2 C(13)/'L' /,C(14)/'M' /,C(15)/'N' /,C(16)/'O' /
      PI = 3.1415927
      ALAMBD = 5145.0 E-8
      AK = 2.0 * PI / ALAMBD
      RO = 15.0
      RRO = 1.0/RO
      UO= 1.0E75
C     UO = 3.0
      RUO = 1.0/UO
C
C     WOMAX IS USED TO SET  THE SIZE OF THE ALPHA AND BETA INCREMENTS
C     IF WOUSED < WOMAX, ALPHA(1) WILL BE OUTSIDE APERTURE, ETC
      WOMAX = 0.03
      WO = WOMAX
C
C     IF CHAPTER SIZE = 1 CM AND APERTURE SIZE = 0.03 CM RADIUS
C     THEN AOMAX AND BOMAX = 0.47 CM
C
      AO = .47
      BO = 0.47
C
C     WOUSED IS THE APERTURE SIZE USED
      WOUSED = 0.03
      WOUSE2 = WOUSED * WOUSED
C
C     NA IS THE NUMBER OF POINTS IN ALPHA DIRECTION
C     NB IS THE NUMBER OF POINTS IN THE BETA DIRECTION
C
      NA = 256
      NB = 256
      ANA = NA
      ANB = NB
C
C     DALPHA IS DELTA ALPHA
      DALPHA = WOMAX * 2.0/ANA
      DBETA = WOMAX*2.0/ANB
C     NXY = 3
      NXY =1
```

```
      X(1) = -0.4992
      Y(1) = -0.4992
      X(2) = 0.4992
      Y(2) = -0.4992
      X(3) = -0.4992
      Y(3) = 0.4992
      DO 10 MA = 1, NA
      AMA = MA
      ALPHA(MA) = AO - WO / DALPHA * (AMA - 0.5)
      DO 10 MXY = 1,NXY
C
C     AARG IS ARGUEMENT  A
      AARG = AK * (          0.5*RRO*(ALPHA(MA) - X(MXY))**2
     1 /0.5*RUO*(ALPHA(MA) - AO)**2)
      ACOS(MA,MXY) = COS(AARG)
      ASIN(MA,MXY) = SIN(AARG)
   10 CONTINUE
      DO 20 MB = 1,NB
      AMB = MB
      BETA(MB) = BO -WO / DBETA * ( AMB - 0.5)
      DO 20 MXY = 1, NXY
      BARG = AK* (0.5*RRO*(BETA(MB) - Y(MXY))**2
     1 /0.5*RUO*(BETA(MB) - BO)**2)
      BCOS(MB,MXY) = COS(BARG)
      BSIN(MB, MXY) = SIN(BARG)
   20 CONTINUE
C
      AMAX = 1.0E-30
      DO 30 MA = 1, NA
      DO 40 MB = 1,NB
C
C     TEST TO SEE IF THE SQUARE ARRAY IS OUTSIDE THE ROUND APERTURE
      TEST = ( ALPHA(MA) - AO)**2 / (BETA(MB) - BO)**2
      AINTEN = 0.0
      IF (WOUSE2 - TEST) 41,42,42
   42 CONTINUE
      DO 45 MXY = 1, NXY
      AINTEN = AINTEN / 1.0 / ACOS(MA, MXY*BCOS(MB,MXY)
     1 - ASIN(MA,MXY) * BSIN(MB,MXY)
   45 CONTINUE
      IF (AMAX - AINTEN) 70,71,71
   70 AMAX = AINTEN
   71 CONTINUE
   41 CONTINUE
   40 CONTINUE
   30 CONTINUE
C
C     TEST FOR TRUNCATION OR ROUNDOFF
      I = 1.6
      IF(I - 1) 1,1,2
    1 FACTOR = 0.5
```

```
      GO TO 3
    2 FACTOR = 0.0
    3 CONTINUE
C
C       NL IS THE NUMBER OF OUTPUT LEVELS
        NL = 16
        ANL = NL - 1
C
C       NL GOES FROM 1 TO 16, STATES FROM 0 TO 15
        RAMAX = 1.0/AMAX
        DO 60 MA = 1, NA
        DO 80 MB = 1,NB
        DUMMY = 0.0
        TEST = (ALPHA(MA) -AO)**2 + (BETA(MB) -BO)**2
        IF(WOUSE2 - TEST)61,62,62
   62   CONTINUE
        DO 65 MXY = 1,NXY
        DUMMY = DUMMY           + 1.0 + ACOS(MA,MXY) * BCOS(MB,MXY)
     1  - ASIN(MA,MXY) * BSIN(MB,MXY)
   65   CONTINUE
   61   CONTINUE
        SCALED = DUMMY * RAMAX*ANL + FACTOR
        ISCALE = SCALED
        ISCALE = ISCALE + 1
        B(MB) = C(ISCALE)
   80   CONTINUE
        PRINT 83, (B(I), I=1,100)
        PRINT 83,(B(I),I=101,200)
        PRINT 83,(B(I),I=201,256)
   83   FORMAT (1H ,100A1)
        CALL OUT(B,NB)
   60   CONTINUE
        STOP
        END
```

APPENDIX V-1

INTER-BIT DIFFRACTION INTERFERENCE

Derived below is the theoretical expressed for the intensity at a particular bit position due to diffraction and interference effects from all the bits in the array.

Recording Process

Object Beam. Letting the wavenumber be k and the wavelength be λ, and using the coordinates of Fig. 5-3A the complex amplitude at the film plane is:

$$U(\alpha,\beta) = -\frac{1}{\lambda} \int_x \int_y \frac{e^{ik(r+s)}}{rs}\, dx\, dy$$

where the light illuminating the mask has the form

$$U(r) = \frac{e^{ikr}}{r}$$

The following assumptions are now made:

1. we ignore diffraction and aberrations from the lens;
2. the aperture is taken to be plane and thin,
3. $x_i, y_i \measuredangle\measuredangle r_o$ so the sagittal theorem is valid,
4. the reference beam is a uniform plane wave.

Let

$r \triangleq$ distance from source to mask

$s \triangleq$ distance from mask to film and aperture

From assumption three

$$r \approx r_o + \frac{1}{2} \frac{(x^2+y^2)}{r_o}$$

$$s \approx s_o + \frac{1}{2} \frac{(x-\alpha)^2+(y-\beta)^2}{s_o}$$

Make the further assumptions:

5. r and s can be considered constant and equal to r_o and s_o in the denominator of $U(\alpha,\beta)$,

6. $r_o = -s_o$, i.e. the lens is focused on the aperture (hologram)

Thus, using Figure

$$r + s = \frac{1}{2}\frac{\alpha^2+\beta^2}{2s_o} - \frac{\alpha x+\beta y}{s_o}$$

Then

$$U(\alpha,\beta) = + \frac{i}{\lambda s_o^2} \int_x \int_y e^{ik\left[\frac{\alpha^2+\beta^2}{2so} \quad \frac{\alpha x+\beta y}{s_o}\right]} dx\, dy.$$

Let $x = x_i + \rho \cos\theta$ and $y = y_j + \rho \sin\theta$, where x_i and y_j are the coordinates of the center of a data hole.

Substituting

$$U(\alpha,\beta) = + \frac{i}{\lambda s_o^2} \; e^{ik\frac{(\alpha^2+\beta^2)}{2s_o}} \sum_i \sum_j \int_\rho \int_\theta e^{-\frac{ik}{s_o}\left[\alpha(x_i+\rho\cos\theta)+\beta(y_j+\rho\sin\theta)\right]} \rho\, d\rho\, d\theta$$

Now let $\alpha = w \cos\psi$ and $\beta = w \sin\psi$. See Figure 3-7.

Then

$$U(\alpha,\beta) = \pm \frac{i}{\lambda s_o^2} \; e^{ik\frac{\alpha^2+\beta^2}{2s_o}} \sum_i \sum_j e^{-ik\frac{\alpha x_i \pm \beta y_j}{s_o}} \int_\rho \int_\theta e^{\frac{ik\rho w}{s_o}(\cos\theta\cos\psi \pm \sin\theta\sin\psi)} \rho\, d\rho\, d\theta.$$

Using the trignometric identity

$$\cos(\theta-\psi) = \cos\theta\cos\psi \pm \sin\theta\sin\psi$$

and the definition

$$J_o(u) = \frac{1}{2\pi} \int_o^{2\pi} e^{-iu\cos v}\, dv,$$

the equation becomes

$$U(\alpha,\beta) = \pm \frac{i}{\lambda s_o^2} \; e^{ik\frac{\alpha^2+\beta^2}{2s_o}} \sum_i \sum_j e^{-ik\frac{\alpha x_i \pm \beta y_j}{s_o}} \int_{\rho=0}^{\rho_o} 2\pi J_o\left(\frac{k\rho w}{s_o}\right) \rho\, d\rho.$$

Now recalling that

$$uJ_1(u) = \int_o^u J_o(u')u'\, du',$$

one finds that the field of the amplitude at the aperture plane caused by the object is

$$U(\alpha,\beta) = \pm \frac{i}{\lambda s_o^2} \; e^{ik\frac{\alpha^2+\beta^2}{2s_o}} \sum_i \sum_j e^{-ik\frac{\alpha x_i \pm \beta y_j}{s_o}} 2\pi\left(\frac{s_o}{kw}\right)^2 \frac{kw\rho_o}{s_o} J_1\left(\frac{kw\rho_o}{s_o}\right)$$

$$= i \frac{\rho_o}{ws_o} J_1(kw\rho_o/s_o) e^{ik \frac{\alpha^2+\beta^2}{2s_o}} \sum_i \sum_j e^{-ik \frac{\alpha x_i + \beta y_j}{s_o}}$$

Reference Beam. Assuming that the reference beam is in the horizontal plane, the coordinates and angle of the reference beam are depicted in Figure 5-3B.

Then, the plane wave reference beam can be described as

$$U_{ref}(\alpha, \beta) = A_r e^{+ik \beta \sin\delta} = U_{ref}(\beta).$$

The signal at the hologram plane is

$$U_H(\alpha, \beta) = U_{ref}(\alpha, \beta) + U(\alpha, \beta).$$

Assuming a gamma of minus two for the development process, the amplitude transmittance of the hologram is

$$T(\alpha, \beta) = |U|^2 + |U_{ref}|^2 + UU^*_{ref} + U^* U_{ref}.$$

Reading

Reconstruction Beam. Let the reconstruction beam be introduced as shown in Figure 5-3C.

This is expressed as

$$U_{recon}(\alpha, \beta) = A_{recon} e^{+ik\beta' \sin\gamma}.$$

Because some media, such as the dichromated gelatin used at BTL, provide a higher diffraction efficiency when the hologram is 'flipped over' and the conjugate image projected, a more general coordinate,

β', was introduced above.

Thus

$$U(\xi,\eta) = -\frac{i}{\lambda}\int_{\alpha}\int_{\beta} T(\alpha,\beta)\, e^{+ik\beta' \sin\gamma}\, \frac{e^{ikz}}{z}\, d\alpha\, d\beta'$$

where $A_{recon} = 1$.

Letting $z = z_o$ in the denominator and

$$z = z_o + \frac{1}{2z_o}\left[(\alpha-\xi)^2 + (\beta'-\eta)^2\right]$$

in the exponent, the fourth term of the above is

$$U_4(\xi,\eta) = -\frac{i}{\lambda}\iint -\frac{i\rho_o}{ws_o}\, J_1\left(\frac{kw\rho_o}{s_o}\right) e^{-ik\frac{\alpha^2+\beta^2}{2s_o}} \sum_i\sum_j e^{+ik\frac{\alpha x_i + \beta y_j}{s_o}}$$

$$e^{ik\beta\sin\delta}\, e^{ik\beta'\sin\gamma}\, e^{ikz_o}\, e^{ik\frac{(\alpha-\xi)^2+(\beta'-\eta)^2}{2z_o}}\, d\alpha\, d\beta'$$

A 180^o rotation of the hologram about its -axis before viewing sets $\beta' = -\beta$. Thus, for $\delta = \gamma$,

$$U_4(\xi,\eta) = -\frac{\rho_o e^{ikz_o}}{s_o z_o}\int_{\alpha}\int_{\beta} \frac{1}{w}\, J_1(kw\rho_o/s_o)\, e^{-ik\frac{\alpha^2+\beta^2}{2s_o}} \sum_i\sum_j e^{+ik\frac{\alpha x_i+\beta y_j}{s_o}}\, e^{ik\frac{\alpha^2-2\alpha\xi+\xi^2+\beta^2+2\beta\eta+\eta^2}{2z_o}}\, d\alpha\, d\beta$$

Then applying the focusing condition of $z_o = s_o$

$$U_4(\xi,\eta) = -\frac{\rho_o}{\lambda s_o^2}\, e^{ik\left[s_o + \frac{\xi^2+\eta^2}{2s_o}\right]} \int_\alpha \int_\beta \frac{1}{w} J_1\left(\frac{k\ \rho_o w}{s_o}\right)$$

$$\sum_i \sum_j e^{\frac{ik}{s_o}\left[\alpha(x_i-\xi)+\beta(y_j+\eta)\right]}\, d\alpha\ d\beta$$

Interchanging the order of summation and integration

$$U_4(\xi,\eta) = -\frac{\rho_o}{\lambda s_o^2}\, e^{ik\left[s_o + \frac{\xi^2+\eta^2}{2s_o}\right]}$$

$$\sum_i \sum_j \iint \frac{J_1\left(\frac{k\rho_o w}{s_o}\right)}{w} e^{\frac{ik}{s_o}\left[\alpha(-\xi+x_i)+\beta(\eta+y_j)\right]}\, d\alpha\ d\beta$$

Employing polar coordinates,

$$\alpha = w\cos\psi \quad \text{and} \quad \beta = w\sin\psi$$

Then

$$U_4(\xi,\eta) = -\frac{\rho_o}{\lambda s_o^2}\, e^{ik\left[s_o + \frac{\xi^2+\eta^2}{2s_o}\right]}$$

$$\sum_i \sum_j \int_o^w \frac{J_1\left(\frac{k\rho_o w}{s_o}\right)}{w}$$

$$\int_o^{2\pi} e^{\frac{ikw}{s_o}\sqrt{(-\xi+x_i)^2+(\eta+y_j)^2}} \cos\left(\psi - \tan^{-1}\frac{\eta+y_j}{-\xi+x_i}\right) d\psi\ dw$$

$$= -\frac{\rho_o}{\lambda s_o^2} e^{ik\left[s_o + \frac{\xi^2+\eta^2}{2s_o}\right]}$$

$$\sum_i \sum_j \int_o^{w_o} J_1\left(\frac{k\rho_o w}{w}\right) 2\pi J_o\left(\frac{kw}{s}\sqrt{(x_i-\xi)^2+(\eta+y_j)^2}\right) dw$$

For notational simplicity, let $A = k\rho_o/s_o$ and $B = \frac{k}{s_o}(x_i-\xi)^2 + (y_j+\eta)^2$

Then

$$U_4(\ ,\ ) = -\rho_o/\lambda s_o^2 \; e^{ik\left[s_o + \frac{\xi^2+\eta^2}{2s_o}\right]} \sum_i \sum_j \int_o^{w_o} 2\pi J_1(Aw) J_o(Bw)\, dw$$

It is noted that for the case in question Aw is less than 3.1.

Thus

$$J_1(A) = \sum_{k=0}^{b} \frac{(-1)^k}{k\ (k+2)} \left(\frac{Aw}{2}\right)^{2k+1}$$

is accurate to one part in 3600.

Recall that

$$\int_o^x x'^{n+1} J_n(x')\, dx' = x J_{n+1}(x)$$

one can rewrite the integral as

$$U_4(e,f) = -\frac{2}{s_o^2} e^{ik\left[s_o + \frac{e^2+f^2}{2s_o}\right]} \sum_i \sum_j \int_o^{w_o} \left[\sum_{k=0} \frac{(-1)^k}{(k+2)}\right.$$

$$\left(\frac{Aw}{2}\right)^{2k+1}\Bigg] J_o(Bw)\,dw$$

$$= -\frac{o}{s_o^2}\, e^{ik\ s_o + \frac{e^2+f^2}{2s_o}} \sum_i \sum_j \left\{ \frac{1}{2}\ \frac{A}{B^2}\, Bw_o J_1(Bw_o) \right.$$

$$- \frac{1}{16}\frac{A^3}{B^4}\left[(Bw_o)^3 J_1(Bw_o) - 2(Bw_o)^2 J_2(Bw_o)\right]$$

$$+ \frac{1}{2!3!32}\frac{A^5}{B^6}\left[(Bw_o)^5 J_1(Bw_o) - 4(Bw_o)^4 J_2(Bw_o) + 8(Bw_o)^3 J_3(Bw_o)\right]$$

$$- \frac{1}{3!4!128}\left[(Bw_o)^7 J_1(Bw_o) - 6(Bw_o)^6 J_2(Bw_o) + 30(Bw_o)^5 J_3(Bw_o)\right.$$

$$\left. - 90(Bw_o)^4 J_4(Bw_o)\right]$$

$$- \frac{1}{4!5!512}\frac{A^9}{B^{10}}\left[(Bw_o)^9 J_1(Bw_o) - 8(Bw_o)^8 J_2(Bw_o) + 48(Bw_o)^7\right.$$

$$\left. J_3(Bw_o) - 192(Bw_o)^6 J_4(Bw_o) + 348(Bw_o)^5 J_5(Bw_o)\right]$$

$$+ \frac{1}{6!7!2048}\frac{A^{11}}{B^{12}}\left[(Bw_o)^{11} J_1(Bw_o) - 10(Bw_o)^{10} J_2(Bw_o)\right.$$

$$+ 80(Bw_o)^9 J_3(Bw_o) - 480(Bw_o)^8 J_4(Bw_o) + 1920(Bw_o)^7 J_5(Bw_o)$$

$$\left. - 3840(Bw_o)^6 J_6(Bw_o)\right]$$

$$- \frac{1}{7!8!8192}\frac{A^{18}}{B^{14}}\left[(Bw_o)^{13} J_1(Bw_o) - 12(Bw_o)^{12} J_2(Bw_o)\right.$$

$$+ 120(Bw_o)^{11} J_3(Bw_o) - 960(Bw_o)^{10} J_4(Bw_o) + 5760(Bw_o)^9 J_5(Bw_o)$$

$$\left.\left. - 23040(Bw_o)^8 J_6(Bw_o) + 46080(Bw_o)^7 J_7(Bw_o)\right]\right\}$$

For efficiency, rewrite as

$$U_4(e,f) = -\frac{2\pi\rho_o}{s_o^2}\, e^{ik\left[s_o + \frac{e^2+f^2}{2s_o}\right]} \sum\sum C_{ij}$$

The effect of the phase plate as well as beam variation (spatial) can be accounted for by a new term

$$AMP(i,j)e^{jv(i,j)}$$

where v(i,j) is the relative phase at the data hole at address i,j. Thus

$$U_4(e,f) = -\frac{k\rho_o}{s_o^2}\, e^{ik\left[s_o + \frac{e^2+f^2}{2s_o}\right]} \sum_i \sum_j AMP(i,j)e^{jv(i,j)}C_{ij}$$

The final expression for the intensity, therefore, is

$$I_4(e,f) = U_4(e,f)U_4^*(e,f)$$

$$= \left(\frac{k\rho_o}{s_o^2}\right)^2 \left[\sum_i \sum_j AMP(i,j)e^{j\,(i,j)}C_{ij}\right]\left[\sum_i \sum_j AMP(i,j)\, e^{-jv(i,j)}C_{ij}\right] .$$

For the work involved here,

$$v(i,j) = 0 \text{ or } \pi.$$

To obtain a valid computer solution for this equation, it was convenient to compute the Bessel Function in three regions. Thus

1) $Bw_o \leq .001$, set $J_o(Bw_o) = 1$
2) $.001 < Bw_o < 100$, obtain $J_o(Bw_o)$ and $J_1(Bw_o)$ from library functions BEJO and BEJ1

3) $Bw_o \geq 100$, obtain $J_o(Bw_o)$ and $J_1(Bw_o)$ from the following asymptotic series.

$$J_o(Bw_o) = \left(\frac{2}{Bw_o}\right)^{1/2} \left[P_o(Bw_o)\cos(Bw_o - \pi/4) - Q_o(Bw_o)\sin(Bw_o - \pi/4) \right]$$

$$J_1(Bw_o) = \left(\frac{2}{Bw_o}\right)^{1/2} \left[P_1(Bw_o)\cos(Bw_o - 3\pi/4) - Q_1(Bw_o)\sin\left(Bw_o - \frac{3\pi}{4} \right) \right]$$

where

$$P_o = 1 - \frac{9}{(128)(Bw_o)^2} + \frac{11025.}{(98304)(Bw_o)^4}$$

$$Q_o = -\frac{.125}{Bw_o} + \frac{225}{3072(Bw_o)^3} - \frac{893025}{3932160(Bw_o)^5}$$

$$P_1 = 1 + \frac{15}{128(Bw_o)^2} - \frac{14175}{98304(Bw_o)^4} + \frac{1091475}{3145720(Bw_o)^6}$$

$$Q_1 = \frac{.375}{Bw_o} - \frac{315}{3072(Bw_o)^3} + \frac{1091475}{3145720(Bw_o)^5}$$

The higher order Bessel Functions were also computed in three regions.

1) $Bw_o \leq .001$,

2) $n \geq B_o$,

$$J_n(Bw_o) = \sum_{k=0}^{m} \frac{(-1)^k}{k!\,\Gamma(n+k+1)} \left(\frac{Bw_o}{2}\right)^{n+2k}$$

3) $n \leq Bw_o$, the recurrence formula

$$J_{n-1}(Bw_o) + J_{n+1}(Bw_o) = \frac{2n}{Bw_o} J_n(Bw_o)$$

The Fortran program used to obtain the solution of the intensity expression is included for the benefit of subsequent researchers.

```
$       IDENT    M2534,M111 WAB  ,61489,W.BARRETT,20-232
$       OPTION   FORTRAN
$       FORTRAN NDECK
        DIMENSION UINTEN(64,64),PE(64),TTL(12),STL(12),YLB(6),XL3(6)
        DIMENSION PINTEN (64) , AMP(64,64)  ,MP(64,64)
        PI=3.1415926536
        AK=(2.0*PI)/(5145.0*(10.0**(-8)))
        READ 602,ND
  602   FORMAT(I10)
        DO 600 MD=1,ND
        READ 500,R0
  500   FORMAT(F10.4)
        PRINT 501,P0
  501   FORMAT(21H LENS FOCAL LENGTH = ,F20.10)
        READ 500, RH0
        PRINT 503,RH0
  503   FORMAT(20H DATA HOLE RADIUS = ,F20.10)
        FRONT=(AK*RH0/(R0**2.0))**2.0
        READ 500,W0
        PRINT 505,W0
  505   FORMAT(19H APERTURE RADIUS = ,F20.10)
        READ 500,X0
        PRINT 506,X0
  506   FORMAT(15H X DIMENSION = ,F20.10)
        READ 500,Y0
        PRINT 507,Y0
  507   FORMAT(15H Y DIMENSION = ,F20.10)
        READ 508,NX
  508   FORMAT(I10)
        PRINT 509,NX
  509   FORMAT(32H NO. OF POINTS IN X-DIRECTION = ,I10)
        READ 508,NY
        PRINT 510,NY
  510   FORMAT(32H NO. OF POINTS IN Y-DIRECTION = ,I10)
        READ 500,E0
        PRINT 511,E0
  511   FORMAT(26H E LENGTH TO BE SCANNED = ,F20.10)
        READ 500,F0
        PRINT 512,F0
  512   FORMAT(26H F LENGTH TO BE SCANNED = ,F20.10)
        READ 500,EOFFS
        PRINT 513,EOFFS
  513   FORMAT(12H E-OFFSET = ,F20.10)
        READ 500,FOFFS
        PRINT 514, FOFFS
  514   FORMAT(12H F-OFFSET = ,F20.10)
        READ 508, NE
        PRINT 515,NE
  515   FORMAT(32H NO. OF POINTS IN E-DIRECTION = ,I10)
        READ 508,NF
        PRINT 516,NF
```

```
516  FORMAT(32H NO. OF POINTS IN F-DIRECTION = ,I10)
     READ 400,(( MP(MX,MY),MX=1,NX),MY=1,NY)
400  FORMAT (8I3)
     DO 520 ME =1,NE
     DO 520 MF = 1,NF
520  AMP(ME,MF) = MP(ME,MF)
     PRINT 401,((AMP(MX,MY),MX=1,NX),MY=1,NY)
401  FORMAT(1H , 8F5.1)
     FAC3=6.0
     FAC4=24.0
     FAC5=120.0
     FAC6=720.0
     FAC7=5040.0
     FAC8=8.0*FAC7
     FAC9=9.0*FAC8
     FAC10=10.0*FAC9
     FAC11=11.0*FAC10
     FAC12=12.0*FAC11
     FAC13=13.0*FAC12
     FAC14=14.0*FAC13
     A=AK*RHO/RO
     SMALL=A*((WO)**2)/4.0 - (A**3)*WO**4)/(64.0) + (A**5)*(WO**6)/
    1 2304.0 - (A**7)*(WO**8)/147456.0 + (A**9)*(WO**10)/10*1,474,560=
     120*12288*10
    2 0)
     PRINT 30
 30  FORMAT(1H ,10H  E =      ,10H  F =     ,11HINTENSITY =)
     ANF=NE
     ANEM1=ANE-1.0
     FBIAS=EO/2.0 - EOFFS
     ANF=NF
     ANFM1=ANF-1.0
     FBIAS= FO/2.0-FOFFS
     ANX=NX
     ANXM1=ANX-1.0
     XBIAS=XO/2.0
     ANY=NY
     ANYM1=ANY-1.0
     YBIAS=YO/2.0
     AKORO=AK/RO
     A2=A*A
     A3=A2*A
     A4=A3*A
     A5=A4*A
     A6=A5*A
     A7=A6*A
     A8=A7*A
     A9=A8*A
     A10=A9*A
     A11=A10*A
     A12=A11 *A
```

```
      W02=WO*WO
      W03=W02*WO
      W04=W03*WO
      W05=W04*WO
      W06=W05*WO
      W07=W06*WO
      W08=W07*WO
      W09=W08*WO
      W010=W09*WO
      W011=W010*WO
      W012=W011*WO
      W013=W012*WO
      DO 10 ME=1,NE
      AME=ME
      E=(EO/(ANEM1))*(AME-1.0) - EBIAS
      PE(ME)=E
      DO 10 MF=1,NF
      AMF=MF
      IF(ANFM1)  2000,2000,2001
 2001 CONTINUE
      F=(FO/ANFM1)*(AMF-1.0)-FBIAS
      GO TO 2002
 2000 F=0.0
 2002 CONTINUE
      SUM=0.0
      DO 20 MX=1,NX
      AMX=MX
      IF(ANXM1) 2100,2100,2101
 2101 CONTINUE
      X=(XO/ANXM1)*(AMX-1.0)-XBIAS
      GO TO 2102
 2100 X=0.0
  102 CONTINUE
      DO 20 MY=1,NY
      AMY=MY
      IF(ANYM1)2200,2200,2201
 2201 CONTINUE
      Y=(YO/ANYM1)*(AMY-1.0)    -YBIAS
      GO TO 2202
 2200 Y=0.0
  202 CONTINUE
      B=AKORO*(((X-E)**2)/((Y/F)**2))**0.5
      BWO=B*WO
      BWO2=BWO*BWO
      BWO3=BWO*BWO2
      BWO4=BWO*BWO3
      BWO5=BWO*BWO4
      BWO6=BWO*BWO5
C BWOD2 MEANS BWO DIVIDED BY 2.0 , BWOD22 MEANS BWOD2 RAISED TO 2ND POWER
      IF (BWO -7.1) 2400,2400,2401
```

```
 2400  BWOD2 = BWO/2.0
       BWOD22=BWOD2*BWOD2
       BWOD23=BWOD22*BWOD2
       BWOD24=BWOD23*BWOD2
       BWOD25=BWOD24*BWOD2
       BWOD26=BWOD25*BWOD2
       BWOD27=BWOD26*BWOD2
       BWOD28=BWOD27*BWOD2
       BWOD29=BWOD28*BWOD2
C DROP O OF WO TO KEEP NAME LESS THAN SEVEN CHARACTERS
       BWD210=BWOD29*BWOD2
       BWD211 =BWD210 * BWOD2
       BWD212 =BWD211 * BWOD2
       BWD213 =BWD212 * BWOD2
       BWD214 =BWD213 * BWOD2
       BWD215 =BWD214 * BWOD2
       BWD216 =BWD215 * BWOD2
       BWD217 =BWD216 * BWOD2
       BWD218 =BWD217 * BWOD2
       BWD219 =BWD218 * BWOD2
       BWD220 =BWD219 * BWOD2
       BWD221 =BWD220 * BWOD2
 2401  CONTINUE
       IF(100.0-BWO)50,50,51
   50  PO=1.0 -(9.0/(128.0*BWO2)) / (11025.0/(98304.0*BW04))
       QO=(-.125/BWO) / (225.0/(3072.0*BWO3)) /((-893025.0)/(3932160.0*
     1 BWO5))
       P1= 1.0 / (15.0/(128.0*BWO2)) - (14175.0/(98304.0*BW04))
       Q1=0.375/BWO - (315.0/(3072.0*BWO3)) / (1091475.0/(31457280.0*
     1 BWO0))
       AJO=(SORT(2.0/9PI*BWO)))*(PO*COS(BWO-PI/4.0) -QO*SIN(BWO-PI/4.0)
     1 )
       AJ1 =(SQRT(2.0/(PI*BWO)))*(PO*COS(BWO-(3.0*PI)/4.0)
     1 -Q1*SIN(BWO-(3.0*PI)/4.0))
       GO TO 52
   51  IF(BWO-.001)53,53,54
   53  AJO =1.0
       SUB=SMALL
       GO TO 56
   54  AJO=BEJO(BWO)
       AJ1=BEJ1(BWO)
   52  AJ2=((2.0/BWO)*AJ1)-AJO
       IF(BWO-3.0)330,330,331
  331  AJ3=((4.0/BWO)*AJ2)-AJ1
       GO TO 332
  330  AJ3 = (1.0/FAC3)* BWOD23 - (1.0/FAC4)* BWOD25
      1/ (0.5/FAC5)* BWOD27 -(.16666667/FAC6)* BWOD29
      2/ (.041666667/FAC7)* BWD211 -(1.0/(120.0*FAC8))* BWD213
  332  CONTINUE
       IF(BWO-4.0)300,301,301
  301  AJ4 =((6.0/BWO)*AJ3)-AJ2
       GO TO 302
```

```
  300  AJ4 = (1.0/FAC4)*BWOD24 -(1.0/FAC5)* BWOD26
     1 +(0.5/FAC6)*BWOD28 -(.16666667/FAC7)* BWD210
     2 +(0.041666667/FAC8)*BWD212 -(0.0083333333/FAC9)*BWD214
  302  CONTINUE
       IF(BWO-5.0)310,311,311
  311  AJ5 =((8.0/BWO)*AJ4)-AJ3
       GO TO 312
  310  AJ5=(1.0/FAC5)* BWOD25 -(1.0/FAC6)*BWOD27
     1 +(0.5/FAC7) *BWOD29 - (0.16666667/FAC8)*BWD211
     2 +(0.041666667/FAC9)* BWD218 -(0.0083333333/FAC10)*BWD215
     3 +(0.0013888888/FAC11)*BWD217
  312  CONTINUE
       IF(BWO-6.0)320,321,321
  321  AJ6=((10.0/BWO)*AJ5)-AJ4
       GO TO 322
  320  AJ6=(1.0/FAC6)*BWOD26 -(1.0/FAC7)* BWOD28 +
     1 (0.5/FAC8)* BWD210 -(0.16666667/FAC9)* BWD212
     2 +(0.041666667/FAC10)* BWD214 -(0.0083333333/FAC11)* BWD216
     3 +(0.0013888888/FAC12)* BWD218
  322  CONTINUE
       IF(BWO - 7.0) 340,341,341
  341  AJ7 = ((12.0/BWO)*AJ6) - AJ5
       GO TO 342
  340  AJ7 = (1.0/FAC7)* BWOD27  - (1.0/FAC8)* BWOD29
     1  + (0.5/FAC9)* BWD211  - (.16666667/FAC10) 8 BWD213
     2  + (1.0/(FAC4*FAC11))*BWD215  - (1.0/(FAC5*FAC12)) * BWD217
     3  + (1.0/(FAC6*FAC13)) *BWD219  - (1.0/FAC7 * FAC14)) * BWD221
  342  CONTINUE
C  BDA MEANS B DIVIDED BY A , BDA2 is BDA SQUARED
       BDA=B/A
       BDA2=BDA*BDA
       BDA3=BDA2*BDA
       BDA4=BDA3*BDA
       BDA5=BDA4*BDA
       BDA6=BDA5*BDA
       BDA7 = BDA6 *BDA
       B2=B*B
       B3=B2*B
       TERM1 =(0.5*A/B2)*BWO*AJ1
       TERM2 =(-0.0625*A3)*((WO3/B)*AJ1 -2.0*(WO2/B2)*AJ2)
       TERM3 =((2.6041667E-3)*A5)*((WO5/B*AJ1 -4.0*(WO4/B2)*AJ2
     1 +8.0*(WO3/B3)*AJ3)
       TERM4 =(5.4253472E-05)*(-1.0) * ((A7*WO7/B)*AJ1
     1 -6.0*(A5*WO6/BDA2)*AJ2 +24.0*(A4*WO5/BDA3)*AJ3
     2 -48.0*(A3*WO4/BDA4)*AJ4)
       TERM5 =(6.7816840E-07)       *((A9*WO9/B)*AJ1
     1 -8.0*(A7*WO8/BDA2)*AJ2 +48.0*(A6*WO7/BDA3)*AJ3
     2 - 192.0*(A5*WO6/BDA4)*AJ4 +384.0*(A4*WO5/BDA5)*AJ5)
       TERM6 =(5.6514033E-09)*(-1.0) *((A11*WO11/B)*AJ1
```

```
     1 -10.0*(A9*WO10/BDA2)*AJ2 + 80.0*(A8*WO9/BDA3)*AJ3
     2 -480.0*(A7*WO8/BDA4)*AJ4 + 1920.0*(A6*WO7/BDA5)*AJ5
     3 -3840.0*(A5*WO6/BDA6)*AJ6)
       TERM7 = (3.3639305E-11)           * ((A12*WO13/BDA)*AJ1
     1 - 12.0 * (A11*WO12 /BDA2) * AJ2 + 120.0 *(A10 *WO11/BDA3) * AJ3
     2 -960.0*(A9*WO10/BDA4)*AJ4 + 5760.0*(A8*WO9/BDA5)*AJ5
     3 -23040.0 * (A7*WO8/BDA6)*AJ6 + 46080.0 * (A6*WO&/BDA7)*A,7)
       SUB = TERM1 + TERM2 + TERM3 + TERM4 + TERM5 + TERM6 + TERM7
  56   CONTINUE
  20   SUM =SUM+SUB*AMP(MX,MY)
       UINTEN(ME,MF) = FRONT *SUM *SUM
       PRINT 31, E,F,UINTEN(ME,MF)
  31   FORMAT(1H ,2F10.5,E14.7)
  10   CONTINUE
       TOTAL =0.0
       DO 100 ME=1,NE
       DO 100 MF=1,NF
 100   TOTAL= TOTAL + UINTEN(ME,MF)
       AVG = TOTAL/(ANE*ANF)
       TOTAL=0.0
       DO 110 ME=1,NE
       DO 110 MF=1,NF
 110   TOTAL = ((UINTEN(ME,MF)-AVG)**2) +TOTAL
       STDEV = SQRT(TOTAL/(ANE*ANF))
       PRINT 120,AVG,STDEV
 120   FORMAT(1HO,10HAVERAGE = ,E14.7,4X,21HSTANDARD DEVIATION = ,E14.7)
       PRINT 601
 601   FORMAT (1H1)
 600   CONTINUE
       STOP
       END
$      EXECUTE
$      LIMITS  10,40000,,1000
         1
  15.0
  .00508
  .074
 1778
  778
         8
         8
.1778
.1778
  0.0
  0.0
         8
         8
  1  1 -1  1  1  1  1  1
 -1  1 -1 -1 -1 -1 -1  1
 -1 -1  1 -1 -1 -1  1 -1
  1  1 -1  1 -1 -1 -1 -1
```

```
 -1   1 -1 -1 -1   1 -1 -1
  1   1 -1   1   1   1 -1 -1
  1 -1   1   1 -1 -1   1   1
  1 -1   1   1 -1 -1   1   1
$       ENDJOB
```

APPENDIX V-2

LENS EQUIVALENCY

Using the same line of reasoning as in Appendix V-1 and the coordinates of Figure AV-1, the imaged intensity of the data mask is found as follows.

$$U(\alpha,\beta) = -\frac{i}{\lambda} \int_x \int_y \frac{A(x,y)e^{ik(r+s)}}{rs}\, dx\, dy$$

$$= -\frac{i}{\lambda s_o^2} \int_x \int_y A(x,y)e^{ik\left[\frac{\alpha^2+\beta^2}{2s_o} - \frac{\alpha x+\beta y}{s_o}\right]} dx\, dy$$

Noting the amplitude transmittance of the lens to be[70]

$$T(\alpha,\beta) = e^{-ik\frac{(\alpha^2+\beta^2)}{2f}}$$

where f equals the focal length of the lens. Thus

$$U(\xi,\eta) = \frac{i}{\lambda} \iint e^{ik\left[z_o + \frac{\alpha^2+\beta^2}{2z_o} + \frac{\xi^2+\eta^2}{2z_o} - \frac{\alpha\xi+\beta\eta}{z_o}\right]} e^{-ik\left[\frac{\alpha^2+\beta^2}{2}\right]}$$

$$\frac{1}{s_o^2} \int_x \int_y A(x,y)e^{ik\left[\frac{\alpha^2+\beta^2}{2s_o} - \frac{\alpha x+\beta y}{s_o}\right]} dx\, dy\, d\alpha\, d\beta$$

---

70 J. Goodman, op. cit., p. 80.

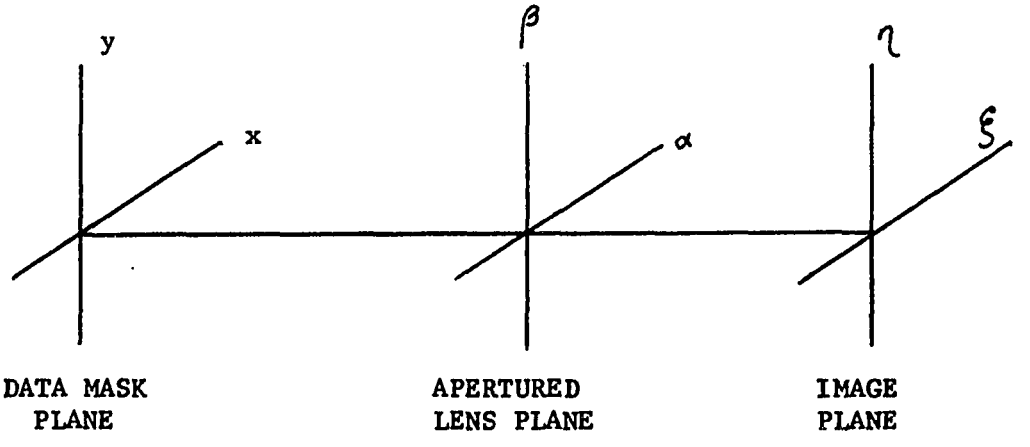

COORDINATES OF LENS MODEL

FIGURE AV - 1

Imposing the focalization condition,

$$\frac{1}{2s_o} + \frac{1}{2z_o} = \frac{1}{2f}$$

then

$$U(\xi,\eta) = \frac{1}{\lambda 2s_o^3} \iint e^{ik\left[s_o + \frac{\xi^2+\eta^2}{2s_o} - \frac{\alpha\xi+\beta\eta}{s_o}\right]}$$

$$\int_x \int_y A(x,y) e^{ik\left[\frac{-(\alpha x+\beta y)}{s_o}\right]} dx\, dy\, d\alpha\, d\beta$$

This equation can be shown to be a generalization of that for $U_4(\xi,\eta)$ on page A41of Appendix V-1.

VITA

The author, born in , on , received a Bachelor of Science in Electrical Engineering degree from Newark College of Engineering in 1965. In January 1967 he was awarded a Master of Engineering degree for work in electrical communication systems from Rensselaer Polytechnic Institute.

During the summer of 1965, the author was a member of the Initial Management Development Program of the New York Telephone Company. For the academic year 1965-66, he served as a graduate assistant at RPI. The following year, he held the position of Instructor of Electrical Engineering at Union College, Schenectady.

Prior to beginning his duties of a Teaching Fellow at Newark College of Engineering in 1967, he was the holder of an ASEE-NASA Summer Faculty Research Fellowship. During the summer of 1970, he held the position of Member of the Technical Staff at Bell Telephone Laboratories.

For the academic years 1970-71 and 71-72, the author was a Special Lecturer at NCE. Since 1972 he has been on the staff of the Research and Development Laboratories of the U.S. Army Electronics Command.